Monomer Sequence Controllable Ring-opening Polymerization for Precise Synthesis of Polyester-based Copolymers

A Dissertation for the Degree of Doctor of Philosophy

Tianle Gao

Graduate School of Chemical Sciences and Engineering

Hokkaido University

June 2024

Acknowledgments

The study presented in this dissertation has been performed under the direction of Professor Takuya Isono, Division of Applied Chemistry, Faculty of Engineering, Hokkaido University. I would like to express the biggest and sincerest appreciation to Professor Takuya Isono and Professor Toshifumi Satoh for their tremendous support as well as thorough guidance, discussions, and words of wisdom throughout this academic journey of mine. I could not have imagined having a better advisor and mentor for the studies and research works in the Ph.D program.

I am also grateful to Assistant Professor Feng Li, Division of Applied Chemistry, Faculty of Engineering, Hokkaido University, for all the helpful suggestions and fruitful discussions. His academic rigor allowed me to grow under his guidance.

Much appreciation is expressed to Professor Tajima and Professor Yamamoto for providing helpful advice as the committee members for the evaluation of my Ph.D. dissertation. Special thanks go to Xiaochao Xia. It was an unforgettable experience and a great honor to have him as my teacher, friend, and an academic comrade from 2019 to 2022. Words cannot fully describe my appreciation but I am lucky to have met him. And I also thank to Yubo Wang, my senior colleagues, accompanied me throughout my five-year journey in Sapporo and provided me with invaluable support and care in numerous ways.

I also thank all the members of Polymer Chemistry Laboratory. All of you are my academic family; and it was great to work alongside with everyone over the years. You have been exceedingly supportive in guiding me both in my personal endeavors and academic pursuits.

The last and not the least, I extend the greatest love and thanks to my family and friends for all the love, encouragement, and support. It would not have been possible without you all.

July 2024 Tianle Gao

Contents

Chapter 1

General Introduction

1.1 Polyester

Synthetic polymeric materials play an indispensable role in various sectors, including food production, clothing, transportation, insulation, healthcare, and medicine. Despite their significant contributions to human welfare, the accumulation of plastic waste poses formidable environmental challenges, including air pollution resulting from open burning,[1] marine ecosystem degradation,[2] and the widespread presence of microplastics.[3] In 2014, global synthetic polymeric material production peaked at 311 million tons and is expected to triple by 2050.[4] The unsustainable generation and disposal of polymers necessitate urgent strides towards establishing a sustainable plastics system.

Vinyl polymers derived from petroleum sources hold a predominant position in the current polymeric materials, owing to their superior properties, such as strength, flexibility, electrical resistivity, and chemical inertness, coupled with well-established production techniques.[5] However, their high depolymerization temperatures due to stable carbon-carbon backbones and limited monomer selectivity resulting from random chain scission present formidable sustainability hurdles.[6] In response, recyclable polymers have emerged over the past two decades and polyesters play a predominant role among them owing to its potentially hydrolysable ester bonds that enable chemical recycling into small molecules, and the renewable monomer resources for polyester synthesis.[7–9]

Polyester-based materials are increasingly replacing their petroleum-based vinyl polymers in various aspects of daily life (Scheme 1.1). For instance, poly(lactide) (PLA), poly(butylene succinate) (PBS), and poly(hydroxyalkanoate) (PHA) are utilized in packaging, foils, and agricultural applications.[10, 11] Additionally, owing to their biocompatibility, polyesters find diverse applications in biomedical fields, such as tissue engineering scaffolds and drug delivery systems.[12–14] Medical sutures fabricated from poly(glycolic acid) (PGA), PLA, and poly(lactide-*co*-glycolide) (PGLA) are gaining traction due to their ability to biodegrade within the human body over several weeks.[15]

To further enhance the functionality of polyesters to meet evolving application demands, structural design and control will be pivotal focuses for future polyester material development.

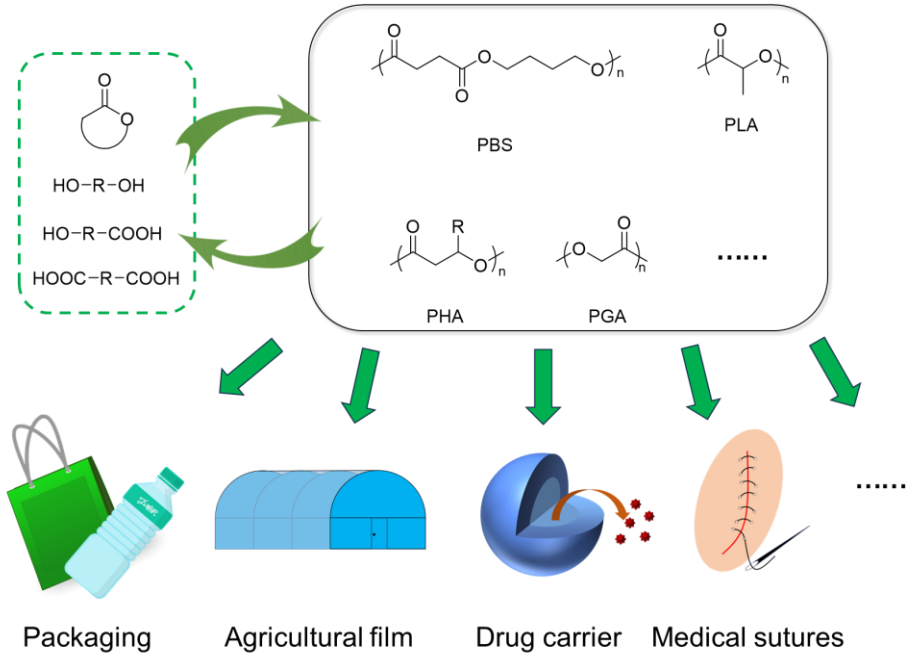

Scheme 1.1. Applications of degradable polyester materials.

1.2 Conventional synthesis method for polyester

1.2.1 Step-growth polymerization

The conventional techniques for synthesizing polyesters involve polycondensation of a diacid with a diol and self-polycondensation of hydroxy carboxylic acid (Scheme 1.2). Advantage of this system is that various combinations of monomers yield diverse polyester structures. However, precise temperature control during polymerization is crucial to eliminate small molecule byproducts (such as water and alcohol).[16]

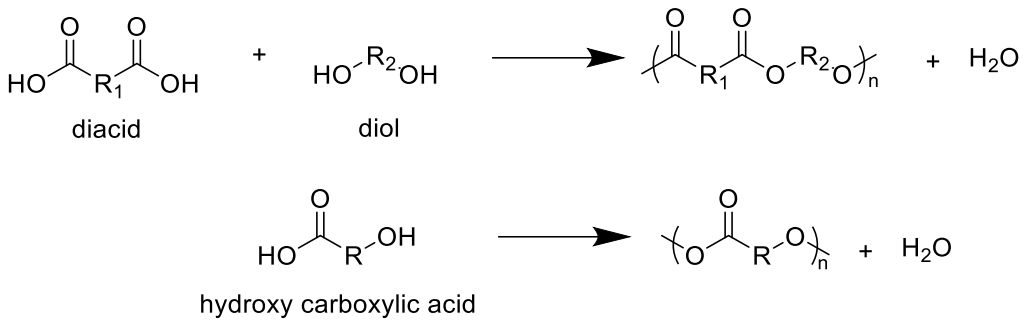

Scheme 1.2. Polycondensation of a diacid with diol and self-polycondensation of hydroxy carboxylic acid.

An illustrative example of polyester synthesized via step-growth polymerization is poly(ethylene terephthalate) (PET), extensively employed in packaging applications due to its robust mechanical properties. PET synthesis involves two stages (Scheme 1.3). Initially, dimethyl terephthalate (DMT) undergoes ester interchange with ethylene glycol, necessitating temperatures ranging from 150 to 210 °C for methanol distillation. Subsequently, the resulting bis(2-hydroxyethyl)terephthalate is subjected to polymerization at 270–280 °C, accompanied by partial vacuum application (0.5–1 torr or 66–133 Pa) for ethylene glycol removal.[16]

Step-growth polymerization for polyester synthesis needs elevated temperatures and small-molecule byproduct elimination to achieve high conversion rates, rendering the process energy-intensive. Furthermore, due to the intrinsic characteristics of step-growth polymerization, the molecular weight dispersity converges to theoretically 2 at high conversion rates. Moreover, the controls over the molecular weight, chain-end functionality, and comonomer composition/sequence are quite difficult. Consequently, to produce polyesters with defined primary structures under milder reaction conditions, extensive research efforts have been dedicated to developing chain-growth synthesis methods.

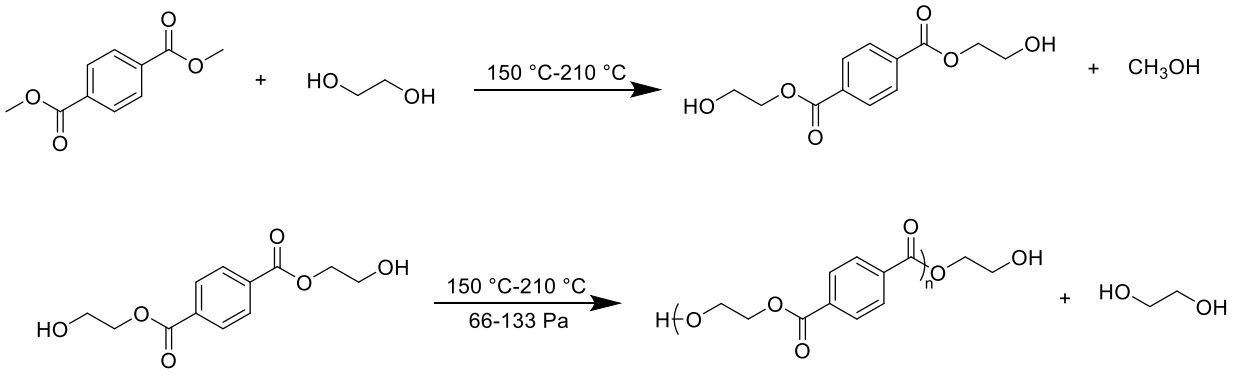

Scheme 1.3. Step-growth polymerization for poly(ethylene terephthalate) synthesis.

1.2.2 Ring-Opening Polymerization

Compared to step-growth polymerizations, chain-growth polymerizations offer superior control over molecular weight and exhibit high atom economy. The ring-opening polymerization (ROP) of cyclic esters and cyclic carbonates stands out as an efficient method for producing polyester and polycarbonate (Scheme 1.4), enabling synthesis under mild conditions and precise control over polymer parameters, including molecular weight, polydispersity, chain-end functionality, regio- and stereoselectivity, and polymer topology.[16–19]

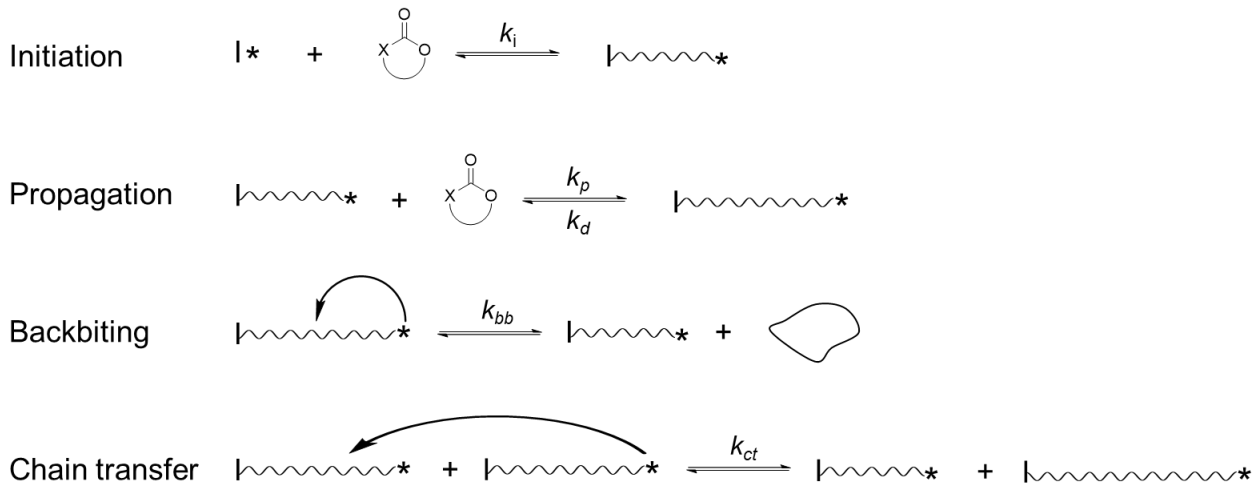

Scheme 1.4. Elementary reactions for cyclic ester and cyclic carbonate ROP.

The term "ring-opening polymerization " encompasses a class of polymerization techniques wherein cyclic monomers serve as substrates for chain extension by the attacking propagating species. Notable examples include ring-opening metathesis polymerization,[20] radical ring-opening polymerizations,[21] cationic ring-opening polymerizations,[22] and anionic ring-opening polymerizations. Since the focus of this dissertation is on the ROP synthesis of polyester, highly related anionic ROP systems for synthesizing polyether, polyester, polycarbonate, and their derivatives are briefly summarized in this section.

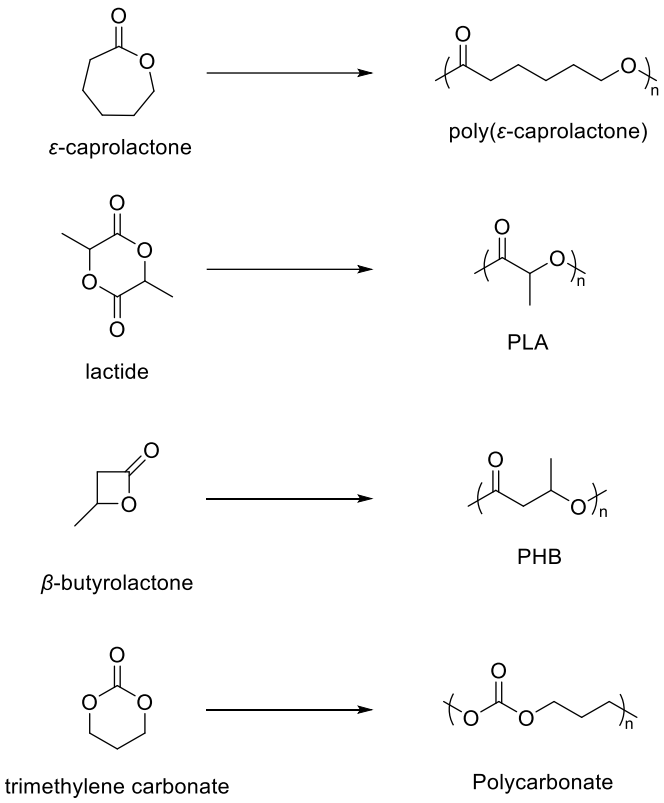

Scheme 1.5. Typical anionic ROP for polyester and polycarbonate synthesis.

Cyclic ester ROP is a versatile technique for the synthesis of well-defined polyesters, including poly(ε-caprolactone), poly(lactic acid) (PLA), and poly(hydroxybutyrate) (PHB) (Scheme 1.5). Additionally, trimethylene carbonate represents a common cyclic carbonate monomer utilized in the ROP process for the synthesis of polycarbonates (Scheme 1.5). Traditional initiators for anionic cyclic ester and cyclic carbonate ROP include alkali metal complexes.[23, 24] However, the strong nucleophilicity of the propagating species often

leads to transesterification, causing loss of control over molecular weight, polydispersity, and end-group fidelity (Scheme 1.4).[25, 26] To address this, metal-ligand catalysts have been developed to produce polyester with high molecular weight and narrow polydispersity. Recently, metal-free organocatalyst systems have shown promising efficiency for polyester and polycarbonate synthesis.[27, 28]

Epoxide ROP is an important category within anionic ROP, which is usually used to synthesize well-defined polyethers, such as poly(ethylene oxide) and poly(propylene oxide). Applications of such polyethers are found in diverse fields such as antifouling coatings,[29] cosmetics,[30] biomedical materials,[31–33] and rubber/plastics.[34, 35] Although cyclic ethers of three- to five-membered ring can be utilized for polyether synthesis via ROP, only epoxides can undergo anionic ROP to yield well-defined polyether. The versatile class of epoxide monomers offers numerous possible polyether structures, attracting significant attention to epoxide ROP research.[36] Conventionally, epoxide ROP initiated by sodium, potassium, or cesium alkoxides suffers from strong basicity-induced irreversible chain transfer to the monomer, particularly with the monomers bearing methylene- or methyl-group substituents at high temperatures, limiting product molecular weight (≤ 5.0 kDa) (Scheme 1.6). The addition of crown ethers or trialkylaluminum mitigates this issue and increases achievable molecular weight (M_n > 10 kDa).[37, 38] Alternatively, organocatalysts enable controlled epoxide ROP, where phosphazene base (*t*-Bu-P_4) catalyst systems exemplifying efficient synthesis of high molecular weight polyether with narrow polydispersity at room temperature.[39]

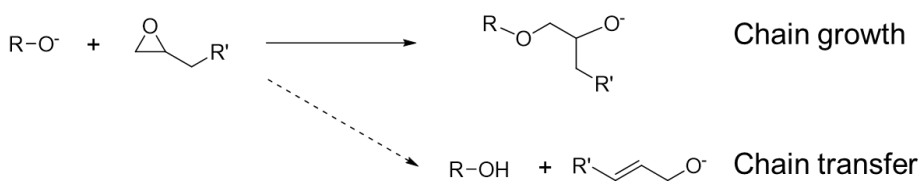

Scheme 1.6. Chain growth and chain transfer on epoxide ROP.

Exploration of cyclic monomers beyond conventional epoxides, cyclic esters, and cyclic carbonates has

led to the utilization of novel cyclic monomers for synthesizing heteroatom-containing polymers such as poly(thioester),[40] poly(thioether),[41] and poly(sulfonylaziridine)s (Scheme 1.7).[42] Under anionic ROP condition, the ROPs of those monomers exhibit precise molecular weight control and afford new structures with high atom economy. Properties and performance of these polymers continue to be investigated, holding promise for addressing contemporary material challenges.

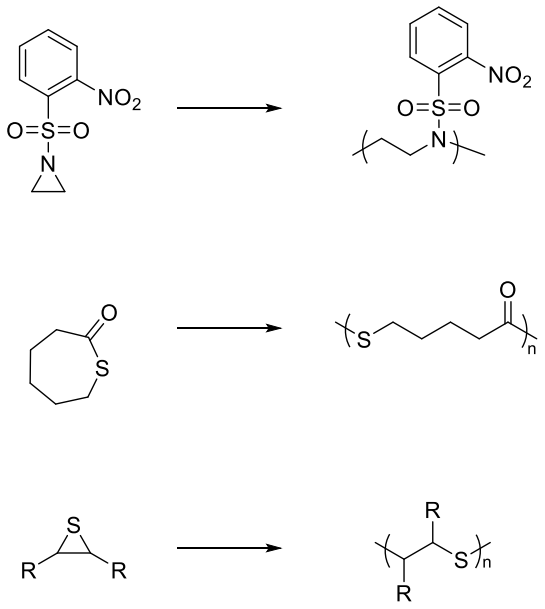

Scheme 1.7. Synthesis of heteroatom-containing polymers via ROP.

As mentioned above, ROP of cyclic ester, cyclic carbonate, and other cyclic monomers could efficiently synthesize well-defined polyester, polycarbonate, polyether, and their derivatives. However, since the thermodynamic driving force for cyclic monomer ROP is the ring strain relief, the monomer reactivity is highly dependent on the ring size and substituents of monomers. This limited the diversity of polymer structures synthesized from ROP.

1.2.3 Ring-opening alternating copolymerization

Polycondensation represents a straightforward technique for fabricating polyesters with diverse structural

characteristics. Meanwhile, controlling molecular weight proves challenging owing to the inherent step-growth polymerization mechanism. Conversely, ROP of cyclic esters yields polyesters with high molecular weights and narrow polydispersity, yet confines the resulting polyester structures within the realm of polymerizable monomers. To overcome this dilemma, ring-opening alternating copolymerizations (ROACs), involving epoxide/cyclic anhydride systems, emerge as a promising alternative for polyester synthesis. This approach not only enables the production of well-defined polyester architectures in a controlled manner owing to its chain-growth mechanism but also offers a wide array of feasible structures due to the availability of diverse epoxides and cyclic anhydrides (Scheme 1.8). Furthermore, the epoxide/CO_2 ROAC method presents a sustainable avenue for polycarbonate synthesis. CO_2 serves as an attractive monomer due to its affordability, low toxic, and abundant supply, addressing environmental concerns associated with climate change. Consequently, it stands as an ideal candidate for sustainable polymer material systems.

	Advantage	Challenge
Polycondensation	Simple process Abundant monomer source	Energy-consume Low molecular weight Broad polydispersity
Cyclic ester ROP	High molecular weight Narrow polydispersity	Limited monomer scope
Epoxide/cyclic anhydride ROAC	High molecular weight Narrow polydispersity Diversity polyester structure	Heteroatom-containing polymers synthesis

Scheme 1.8. Comparison of polyester syntheses by polycondensation, cyclic ester ROP, and epoxide/cyclic anhydride ROAC.

In the ROAC of epoxides and cyclic anhydrides (or CO_2), the cyclic anhydride (or CO_2) exhibits significantly higher reactivity towards nucleophilic attack compared to the epoxide. Upon reaction, the cyclic

anhydride (or CO_2) yields carboxylate (or carbonate), thereby exclusively exposing the epoxide to further nucleophilic attack rather than the cyclic anhydride (or CO_2) (Scheme 1.9a). This mechanism results in the formation of an alternating copolymer structure. Since the pioneering discovery of epoxide/CO_2 ROAC using Et_2Zn/H_2O in 1969 and epoxide/cyclic anhydride ROAC with aluminum porphyrin salt in 1985 by Inoue et al.,[43, 44] substantial efforts have been devoted to catalytic system development in this field. Recently, significant advancements have been achieved, particularly by Williams and Coates, in the development of transition metal catalyst systems, such as metal salen-type catalysts, for epoxide/cyclic anhydride and epoxide/CO_2 ROAC (Scheme 1.9b).[45–49] These catalysts offer precise control over regio- and stereoselectivity during polymerization, in conjunction with a broad spectrum of monomer sources, facilitating the synthesis of polymers with tailored thermal properties.[50, 51]

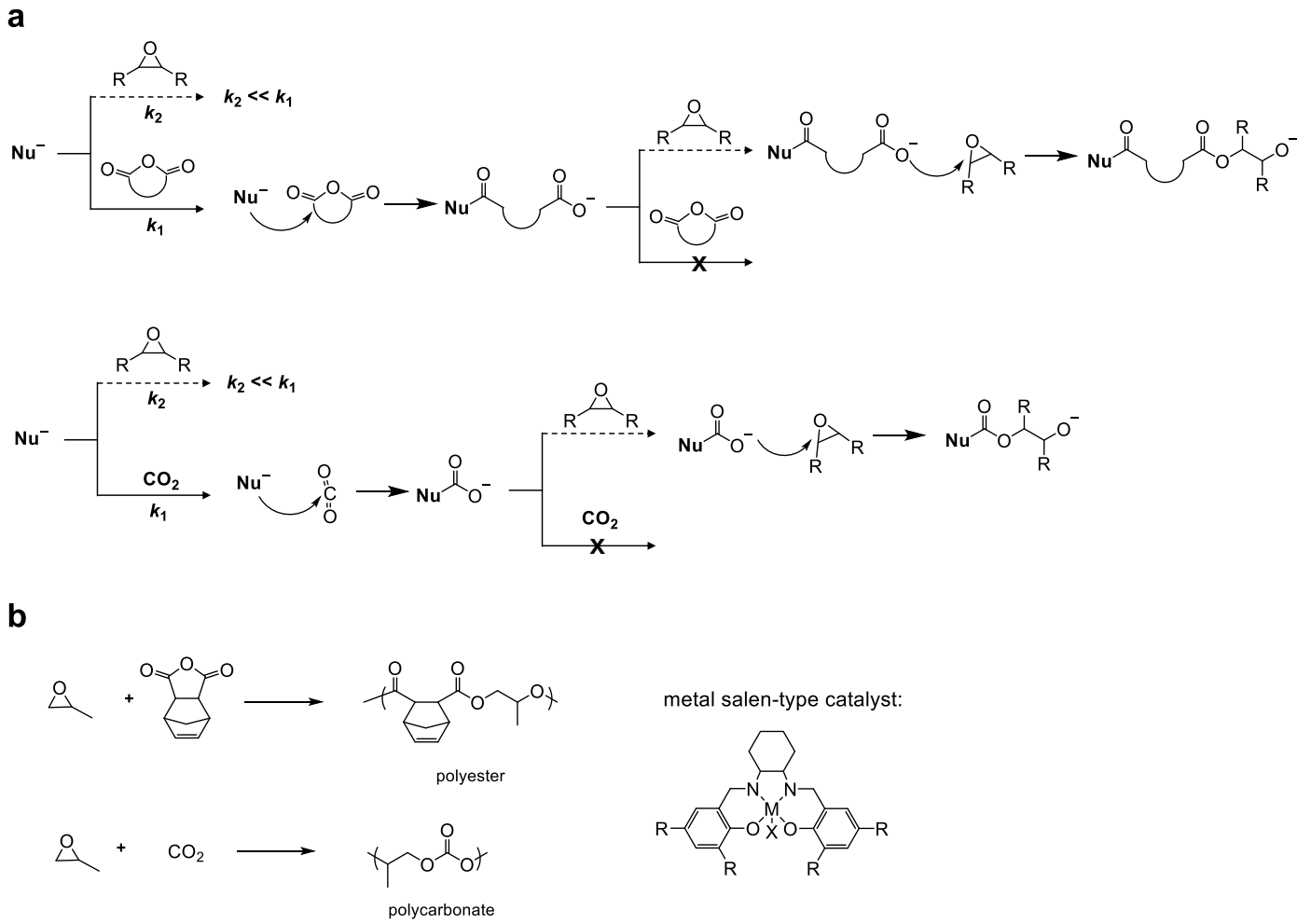

Scheme 1.9. ROAC of epoxide/cyclic anhydride and epoxide/CO_2 and structure of metal salen-type catalyst.

In addition to the transition metal catalysts, organocatalysts also play a pivotal role in ROACs involving epoxide, CO_2, and cyclic anhydride (Scheme 1.10). Organo-bases such as phosphazene base (*tert*-butylimino-tris(dimethylamino)phosphorane(*t*-Bu-P_1)), 1,8-diazabicyclo[5.4.0]undec-7-ene (DBU), 4-dimethylaminopyridine (DMAP), and Triazabicyclodecene (TBD) have demonstrated efficient polymerization and molecular weight controllability in epoxide/cyclic anhydride and epoxide/CO_2 ROAC. Their metal-free nature renders them particularly appealing for synthesizing biomedical polymer materials.[52, 53] Notably, Feng et al. reported the utilization of triethyl borane and a phosphazene base as an efficient cocatalyst system for epoxide/CO_2 ROAC in 2016.[54] Since then, boron-containing catalysts have garnered significant attention for their high efficiency and excellent molecular weight controllability, driving further

advancements in the field.[55–57]

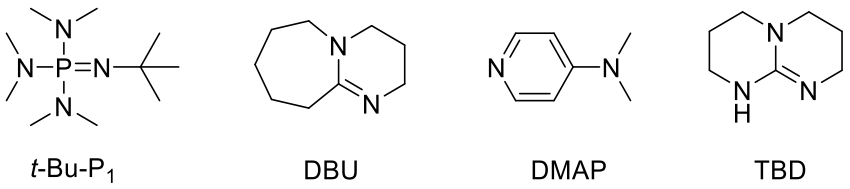

Scheme 1.10. Structure of organocatalysts used in ROAC.

At present, epoxide/cyclic anhydride ROAC stands as a pivotal technique in producing precisely defined polyesters with a diverse main chain structure. The exploration of innovative combinations of cyclic monomers for synthesizing polymers containing heteroatoms holds considerable potential for tackling recyclable polymeric material challenges. Moreover, connecting various ROAC cycles under the same catalytic conditions to establish a self-switchable copolymerization system represents a cutting-edge method for synthesizing block polyesters. This will be further elucidated in the Section 1.3.3.

1.3 Monomer sequence control in polyesters

1.3.1 Monomer sequence of polyester

The performance of polymer materials is highly influenced by the structure of their main chain. Rather than synthesizing homopolymers, copolymerization involving two or more types of monomers enhances the degree of structural control over polymers. The combination of different monomers to form copolymers represents a versatile approach for producing polymer materials with finely tuned physicochemical properties and improved mechanical performance (Scheme 1.11). The properties of copolymers are highly dependent on the arrangement of monomers along the polymer main chain, such as random, alternating, gradient, and block sequences. Therefore, controlling the arrangement of monomers along the polymer main chain is crucial for

producing copolymer materials with the desired performance.

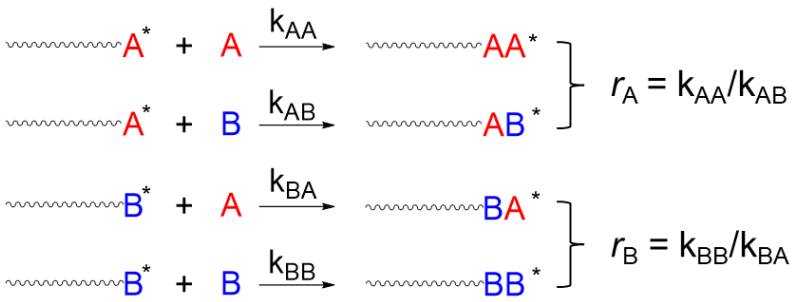

Scheme 1.11. Reactivity ratios are defined by the ratios of the propagation rate constants for adding a monomer (A or B) to a growing chain end of the same identity. $r_A=k_{AA}/k_{AB}$ represents the preference of a chain with a terminal A unit for similar monomers of type A and likewise for r_B.

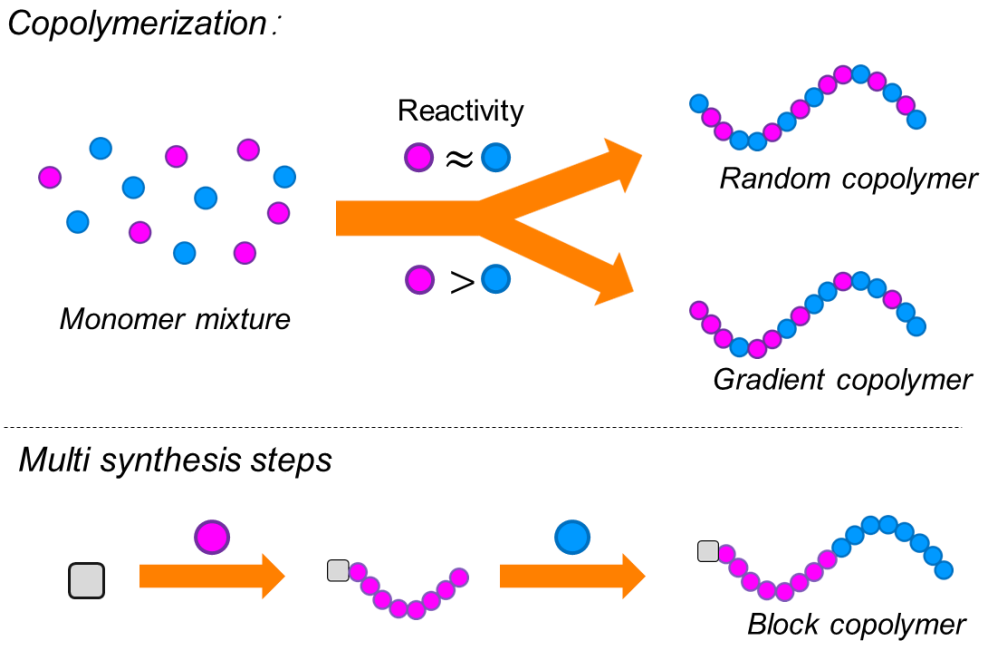

Scheme 1.12. Synthesis of copolymers with different monomer sequences.

The reactivity ratios are defined by the ratios of the propagation rate constants for adding a monomer (A

or B) to a growing chain end of the same identity. $r_A=k_{AA}/k_{AB}$ represents the preference of a chain with a terminal A unit for similar monomers of type A and likewise for r_B (Scheme 1.11). Reactivity ratio between two monomers decided the sequence structure of resulted copolymer (Scheme 1.12) in copolymerization of binary monomer mixture system. Monomers show a similar reactivity ratio during copolymerization yields copolymers with a random monomer sequence, wherein monomer residues adhere to a statistical distribution. Conversely, when copolymerizing two monomers with distinct reactivity ratio, the copolymer exhibits a gradient monomer sequence. Monomer shows higher reactivity ratio aggregated at the α-end and ω-ends are rich of low reactivity ratio monomer. Copolymerization serves as a straightforward method to combine the characteristics of two polymer materials, thereby generating new properties or enhancing existing ones. An exemplary instance of high-value polyester copolymer synthesis involves combining PLA (which typically exhibits poor elasticity) and PCL (poly(ε-caprolactone), known for its poor mechanical properties). The resulting biodegradable materials possess optimal thermomechanical properties suitable for pharmaceutical or biomedical applications.[58, 59]

Block copolymer is the extreme case of copolymers composed of distinct polymer segments linked by covalent bonds. Segmented structure of block copolymers resulted in unique self-assembly behavior that cannot be achieved by random copolymers. Their enhanced performance in terms of morphologies, thermal properties, and elasticity compared to homopolymers, offered a versatile platform for producing polymer materials tailored to diverse application needs, such as drug delivery,[60] data storage device construction,[61–63] nanoporous material synthesis,[64] and nanolithography.[65]

Alongside the enhanced performance of polymer materials, the synthesis of block copolymers poses a significant challenge. In contrast to copolymers with random monomer sequences, the generation of block copolymers cannot typically be achieved through a one-step copolymerization process involving two monomers. Instead, a complex synthesis route or multi-step method is often required for the conventional

generation of block copolymers (Scheme 1. 12).

1.3.2 Conventional block copolymer synthesis

To synthesize block copolymers from monomers with similar reactivity and the same polymerization mechanism, sequential monomer addition stands out as the most commonly employed approach. For instance, employing a dinuclear indium catalyst, a poly(L-lactide)-*b*-poly(D-lactide)-*b*-poly(L-lactide) triblock copolymer was synthesized via a three-step method (Scheme 1.13a).[66] Using the dinuclear indium catalyst, the first poly(L-lactide) block was synthesized through L-lactide ROP at room temperature. Subsequently, after complete consumption of L-lactide, D-lactide was introduced into the reaction flask to initiate D-lactide ROP. This process was repeated for another cycle of L-lactide ROP, resulting in the formation of the poly(L-lactide)-*b*-poly(D-lactide)-*b*-poly(L-lactide) triblock copolymer with a polydispersity index of 1.24.

In cases where block copolymers are synthesized from monomers incompatible under identical conditions, various methods can be employed, such as polymer coupling and utilization of macroinitiators, depending on the specific circumstances. For instance, in synthesizing maltooligosaccharide-*b*-poly(*δ*-decanolactone)-*b*-maltooligosaccharide block copolymers, Satoh's group utilized copper-catalyzed azido−alkyne click reaction to couple ethynyl-end-functionalized maltooligosaccharide with azido-end-functionalized poly(*δ*-decanolactone). These block copolymers, with diverse topologies and narrow polydispersity, exhibited potential as bio-based elastomers (Scheme 1.13b).[67] Moreover, employing an amino functionalized poly(2-deoxy-2-methacrylamido-*D*-glucose) macroinitiator, poly(2-deoxy-2-methacrylamido-*D*-glucose)-*b*-poly(*L*-phenylalanine) block copolymers were synthesized via *L*-phenylalanine *α*-*N*-carboxyanhydride ROP (Scheme 1.13c).[68]

Despite significant efforts in developing synthetic methods for sequence-controlled polyester block

copolymer, achieving large-scale sequence-controlled polyester block copolymer synthesis remains challenging due to constraints such as intricate procedures and time limitations.

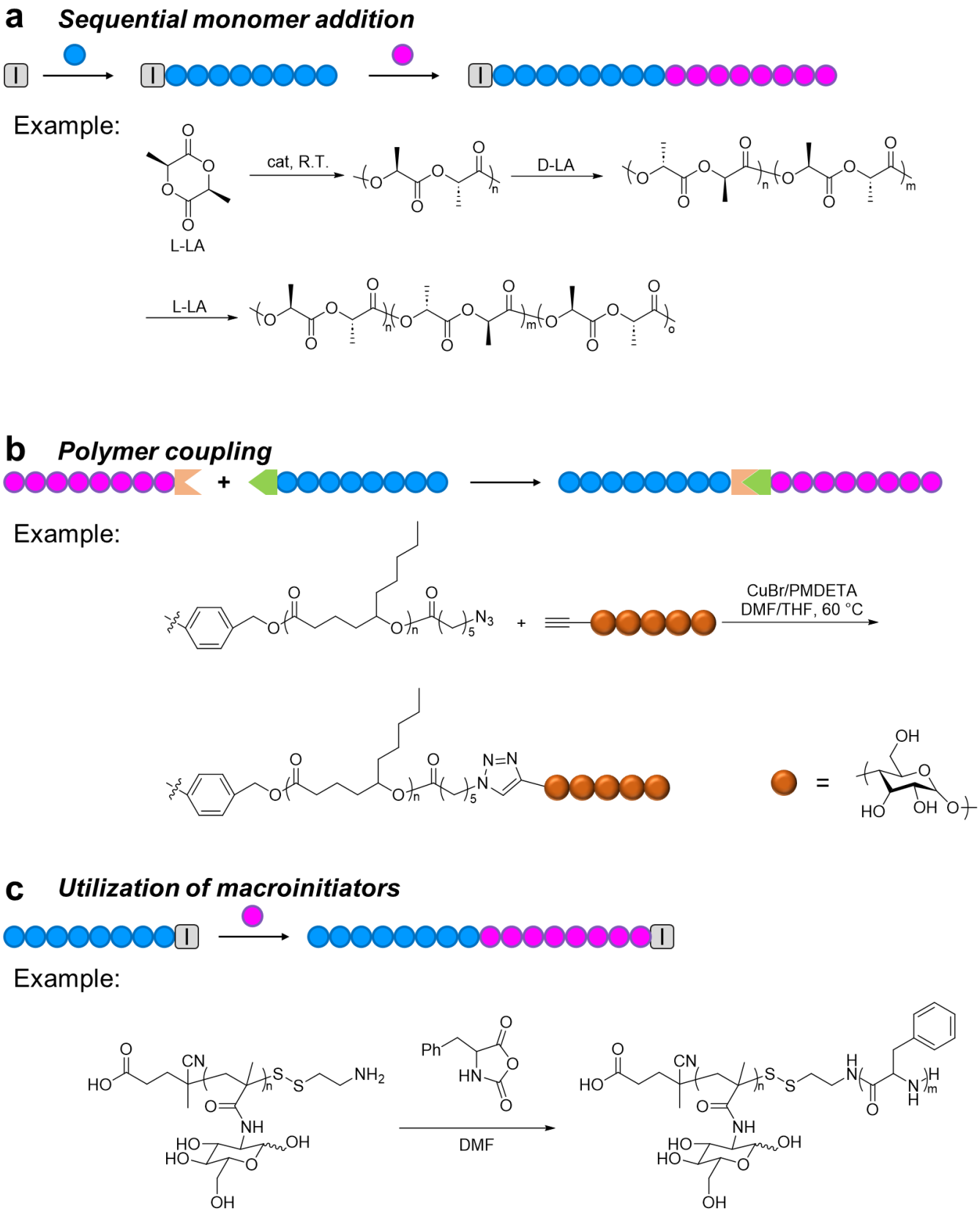

Scheme 1.13. Common synthetic strategies for block copolymers and each example in the polyester-based block copolymer synthesis.

1.3.3. Self-switchable polymerization

To address the limitations on conventional block copolymer synthesis, polymer scientists have developed switchable polymerization systems, enabling the spontaneous, selective transformation of a monomer mixture into a sequence-controlled block copolymer in a single synthetic step (Scheme 1.14).[69–72] In self-switchable copolymerization, different monomers or monomer combinations can undergo polymerization using a single catalyst or cocatalysts, termed "switchable" catalysts. Reactivity trends among monomers decide the polymerization sequence, resulting in the high reactivity monomer polymerizing first, followed by the low reactivity monomer, ultimately yielding a block copolymer with the desired monomer sequence.

In 2008, Coates synthesized diblock copolymers from a monomer mixture of epoxide, anhydride, and CO_2 using a β-diiminate(bdi) zinc catalyst, connecting the epoxide/anhydride ROAC and epoxide/CO_2 ROAC catalytic cycles to produce a polyester-*b*-polycarbonate block copolymer.[73] Williams et al. investigated the same self-switchable copolymerization system using mono-, di-, and trimetallic catalysts.[74–77] Connecting the epoxide/anhydride ROAC and lactone ROP is an effective method for producing block polyester, due to the activity gap between these two catalytic cycles. Both transition metal catalyst systems and organocatalyst systems have been reported for efficiently connecting these two catalytic cycles (Scheme 1.14).[78, 79]

The emergence of new monomers and continuous advancements in polymerization systems have greatly expanded the diversity of structure on polyester block copolymers synthesized via self-switchable copolymerization. This has fueled studies exploring the relationship between structure and properties, offering potential solutions to address issues in polymer-related fields. However, the monomer sequence in synthesized polyester block copolymer is inherently determined by monomer intrinsic reactivity in self-switchable copolymerization systems, necessitating the development of copolymerization systems capable of tailoring monomer sequence regardless of intrinsic reactivity limitations for artificial polyester block copolymer synthesis.

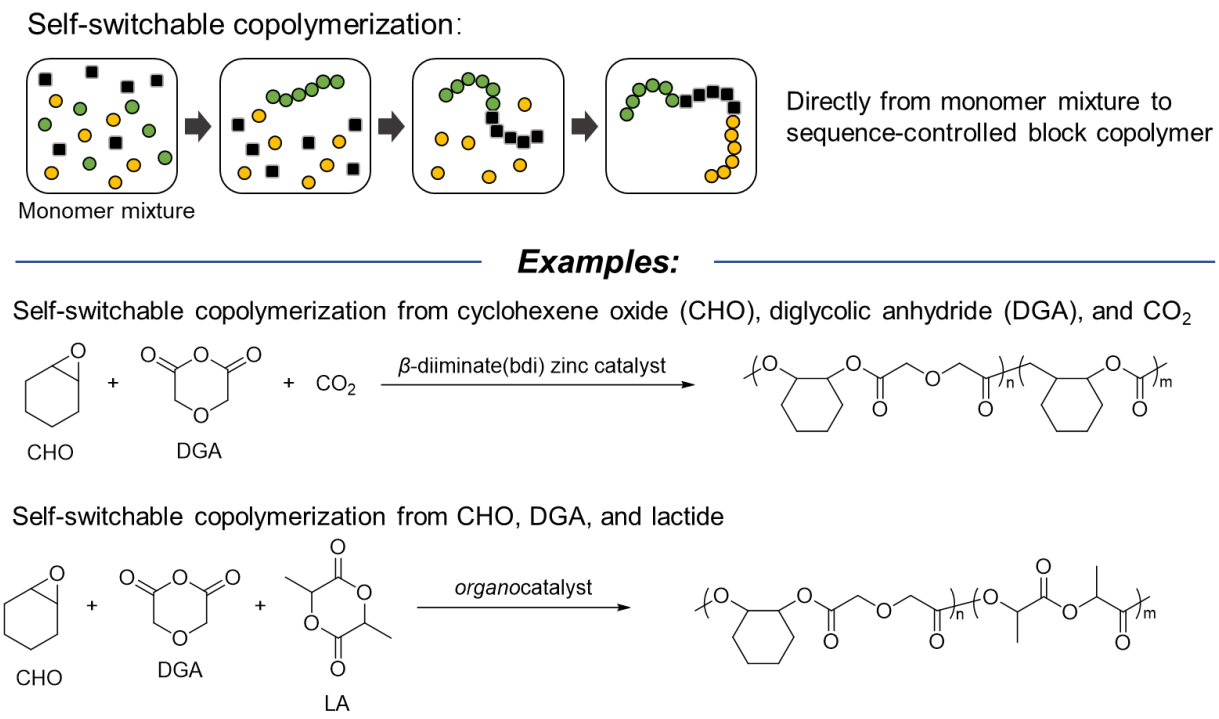

Scheme 1.14. Illustration and examples of self-switchable copolymerization.

1.4 Objectives and outline of this dissertation

Polymeric materials have become ubiquitous in various aspects of human life, yet the exponential increase in demand has led to global concerns regarding their disposal. The need for developing a sustainable plastics system is underscored by environmental and economic considerations. In response to this pressing issue, numerous endeavors have been directed towards designing recyclable polymers and gradually replacing conventional petroleum-based polymers with sustainable alternatives. Among these alternatives, polyesters stand out as a widely used recyclable polymer due to its hydrolyzable ester bonds, utilization of renewable monomer resources, and favorable mechanical properties. However, to elevate polyester performance to the level of current widely used petroleum-based polymers across diverse applications, a broad monomer scope and precise design and tailoring of polymer structure are essential. To achieve this, polymerization systems capable of accommodating a wide range of monomer types to enable precise control of monomer arrangement within the polymer chain are necessary. Additionally, an easily manageable and cost-effective polymerization process is crucial for industrial-scale polyester production.

Addressing these concerns, the aim of this thesis is to develop simple self-switchable copolymerization systems based on ROAC for synthesizing polyesters and related polymers with controllable monomer sequences. In the present study, alkali metal carboxylate (AMC)-catalyzed epoxide/cyclic anhydride ROAC and oxetane/cyclic anhydride ROAC were established for synthesizing polyester homopolymers with diverse structures. The low-cost, easy-to-handle, and low-toxicity nature of AMC endows promising applications in industrial polyester production. By combining two different epoxide/cyclic anhydride ROAC and oxetane/cyclic anhydride ROAC catalytic cycles with the AMC catalyst, block polyesters were synthesized in a one-step process. A comprehensive investigation of polymerization behaviors from two cyclic anhydrides and an epoxide revealed reactivity trends among cyclic anhydrides, ensuring precise control of monomer sequence. Furthermore, the incorporation of aziridine monomer enabled the one-step synthesis of poly(amide ester)-*b*-polyesters with a phosphazene base catalyst. The distinct chemical nature between the two blocks resulted in microphase separation, facilitating the fabrication of block copolymers with the desired microphase-separated morphology.

Tailoring monomer sequence during copolymerization, particularly from the same monomer mixture, could significantly enhance polymer material design, albeit posing challenges due to monomer intrinsic reactivity. At the end of this study, the author addressed the challenge of monomer sequence control regardless of monomer intrinsic reactivity using a binary organocatalyst polymerization system. Poly(amide ester-ester) from ABA-type block to gradient, random-like, reversed gradient, and reversed BAB-type block monomer sequences were successfully synthesized from the same monomers mixture. This copolymerization strategy offers a straightforward approach for producing copolymers with similar chemical compositions but varying monomer sequences, which holds promise for exploring the relationship between monomer sequences and polyester properties.

An outline of this dissertation is as follows:

Chapter 2 elucidates the versatility of the AMC catalyst in ring-opening alternating copolymerization (ROAC) for polyester synthesis and its potential as a switch catalyst for block copolymer production (Figure 1.1). Initially, the ROAC behavior of ethyl glycidyl ether (EGE) with various cyclic anhydrides was investigated, validating this approach as an efficient route to synthesize polyesters with controllable structures. Subsequently, oxetane was successfully copolymerized with cyclic anhydrides, broadening the range of polyester structures achievable via ROAC. Furthermore, AMC was employed in epoxide ring-opening polymerization (ROP), confirming its ability to efficiently synthesize well-defined polyether. Building upon this, the author developed a one-pot, two-step method for synthesizing polyether-*b*-polyester. Covalent bonding between each block was verified through diffusion-ordered NMR spectroscopy, and size-exclusion chromatography measurements demonstrated precise molecular weight controllability. This underscores the potential of AMC as a switch catalyst capable of connecting two or more catalytic cycles for one-step synthesis of block copolymers (Figure 1.1).

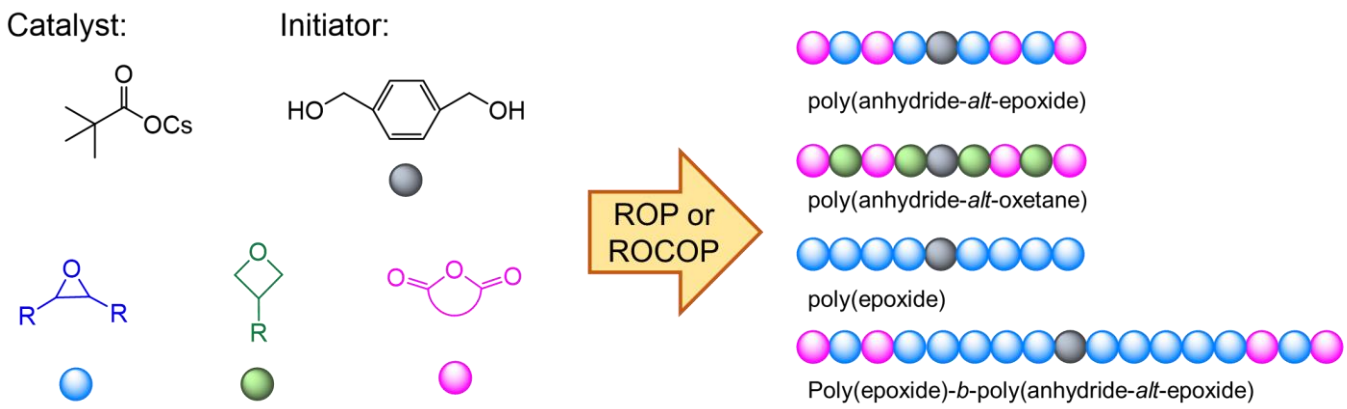

Figure 1.1. Illustration of the chapter 2 outline.

Chapter 3 delves into the capability of AMC to connect two catalytic cycles for one-step synthesis of block polyester (Figure 1.2). The polymerization of epoxide with two cyclic anhydrides was explored to ascertain the reactivity trends among cyclic anhydrides with different structures. Based on the results, polyesters with desired structures and different tapered regions could be precisely synthesized. Similarly, the cyclic anhydride reactivity trend was confirmed in the polymerization of oxetane with two cyclic anhydrides. The incorporation of the oxetane monomer enriched the range of possible polyester structures and enhanced the adjustability of the system.

Building upon the reactivity order of epoxides >> oxetane, a polymerization scheme involving one anhydride, epoxide, and oxetane was executed. Epoxide was first copolymerized with cyclic anhydride to form the first block, followed by copolymerization with oxetane/cyclic anhydride ROAC to form the second block. Furthermore, expanding the range of monomers, a quarterpolymerization involving two different cyclic anhydrides, epoxide, and oxetane was implemented for one-step synthesis of block polyester. This quarterpolymerization system offers a more flexible and adjustable main chain structure and monomer sequence, facilitating the design and synthesis of tailored block polyesters (Figure 1.2).

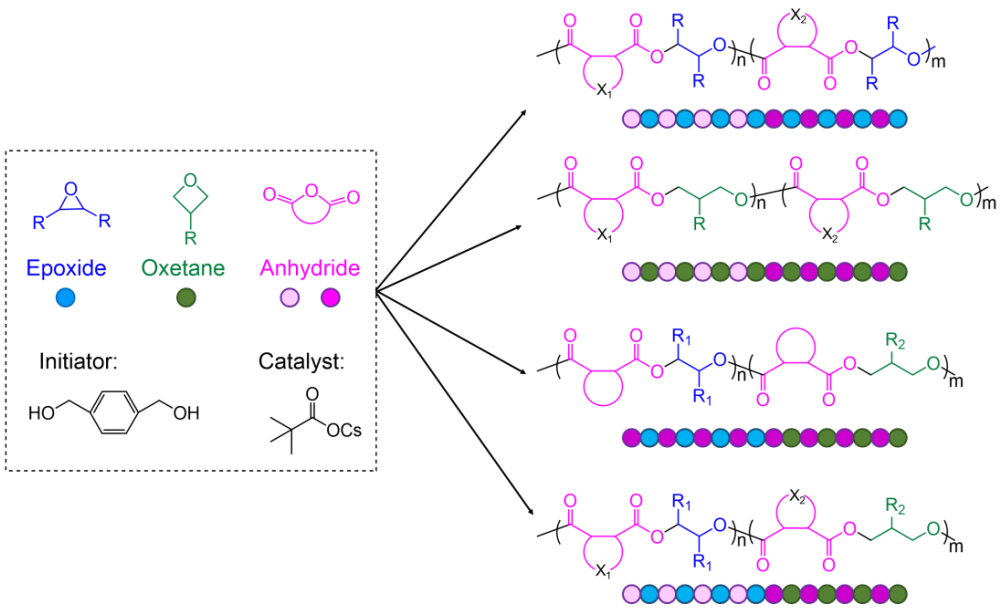

Figure 1.2. Illustration of the chapter 3 outline.

Chapter 4 introduces a self-switchable copolymerization system utilizing aziridine monomer, enabling the synthesis of various poly(amide ester)-based block copolymers with a phosphazene base catalyst (Figure 1.3). The physical properties of these copolymers were investigated. The terpolymerization of aziridine with two cyclic anhydrides was performed, leading to the synthesis of a range of poly(amide ester) block copolymers. Through a comprehensive analysis of the copolymerization behavior, the reactivity trend of the cyclic anhydrides was elucidated. This trend was found to be consistent with that observed in the terpolymerization involving two cyclic anhydrides and one epoxide.

In the conversational self-switchable copolymerization, the difference in chemical nature (or polarity) between the two blocks was not significant enough to induce phase separation. To achieve distinct chemical natures among different blocks in a one-step synthesized block copolymer, this research connected aziridine/cyclic anhydride ROAC with cyclic carbonate ROP under the same catalytic system, resulting in the synthesis of poly(amide ester)-*b*-polycarbonate. Additionally, aziridine/cyclic anhydride ROAC and epoxide/cyclic anhydride ROAC were connected in a quarterpolymerization system to one-step synthesize poly(amide ester)-*b*-polyester. The physical properties were investigated using differential scanning calorimetry and small-angle X-ray scattering measurements, confirming their phase separation behavior.

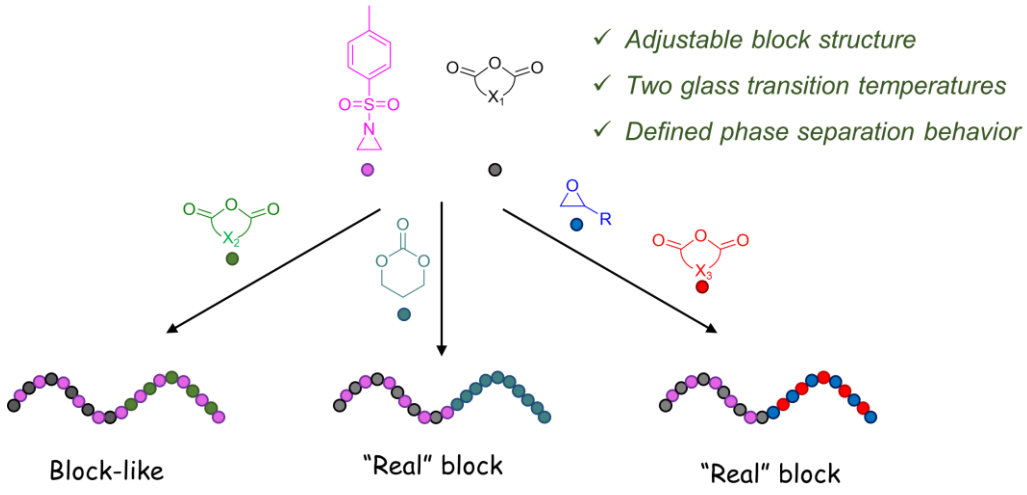

Figure 1.3. Illustration of the chapter 4 outline.

Chapter 5 explores a binary organocatalyzed copolymerization system capable of synthesizing poly(amide ester-ester) copolymers with various monomer sequences from the same monomer mixture (Figure 1.4). The copolymerization behavior of cyclohexene oxide (CHO)/phthalic anhydride (PA) ROAC and *N*-tosyl aziridine (TAz)/PA ROAC under a triethylborane (TEB)/*t*-Bu-P_1-cocatalyzed system was investigated. Interestingly, an opposite effect of TEB on these two ROACs was observed. Building upon this observation, a TEB//*t*-Bu-P_1-cocatalyzed terpolymerization system was devised. By varying the catalyst ratio, poly(TAz-*alt*-PA)-*co*-poly(CHO-*alt*-PA) copolymers with controllable monomer sequences were synthesized. To deepen the understanding of the monomer selectivity mechanism, energy calculations based on density functional theory were conducted. These calculations facilitated the design of other monomer sequence-controlled copolymerization systems, offering insights into the underlying mechanisms governing monomer selectivity in copolymerization reactions.

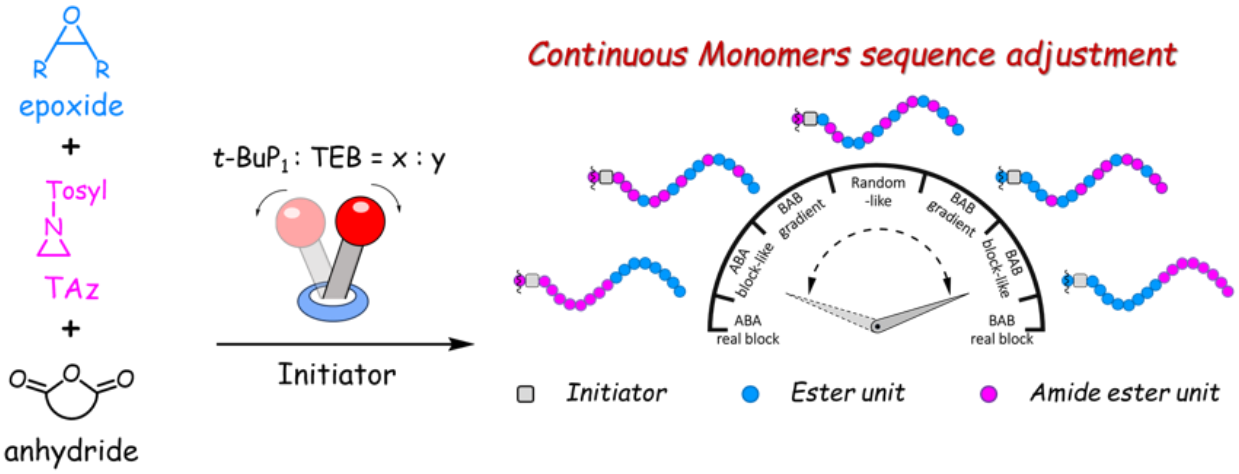

Figure 1.4. Illustration of the chapter 5 outline.

Chapter 6 summarizes the sequence controllable copolymerization systems established in this research as the overall conclusions of this thesis.

1.5 References

1. Velis C A, Cook E. Mismanagement of plastic waste through open burning with emphasis on the global south: a systematic review of risks to occupational and public health. *Environ. Sci. Technol.* **2021**, *55*, 7186-7207.

2. Savoca M S, McInturf A G, Hazen E L. Plastic ingestion by marine fish is widespread and increasing. *Glob. Change Biol*. **2021**, *27*, 2188–2199.

3. Auta H S, Emenike C U, Fauziah S H. Distribution and importance of microplastics in the marine environment: a review of the sources, fate, effects, and potential solutions. *Environ. Int.* **2017**, *102*, 165–176.

4. Agenda, Industry. The new plastics economy rethinking the future of plastics. *The World Economic Forum: Geneva.* **2016**

5. Gironi F, Piemonte V. Bioplastics and petroleum-based plastics: strengths and weaknesses. *Energy. Source. Part A* **2011**, *33*, 1949–1959.

6. Ellis, L. D., Rorrer, N. A., Sullivan, K. P., Otto, M., McGeehan, J. E., Román-Leshkov, Román-Leshkov Y., Wierckx N., Beckham, G. T. Chemical and biological catalysis for plastics recycling and upcycling. *Nature Catalysis* **2021***, 4*, 539–556.

7. Vert M. Aliphatic polyesters: great degradable polymers that cannot do everything. *Biomacromolecules* **2005**, *6*, 538–546.

8. Yao K, Tang C. Controlled polymerization of next-generation renewable monomers and beyond. *Macromolecules* **2013**, *46*,1689–1712.

9. Kobayashi H, Fukuoka A. Synthesis and utilisation of sugar compounds derived from lignocellulosic biomass. Green Chem. **2013**, *15*, 1740–1763.

10. Gross R A, Kalra B. Biodegradable polymers for the environment. *Science* **2002**, *297*, 803–807.

11. Rieger, B., Künkel, A., Coates, G. W., Reichardt, R., Dinjus, E., Zevaco, T. A. (Eds.). Synthetic

biodegradable polymers. *Springer Science & Business Media*. **2012**

12. Meng, C., Zhao, J., Yin, Y., Luo, J., Zhao, L., Jiang, W., Feng, J. Preparation and Characterization of PLA Film/3D Printing Composite Scaffold for Tissue Engineering Application. *Fiber. Polym.* **2020**, *21*, 709–716.

13. Abd Elwakil, M. M., Gao, T., Isono, T., Sato, Y., Elewa, Y. H., Satoh, T., Harashima, H. Engineered ε-decalactone lipomers bypass the liver to selectively in vivo deliver mRNA to the lungs without targeting ligands. *Mater. Horizons* **2021**, *8*, 2251–2259.

14. Bodell, B. D., Taylor, A. C., Patel, P. J. Thoracic endovascular aortic repair: review of current devices and treatments options. tech. *Vasc. Interv. Radiol.*, **2018,** *21*, 137–145.

15. Seitz, J. M., Durisin, M., Goldman, J., Drelich, J. W. Recent advances in biodegradable metals for medical sutures: a critical review. Adv. healthcare mater., **2015**, *4*, 1915–1936.

16. Odian, G. Principles of Polymerization, J*ohn Wiley & Sons: Hoboken.* **2004**,

17. Zhang, X., Fevre, M., Jones, G. O., Waymouth, R. M. Catalysis as an enabling science for sustainable polymers. *Chem. Rev.,* **2018**, *118*, 839–885.

18. uillaume, S. M., Kirillov, E., Sarazin, Y., Carpentier, J. F.Beyond Stereoselectivity, Switchable Catalysis: Some of the Last Frontier Challenges in Ring-Opening Polymerization of Cyclic Esters. *Chem. Eur.* **2015**, *21*, 7988−8003.

19. Dechy Cabaret, O., Martin Vaca, B., Bourissou, D. Controlled ring-opening polymerization of lactide and glycolide. *Chem. Rev.* **2004**, *104*, 6147−6176.

20. Monfette, S., Fogg, D. E. Equilibrium ring-closing metathesis. *Chem. Rev*., **2009**, *109*, 3783–3816.

21. Tardy, A., Nicolas, J., Gigmes, D., Lefay, C., Guillaneuf, Y. Radical ring-opening polymerization: Scope, limitations, and application to (bio) degradable materials. *Chem. Rev*., **2017**, *117*, 1319–1406.

22. Chutayothin, P., Ishida, H. Cationic ring-opening polymerization of 1, 3-benzoxazines: mechanistic study

using model compounds. *Macromolecules* **2010**, *43*, 4562–4572.

23. Jedliński, Z., Wałach, W., Kurcok, P., Adamus, G., Polymerization of lactones, 12. Polymerization of L-dilactide and L, D-dilactide in the presence of potassium methoxide. *Macromol. Chem. Phys.* **1991**, *192*, 2051–2057.

24. Quirk, R. P., Zhuo, Q., Jang, S. H., Lee, Y., Lizarraga, G. Principles of Anionic Polymerization: An introduction. *ACS Symp. Ser.* **1998**, *696*, 2−27.

25. Sarazin Y., Carpentier J. F. Discrete cationic complexes for ring-opening polymerization catalysis of cyclic esters and epoxides. *Chem. Rev.*, **2015**, *115*, 3564–3614.

26. Dijkstra P. J., Du H., Feijen J. Single site catalysts for stereoselective ring-opening polymerization of lactides. *Polym. Chem.*, **2011,** *2*, 520–527.

27. Kamber, N. E., Jeong, W., Waymouth, R. M., Pratt, R. C., Lohmeijer, B. G., Hedrick, J. L. Organocatalytic ring-opening polymerization. *Chem. Rev.*, **2007,** *107*, 5813–5840.

28. Makiguchi K, Satoh T, Kakuchi T. Diphenyl phosphate as an efficient cationic organocatalyst for controlled/living ring-opening polymerization of δ-valerolactone and ε-caprolactone. *Macromolecules,* **2011**, *44*, 1999–2005.

29. Kang, T., Banquy, X., Heo, J., Lim, C., Lynd, N. A., Lundberg, P., Oh, D. X., Lee, H. K., Hong, Y. K., Hwang, D. S., Waite, J. H., Israelachvili, J. N., Hawker, C. J. Mussel-inspired anchoring of polymer loops that provide superior surface lubrication and antifouling properties. *ACS Nano* **2016,** *10*, 930−937

30. Paderes, M. C., James, C., Jamieson, S. A., Mai, A. H., Limon, J. H., Dolatkhani, M., Fernandez-Prieto, S., De Borggraeve, W. M., Fratini, E. Tuning the Properties of Polyether Alkyl Urea Derivatives as Rheology Modifiers in Cosmetic Solvents. *ACS Appl. Polym. Mater.* **2020**, *2*, 2902–2909.

31. Obermeier, B., Wurm, F., Mangold, C., Frey, H. Multifunctional Poly(Ethylene Glycol)s. *Angew. Chemie Int. Ed.* **2011,** *50*, 7988–7997.

32. Kim, M., Park, J., Lee, K. M., Shin, E., Park, S., Lee, J., Lim, C., Kwak, S. K., Lee, D. W., Kim, B.-S.

Peptidomimetic Wet-Adhesive PEGtides with Synergistic and Multimodal Hydrogen Bonding. *J. Am. Chem. Soc.* **2022,** *144*, 6261–6269.

33. Son, I., Lee, Y., Baek, J., Park, M., Han, D., Min, S. K., Lee, D., Kim, B. S. PH-Responsive Amphiphilic Polyether Micelles with Superior Stability for Smart Drug Delivery. *Biomacromolecules* **2021,** *22*, 2043–2056.

34. Hill, F. B., Young, C. A., Nelson, J. A., Arnold, R. G. Glycol, P. Urethane Rubber from a Polyether Glycol Properties of Raw Polymer and Vulcanizates-Properties of Raw Polymer and Vulcanizates. *Industrial & Engineering Chemistry* **1956,** *48*, 927–929.

35. Johnson, G. H., Mancl, L. A., Schwedhelm, E. R., Verhoef, D. R., Lepe, X. Clinical Trial Investigating Success Rates for Polyether and Vinyl Polysiloxane Impressions Made with Full-Arch and Dual-Arch Plastic Trays. *J. Prosthet. Dent.* **2010,** *103*, 13–22.

36. Herzberger, J., Niederer, K., Pohlit, H., Seiwert, J., Worm, M., Wurm, F. R., Frey, H. Polymerization of Ethylene Oxide, Propylene Oxide, and Other Alkylene Oxides: Synthesis, Novel Polymer Architectures, and Bioconjugation. *Chem. Rev.* **2016**. *116*, 2170−2243.

37. Stolarzewicz, A., Neugebauer, D., Grobelny, Z. Influence of the Crown Ether Concentration and the Addition of Tert-butyl Alcohol on Anionic Polymerization of (Butoxymethyl)Oxirane Initiated by Potassium Tert-butoxide. *Macromol. Chem. Phys.* **1995,** *196*, 1295–1300.

38. Billouard, C., Desbois, P., Deffieux, A. “Controlled” High-Speed Anionic Polymerization of Propylene Oxide Initiated by Alkali Metal Alkoxide/Trialkylaluminum Systems. *Macromolecules* **2004,** *37*, 4038–4043.

39. Takuya I. Synthesis of functional and architectural polyethers via the anionic ring-opening polymerization of epoxide monomers using a phosphazene base catalyst, *Polym. J.*, **2021,** *53*, 753–764.

40. Overberger, C. G., Weise, J. K. Anionic ring-opening polymerization of thiolactones. *J. Am. Chem. Soc.* **1968,** *90*, 3533-3537.

41. Vo, C. D., Kilcher, G., Tirelli, N. Polymers and sulfur: what are organic polysulfides good for? Preparative strategies and biological applications. *Macromol. Rapid Commun.* **2009,** *30*, 299–315.

42. Mbarushimana, P. C., Liang, Q., Allred, J. M., Rupar, P. A. Polymerizations of nitrophenylsulfonyl-activated aziridines. *Macromolecules.* **2018,** *51,* 977−983.

43. Inoue, S., Koinuma, H., Tsuruta, T. Copolymerization of carbon dioxide and epoxide. *J. Polym. Sci. Lett.* **1969,** *7*, 287-292.

44. Aida, T., Inoue, S. Catalytic reaction on both sides of a metalloporphyrin plane. Alternating copolymerization of phthalic anhydride and epoxypropane with an aluminum porphyrin-quaternary salt system. *J. Am. Chem. Soc.* **1985,** *107*, 1358-1364.

45. Diment, W. T., Lindeboom, W., Fiorentini, F., Deacy, A. C., Williams, C. K. Synergic heterodinuclear catalysts for the ring-opening copolymerization (ROCOP) of epoxides, carbon dioxide, and anhydrides. *Acc. Chem. Res*. **2022,** *55,* 1997−2010.

46. Longo, J. M., Sanford, M. J., Coates, G. W. Ring-opening copolymerization of epoxides and cyclic anhydrides with discrete metal complexes: structure–property relationships. *Chem. Rev.* **2016,** *116,* 15167−15197.

47. Shellard, E. J., Diment, W. T., Resendiz-Lara, D. A., Fiorentini, F., Gregory, G. L., Williams, C. K. Al (III)/K (I) Heterodinuclear Polymerization Catalysts Showing Fast Rates and High Selectivity for Polyester Polyols. *ACS Catal,* **2024,** *14,* 1363–1374.

48. Lidston, C. A., Severson, S. M., Abel, B. A., Coates, G. W. Multifunctional catalysts for ring-opening copolymerizations. *ACS Catal.* **2022,** *12,* 11037–11070.

49. Kember, M. R., Knight, P. D., Reung, P. T., Williams, C. K. Highly active dizinc catalyst for the copolymerization of carbon dioxide and cyclohexene oxide at one atmosphere pressure. *Angew. Chem. Int. Ed.* **2009,** *48,* 931–933.

50. Longo, J. M., Sanford, M. J., Coates, G. W. Ring-opening copolymerization of epoxides and cyclic

anhydrides with discrete metal complexes: structure–property relationships. *Chem. Rev.* **2016,** *116,* 15167−15197.

51. Lu, X. B., Ren, W. M., Wu, G. P. CO_2 copolymers from epoxides: catalyst activity, product selectivity, and stereochemistry control. *Acc. Chem. Res.* **2012,** *45,* 10, 1721–1735.

52. Li, H., Zhao, J., Zhang, G. Self-buffering organocatalysis tailoring alternating polyester. *ACS Macro Lett.* **2017,** *6*, 1094–1098.

53. Ji H., Wang B., Pan Li., Li Y., Lewis pairs for ring-opening alternating copolymerization of cyclic anhydrides and epoxides. *Green Chem.* **2018,** *20*, 641-648.

54. Zhang, D., Boopathi, S. K., Hadjichristidis, N., Gnanou, Y., Feng, X. Metal-Free Alternating Copolymerization of CO_2 with Epoxides: Fulfilling "Green" Synthesis and Activity. *J. Am. Chem. Soc.* **2016,** *138*, 11117–11120.

55. Luo, H., Zhou, Y., Li, Q., Zhang, B., Cao, X., Zhao, J., Zhang, G. Oxygenated boron species generated in situ by protonolysis enables precision synthesis of alternating polyesters. *Macromolecules* **2023**, *56,* 1907–1920.

56. Wang, J., Zhu, Y., Li, M., Wang, Y., Wang, X., Tao, Y. Tug-of-War between Two Distinct Catalytic Sites Enables Fast and Selective Ring-Opening Copolymerizations. *Angew. Chem*. **2022**, *134*, e202208525.

57. Yang, G. W., Zhang, Y. Y., Xie, R., Wu, G. P. Scalable bifunctional organoboron catalysts for copolymerization of CO_2 and epoxides with unprecedented efficiency. *J. Am. Chem. Soc.* **2020,** *142,* 12245−12255.

58. Jung, Y.; Park, M. S.; Lee, J. W.; Kim, Y. H.; Kim, S.-H.; Kim, S.H. Cartilage Regeneration with Highly-Elastic Three-Dimensional Scaffolds Prepared from Biodegradable Poly(*L*-Lactide-*Co*-*ε*-Capro-lactone). *Biomaterials* **2008,** *29*, 4630−4636.

59. Jehanno, C.; Mezzasalma, L.; Sardon, H.; Ruipérez, F.; Coulembier, O.; Taton, D. Benzoic Acid as an Efficient Organocatalyst for the Statistical Ring-Opening Copolymerization of ε-Caprolactone and *L*-

Lactide: A Computational Investigation. *Macromolecules* **2019,** *52*, 9238–9247,

60. Cabral, H., Miyata, K., Osada, K., Kataoka, K. Block copolymer micelles in nanomedicine applications. *Chem. Rev.* **2018,** *118,* 6844–6892.

61. Hsu, L. C., Isono, T., Lin, Y. C., Kobayashi, S., Chiang, Y. C., Jiang, D. H., Hung, C. C., Ercan, E., Yang, W. C., Hsieh, H. C., Tajima, K., Satoh, T., Chen, W. C. Stretchable OFET Memories: Tuning the Morphology and the Charge-Trapping Ability of Conjugated Block Copolymers Through Soft Segment Branching. ACS Appl. Mater. Interfaces. **2021,** *13*, 2932–2943.

62. Oh, J. Y., Rondeau-Gagné, S., Chiu, Y. C., Chortos, A., Lissel, F., Wang, G. N., Schroeder, B. C., Kurosawa, T., Lopez, J., Katsumata, T., Xu, J., Zhu, C., Gu, X., Bae, W. G., Kim, Y., Jin, L., Chung, J. W., Tok, J. B. H., Bao, Z. Intrinsically Stretchable and Healable Semiconducting Polymer for Organic Transistors. *Nature.* **2016,** *539,* 411–415.

63. Chiu, Y. C., Otsuka, I., Halila, S., Borsali, R., Chen, W. C. High-Performance Nonvolatile Transistor Memories of Pentacence Using the Green Electrets of Sugar-Based Block Copolymers and Their Supramolecules. *Adv. Funct. Mater.* **2014,** *24,* 4240–4249.

64. Hsueh, H. Y., Yao, C., Ho, R. M. Well-ordered nanohybrids and nanoporous materials from gyroid block copolymer templates. *Chem Soc Rev,* **2015,** *44,* 1974–2018.

65. Bates, C. M., Maher, M. J., Janes, D. W., Ellison, C. J., Willson, C. G. Block copolymer lithography. Macromolecules, 2014, 47, 2–12.

66. Aluthge, D. C., Xu, C., Othman, N., Noroozi, N., Hatzikiriakos, S. G., Mehrkhodavandi, P. PLA–PHB–PLA triblock copolymers: synthesis by sequential addition and investigation of mechanical and rheological properties. *Macromolecules* **2013**, *46*, 3965-3974.

67. Isono, T., Nakahira, S., Hsieh, H. C., Katsuhara, S., Mamiya, H., Yamamoto, T., Chen, W., Borsali R., Tajima, K., Satoh, T. Carbohydrates as hard segments for sustainable elastomers: carbohydrates direct the self-assembly and mechanical properties of fully bio-based block copolymers. *Macromolecules* **2020,** *53*,

5408-5417.

68. Levit, M., Zashikhina, N., Dobrodumov, A., Kashina, A., Tarasenko, I., Panarin, E., Fiorucci, S., Korzhikova-Vlakh, E., Tennikova, T. Synthesis and characterization of well-defined poly(2-deoxy-2-methacrylamido-*d*-glucose) and its biopotential block copolymers via RAFT and ROP polymerization. *Eur. Polym. J.* **2018**, *105*, 26–37.

69. Pfeifer, S., Lutz, J.-F. A Facile Procedure for Controlling Monomer Sequence Distribution in Radical Chain Polymerizations. *J. Am. Chem. Soc.* **2007**, *129* 9542−9543.

70. Moatsou, D., Hansell, C. F., O'Reilly, R. K. Precision polymers: a kinetic approach for functional poly(norbornenes). *Chem. Sci.* **2014,** *5*, 2246−2250.

71. Gleede, T., Rieger, E., Blankenburg, J., Klein, K., Wurm, F. R. Fast Access to Amphiphilic Multiblock Architectures by the Anionic Copolymerization of Aziridines and Ethylene Oxide. *J. Am. Chem. Soc.* **2018,** *140*, 13407−13412.

72. Zhao, Y., Jung, J., Nozaki, K. One-Pot Synthesis of PolyethyleneBased Block Copolymers via a Dual Polymerization Pathway. *J. Am. Chem. Soc.* **2021,** *143*, 18832−18837.

73. Jeske, R. C., Rowley, J. M., Coates, G. W. Pre-rate-Determining Selectivity in the Terpolymerization of Epoxides, Cyclic Anhydrides, and CO_2: A One-Step Route to Diblock Copolymers. *Angew. Chem. Int. Ed. Engl.* **2008,** *120,* 6130–6133.

74. Romain, D. C., Williams, C. K. Chemoselective Polymerization Control: From Mixed-Monomer Feedstock to Copolymers. *Angew. Chem. Int. Ed. Engl.* **2014,** *53,* 1607–1610.

75. Stößer, T., Mulryan, D., Williams, C. K. Switch Catalysis To Deliver Multi-Block Polyesters from Mixtures of Propene Oxide, Lactide, and Phthalic Anhydride. *Angew. Chem. Int. Ed. Engl.* **2018,** *57,* 16893–16897.

76. Chen, T. T. D., Zhu, Y., Williams, C. K. Pentablock Copolymer from Tetracomponent Monomer Mixture Using a Switchable Dizinc Catalyst. *Macromolecules.* **2018,** *51,* 5346–5351.

77. Plajer, A. J., Williams, C. K. Heterotrimetallic Carbon Dioxide Copolymerization and Switchable Catalysts: Sodium Is the Key to High Activity and Unusual Selectivity. *Angew. Chem. Int. Ed. Engl.* **2021,** *60,* 13372–13379.

78. Xia, X. C.; Ryota, S.; Takojima, K.; Jiang, D. H.; Isono, T.; Satoh, T. Smart access to sequentially and architecturally controlled block polymers via a simple catalytic polymerization system. *ACS Catal.* **2021,** 11, 5999– 6009.

79. Ji, H. Y., Wang, B., Pan, L., Li, Y. S. One-Step Access to Sequence-Controlled Block Copolymers by Self-Switchable Organocatalytic Multicomponent Polymerization. *Angew. Chem. Int. Ed. Engl.* **2018**, *57*, 16888–16892.

Chapter 2

Alkali metal carboxylate-catalyzed ring-opening polymerization for the synthesis of polyesters, polyethers, and their block copolymers

2.1 Introduction

The thermodynamic driving force for cyclic ester ring-opening polymerization (ROP) processes arises from the relief of the monomer ring strain. This phenomenon obviates the necessity for high energy input, allowing polymerization to proceed under milder conditions compared to conventional polycondensation methods. Additionally, the living/controlled nature of cyclic ester ROP facilitates precise control over molecular weight and prevents the formation of small molecule byproducts.[1] Nevertheless, the limited availability of polymerizable cyclic esters constrains the structural diversity of polyesters synthesized via ROP. Ring-opening alternating copolymerization (ROAC) of cyclic anhydrides and epoxides presents an alternative approach for the synthesis of structure-defined polyesters, garnering considerable attention. By employing two distinct monomer types, the ROAC method vastly expands the spectrum of potential polymer structures, with over 400 conceivable polymer configurations stemming from a diverse array of epoxides and cyclic anhydrides, implying a corresponding diversity in polyester properties.[2]

In the realm of epoxide/cyclic anhydride ROAC, organometallic catalytic systems have enjoyed widespread adoption owing to their high efficiency. However, challenges such as the presence of toxic metal residues and costly synthetic procedures have hindered their widespread application.[2–4] Consequently, the quest for metal-free catalysts for ROAC has emerged as a prominent research focus. While organic Lewis pairs and phosphazene base derivatives have exhibited high catalytic activity and excellent control over molecular weight, their application in industrial polyester production is impeded by high costs or complex synthetic protocols.[5–7]

Satoh's group recently introduced an efficient and straightforward alkali metal carboxylate (AMC) catalyst for the ROP of cyclic esters and cyclic carbonates.[8–10] In the AMC-catalyzed cyclic ester ROP system, polymerization is facilitated by the interaction of the AMC carboxylate group on the alcohol initiator as well as the countercations on the monomer carbonyl group. Based on this catalytic behavior, it is plausible to envision the potential of AMC in promoting the ROAC of epoxides and cyclic anhydrides. Notably, the basicity of AMC can be tailored by varying carboxylate moieties and countercations, enabling controlled/living polymerization. The low cost, ease of handling, and low toxicity of AMC makes it a

promising candidate for industrial polyester production. To establish a simple and easy-handing ROAC system that enables the synthesis of well-defined polyester with a diverse main chain structure. In this chapter, the author investigates AMC-catalyzed epoxide/cyclic anhydride ROAC. Furthermore, to explore the diversity of polyester structures, the behavior of oxetane/cyclic anhydride ROAC is also examined. Additionally, following confirmation of AMC's catalytic activity in epoxide ROP, a one-pot/two-step method is employed to synthesize polyether-*b*-polyester. The successful synthesis of a series of polyesters and its copolymers implied AMC's potential for large-scale polyester production.

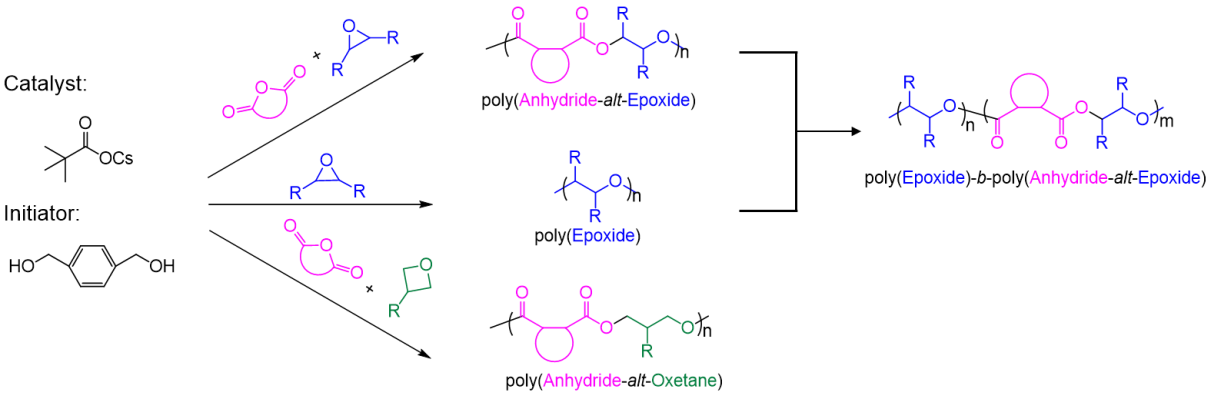

Scheme 2.1. Cesium pivalate-catalyzed epoxide/cyclic anhydride ROAC, oxetane/cyclic anhydride ROAC, epoxide ROP, and one-pot/two step synthesis of polyether-*b*-polyester.

2.2 Experimental Section

2.2.1 Materials

2-Ethylhexyl glycidyl ether (EHGE; >98.0%, Tokyo Kasei Kogyo Co., Ltd. (TCI)), allyl glycidyl ether (AGE; >99.0%, TCI), benzyl glycidyl ether (BGE; >97.0%, TCI), 1,2-epoxycyclohexane (CHO; >98.0%, TCI) 1,2-Butylene oxide (BO; >99.0%, TCI), ethyl glycidyl ether (EGE; >98.0%, TCI), propylene oxide (PO; >99.0%, TCI), 3-((allyloxy)methyl)-3-ethyloxetane (AMEO; >98.0%, TCI), Trimethylene oxide (TO; >99.0%, TCI), and 3-ethyl-3-(phenoxymethyl)oxetane (EPO; >97.0%, TCI), and 3-phenyl-1-propanol (PPA; >98%, TCI) were distilled over CaH_2 under reduced pressure and stored under nitrogen atmosphere. 5-

norbornene-endo-2,3-dicarboxylic anhydride (NA; > 99%, Sigma−Aldrich), diglycolic anhydride (DGA; >98.0%, TCI), succinic anhydride (SA; >95.0%, TCI), diphenic Anhydride (DA; >98.0%, TCI), and phthalic anhydride (PA; >98.0%, TCI) were recrystallized and then purified by the way of sublimation before use. Cesium pivalate (>97.0%, TCI) was dried by heating at 100°C under high vacuum for at least 72 h prior to use. 1,4-benzenedimethanol (BDM; >99.0%, TCI) was used as received. All manipulations were performed using a standard Schlenk technique or in an argon-filled UNILAB Plus glovebox unless otherwise mentioned.

2.2.2 Instruments

The polymerization was carried out in a gas purification system (molecular sieves and copper catalyst) equipped MBRAUN stainless steel glovebox in a dry argon atmosphere (H_2O, O_2 <0.1 ppm). The moisture and oxygen contents in the glovebox were monitored with MB-MO-SE 1 and MB-OX-SE 1, respectively.

The size exclusion chromatography (SEC) is utilizing a Shodex GPC-101 system equipped with a Shodex K-G guard column and a set of two Shodex K-805L columns (linear, 8 mm × 300 mm; bead size, 5 μm; exclusion limit, 4×10^6). The measurement was performed in THF (flow rate, 1.0 mL min^{-1}) at 40 °C. Polystyrene (PS) standard samples were used for calibration.

^{1}H NMR spectra were recorded at 25 °C on a JEOL JNMA400II instrument (400 MHz) using chloroform-d_1 as the solvent and chemical shifts were referenced to an internal standard. DOSY NMR analyses were carried out at 30 ºC on a JEOL JNMA400II instrument (400 MHz) with at least 15 gradient increments using the ledbpgp2s sequence.

DSC7000X differential scanning calorimeter (DSC) measurement was conducted under a nitrogen atmosphere. The obtained triblock copolymer was heated from 20°C to 200 °C at a rate of 10 °C/min, staying at 200 °C for 5 min to erase thermal history. Then the sample was cooled to -100 °C at a rate of 10 °C/min,

keeping at -100 °C for 5 minutes. Finally, the sample was heated to 200 °C at a rate of 10 °C/min.

2.2.3 Synthesis detail

Copolymerization of diglycolic anhydride (DGA)/ethyl glycidyl ether (EGE) catalyzed by cesium pivalate.

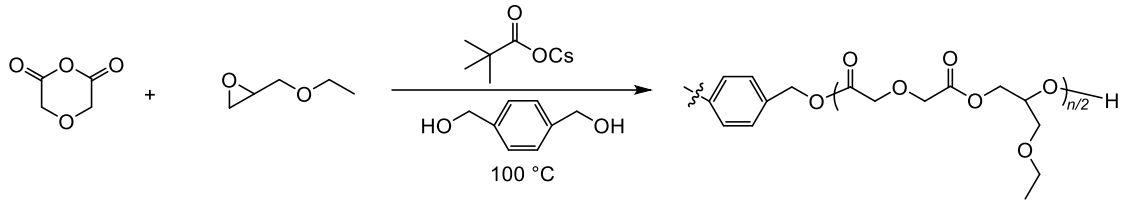

Scheme 2.2. Copolymerization of DGA and EGE catalyzed by cesium pivalate.

In an argon-filled glovebox, cesium pivalate (9.3 mg, 0.02 mmol), BDM (5.5mg, 0.04 mmol), DGA (116.1 mg, 1.0 mmol), and EGE (306.0 mg, 3.0 mmol) were placed in an oven-dried reaction vessel with a magnetic stir. The reaction mixture was stirred at 100 °C under an argon atmosphere in an oil bath. During polymerization, a crude aliquot was time-regularly obtained from the system by a syringe in an argon flow and monitored by ^{1}H NMR spectroscopy to determine monomer conversion. After the defined time, the polymerization was terminated by diluting the reaction mixture with dichloromethane (CH_2Cl_2). The reaction mixture was purified by reprecipitation from a CH_2Cl_2 solution into cold methanol. The purified polymers were dried under vacuum at room temperature for the next analysis.

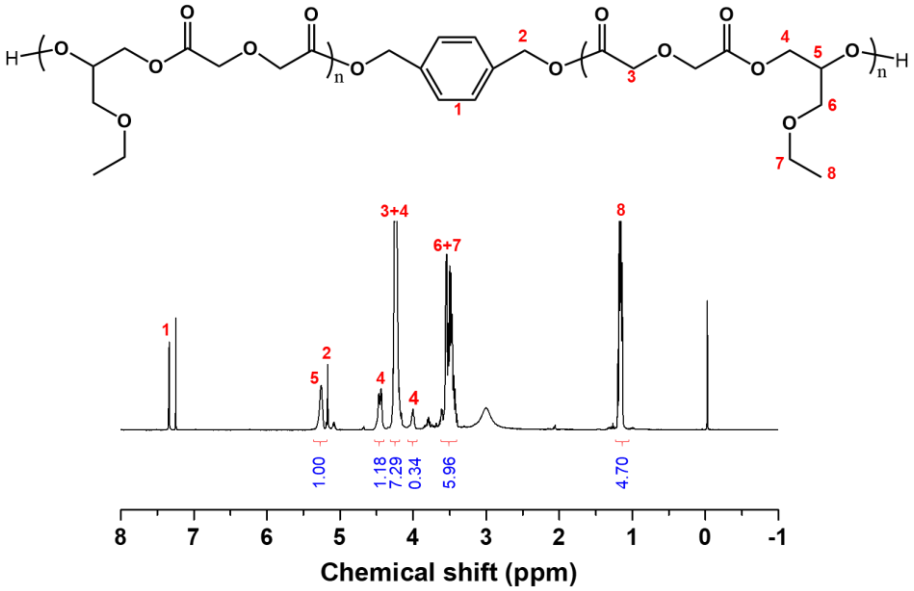

Figure 2.1. ^{1}H NMR ($CDCl_3$) spectrum of the resultant copolymer synthesized from DGA and EGE (entry 1 in Table 2.1).

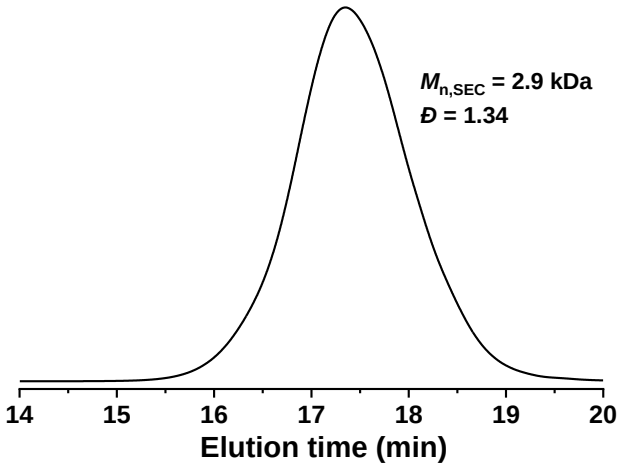

Figure 2.2. SEC (THF) trace of the resultant copolymer synthesized from DGA and EGE (entry 1 in Table 2.1).

Copolymerization of succinic anhydride (SA)/EGE catalyzed by cesium pivalate.

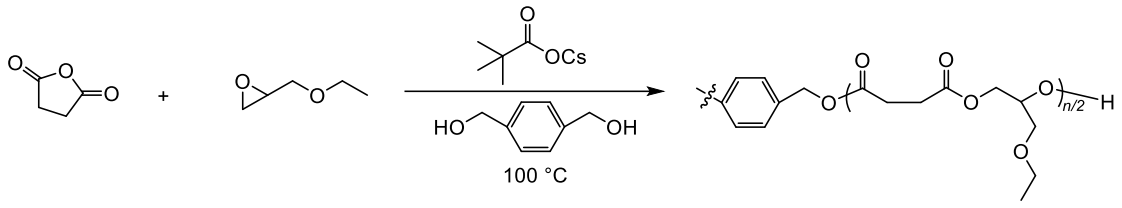

Scheme 2.3. Copolymerization of SA and EGE catalyzed by cesium pivalate.

In an argon-filled glovebox, cesium pivalate (9.3 mg, 0.02 mmol), BDM (5.5mg, 0.04 mmol), SA (100.1 mg, 1.0 mmol), and EGE (306.0 mg, 3.0 mmol) were placed in an oven-dried reaction vessel with a magnetic stir. The reaction mixture was stirred at 100 °C under an argon atmosphere in an oil bath. During polymerization, a crude aliquot was time-regularly obtained from the system by a syringe in an argon flow and monitored by ^{1}H NMR spectroscopy to determine monomer conversion. After the defined time, the polymerization was terminated by diluting the reaction mixture with dichloromethane (CH_2Cl_2). The reaction mixture was purified by reprecipitation from a CH_2Cl_2 solution into cold methanol. The purified polymers were dried under vacuum at room temperature for the next analysis.

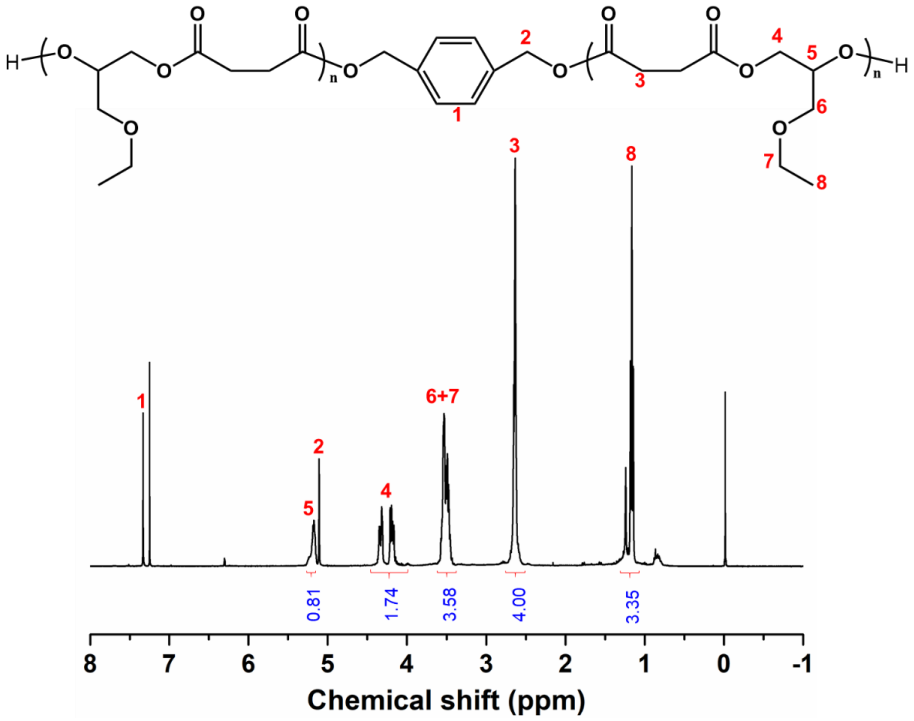

Figure 2.3. ^{1}H NMR ($CDCl_3$) spectrum of the resultant copolymer synthesized from SA and EGE (entry 2 in Table 2.1).

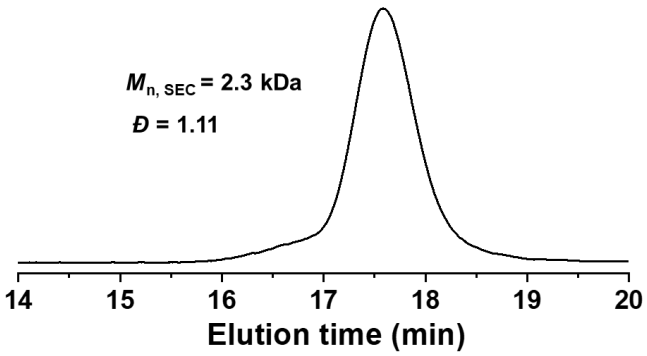

Figure 2.4. SEC (THF) trace of the resultant copolymer synthesized from SA and EGE (entry 2 in Table 2.1).

Copolymerization of 5-norbornene-endo-2,3-dicarboxylic anhydride (NA)/EGE catalyzed by cesium pivalate.

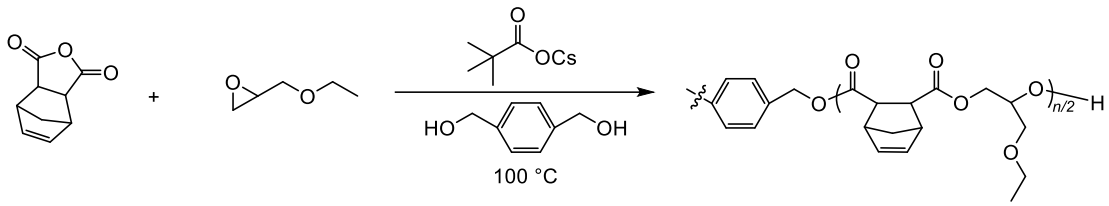

Scheme 2.4. Copolymerization of NA and EGE catalyzed by cesium pivalate.

In an argon-filled glovebox, cesium pivalate (9.3 mg, 0.02 mmol), BDM (5.5mg, 0.04 mmol), NA (162.2 mg, 1.0 mmol), and EGE (306.0 mg, 3.0 mmol) were placed in an oven-dried reaction vessel with a magnetic stir. The reaction mixture was stirred at 100 °C under an argon atmosphere in an oil bath. During polymerization, a crude aliquot was time-regularly obtained from the system by a syringe in an argon flow and monitored by ^{1}H NMR spectroscopy to determine monomer conversion. After the defined time, the polymerization was terminated by diluting the reaction mixture with dichloromethane (CH_2Cl_2). The reaction mixture was purified by reprecipitation from a CH_2Cl_2 solution into cold methanol. The purified polymers were dried under vacuum at room temperature for the next analysis.

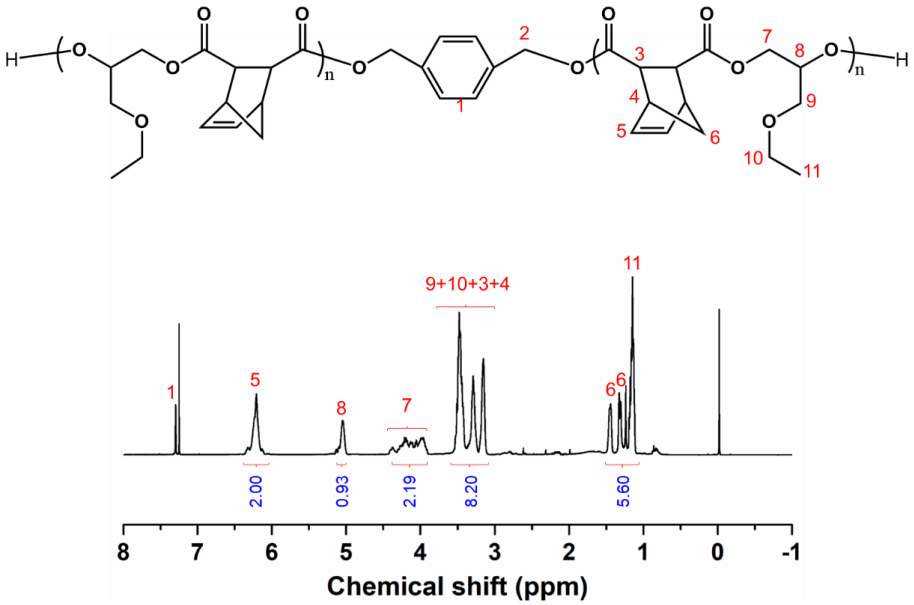

Figure 2.5. ^{1}H NMR ($CDCl_3$) spectrum of the resultant copolymer synthesized from NA and EGE (entry 3 in Table 2.1).

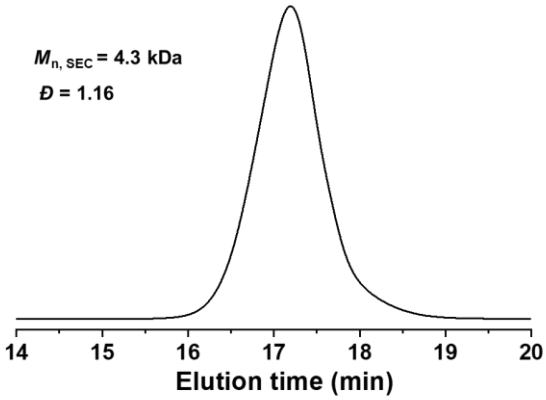

Figure 2.6. SEC (THF) trace of the resultant copolymer synthesized from NA and EGE (entry 3 in Table 2.1).

Copolymerization of phthalic anhydride (PA)/EGE catalyzed by cesium pivalate.

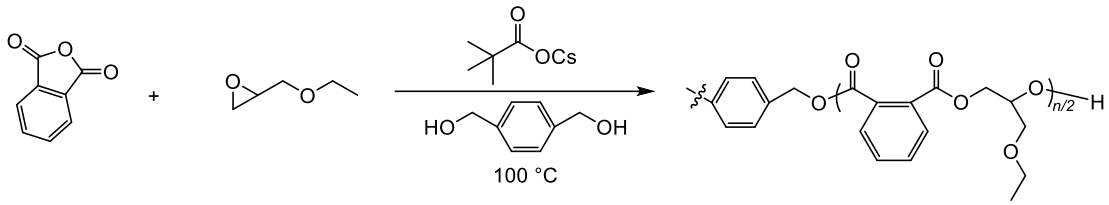

Scheme 2.5. Copolymerization of PA and EGE catalyzed by cesium pivalate.

In an argon-filled glovebox, cesium pivalate (9.3 mg, 0.02 mmol), BDM (5.5mg, 0.04 mmol), PA (148.1 mg, 1.0 mmol), and EGE (306.0 mg, 3.0 mmol) were placed in an oven-dried reaction vessel with a magnetic stir. The reaction mixture was stirred at 100 °C under an argon atmosphere in an oil bath. During polymerization, a crude aliquot was time-regularly obtained from the system by a syringe in an argon flow and monitored by ^{1}H NMR spectroscopy to determine monomer conversion. After the defined time, the polymerization was terminated by diluting the reaction mixture with dichloromethane (CH_2Cl_2). The reaction mixture was purified by reprecipitation from a CH_2Cl_2 solution into cold methanol. The purified polymers were dried under vacuum at room temperature for the next analysis.

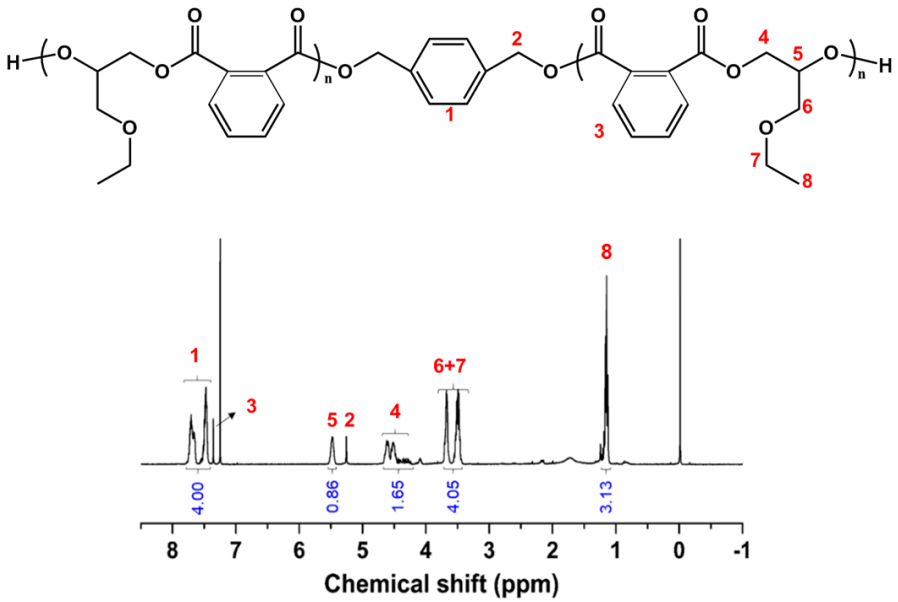

Figure 2.7. ^{1}H NMR spectrum of the resultant copolymer synthesized from PA and EGE (entry 4 in Table 2.1).

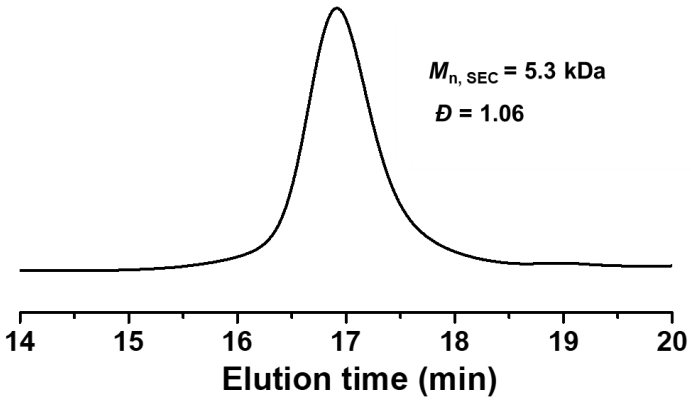

Figure 2.8. SEC (THF) trace of the resultant copolymer synthesized from PA and EGE (entry 4 in Table 2.1).

Copolymerization of PA/3-ethyl-3-(phenoxymethyl)oxetane (EPO) catalyzed by cesium pivalate.

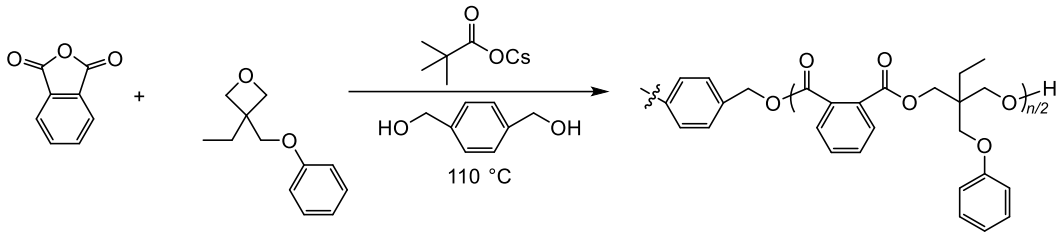

Scheme 2.6. Copolymerization of PA and EPO catalyzed by cesium pivalate.

In an argon-filled glovebox, cesium pivalate (18.6 mg, 0.04 mmol), BDM (5.5mg, 0.04 mmol), PA (88.9 mg, 0.6 mmol), and EPO (692.1 mg, 3.6 mmol) were placed in an oven-dried reaction vessel with a magnetic stir. The reaction mixture was stirred at 130 °C under an argon atmosphere in an oil bath. During polymerization, a crude aliquot was time-regularly obtained from the system by a syringe in an argon flow and monitored by ^{1}H NMR spectroscopy and SEC to determine monomer conversion and molar mass. After the defined time, the polymerization was terminated by diluting the reaction mixture with CH_2Cl_2. The reaction mixture was purified by reprecipitation from a CH_2Cl_2 solution into cold methanol. The purified polymers were dried under vacuum at room temperature for the next analysis.

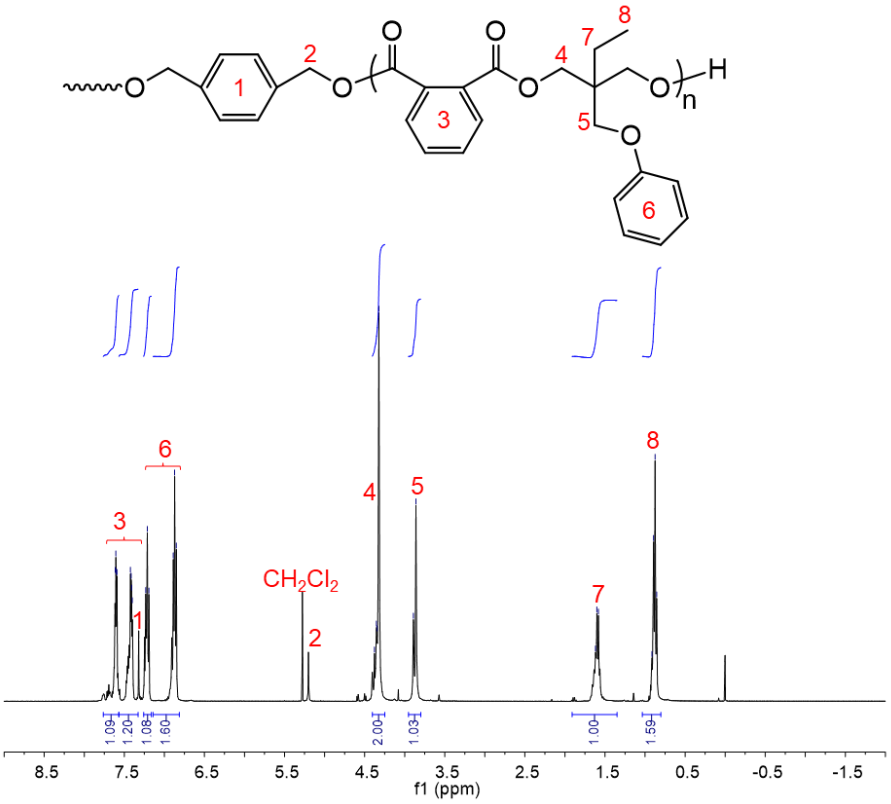

Figure 2.9. ^{1}H NMR ($CDCl_3$) spectrum of the resultant polymer synthesized from PA and EPO (entry 2 in Table 2.2).

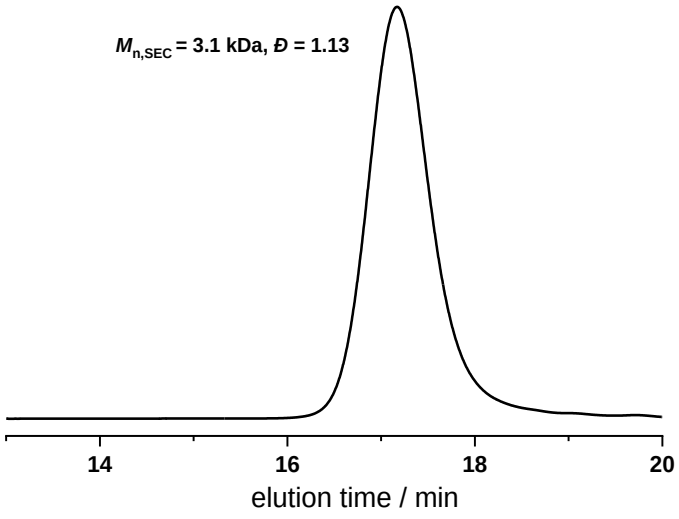

Figure 2.10. SEC (THF) trace of the resultant polymer synthesized from PA and EPO (entry 2 in Table 2.2).

Copolymerization of PA/3-((allyloxy)methyl)-3-ethyloxetane (AMEO) catalyzed by cesium pivalate.

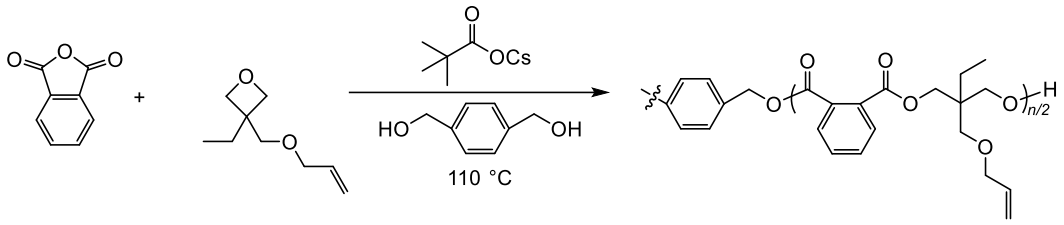

Scheme 2.7. Copolymerization of PA and AEMO catalyzed by cesium pivalate.

In an argon-filled glovebox, cesium pivalate (18.6 mg, 0.04 mmol), BDM (5.5mg, 0.04 mmol), PA (88.9 mg, 0.6 mmol), and AMEO (562.4 mg, 3.6 mmol) were placed in an oven-dried reaction vessel with a magnetic stir. The reaction mixture was stirred at 130 °C under an argon atmosphere in an oil bath. During polymerization, a crude aliquot was time-regularly obtained from the system by a syringe in an argon flow and monitored by ^{1}H NMR spectroscopy and SEC to determine monomer conversion and molar mass. After the defined time, the polymerization was terminated by diluting the reaction mixture with CH_2Cl_2. The reaction mixture was purified by reprecipitation from a CH_2Cl_2 solution into cold methanol. The purified polymers were dried under vacuum at room temperature for the next analysis.

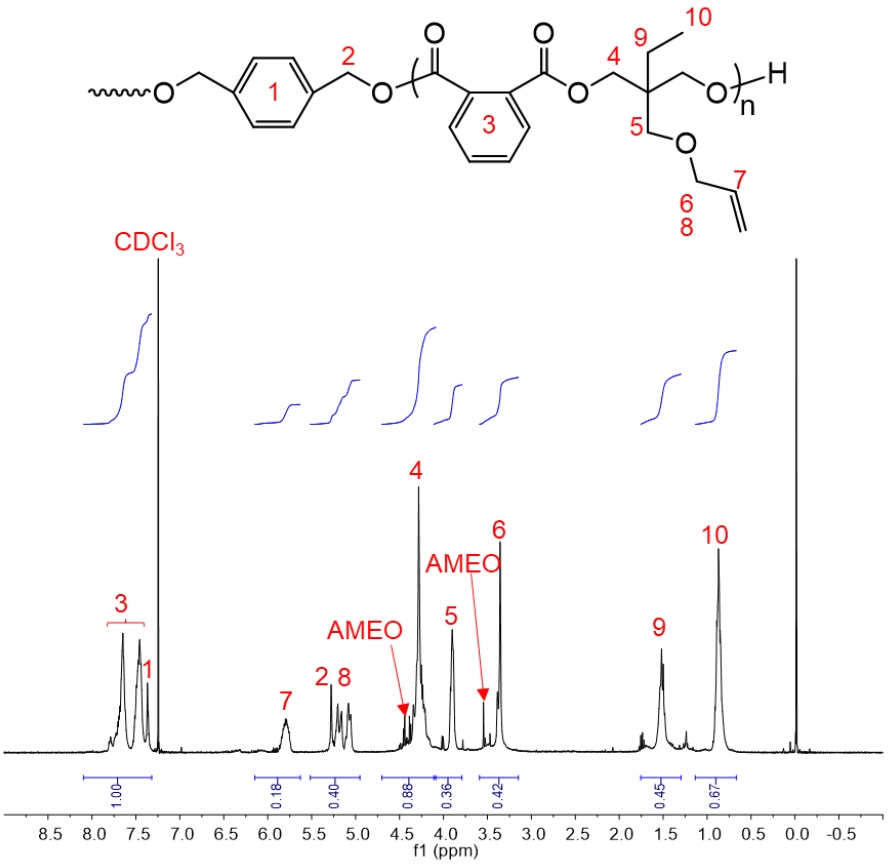

Figure 2.11. ^{1}H NMR ($CDCl_3$) spectrum of the resultant polymer synthesized from PA and AMEO (entry 5 in Table 2.2).

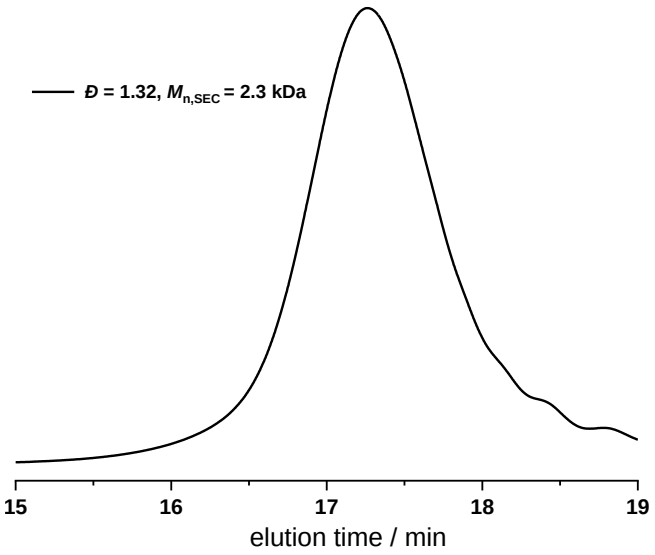

Figure 2.12. SEC (THF) trace of the resultant polymer synthesized from PA and AMEO (entry 5 in Table 2.2).

Copolymerization of PA/Trimethylene oxide (TO) catalyzed by cesium pivalate.

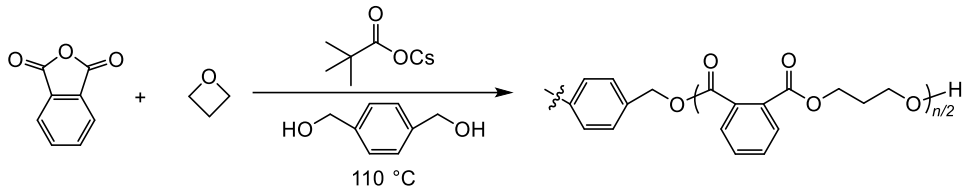

Scheme 2.8. Copolymerization of PA and TO catalyzed by cesium pivalate.

In an argon-filled glovebox, cesium pivalate (18.6 mg, 0.04 mmol), BDM (5.5mg, 0.04 mmol), PA (118.5 mg, 0.8 mmol), and TO (208 mg, 3.6 mmol) were placed in an oven-dried reaction vessel with a magnetic stir. The reaction mixture was stirred at 130 °C under an argon atmosphere in an oil bath. During polymerization, a crude aliquot was time-regularly obtained from the system by a syringe in an argon flow and monitored by ^{1}H NMR spectroscopy and SEC to determine monomer conversion and molar mass. After the defined time, the polymerization was terminated by diluting the reaction mixture with CH_2Cl_2. The reaction mixture was purified by reprecipitation from a CH_2Cl_2 solution into cold methanol. The purified polymers were dried under vacuum at room temperature for the next analysis.

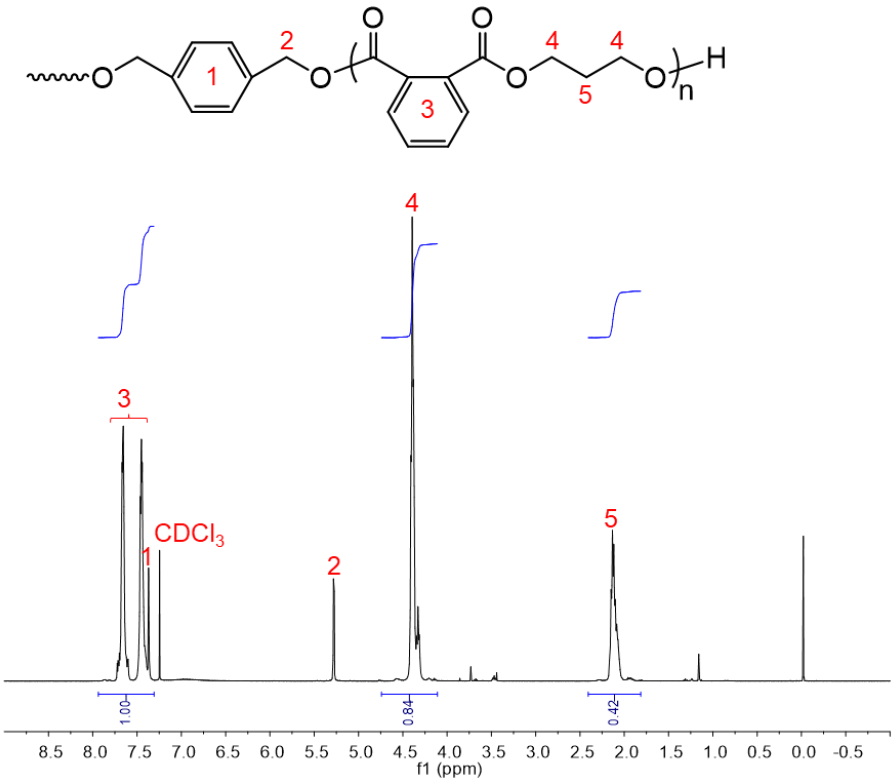

Figure 2.13. ^{1}H NMR ($CDCl_3$) spectrum of the resultant polymer synthesized from PA and TO (entry 6 in Table 2.2).

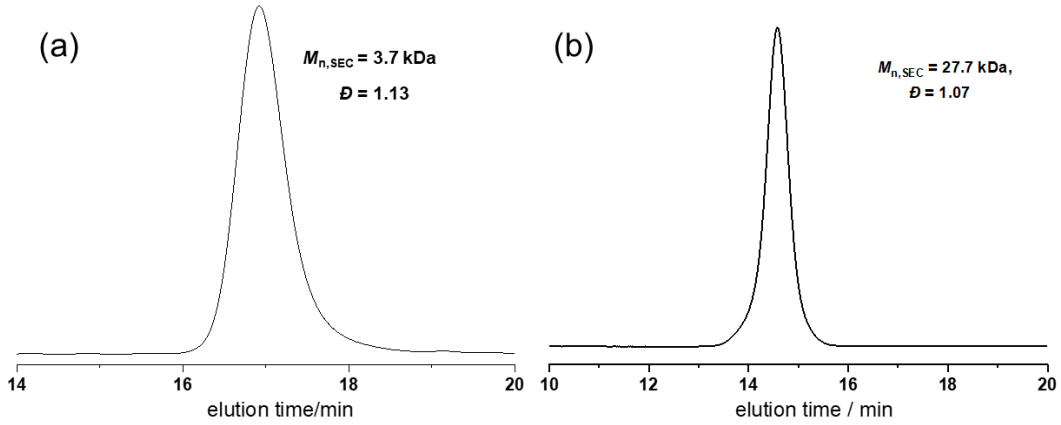

Figure 2.14. SEC (THF) trace of the resultant poly(PA-*alt*-TO) block copolymer: (a) $[PA]_0/[TO]_0/[BDM]_0/[t\text{-}BuCO_2Cs]_0$ = 20/90/1/1 (entry 6 in Table 2.2); (b) $[PA]_0/[TO]_0/[BDM]_0/[t\text{-}BuCO_2Cs]_0$ = 484/2178/1/1 (entry 7 in Table 2.2).

Copolymerization of diphenic anhydride (DA)/EPO catalyzed by cesium pivalate.

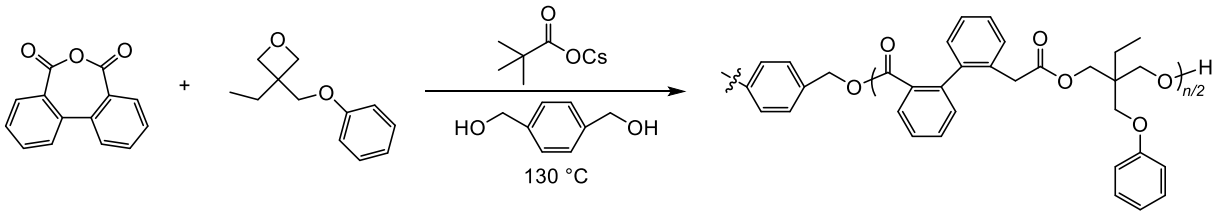

Scheme 2.9. Copolymerization of DA and EPO catalyzed by cesium pivalate.

In an argon-filled glovebox, cesium pivalate (18.6 mg, 0.04 mmol), BDM (5.5mg, 0.04 mmol), DA (134.5 mg, 0.6 mmol), and EPO (692.1 mg, 3.6 mmol) were placed in an oven-dried reaction vessel with a magnetic stir. The reaction mixture was stirred at 130 °C under an argon atmosphere in an oil bath. During polymerization, a crude aliquot was time-regularly obtained from the system by a syringe in an argon flow and monitored by ^{1}H NMR spectroscopy and SEC to determine monomer conversion and molar mass. After the defined time, the polymerization was terminated by diluting the reaction mixture with CH_2Cl_2. The reaction mixture was purified by reprecipitation from a CH_2Cl_2 solution into cold methanol. The purified polymers were dried under vacuum at room temperature for the next analysis.

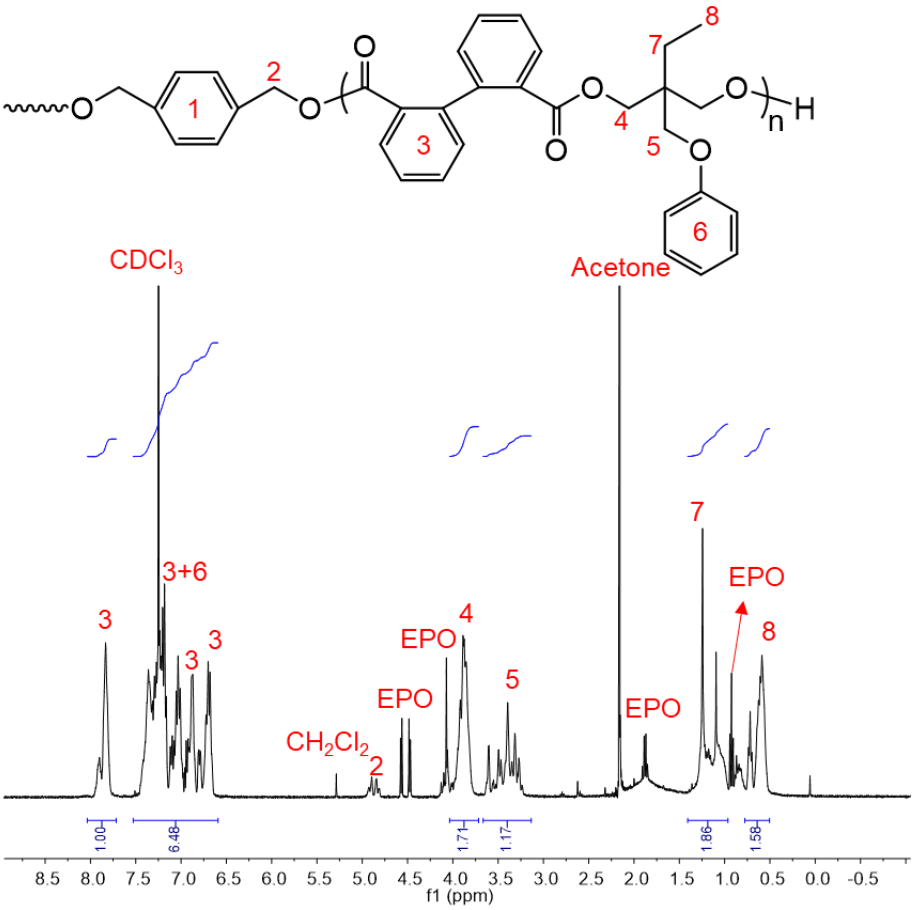

Figure 2.15. ^{1}H NMR ($CDCl_3$) spectrum of the resultant polymer synthesized from DA and EPO (entry 8 in Table 2.2).

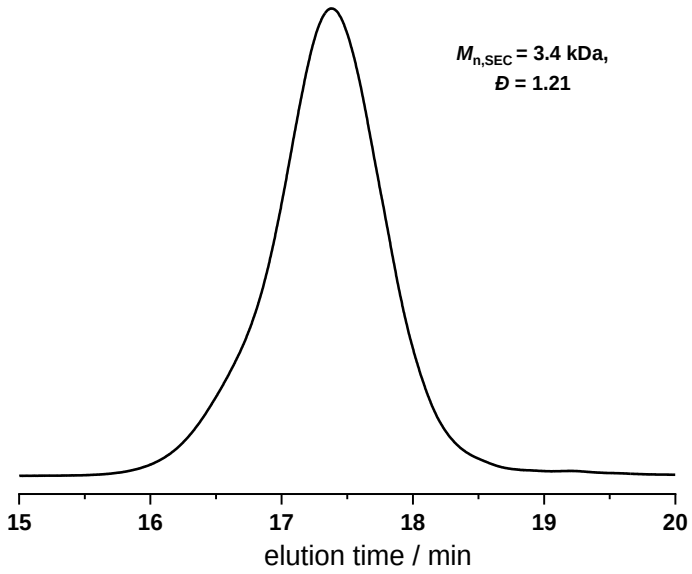

Figure 2.16. SEC (THF) trace of the resultant polymer synthesized from DA and EPO (entry 8 in Table 2.2).

Copolymerization of DGA/TO catalyzed by cesium pivalate.

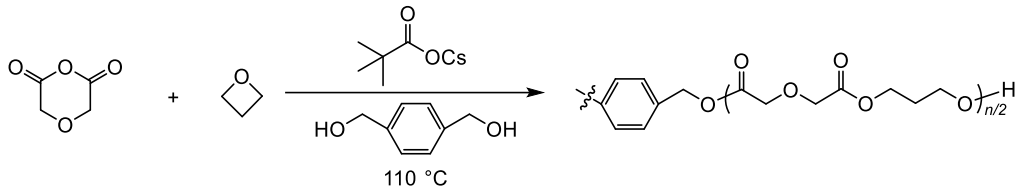

Scheme 2.10. Copolymerization of DGA and TO catalyzed by cesium pivalate.

In an argon-filled glovebox, cesium pivalate (18.6 mg, 0.04 mmol), BDM (5.5mg, 0.04 mmol), DGA (69.6 mg, 0.6 mmol), and TO (208 mg, 3.6 mmol) were placed in an oven-dried reaction vessel with a magnetic stir. The reaction mixture was stirred at 110 °C under an argon atmosphere in an oil bath. During polymerization, a crude aliquot was time-regularly obtained from the system by a syringe in an argon flow and monitored by ^{1}H NMR spectroscopy and SEC to determine monomer conversion and molar mass. After the defined time, the polymerization was terminated by diluting the reaction mixture with CH_2Cl_2. The reaction mixture was purified by reprecipitation from a CH_2Cl_2 solution into cold methanol. The purified polymers were dried under vacuum at room temperature for the next analysis.

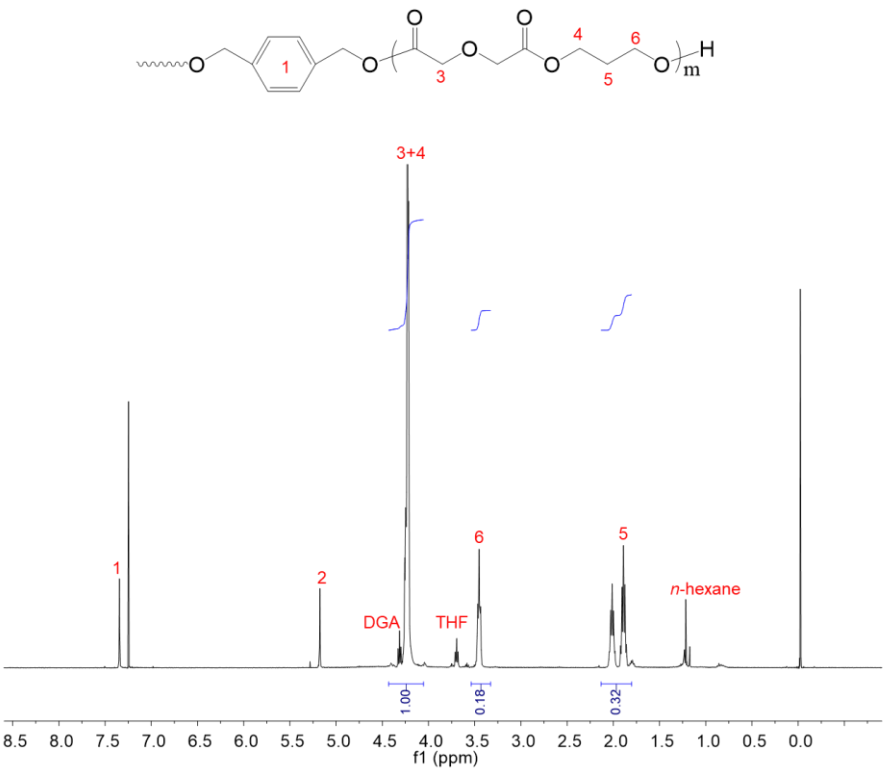

Figure 2.17. ^{1}H NMR ($CDCl_3$) spectrum of the resultant polymer synthesized from DGA and TO (entry 9 in Table 2.2).

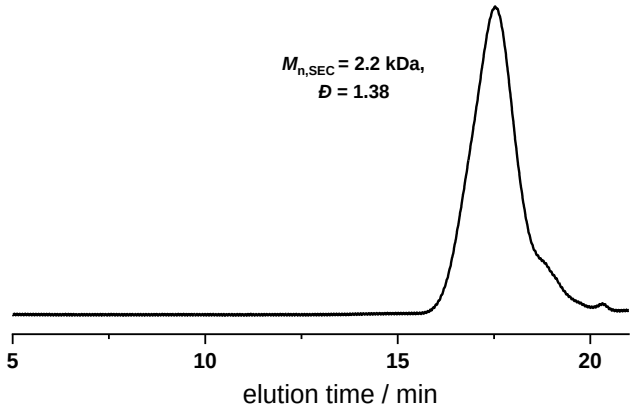

Figure 2.18. SEC (THF) trace of the resultant polymer synthesized from DGA and TO (entry 9 in Table 2.2).

Polymerization of 2-ethylhexyl glycidyl ether (EHGE) catalyzed by cesium pivalate.

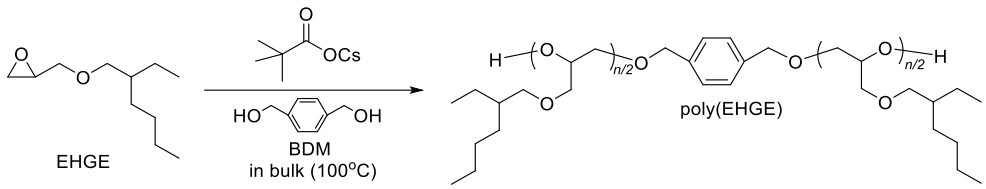

Scheme 2.11. Polymerization of EHGE catalyzed by cesium pivalate.

In an argon-filled glovebox, cesium pivalate (5.09 mg, 21.7 μmol), BDM (6.00 mg, 43.5 μmol), and EHGE (444 mg, 2.39 mmol) were placed in an oven-dried reaction vessel with a magnetic stir. The reaction mixture was stirred at 100 °C under an argon atmosphere in an oil bath. During polymerization, a crude aliquot was time-regularly obtained from the system by a syringe in an argon flow and monitored by ^{1}H NMR spectroscopy and SEC to determine monomer conversion and molar mass. After the defined time, the polymerization was terminated by diluting the reaction mixture with CH_2Cl_2. The reaction mixture was purified by reprecipitation from a CH_2Cl_2 solution into cold methanol. The purified polymers were dried under vacuum at room temperature for the next analysis.

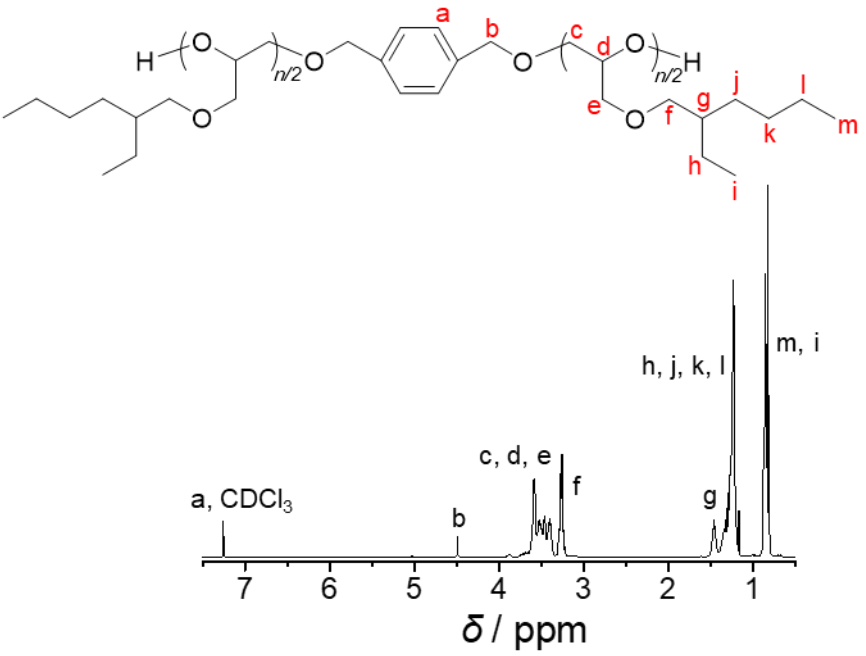

Figure 2.19. ^{1}H NMR ($CDCl_3$) spectrum of the resultant polymer synthesized from EHGE (entry 2 in Table 2.3).

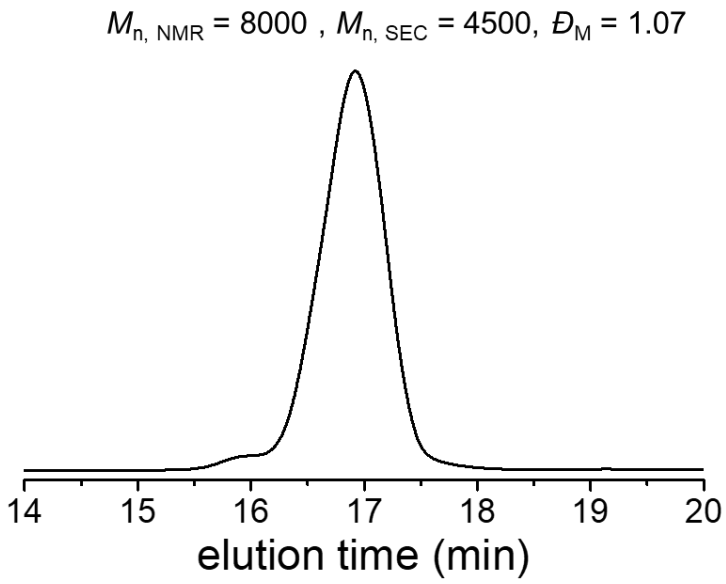

Figure 2.20. SEC (THF) trace of the resultant polymer synthesized from EHGE (entry 2 in Table 2.2).

Polymerization of ethyl glycidyl ether (EGE) catalyzed by cesium pivalate.

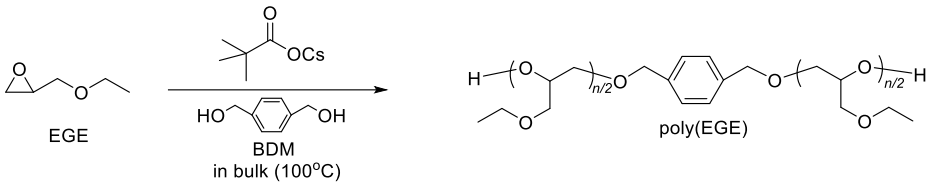

Scheme 2.12. Polymerization of EGE catalyzed by cesium pivalate.

In an argon-filled glovebox, ethyl glycidyl ether (EGE) (488 mg, 4.78 mmol), BDM (12.0 mg, 87.0 µmol), and cesium pivalate (10.2 mg, 43.5 µmol) were placed in an oven-dried reaction vessel with a magnetic stir. The reaction mixture was stirred at 100 °C under an argon atmosphere in an oil bath. During polymerization, a crude aliquot was time-regularly obtained from the system by a syringe in an argon flow and monitored by ^{1}H NMR spectroscopy and SEC to determine monomer conversion and molar mass. After the defined time, the polymerization was terminated by diluting the reaction mixture with CH_2Cl_2. The reaction mixture was purified by reprecipitation from a CH_2Cl_2 solution into cold methanol. The purified polymers were dried under vacuum at room temperature for the next analysis.

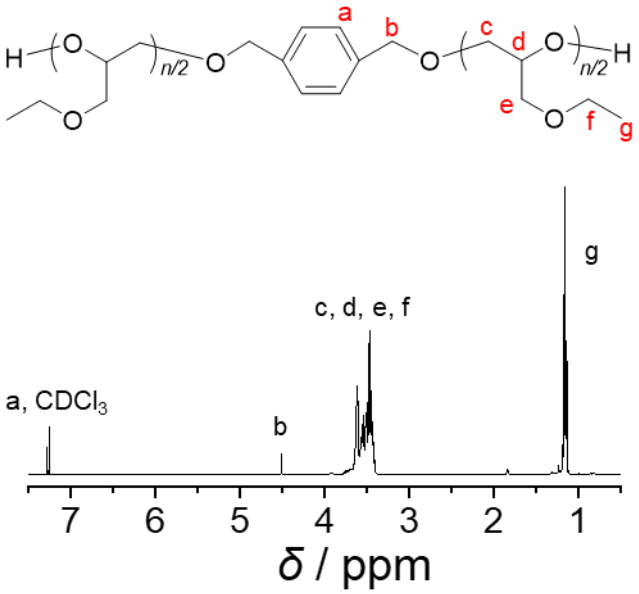

Figure 2.21. ^{1}H NMR spectrum of poly(EGE) (entry 1 in Table 2.4).

Polymerization of allyl glycidyl ether (AGE) catalyzed by cesium pivalate.

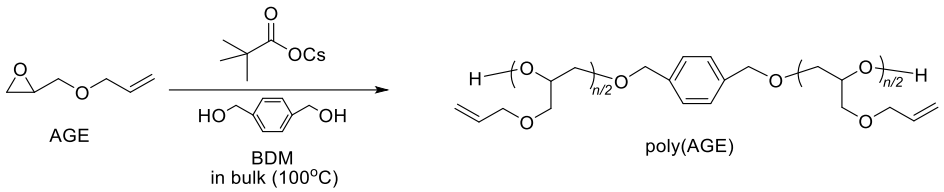

Scheme 2.13. Polymerization of AGE catalyzed by cesium pivalate.

In an argon-filled glovebox, allyl glycidyl ether (AGE) (454 mg, 3.99 mmol), BDM (10.0 mg, 72.5 µmol) and cesium pivalate (8.48 mg, 36.2 µmol) were placed in an oven-dried reaction vessel with a magnetic stir. The reaction mixture was stirred at 100 °C under an argon atmosphere in an oil bath. During polymerization, a crude aliquot was time-regularly obtained from the system by a syringe in an argon flow and monitored by ^{1}H NMR spectroscopy and SEC to determine monomer conversion and molar mass. After the defined time, the polymerization was terminated by diluting the reaction mixture with CH_2Cl_2. The reaction mixture was purified by reprecipitation from a CH_2Cl_2 solution into cold methanol. The purified polymers were dried under vacuum at room temperature for the next analysis.

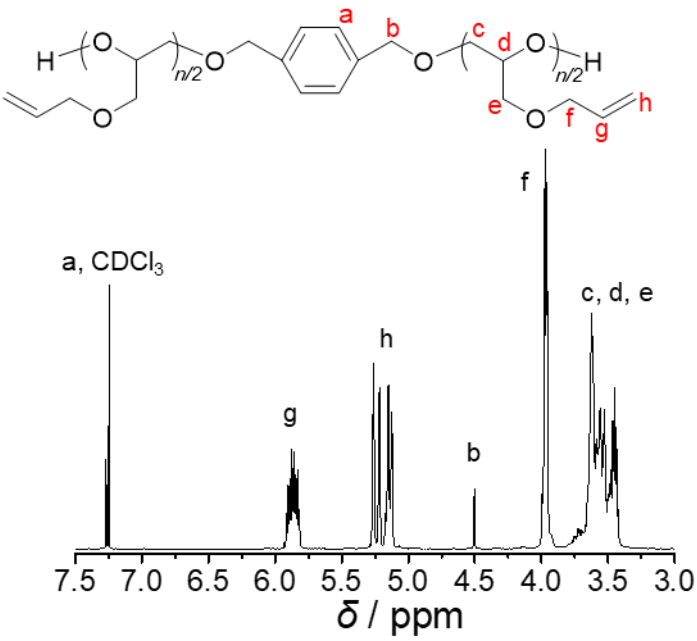

Figure 2.22. ^{1}H NMR spectrum of poly(AGE) (entry 2 in Table 2.4).

Polymerization of benzyl glycidyl ether (BGE) catalyzed by cesium pivalate.

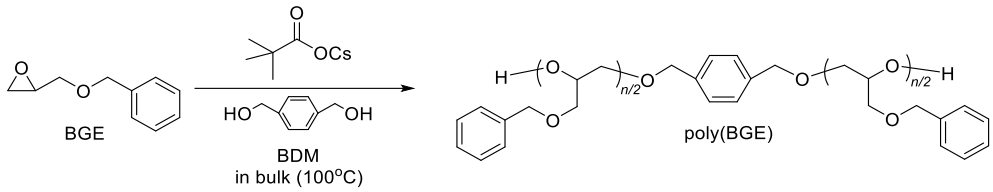

Scheme 2.14. Polymerization of BGE catalyzed by cesium pivalate.

In an argon-filled glovebox, benzyl glycidyl ether (BGE) (392 mg, 2.39 mmol), BDM (6.00 mg, 43.5 µmol) and cesium pivalate (5.09 mg, 21.7 µmol) were placed in an oven-dried reaction vessel with a magnetic stir. The reaction mixture was stirred at 100 °C under an argon atmosphere in an oil bath. During polymerization, a crude aliquot was time-regularly obtained from the system by a syringe in an argon flow and monitored by ^{1}H NMR spectroscopy and SEC to determine monomer conversion and molar mass. After the defined time, the polymerization was terminated by diluting the reaction mixture with CH_2Cl_2. The reaction mixture was purified by reprecipitation from a CH_2Cl_2 solution into cold methanol. The purified polymers were dried under vacuum at room temperature for the next analysis.

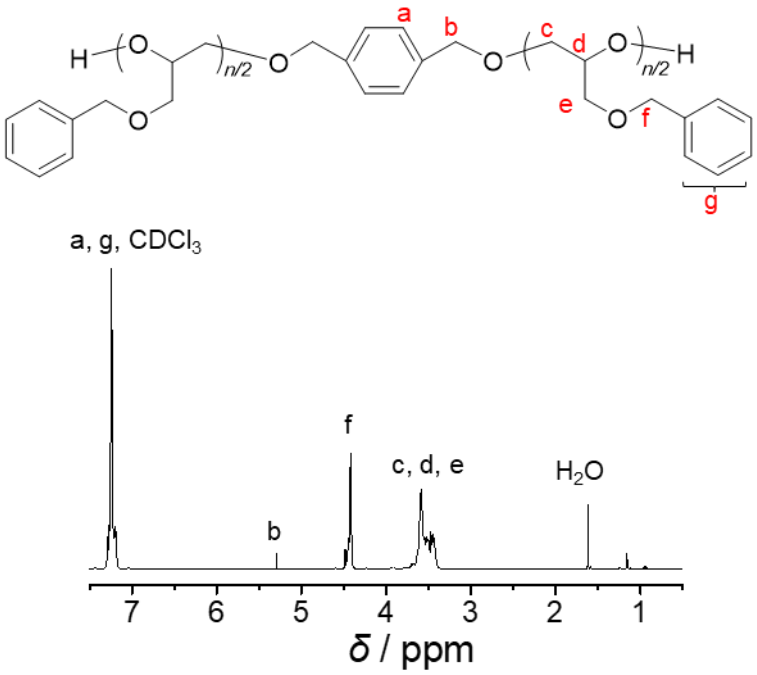

Figure 2.23. ^{1}H NMR spectrum of poly(BGE) (entry 3 in Table 2.4).

Polymerization of styrene oxide (SO) catalyzed by cesium pivalate.

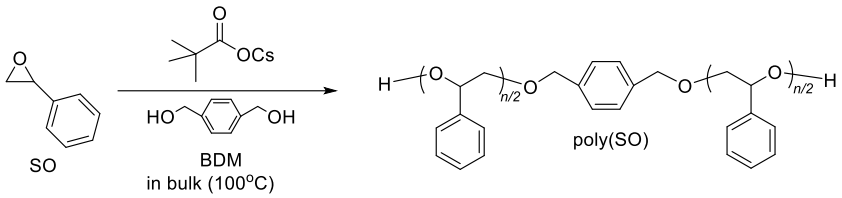

Scheme 2.15. Polymerization of SO catalyzed by cesium pivalate.

In an argon-filled glovebox, styrene oxide (SO) (287 mg, 2.39 mmol), BDM (6.00 mg, 43.5 µmol) and cesium pivalate (5.09 mg, 21.7 µmol) were placed in an oven-dried reaction vessel with a magnetic stir. The reaction mixture was stirred at 100 °C under an argon atmosphere in an oil bath. During polymerization, a crude aliquot was time-regularly obtained from the system by a syringe in an argon flow and monitored by ^{1}H NMR spectroscopy and SEC to determine monomer conversion and molar mass. After the defined time, the polymerization was terminated by diluting the reaction mixture with CH_2Cl_2. The reaction mixture was purified by reprecipitation from a CH_2Cl_2 solution into cold methanol. The purified polymers were dried under vacuum at room temperature for the next analysis.

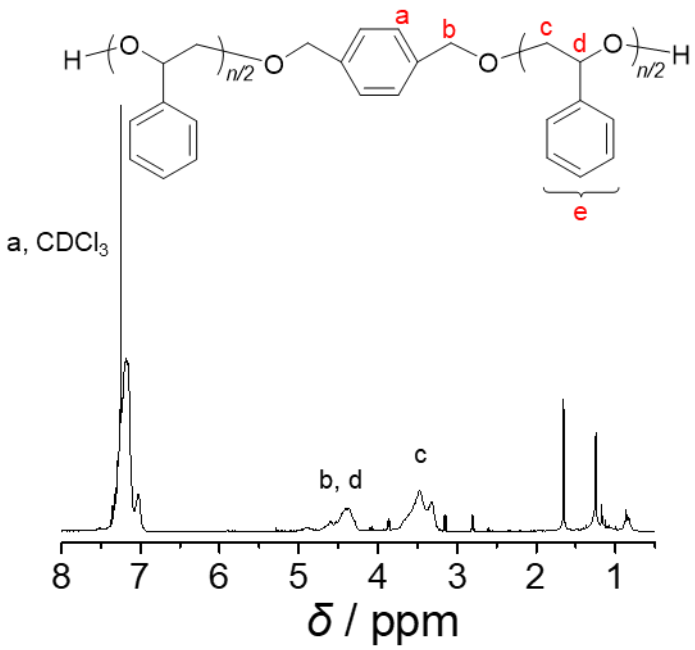

Figure 2.24. ^{1}H NMR spectrum of poly(SO) (entry 4 in Table 2.4).

Polymerization of 1,2-epoxyhexane (EH) catalyzed by cesium pivalate.

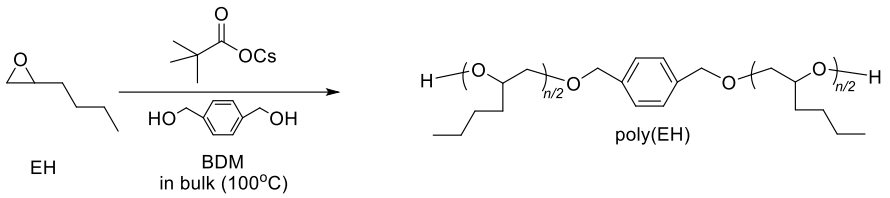

Scheme 2.16. Polymerization of EH catalyzed by cesium pivalate.

In an argon-filled glovebox, 1,2-epoxyhexane (EH) (399 mg, 3.99 mmol), BDM (10.0 mg, 72.5 µmol) and cesium pivalate (8.48 mg, 36.2 µmol) were placed in an oven-dried reaction vessel with a magnetic stir. The reaction mixture was stirred at 100 °C under an argon atmosphere in an oil bath. During polymerization, a crude aliquot was time-regularly obtained from the system by a syringe in an argon flow and monitored by ^{1}H NMR spectroscopy and SEC to determine monomer conversion and molar mass. After the defined time, the polymerization was terminated by diluting the reaction mixture with CH_2Cl_2. The reaction mixture was purified by reprecipitation from a CH_2Cl_2 solution into cold methanol. The purified polymers were dried under vacuum at room temperature for the next analysis.

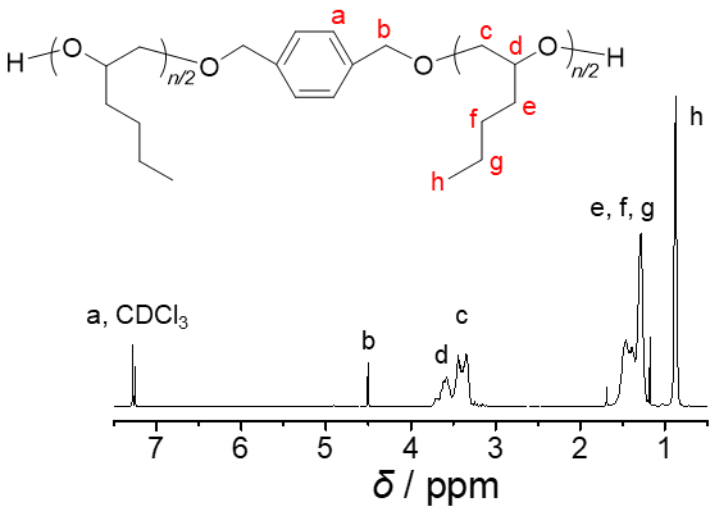

Figure 2.25. ^{1}H NMR spectrum of poly(EH) (entry 5 in Table 2.4).

Polymerization of 1,2-butylene oxide (BO) catalyzed by cesium pivalate.

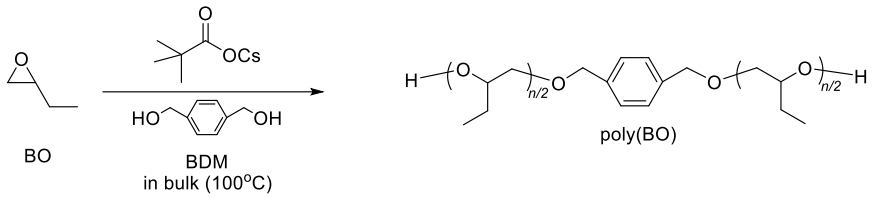

Scheme 2.17. Polymerization of BO catalyzed by cesium pivalate.

In an argon-filled glovebox, 1,2-butylene oxide (BO) (344 mg, 4.78 mmol), BDM (6.00 mg, 43.5 µmol) and cesium pivalate (5.09 mg, 21.7 µmol) were placed in an oven-dried reaction vessel with a magnetic stir. The reaction mixture was stirred at 100 °C under an argon atmosphere in an oil bath. During polymerization, a crude aliquot was time-regularly obtained from the system by a syringe in an argon flow and monitored by ^{1}H NMR spectroscopy and SEC to determine monomer conversion and molar mass. After the defined time, the polymerization was terminated by diluting the reaction mixture with CH_2Cl_2. The reaction mixture was purified by reprecipitation from a CH_2Cl_2 solution into cold methanol. The purified polymers were dried under vacuum at room temperature for the next analysis.

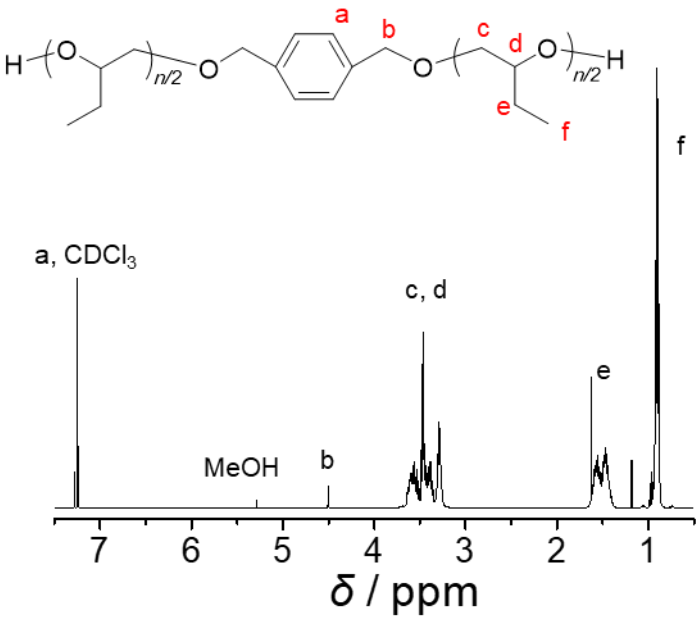

Figure 2.26. ^{1}H NMR spectrum of poly(BO) (entry 6 in Table 2.4).

Polymerization of 1,2-epoxycyclohexane (CHO) catalyzed by cesium pivalate.

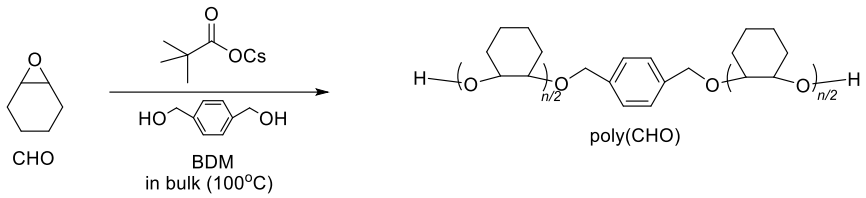

Scheme 2.18. Polymerization of CHO catalyzed by cesium pivalate.

In an argon-filled glovebox, cyclohexene oxide (CHO) (234 mg, 2.39 mmol), BDM (6.00 mg, 43.5 μmol) and cesium pivalate (5.09 mg, 21.7 μmol) were mixed in a test tube. The reaction performed at 100 °C while stirring, and no polymer formation was found even after 48 h.

Polymerization of epichlorohydrin (ECH) catalyzed by cesium pivalate.

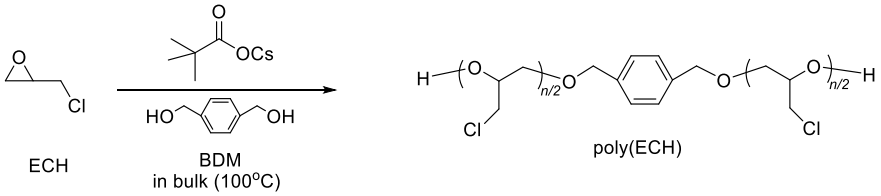

Scheme 2.19. Polymerization of ECH catalyzed by cesium pivalate.

In an argon-filled glovebox, epichlorohydrin (ECH) (220 mg, 2.39 mmol), BDM (6.00 mg, 43.5 μmol) and cesium pivalate (5.09 mg, 21.7 μmol) were mixed in a test tube. The reaction was performed at 100 °C while stirring, and no polymer formation was found even after 48 h.

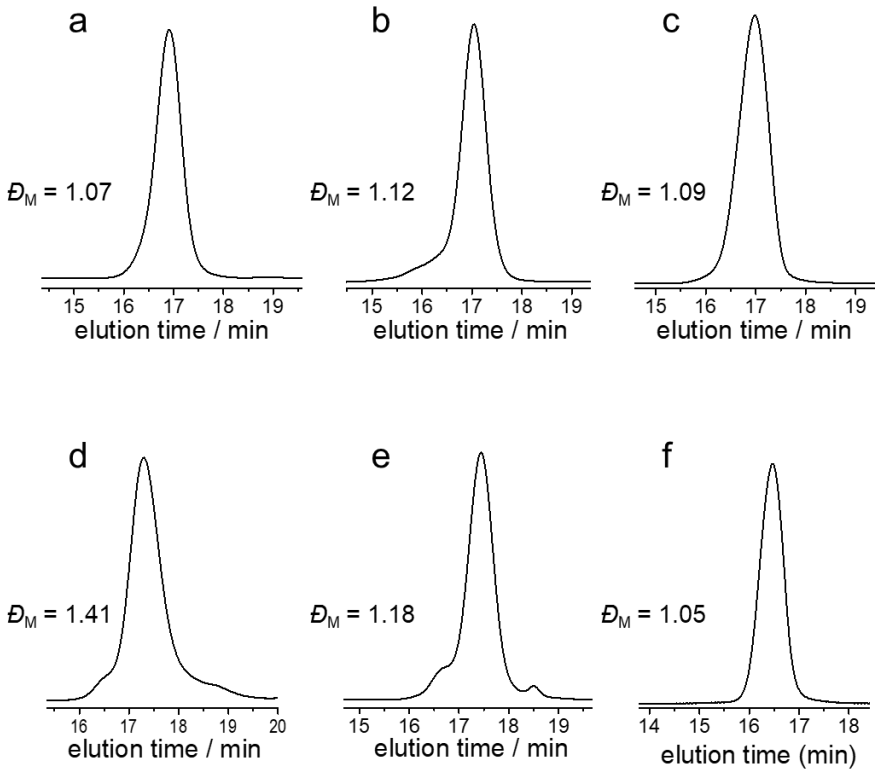

Figure 2.27. SEC trace of different polyether. (a) poly(EGE), (b) poly(AGE), (c) poly(BGE), (d) poly(SO), (e) poly(EH), and (f) poly(BO) synthesized by the cesium pivalate-catalyzed ROPs (entries 1-6 in Table 2.4).

Synthesis of polyester-polyether block polymer

In an argon-filled glovebox, butylene oxide (BO) (501 mg, 6.96 mmol), BDM (6.00 mg, 43.5 μmol) and cesium pivalate (5.09 mg, 21.7 μmol) were placed in an oven-dried reaction vessel with a magnetic stir. The reaction mixture was stirred at 100 °C under an argon atmosphere in an oil bath. During polymerization, a crude aliquot was time-regularly obtained from the system by a syringe in an argon flow and monitored by ^{1}H NMR spectroscopy and SEC to determine monomer conversion and molar mass. After 4 hours, the reaction mixture was cooled down to room temperature. Subsequently, NA (285 mg, 1.74 mmol) in 0.6 mL THF solvent was added into the test tube through syringe and increase the reaction temperature to 100 °C to start the ROAC. After 6 hours, the polymerization was terminated by diluting the reaction mixture with CH_2Cl_2. The reaction

mixture was purified by reprecipitation from a CH_2Cl_2 solution into cold methanol. The purified polymers were dried under vacuum at room temperature for the next analysis.

2.3 Results and Discussion

2.3.1 Cesium pivalate-catalyzed ring-opening alternating copolymerization of epoxide and cyclic anhydride

In the previous study by Satoh's group, the catalytic behaviors of a series (alkali metal carboxylate) AMC catalyst on EGE/PA ROAC were examined. Among the AMC, cesium pivalate (*t*-$BuCO_2Cs$) possessing the highest basicity showed the highest catalytic activity, and it was used to one-step synthesize block polyester via ring-opening copolymerization (ROCOP) from cyclic ester, epoxide, and cyclic anhydride.[10] However, a comprehensive study of ROAC of epoxide with different cyclic anhydrides for polyester homopolymer synthesis is needed for a better understanding of the polymerization mechanisms. Therefore, the effect of anhydride structure on anhydride/epoxide ROAC was examined using four cyclic anhydrides [diglycolic anhydride (DGA), succinic anhydride (SA), 5-norbornene-endo-2,3-dicarboxylic anhydride (NA), and phthalic anhydride (PA)]. Using EGE as the model epoxide with *t*-$BuCO_2Cs$ and 1,4-benzenedimethanol (BDM) as the catalyst and initiator, respectively, ROAC was performed at 100 °C with an $[anhydride]_0/[EGE]_0/[BDM]_0/[t\text{-}BuCO_2Cs]$ ratio of 50/150/2/1 (Table 2.1, Figure 2.28a). Copolymerization was slowest with DGA, which gave a product with a perfect alternating sequence but a relatively broad distribution ($Đ$ = 1.34; entry 1, Table 2.1, Figures 2.1 and 2.2). Copolymerization proceeded more rapidly with both SA and NA, and better control was achieved ($Đ \leq 1.16$; entries 2 and 3, Table 2.1, Figures 2.3–2.6). The fastest copolymerization and best control were obtained with PA, which provided a narrow, monomodal distribution ($Đ$ = 1.06; entry 4, Table 2.1, Figures 2.7 and 2.8). Anhydride consumption followed zero-order kinetics (Figure 2.28b), with turnover frequencies (TOFs) decreasing in the order TOF_{PA} (68.6 h^{-1}) > TOF_{NA}

(20.0 h^{-1}) > TOF_{SA} (15.0 h^{-1}) > TOF_{DGA} (6.1 h^{-1}). These results confirmed the capability of AMC as an efficient catalyst for the synthesis of well-defined polyester with diverse structures via epoxide/cyclic anhydride ROAC.

Table 2.1. ROAC of PA and EGE catalyzed by cesium pivalate [a]

entry	monomers	time (h)	conv. [b] (%)	TOF (h^{-1})	$M_{n,th}$ [c] (kDa)	$M_{n,NMR}$ [b] (kDa)	$M_{n,SEC}$ [d] (kDa)	$Đ$ [d]
1	DGA/EGE	6.9	84.0	6.1	4.7	4.5	2.9	1.34
2	SA/EGE	2.3	69.1	15.0	3.6	3.6	2.3	1.11
3	NA/EGE	2.3	92.0	20.0	6.3	6.3	4.3	1.16
4	PA/EGE	0.7	96.1	68.6	6.1	6.0	5.3	1.06

[a]Polymerization conditions: $[anhydride]_0/[EGE]_0/[BDM]_0/[t\text{-}BuCO_2Cs]$ = 50/150/2/1, in the bulk under an Ar atmosphere at 100 °C. [b]Determined by ^1H NMR analysis of the obtained polymer in $CDCl_3$. [c]Calculated using $[anhydride]_0/[I]_0 \times conv. \times$(M.W.of anhydride+ M.W.of epoxide) + (M.W.of initiator). [d]Determined by SEC analysis of the obtained polymer in THF with a PSt standard.

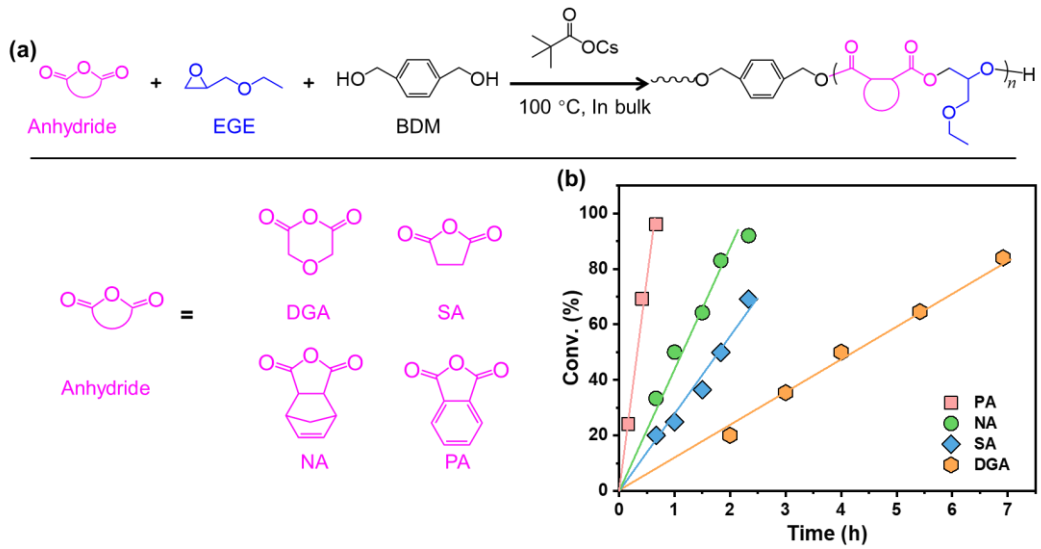

Figure 2.28. Catalytic performance of alkali metal carboxylates for anhydride/EGE ROAC. (a) Anhydride/EGE ROAC catalyzed by *t*-$BuCO_2Cs$. (b) Zero-order kinetic plots for PA/EGE, NA/EGE, SA/EGE, and DGA/EGE ROACs.

2.3.2 Cesium pivalate catalyzed ring-opening alternating copolymerization of oxetane and cyclic anhydride

After the successful establishment of cesium pivalate-catalyzed epoxide/cyclic anhydride ROAC, the author selected four-member cyclic ether, i.e., oxetane, instead of epoxide to copolymerize with anhydrides. This could further expand the polyester structures synthesized from ROAC. Initially, ROAC of PA with 3-ethyl-3-(phenoxymethyl)oxetane (EPO) was carried out using cesium pivalate and BDM as the catalyst and bidirectional initiator at 100 °C, with a $[anhydride]_0/[oxetane]_0/[BDM]_0/[t\text{-}BuCO_2Cs]$ ratio of 15/90/1/1. The copolymerization of PA with EPO reached around 2% in 30 h (entry 1 in Table 2.2), indicating a very low polymerization rate at this temperature. Accordingly, the author attempted to increase the reaction temperature from 100 to 130 °C, and the ROAC reached 86.0% in 19 h, resulting in a perfect alternating sequence distribution with a narrow dispersity ($Đ$ = 1.13, entry 2 in Table 2.2 and Figures 2.9 and 2.10).

Table 2.2. ROCP of anhydrides and oxetanes catalyzed by cesium pivalate [a]

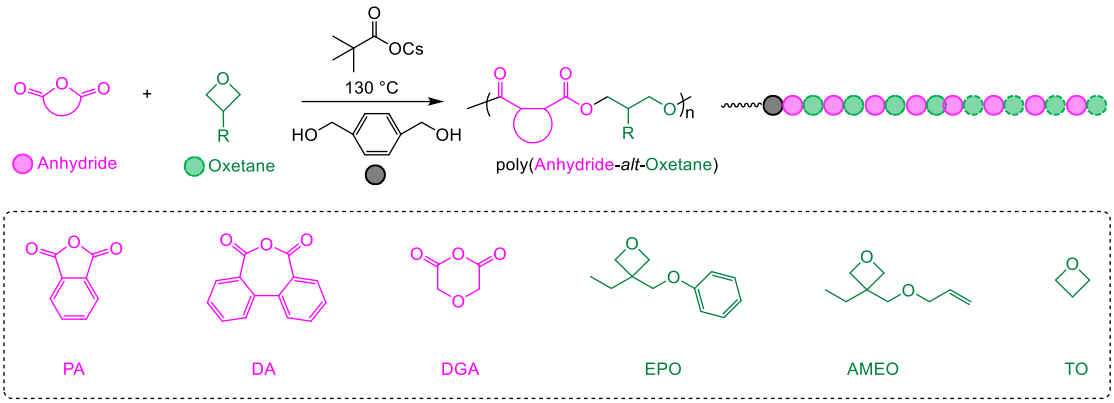

entry	monomers	Initiator	time (h)	conv. [b] (%) (anhydride)	TOF [b] (h^{-1})	$M_{n,th}$ [c](kDa)	$M_{n,NMR}$ [b](kDa)	$M_{n,SEC}$ [d](kDa)	$Đ$ [d]
[e]1	PA/EPO	BDM	30	2.0					
2	PA/EPO	BDM	19	86.0	0.68	4.4	4.3	3.1	1.13
[f]3	PA/EPO	BDM	56	175	n.d.	9.1	8.9	7.3	1.13
[g]4	PA/EPO	BDM	25.5	96.2	n.d.	6.7	6.7	6.4	1.08
5	PA/AMEO	BDM	44	78.6	0.27	3.7	3.5	2.3	1.32
[g]6	PA/TO	BDM	4	91.6	3.44	3.9	3.8	3.7	1.13
[h]7	PA/TO	BDM	120	89.8	n.d.	89.7	83.1	27.7	1.07
8	DA/EPO	BDM	18	99.0	0.83	6.3	6.2	3.4	1.21
[i]9	DGA/TO	BDM	72	99.0	n.d.	2.7	3.0	2.2	1.38

[a]Polymerization conditions at a $[anhydride]_0/[oxetane]_0/[BDM]_0/[t\text{-}BuCO_2Cs]_0$ ratio of 15/90/1/1 at 130 °C in the bulk under an Ar atmosphere. [b]Determined by ^1H NMR analysis of the obtained polymer in $CDCl_3$ and TOF = turnover frequency. [c]Calculated using $[anhydride]_0/[I]_0 \times conv. \times$(M.W.of anhydride+ M.W.of oxetane) + (M.W.of initiator). [d]Determined by SEC analysis of the obtained polymer in THF with a PSt standard. [e]The polymerization was performed at 100 °C. [f]The initial ratio of $[PA]_0/[EPO]_0/[BDM]_0/[t\text{-}BuCO2Cs]_0$ is 15/90/1/1, and the additional 15 eq. of PA was introduced after PA was fully consumed in 29 h. [g]$[PA]_0/[TO]_0/[BDM]_0/[t\text{-}BuCO_2Cs]_0$ = 20/90/1/1. [h]$[PA]_0/[TO]_0/[BDM]_0/[t\text{-}BuCO2Cs]_0$ = 484/2178/1/1. [i]Polymerization was performed at 110 °C.

After PA was fully consumed in 29 h ($M_{n,SEC}$ = 5.5 kDa), 15 eq. of PA was introduced to verify the living polymerization behavior of the catalytic system. The addition of PA immediately restarted the propagation from the terminus of poly(PA-*alt*-EPO), in which $M_{n,\,NMR}$ values increased from 5.5 to 7.3 kDa when PA conversion reached 175% in 56 h and dispersity remained narrow ($Đ$ = 1.13, entry 3 in Table 2.2 and Figures 2.29 and 2.30), indicating living behavior.

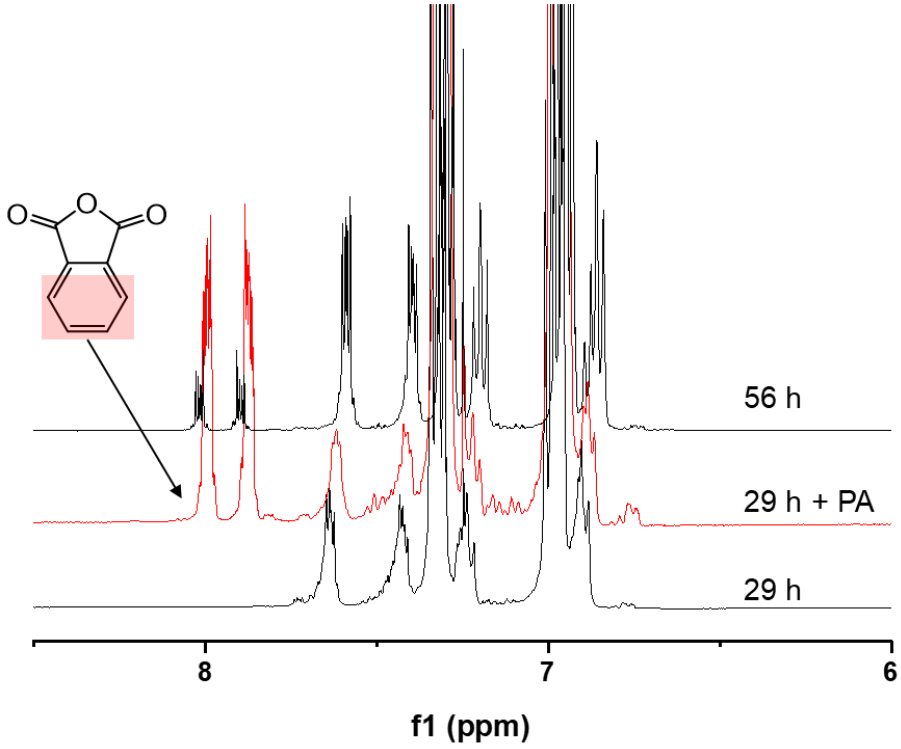

Figure 2.29. ^{1}H NMR ($CDCl_3$) spectra of crude aliquots withdrawn from the reaction system for monitoring the conversion of PA and the formation of resultant polymers (entry 3 in Table 2.2).

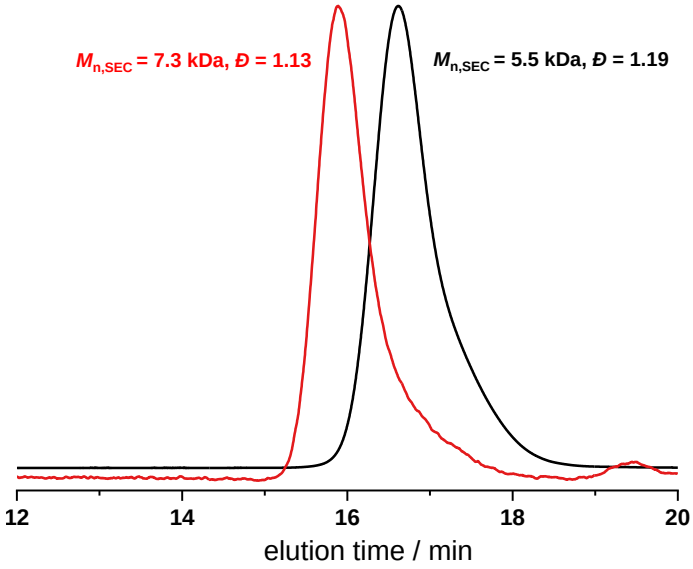

Figure 2.30. SEC (THF) trace of the resultant polymer (entry 3 in Table 2.2).

The molecular weight $M_{n,\,NMR}$ values of the obtained copolymer poly(PA-*alt*-EPO) correlated linearly with PA conversion (entry 4 in Table 2.2 and Figure 2.31a), and the elution peak maximum continuously shifted toward shorter elution times (higher molecular weights) as polymerization progressed (Figure 2.31b). Kinetic analysis revealed that the ROAC of PA with EPO followed zero-order kinetics (Figure 2.31c).

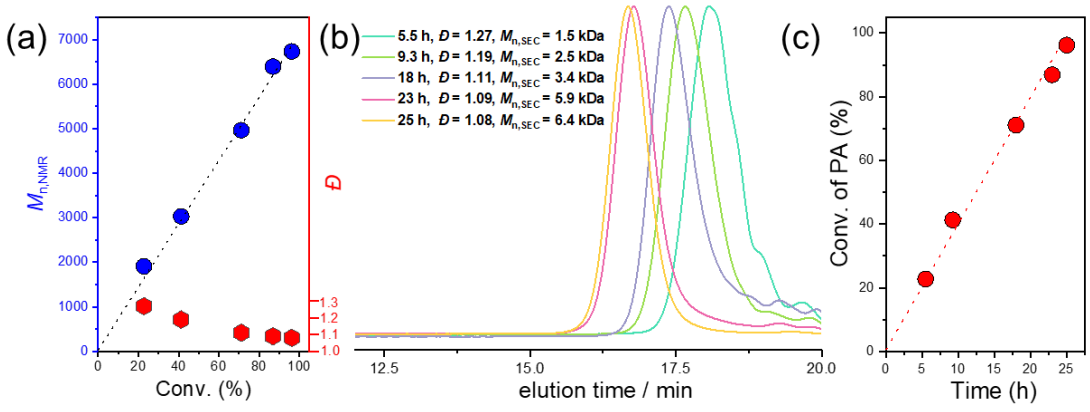

Figure 2.31. Kinetics analysis of the PA/EPO ROAC (entry 4 in Table 2.2): (a) Dependence of $M_{n,NMR}$ and $Đ$ on the monomer conversion. (b) Evolution of SEC traces (THF). (c) Zero-order kinetic plot for the PA/EPO ROAC.

Matrix-assisted laser desorption ionization time-of-flight mass spectrometry (MALDI-TOF MS) was utilized to confirm the structure and terminal functional groups of the obtained poly(PA-*alt*-EPO). The major series of repeated peaks corresponded to the sodium adduct of poly(PA-*alt*-EPO) with BDM as the initiator and two PA as the two end groups of the chains (Figure 2.32). Also assignable to BDM-initiated poly(PA-*alt*-EPO) were two minor series of peaks with two EPOs at two chain ends or PA and EPO at two chain ends, respectively. This indicates that the insertion rate of PA is significantly higher than that of EPO and the slow insertion of EPO is the rate-determining step for polyester formation, which results in the rapid occupation of chain ends by PA. Other minor series of peaks are resulted from polymerization initiated by water. The results indicate that the copolymers have perfectly alternating units of PA and EPO, with no transesterification side reaction occurring during polymerization.

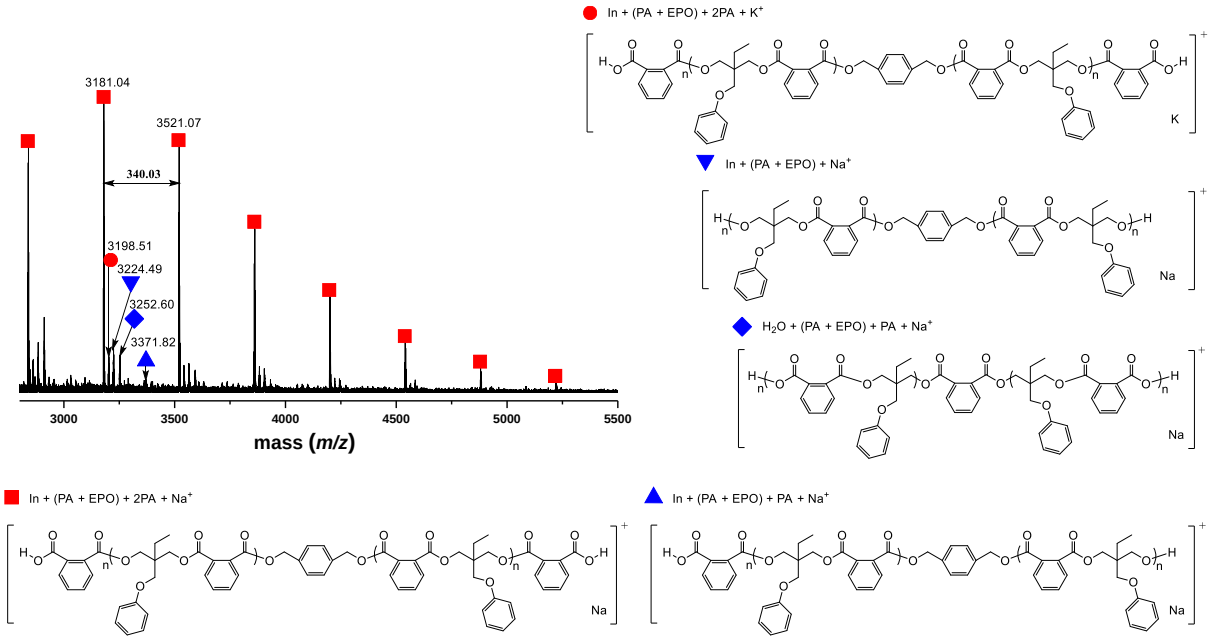

Figure 2.32. MALDI-TOF MS of the poly(PA-*alt*-EPO) from entry 2 in Table 2.2.

On the basis of the above-mentioned studies, as well as the observation that cesium pivalate activates EPO monomer via the interaction between cesium and cyclic ether oxygen atom on Fourier transform infrared (FT-IR) spectroscopy measurement (Figure 2.33), a plausible mechanism for the copolymerization of PA and EPO is proposed (Scheme 2.20). The carboxylate activates the initiator via H-bonding, and a cesium cation

activates the carbonyl group of the anhydride. Because the hydroxyl group of the initiator is nucleophilic and PA activated by a cesium cation shows extremely high electrophilicity, the activated PA is prone to nucleophilic attack from the cesium pivalate-activated hydroxyl group. The forming carboxylate species is sufficiently reactive to react with the cesium cation-activated EPO via nucleophilic attack, resulting in the formation of a copolymer with a perfect alternating chemical structure. During the copolymerization, the insertion rate of PA is significantly higher than that of EPO so that the slow insertion of EPO is the rate-determining step for polyester formation.

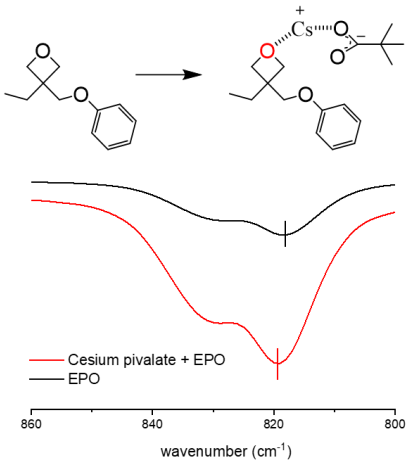

Figure 2.33. Fourier transform infrared (FT-IR) spectrum of EPO and EPO mixed with cesium pivalate.

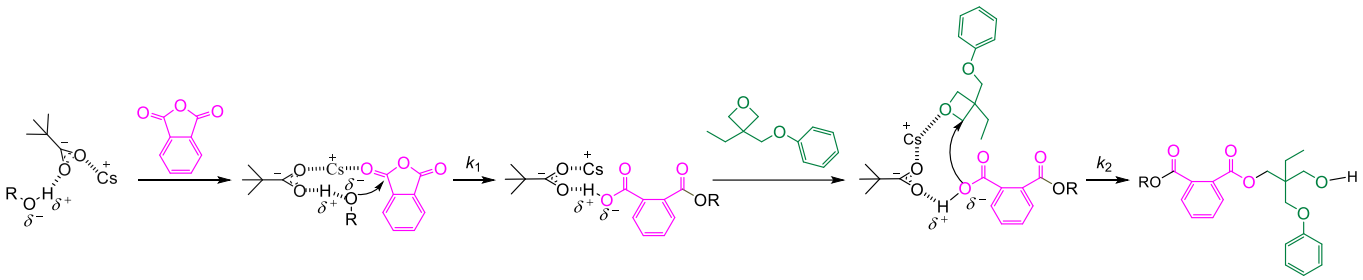

Scheme 2.20. Proposed mechanism of ROAC from a mixture of PA and EPO with cesium pivalate as the catalyst and alcohol as the initiator.

A variety of cyclic anhydrides and oxetanes were evaluated in order to confirm the potential of the copolymerization for a large library of structurally and functionally diverse monomers. Using PA as a model anhydride, the current catalysis system was applied to two additional oxetanes. A less active 3-((allyloxy)methyl)-3-ethyloxetane (AMEO) was copolymerized with PA, producing a functional copolymer for postpolymerization modification (entry 5 in Table 2.2 and Figures 2.11 and 2.12). TO has the highest activity of these monomers because of without any substituent. After 4h, the PA conversion reached 91.6%, resulting in copolymers with a narrow dispersity (entry 6 in Table 2.2 and Figures 2.13 and 2.14a). The MALDI-TOF MS results indicated that the major series of peaks corresponded to the sodium adduct of poly(PA-*alt*-TO) containing BDM as the initiator and two PA or two TO at the two chain ends, and that no transesterification side reaction was observed (Figure 2.34). The molecular weight of poly(PA-*alt*-TO) can reach as high as 27.7 kDa when increasing monomer/initiator ratio (entry 7 in Table 2.2 and Figure 2.14b).

Then, utilizing EPO as the oxetane-type monomer, numerous anhydrides were investigated. Compared to PA, faster conversion of diphenyl anhydride (DA) was observed during copolymerization of DA/EPO (entry 8 in Table 2.2 and Figures 2.15 and 2.16), which was consistent with the increased reactivity brought about by the ring strain of the seven-membered anhydride.[11] Comparing to TO, EPO is very difficult to be completely removed from polymers during the purification process, which resulted in that signals of EPO were observed in ^{1}H NMR spectrum. Additionally, DGA was used to react with TO, resulting in the poly(DGA-*alt*-TO) (entry 9 in Table 2.2 and 2.17 and 2.18). These results confirmed the substitution of epoxide with oxetane to process ROAC with cyclic anhydride as an efficient method for polyester synthesis, which enriched the polyester structures obtained from ROAC.

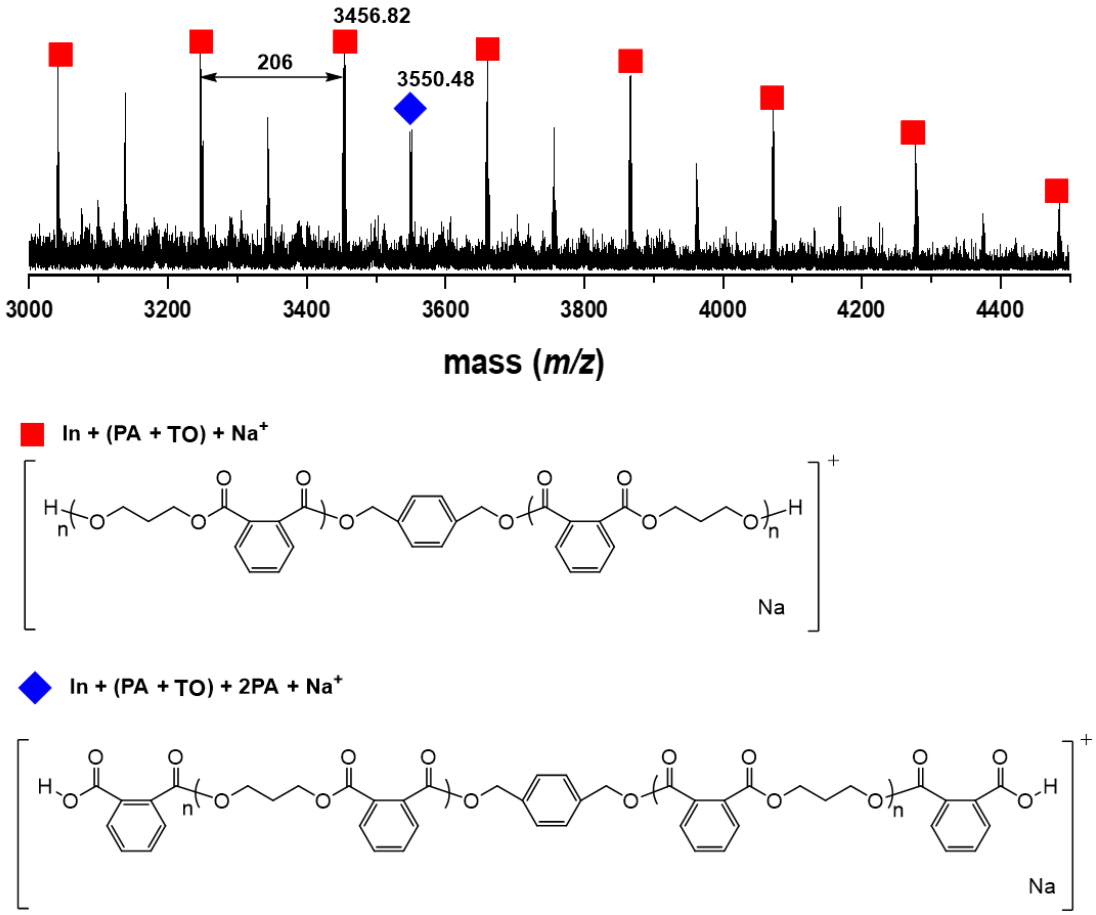

Figure 2.34. MALDI-TOF MS of the poly(PA-*alt*-TO) from entry 6 in Table 2.2.

2.3.3 Cesium pivalate-catalyzed ring-opening polymerization of epoxide and application for one-pot synthesizing polyether-*b*-polyester

During the cesium pivalate-catalyzed epoxide/cyclic anhydride ROAC, epoxides act as polar solvents to weaken the coulombic interaction between the metal cation (Lewis acid) and carboxylate anion (Lewis base). Coordination with metal cations activates epoxides toward nucleophilic attack, while carboxylates are sufficiently reactive to attack the activated epoxides and induce their ring-opening. The potassium carboxylates was reported to initiate the anionic ROP of epoxides in the presence of a crown ether.[12] However, the above-mentioned epoxide/cyclic anhydride ROAC studies suggest that the role of AMCs can change from initiator to catalyst in the coexistence of an alcohol initiator, therefore, the AMC catalyst combined with an alcohol initiator is promising to carry out the epoxide ROP and synthesize polyether (Scheme 2.21).

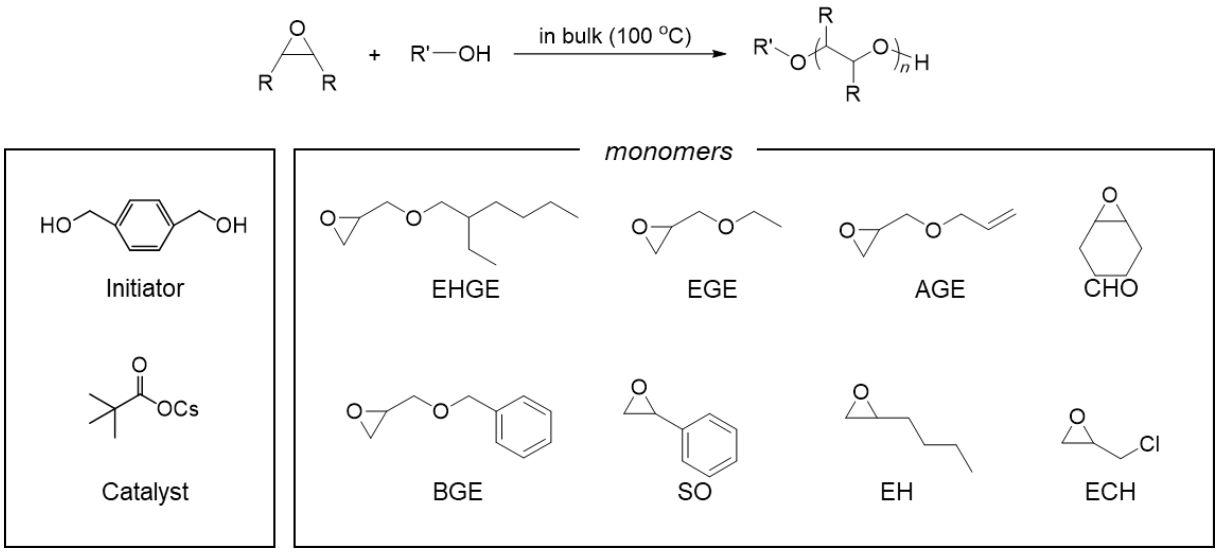

Scheme 2.21. Ring-opening polymerization of epoxides catalyzed by cesium pivalate.

Table 2.3. Results of cesium pivalate–catalyzed ring-opening polymerization of 2-ethylhexyl glycidyl ether[a]

Entry	$[EHGE]_0/[BDM]_0/[t\text{-}BuCO_2Cs]$	Temp. (°C)	Conv.[b] (%)	Time (h)	$M_{n,th}$[c] (kDa)	$M_{n,NMR}$[b] (kDa)	$M_{n,SEC}$[d] (kDa)	$Đ$[d]
1	25/1.0/0.50	100	98	1.8	4.5	5.0	3.7	1.06
2	55/1.0/0.50	100	75	2.3	7.6	8.0	4.5	1.07
3	110/1.0/0.50	100	91	6.0	18.6	19.3	8.8	1.13
4	55/1.0/0.35	100	72	7.5	7.3	6.1	4.4	1.07
5	55/1.0/0.20	100	98	16	10.0	10.2	6.7	1.11

[a]All polymerizations were performed with 43.5 μmol BDM and varied epoxides and catalyst loading in bulk. [b]Calculated from ^{1}H NMR data. [c]$M_{n,th} = [M]_0/[initiator]_0 \times (conv.) \times (M.W.\ of\ monomer) + (M.W.\ of\ initiator)$. [b]Determined by ^{1}H NMR analysis of the obtained polymer in $CDCl_3$. [d]Determined by SEC analysis of the obtained polymer in THF with a PSt standard.

2-ethylhexyl glycidyl ether (EHGE) was selected as the epoxide monomer for investigation. Initially, the ROP of EHGE was performed in the bulk at 100 °C under Ar using cesium pivalate (catalyst) and BDM (initiator) at a $[EHGE]_0/[BDM]_0/[t\text{-}BuCO_2Cs]$ molar ratio of 55/1.0/0.5. Polymerization was monitored by ^{1}H NMR spectroscopy and was terminated when the EHGE conversion reached 75% (entry 2 in Table 2.3).

During polymerization, the dispersity ($Đ$) of poly(EHGE) remained low (1.05−1.07), and the number-averaged molecular weight determined by $M_{n,NMR}$ linearly increased with increasing EHGE conversion (Figure 2.35), which indicated the controlled/living nature of the system. The ^{1}H NMR spectrum of poly(EHGE) (Figures 2.19) agreed with its expected structure, and $M_{n,NMR}$ (8.0 kDa) was close to the theoretical value ($M_{n,th}$) of 7.6 kDa. The SEC trace of poly(EHGE) exhibited a single elution peak with a rather low $Đ$ of 1.07 (Figure 2.20).

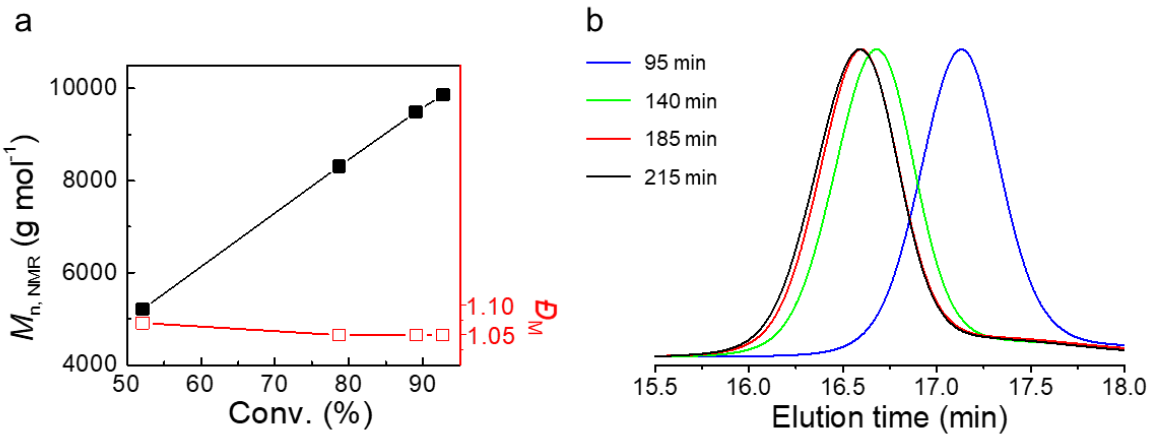

Figure 2.35. (a) Dependence of $M_{n,NMR}$ (■) and $Đ$ (□) on 2-ethylhexyl glycidyl ether conversion, (b) size exclusion chromatography traces of poly(2-ethylhexyl glycidyl ether) obtained at different polymerization times.

MALDI-TOF MS of poly(EHGE) synthesized using the cesium pivalate/BDM system demonstrated the absence of pivalate-initiated species (entry 2 in Table 2.3 and Figure 2.36) and featured two series of peaks. The major series was assigned to BDM-initiated poly(EHGE) with the expected chemical structure, and the peak at *m/z* 5563.81 was in line with the theoretical mass of the desired BDM-initiated poly(EHGE) with a degree of 29 (calculated for $[M + Na]^+$ = 5563.71). The minor series was assigned to water-initiated poly(EHGE) (calculated for $[M + Na]^+$ = 5628.87, n = 30). Importantly, no signals attributable to carboxylate-initiated poly(EHGE) (calculated $[M + Na]^+$ = 5712.96, n = 30) and chain-transfer products (calculated [M +

Na]$^+$ = 5798.13, n = 30) were observed.

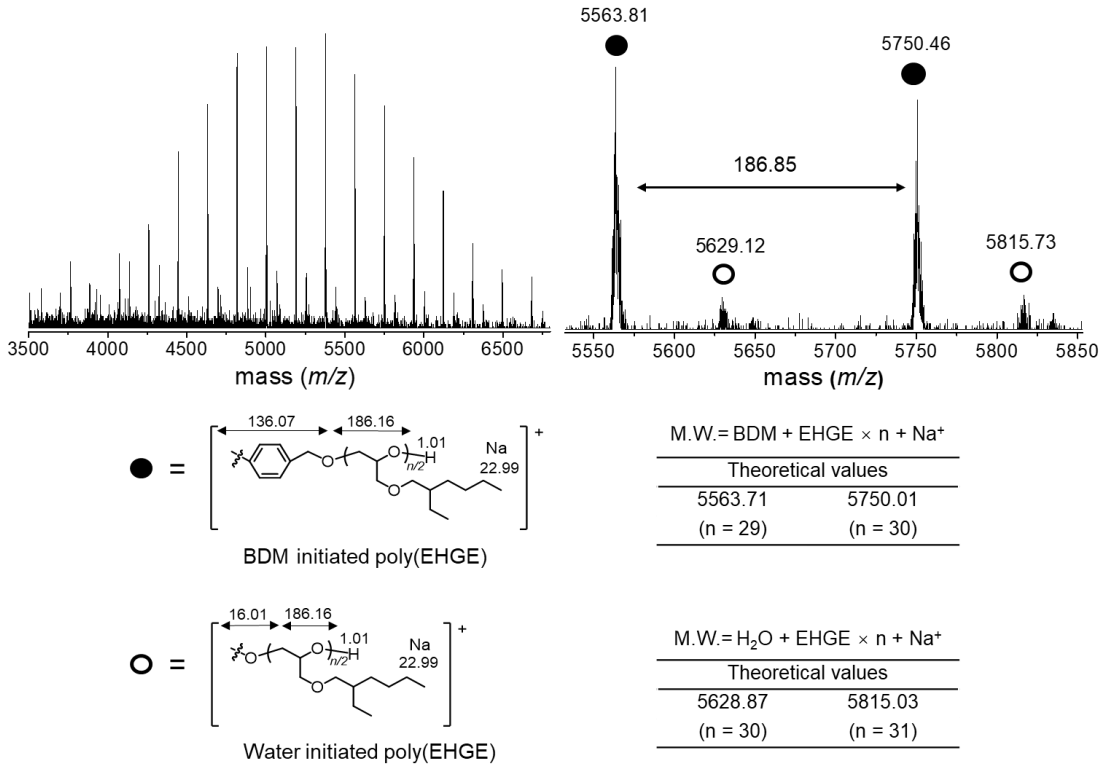

Figure 2.36. MALDI-TOF MS of poly(EHGE) synthesized in the presence of BDM initiator (polymerization was impended in bulk under Ar atmosphere with the $[EHGE]_0/[BDM]_0/[(CH_3)_3CCOOCs]$ ratio of 55/1.0/0.5 at 100°C, entry 2 in Table 2.3).

The polymerization rate could be easily regulated by varying the catalyst loading (entries 4 and 5 in Table 2.3), while the molecular weight distribution of the obtained polymer remained low ($Đ$ = 1.07 and 1.11). At the catalyst/initiator molar ratio of 0.5/1.0, $M_{n,NMR}$ could be regulated in the range of 5.0–20.0 kDa by adjusting the monomer/initiator ratio (entries 1−3 in Table 2.3). Chain extension experiments were executed to confirm the living nature of the system. Poly(EHGE) ($M_{n,SEC}$ = 4.9 kDa, $Đ$ = 1.10) was first prepared at an initial feed ratio of $[EHGE]_0/[BDM]_0/[t\text{-}BuCO_2Cs]$ = 55/1.0/0.5, and 55 eq. of additional EHGE was introduced after complete monomer consumption. This addition immediately restarted chain propagation from the poly(EHGE) terminus to afford poly(EHGE) with a higher number-average molecular weight ($M_{n,SEC}$ = 8.6 kDa, $Đ$ = 1.13) (Figure 2.37), which confirmed that the present system enabled good control over polymerization and

exhibited a controlled/living nature.

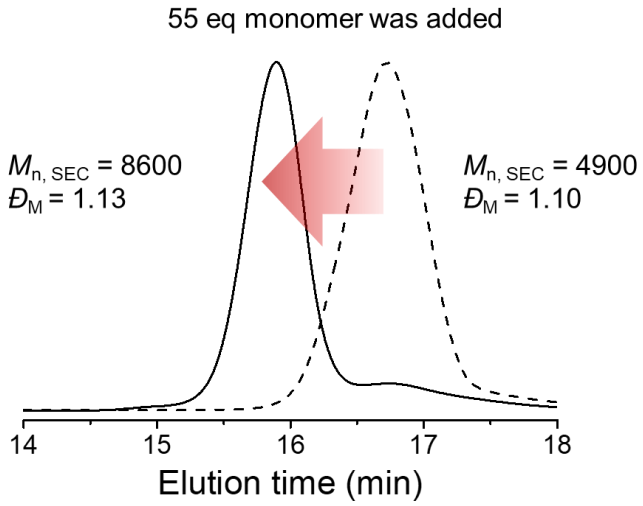

Figure 2.37. SEC traces of the poly(EHGE)s obtained after the first (solid line) and second (dotted line) feeds of EHGE. The M_n values are given in Da.

To investigate the monomer scope and limitations on the established epoxide ROP system, the author examined the cesium pivalate-catalyzed ROP of alkyl-substituted epoxides (1,2-epoxyhexane (EH), cyclohexene oxide (CHO), 1,2-butylene oxide (BO), and epichlorohydrin (ECH)), styrene oxide (SO), and glycidyl ethers (ethyl glycidyl ether (EGE), allyl glycidyl ether (AGE), and benzyl glycidyl ether (BGE)) (Scheme 2.21, Table 2.4). SO showed low reactivity and was fully consumed only after 48 h to afford poly(SO) with a relatively high $Đ$ of 1.41. A higher polymerization rate and better polymerization control were achieved in the case of EH, which was converted into well-defined poly(EH) with a monomodal molecular weight distribution ($Đ$ = 1.18). The highest reactivity and the best molecular weight controllability ($Đ$ = 1.05) among the alkyl-substituted epoxides were obtained for BO, which featured short alkyl substituents. Besides, by applying a high monomer-to-initiator ratio, a high molecular weight poly(1,2-butylene oxide) (poly(BO)) was obtained with a narrow $Đ$ ($M_{n,SEC}$ = 32 kDa, $Đ$ = 1.29; entry 7 in Table 2.4). Compared to alkyl-substituted epoxides, glycidyl ethers exhibited higher polymerization rates. EGE possesses a structure similar to that of

EHGE but exhibited higher ROP reactivity and afforded poly(EGE) with low dispersity ($Đ$ = 1.07). Even faster polymerization was observed for the ROP of BGE, and the related polymerization controllability remained high ($Đ$ = 1.09). To examine the feasibility of functional polyether synthesis, the author tested a monomer with a double bond on the substituent (AGE), obtaining a well-defined functional polyether (poly(AGE), $Đ$ = 1.12). In a previously reported potassium alkoxide/naphthalenide-initiated AGE polymerization system, polymerization was often accompanied by the isomerization of the allyl repeating unit at temperatures above 40 °C.[14] However, ^{1}H NMR analysis showed that in the present polymerization, the allyl group of AGE was not isomerized even at 100 °C (Figure 2.22), which indicated the presented system allowed for post-polymerization modification. The polymerizations of CHO and ECH were unsuccessful. In the case of CHO, the initiator/propagating chain end may be less accessible to the sterically encumbered 1,2-disubstituted epoxide ring. In the case of ECH, a strong electron-withdrawing group on the α-carbon decreases the electron density on the oxyanionic end of the growing chain, thus significantly reducing its ability to nucleophilically attack the monomer. Alternatively, the carboxylate can directly attack the chloromethylene group of ECH. The SEC traces and ^{1}H NMR spectra of the obtained polyethers are presented in Figures 2.21−2.27. This study demonstrated that AMCs can be used as simple and efficient catalysts for the ROP of epoxides a to obtain polyethers with predictable molecular weights, low dispersity, and diversity structures.

Table 2.4. Results of cesium pivalate–catalyzed ring-opening polymerization of various epoxides [a]

Entry	Monomer	$[M]_0/[BDM]_0/[t\text{-}BuCO_2Cs]$	Conv. (%)[b]	Time (h)	$M_{n,th}$[c] (kDa)	$M_{n,NMR}$[d] (kDa)	$M_{n,SEC}$[e] (kDa)	$Đ$[e]
1	EGE	55/1.0/0.5	80	1.6	4.5	6.0	4.5	1.07
2	AGE	55/1.0/0.5	93	3.0	5.8	6.4	4.1	1.12
3	BGE	55/1.0/0.5	89	1.3	8.0	ND[f]	4.3	1.09
4	SO	55/1.0/0.5	99	48	6.5	ND[f]	2.2	1.41
5	EH	55/1.0/0.5	80	13	4.4	3.0	2.6	1.18
6	BO	110/1.0/0.5	82	8.0	6.5	7.3	5.9	1.05
7	BO	1,400/1.0/1.0	96	48	96.9	ND[f]	31.9	1.29
8	CHO	55/1.0/0.5	-	-	-	-	-	-
9	ECH	55/1.0/0.5	-	-	-	-	-	-

[a]All polymerizations were performed with 43.5 μmol BDM with varied epoxides and catalyst loading at 100 °C in bulk. [c]Calculated from ^{1}H NMR data. [b]$M_{n,th} = [M]_0/[initiator]_0 \times (conv.) \times (M.W.\ of\ monomer) + (M.W.\ of\ initiator)$. [d]Determined by ^{1}H NMR analysis of the obtained polymer in $CDCl_3$. [e]$M_{n,SEC}$ and $Đ_M$ were estimated by size exclusion chromatography using polystyrene calibration in tetrahydrofuran at 40 °C. [f]Not determined, as the ^{1}H NMR signals of the initiator residue overlapped with the signals from polymer main chain or was too small.

According to the ability of AMCs to efficiently promote the ROAC of cyclic anhydrides and epoxides, the author employed the same system to achieve the one-pot synthesis of a polyether-polyester block copolymer using the second feeding of a cyclic anhydride into the epoxide polymerization mixture (Scheme 2.22). A poly(BO) diol was prepared using cesium pivalate as the catalyst and BDM as the initiator at a $[BO]_0/[BDM]_0/[$ *t*-$BuCO_2Cs]$ molar ratio of 160/1/0.5 at 100 °C. When the BO conversion reached 36.3%, 40 eq. (with respect to BDM) of NA was added to start the ROAC of BO and NA. The product obtained at a NA consumption of 44.6% exhibited a SEC elution peak in a higher-molecular-weight region (Figure 2.38) compared to that observed for PBO diol, and ^{1}H NMR analysis confirmed the chemical structure of each block (Figure 2.39). The integral intensity of the signal assigned to the alkenyl protons on the norbornene ring (i) was two times that of the signal assigned to the methine group (k) of the epoxide of the poly(BO-*alt*-NA)

block, which implied that during ROAC, NA and BO were consumed in equal amounts. In addition, the DOSY NMR spectrum of the obtained block copolymer showed only one diffusion coefficient (except for the solvent signal), which confirmed that the two blocks were covalently linked (Figure 2.40). These results indicated the successful synthesis of a poly(BO-*alt*-NA)-*b*-PBO-*b*-poly(BO-*alt*-NA) triblock copolymer via the formation of PBO diol and the subsequent bidirectional growth of poly(BO-*alt*-NA). The low $Đ$ (1.05) of this copolymer suggested good molecular weight controllability. The DSC analysis of poly(BO-*alt*-NA)-*b*-PBO-*b*-poly(BO-*alt*-NA) (Figure 2.41) revealed two T_g values ($T_{g,\ poly(BO)block} \approx -65$ °C; $T_{g,\ poly(BO\text{-}alt\text{-}NA)block} \approx 54$ °C) that originated from PBO and poly(BO-*alt*-NA) blocks and were comparable to those of the corresponding homopolymers ($T_{g,\ poly(BO)block} \approx -73$ °C;[13] $T_{g,\ poly(BO\text{-}alt\text{-}NA)} \approx 53$ °C, Figure 2.42). This finding implies that the PBO and poly(BO-*alt*-NA) blocks were microphase-separated and suggests that the corresponding copolymer can be used as a thermoplastic elastomer.

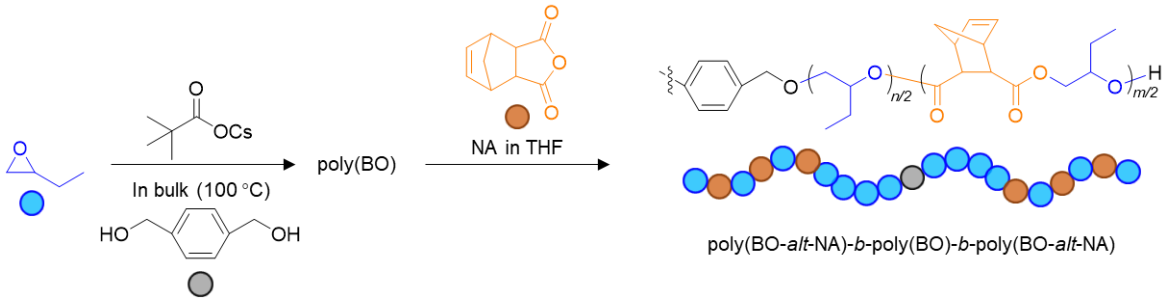

Scheme 2.22. One-pot synthesis of polyether-polyester block copolymer.

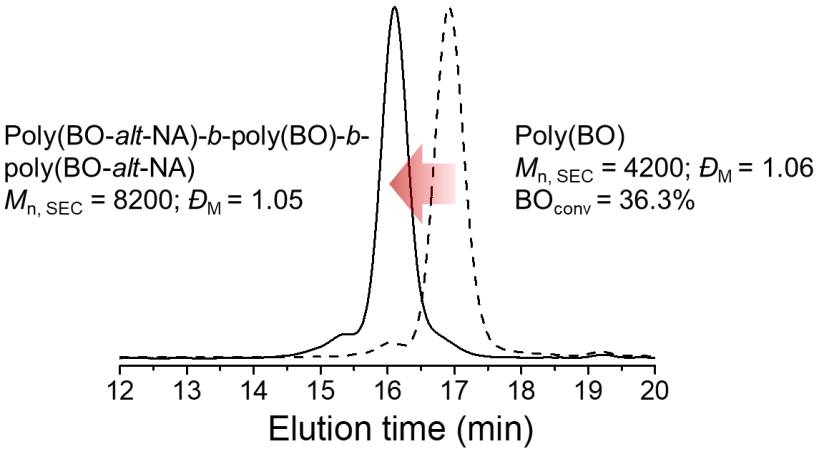

Figure 2.38. SEC traces of poly(butylene oxide) diol (dotted line) and poly(butylene oxide-*alt*-5-norbornene-2,3-dicarboxylic anhydride)-*b*-poly(butylene oxide)-*b*-poly(butylene oxide-*alt*-5-norbornene-2,3-dicarboxylic anhydride) (solid line).

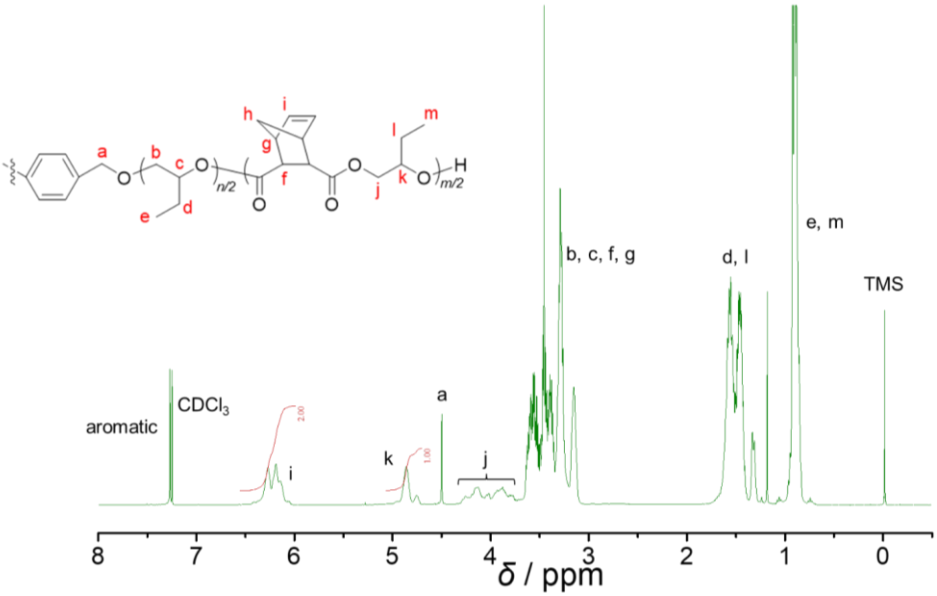

Figure 2.39. ^{1}H NMR spectrum of poly(BO-*alt*-NA)-*b*-poly(BO)-*b*-poly(BO-*alt*-NA).

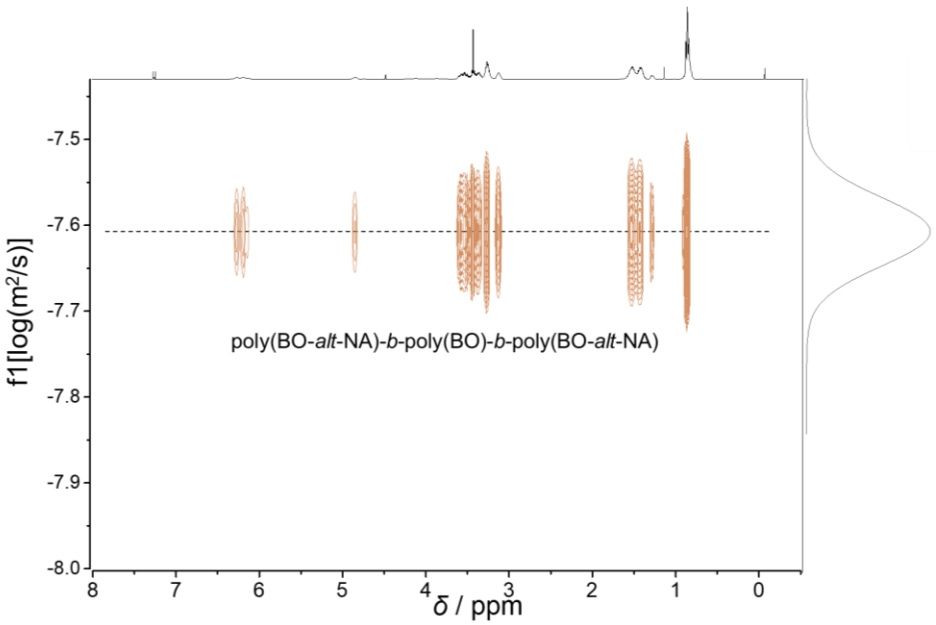

Figure 2.40. DOSY ($CDCl_3$) spectrum of poly(BO-*alt*-NA)-*b*-poly(BO)-*b*-poly(BO-*alt*-NA).

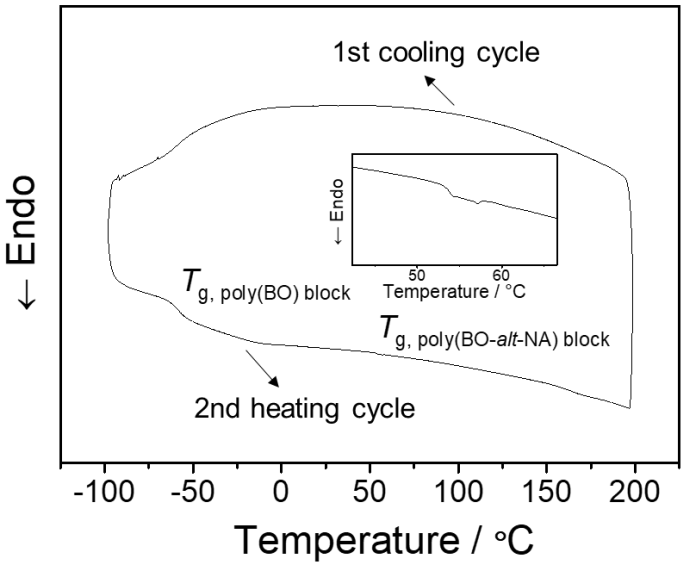

Figure 2.41. DSC trace of isotactic poly(BO-*alt*-NA)-*b*-poly(BO)-*b*-poly(BO-*alt*-NA).

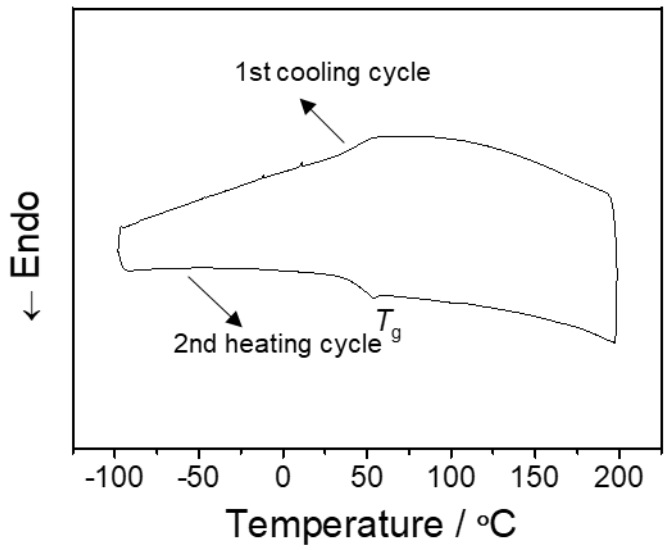

Figure 2.42. DSC trace of poly(BO-*alt*-NA).

2.4 Conclusion

In this chapter, the author elucidated the remarkable catalytic efficacy of cesium pivalate in carrying out epoxide/cyclic anhydride ring-opening alternating copolymerization (ROAC), oxetane/cyclic anhydride ROAC, and epoxide ring-opening polymerization (ROP). The diverse combinations of epoxides and cyclic anhydrides employed yielded a spectrum of polyester structures, all exhibiting narrow molecular weight dispersity. Leveraging the advantageous attributes of the cesium pivalate catalyst, including its affordability, ease of handing, and low toxicity, suggests promising prospects for its application in both laboratory-scale and industrial-scale polyester production. Moreover, the successful implementation of a one-pot/two-step synthesis for polyether-polyester block copolymers underscores the versatility of cesium pivalate as a switchable catalyst capable of connecting different catalytic cycles. In the subsequent chapter, the author will delve into utilizing cesium pivalate to connect various catalytic cycles for the synthesis of block polyesters.

2.5 References

1. Kamber, N. E., Jeong, W., Waymouth, R. M., Pratt, R. C., Lohmeijer, B. G., Hedrick, J. L. Organocatalytic ring-opening polymerization. *Chemical reviews* **2007**, *107*, 5813-5840.
2. Longo J M, Sanford M J, Coates G W. Ring-opening copolymerization of epoxides and cyclic anhydrides with discrete metal complexes: structure–property relationships. *Chemical reviews* **2016**, *116*, 15167-15197.
3. Jeske, R. C.; DiCiccio, A. M.; Coates, G. W. Alternating copolymerization of epoxides and cyclic anhydrides: an improved route to aliphatic polyesters. *J. Am. Chem. Soc.* **2007**, *129*, 11330-11331.
4. Plajer, Alex J., and Charlotte K. Williams. Heterocycle/Heteroallene Ring-Opening Copolymerization: Selective Catalysis Delivering Alternating Copolymers. *Angew. Chem. Int. Ed.* **2022**, *61*, e202104495.
5. Hu, L. F., Zhang, C. J., Wu, H. L., Yang, J. L., Liu, B., Duan, H. Y., Zhang, X. H. Highly active organic lewis pairs for the copolymerization of epoxides with cyclic anhydrides: Metal-free access to well-defined aliphatic polyesters. *Macromolecules* **2018** *51*, 3126-3134.
6. Wang, J., Zhu, Y., Li, M., Wang, Y., Wang, X., & Tao, Y. Tug-of-War between Two Distinct Catalytic Sites Enables Fast and Selective Ring-Opening Copolymerizations. *Angew. Chem. Int. Ed.* **2022** *134*, e202208525.
7. Xie, R., Zhang, Y. Y., Yang, G. W., Zhu, X. F., Li, B., Wu, G. P. Record Productivity and Unprecedented Molecular Weight for Ring-Opening Copolymerization of Epoxides and Cyclic Anhydrides Enabled by Organoboron Catalysts. *Angew. Chem. Int. Ed.* **2021**, *133*, 19402-19410.
8. Li, F., Suzuki, R., Gao, T., Xia, X., Isono, T., Satoh, T. Alkali Metal Carboxylates: Simple, Efficient, and Industrial Relevant Catalysts for Controlled Polymer Synthesis. *Bull. Chem. Soc. Jpn.* **2023**, *96*, 1003-1018.
9. Takojima, K.; Saito, T.; Vevert, C.; Ladelta, V.; Bilalis, P.; Watanabe, J.; Hatanaka, S.; Konno, T.;

Yamamoto, T.; Tajima, K.; Hadjichristidis, N.; Isono, T.; Satoh, T. Facile synthesis of poly (trimethylene carbonate) by alkali metal carboxylate-catalyzed ring-opening polymerization. *Polym. J.* **2020**, *52*, 103–110.

10. Xia, X., Suzuki, R., Takojima, K., Jiang, D. H., Isono, T., & Satoh, T.. Smart access to sequentially and architecturally controlled block polymers via a simple catalytic polymerization system. *ACS catalysis*, **2022,** *11*, 5999-6009.
11. McGuire, T. M., Clark, E. F., Buchard, A. Polymers from sugars and cyclic anhydrides: ring-opening copolymerization of a d-xylose anhydrosugar oxetane. *Macromolecules* **2021**, *54*, 5094-5105.
12. Koinuma, H.; Naito, K.; Hirai, H. Anionic polymerization of oxiranes and cyclic siloxanes initiated with potassium salt-crown ether systems. *Makromol. Chem.* **1982**, *183*, 1383– 1392.
13. Lai, J.; Trick, G. S. Glass Transformation Temperatures of Polymers of Olefin Oxides and Olefin Sulfides. J. Polym. *Sci. Part A-1 Polym. Chem.* **1970**, *8*, 2339– 2350,
14. Lee, B. F.; Kade, M. J.; Chute, J. A.; Gupta, N.; Campos, L. M.; Fredrickson, G. H.; Kramer, E. J.; Lynd, N. A.; Hawker, C. J. Poly(Allyl Glycidyl Ether)-A Versatile and Functional Polyether Platform. *J. Polym. Sci. Part A Polym. Chem.* **2011**, *49*, 4498–4504.

Chapter 3

Self-switchable Copolymerization: From Epoxide, Oxetane, and Cyclic Anhydride to Block Copolyester

3.1 Introduction

The integration of chemically different homopolymers gives rise to block copolymers with tunable physicochemical and morphological properties.[1,2] One of the most interesting properties of block copolymers is their ability to self-assemble into micellar aggregate in selective solvents and into microphase-separated structures in the bulk and thin film states. For example, amphiphilic block copolymers enable the encapsulation of various types of therapeutics in the micelle core through self-assembly, and thus, they have been widely employed as nanocarriers for drug delivery.[3] The immiscibility among different block segments results in a microphase separation with a variety of nanoscale periodic morphologies, such as lamella, cylinder, and spheres. Such nanostructures have found applications in advanced nanotechnological fields, such as data storage device construction,[4–6] nanoporous material synthesis,[7] and nanolithography.[8] In addition, the microphase separation is important for thermoplastic elastomers, where the "hard–soft–hard" type triblock sequence is essential to endow the block copolymers with elastic properties.

Traditional block copolymer synthesis strategies involve multi-reaction steps that are time-, effort-, and energy-intensive.[9–12] To tackle these problems, self-switchable polymerization has emerged as an attractive catalytic approach for the direct synthesis of block copolymers from a monomer mixture, without the need for intermediary isolation, purification, and protection/deprotection steps.[13] Self-switchable polymerization utilizes switch catalysts and cocatalysts that connect different catalytic cycles. Sequence-controlled block copolymers are synthesized from a monomer mixture via smooth and orderly switching between different catalytic cycles without sequential monomer addition. Self-switchable polymerization was implemented in 1985 by Inoue who performed the copolymerization of epoxide/anhydride and lactone to obtain oxygen-rich block copolymers.[14] In 2008, Coates synthesized polyester-*b*-polycarbonate diblock copolymers from a monomer mixture of epoxide, anhydride, and CO_2 using a β-diiminate(bdi) zinc catalyst to connect the epoxide/anhydride ring-opening alternating copolymerization (ROAC) and epoxide/CO_2 ROAC.[15] In 2014,

Williams employed “switch catalysis” to obtain polycarbonate-*b*-polyesters from a mixture of cyclohexene oxide/CO_2/*ε*-caprolactone.[16] Significant progress has been made by Williams, Romain, and Rieger in incorporating epoxide/CO_2 ROAC, epoxide/anhydride ROAC, and cyclic ester ring-opening polymerization (ROP) catalytic cycles using mono-, di-, and trimetallic catalysts.[17–21] Recently, organocatalysts that can switch between different catalytic cycles during copolymerization have been developed as alternatives to transition metal catalysts. In 2016, Feng reported the use of triethyl borane and a phosphazene base as an efficient cocatalyst system for epoxide/CO_2 ROAC.[22] Boron-containing catalysts have since been the focus of further development due to their high efficiency and excellent molecular weight controllability. They have been applied to various self-switchable polymerization systems involving epoxide/CO_2 ROAC, epoxide/anhydride ROAC, cyclic ester ROP, and epoxide ROP.[22–24] Although organocatalysts are simpler and more environmentally benign than transition-metal complex catalysts, they tend to be less active even at a high temperature. Furthermore, their strong basicity hinders the expansion of the synthetic scope for application and high production costs also limit their applicability for industrial block copolyester synthesis.[25–27] In the last chapter, the author introduced the excellent catalytic performance of alkali metal carboxylate (AMC) on epoxide/cyclic anhydride ROAC, oxetane/cyclic anhydride ROAC, and epoxide ROP, as well as the capability to connect two catalytic cycles for polyether-polyester block copolymer synthesis. These demonstrations imply the possibility of using AMC catalyst that efficiently and spontaneously links different catalytic cycles to construct a self-switchable copolymerization system. The low-cost and easy-handing nature of AMC catalyst could address the recent concerns of the previous self-switchable copolymerization systems. In this chapter, the author studied the polymerization behavior that using the AMC to bridge two catalytic cycles among different epoxide/cyclic anhydrides ROAC and oxetane/cyclic anhydrides ROAC. Monomer sequences of the synthesized polymers were discussed to summarize the monomer reactivity trends and to guide later researchers to produce block copolymers with desired monomer sequence structures (Scheme 3.1).

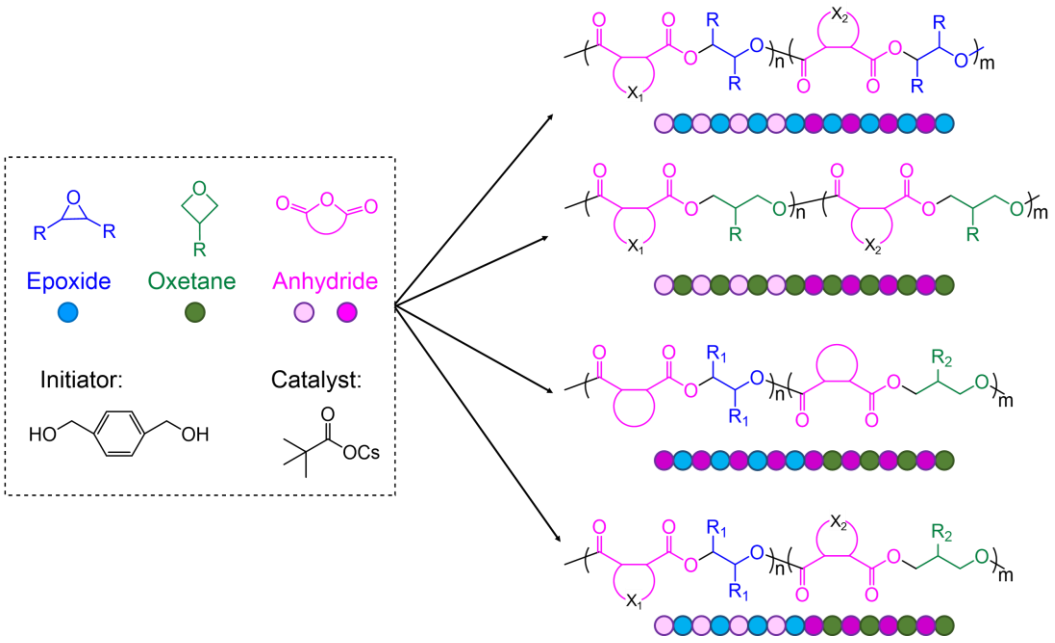

Scheme 3.1. Cesium pivalate-catalyzed self-switchable copolymerization from different epoxide/cyclic anhydride ROAC and oxetane/cyclic anhydride ROAC.

3.2 Experimental Section

3.2.1 Materials

Allyl glycidyl ether (AGE; >99.0%, Tokyo Kasei Kogyo Co., Ltd. (TCI)), 1,2-epoxycyclohexane (CHO; >98.0%, TCI), 1,2-butylene oxide (BO; >99.0%, TCI), ethyl glycidyl ether (EGE; >98.0%, TCI), benzyl elycidyl ether (BGE; >97.0%, TCI), 1,2-epoxycyclohexane (CHO; >98.0%, TCI), 2-ethylhexyl glycidyl ether (EHGE; >98.0%, TCI), 3-((allyloxy)methyl)-3-ethyloxetane (AMEO; >98.0%, TCI), trimethylene oxide (TO; >99.0%, TCI), 3-ethyl-3-(phenoxymethyl)oxetane (EPO; >97.0%, TCI), 2,2,3,3,4,4-hexafluoropentanedioic anhydride (HFA; >97.0%, TCI), allylsuccinic anhydride (AA; >97.0%, TCI), and 3-phenyl-1-propanol (PPA; >98%, TCI) were distilled over CaH_2 under reduced pressure and stored under nitrogen atmosphere. 5-Norbornene-endo-2,3-dicarboxylic anhydride (NA; > 99%, Sigma−Aldrich), diglycolic anhydride (DGA; >98.0%, TCI), succinic anhydride (SA; >95.0%, TCI), diphenic anhydride (DA; >98.0%, TCI), phthalic anhydride (PA; >98.0%, TCI), 4-bromophthalic anhydride (BPA; >97.0%, TCI),

n-octylsuccinic anhydride (OSA, >98.0%, TCI), and glutaric anhydride (GA; >98.0%, TCI) were recrystallized and then purified by sublimation before use. Cesium pivalate (>97.0%, TCI) was dried by heating at 100°C under high vacuum for at least 72 h prior to use. *α*-Terpinene (>99.0%, TCI), maleic anhydride (MA; >99.0%, TCI), and 1,4-benzenedimethanol (BDM; >99.0%, TCI) was used as received.

3.2.2 Instruments

The polymerization was carried out in a gas purification system (molecular sieves and copper catalyst) equipped MBRAUN stainless steel glovebox in a dry argon atmosphere (H_2O, O_2 <0.1 ppm). The moisture and oxygen contents in the glovebox were monitored with MB-MO-SE 1 and MB-OX-SE 1, respectively.

The size exclusion chromatography (SEC) is utilizing a Shodex GPC-101 system equipped with a Shodex K-G guard column and a set of two Shodex K-805L columns (linear, 8 mm × 300 mm; bead size, 5 μm; exclusion limit, 4×10^6). The measurement was performed in THF (flow rate, 1.0 mL min^{-1}) at 40 °C. Polystyrene (PS) standard samples were used for calibration.

^{1}H NMR spectra were recorded at 25 °C on a JEOL JNMA400II instrument (400 MHz) using chloroform-d_1 as the solvent and chemical shifts were referenced to an internal standard. DOSY NMR analyses were carried out at 30 ºC on a JEOL JNMA400II instrument (400 MHz) with at least 15 gradient increments using the ledbpgp2s sequence.

3.2.3. Synthesis detail

Synthesis of the *rac-cis-endo*-1-isopropyl-4-methyl-bicyclo[2.2.2]oct-5-ene-2,3-dicarboxylic anhydride (DPMA)

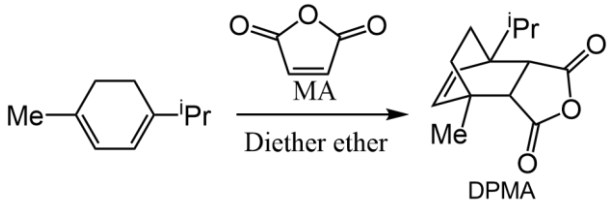

Scheme 3.2. Synthesis of the DPMA.

DPMA was synthesized according to literature procedure.[28] Maleic anhydride (3.4 g, 34 mmol) was dissolved in 100 mL of diethyl ether in a 250-mL round bottom flask. Technical grade α-terpinene (5.0 g, 35 mmol) was then added. The mixture immediately turned yellow. The flask was fitted with a condenser, and the mixture was refluxed for 36 h. After cooling the mixture to 22 °C, the solvent was removed by rotary evaporation to give a yellow oil. The crude mixture was purified by flash column chromatography using 15% ethyl acetate/hexanes as the eluent (R_f = 0.44) to give a colorless oil that solidified upon standing; the solid was dried overnight before use.

Competitive copolymerization of two anhydrides and ethyl glycidyl ether (EGE) catalyzed by cesium pivalate.

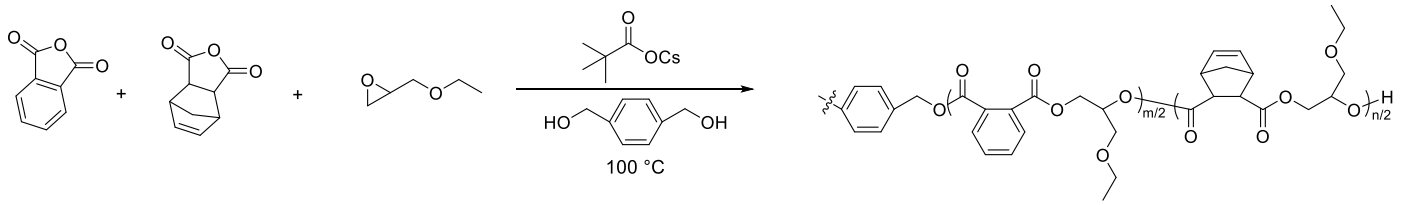

Scheme 3.3. Competitive copolymerization of two anhydrides and EGE catalyzed by cesium pivalate.

A typical procedure is presented as follows: In an argon-filled glovebox, cesium pivalate (9.3 mg, 0.02 mmol), 1,4-benzenedimethanol (BDM) (5.5 mg, 0.04 mmol), phthalic anhydride (PA) (74.1 mg, 0.5 mmol), 5-norbornene-endo-2,3-dicarboxylic anhydride (NA) (81.1mg, 0.5 mmol), and ethyl glycidyl ether (EGE) (306.4 mg, 3.0 mmol) were placed in an oven-dried reaction vessel with a magnetic stir. The reaction mixture was stirred at 100 °C under an argon atmosphere in an oil bath. During polymerization, a crude aliquot was time-regularly obtained from the system by a syringe under an argon flow and monitored by ^{1}H NMR spectroscopy and SEC to determine monomer conversion and molar mass. After the defined time, the polymerization was terminated by diluting the reaction mixture with dichloromethane (CH_2Cl_2). The reaction mixture was purified by reprecipitation from a CH_2Cl_2 solution into cold methanol. The purified polymers were dried under vacuum at room temperature for the next analysis. Other competitive copolymerizations of two anhydrides/epoxides were performed as the same procedure.

The copolymerization of NA/DA/3-ethyl-3-(phenoxymethyl)oxetane (EPO) catalyzed by the cesium pivalate.

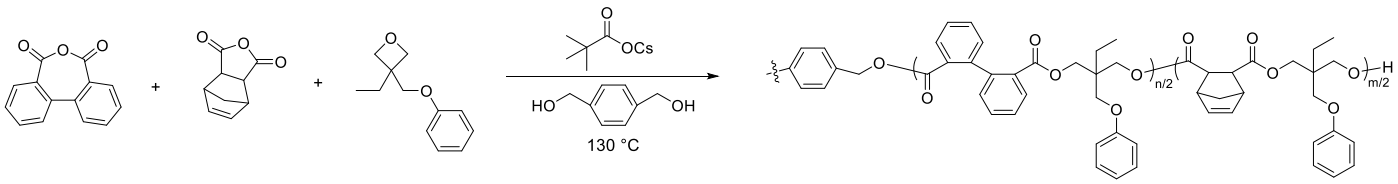

Scheme 3.4. Copolymerization of NA/DA/EPO catalyzed by the cesium pivalate.

In an argon-filled glovebox, cesium pivalate (18.6 mg, 0.04 mmol), BDM (5.5 mg, 0.04 mmol), DA (134.5 mg, 0.6 mmol), NA (97.3mg, 0.6 mmol), and EPO (691.9 mg, 3.6 mmol) were placed in an oven-dried reaction vessel with a magnetic stir. The reaction mixture was stirred at 130 °C under an argon atmosphere in an oil bath. During polymerization, a crude aliquot was time-regularly obtained from the system by a syringe in an argon flow and monitored by ^{1}H NMR spectroscopy and SEC to determine monomer conversion and

molar mass. After the defined time, the polymerization was terminated by diluting the reaction mixture with dichloromethane (CH_2Cl_2). The reaction mixture was purified by reprecipitation from a CH_2Cl_2 solution into cold methanol, and the obtained polymers were purified again by dialysis. The purified polymers were dried under vacuum at room temperature for the next analysis.

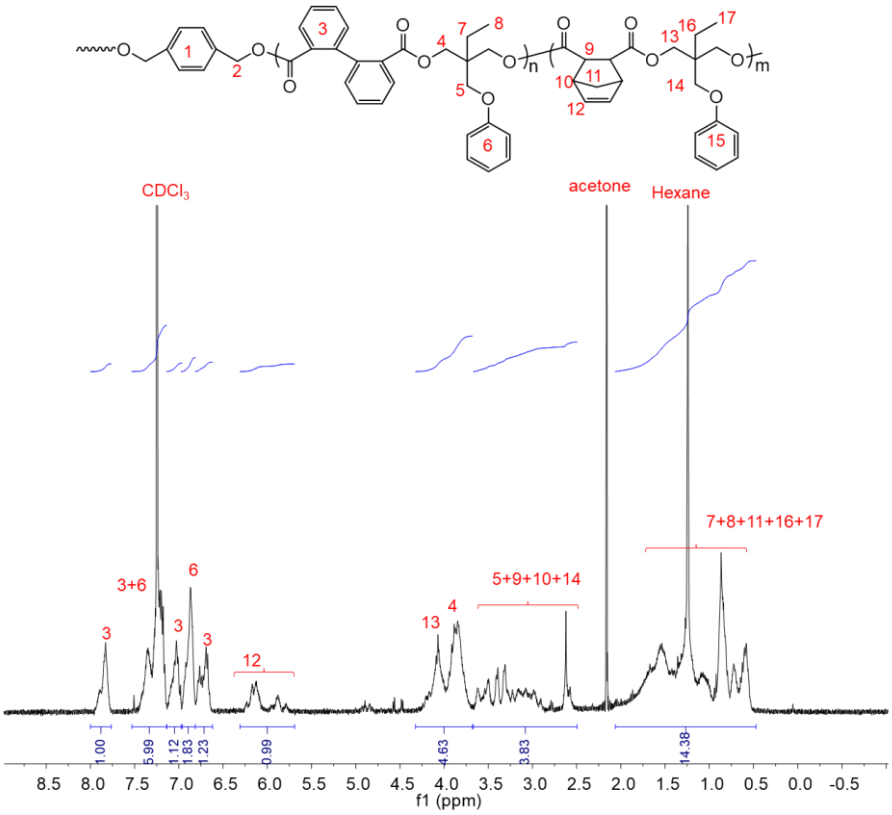

Figure 3.1. ^{1}H NMR ($CDCl_3$) spectrum of the resultant polymer synthesized from NA, DA, and EPO.

Copolymerization of PA/1,2-epoxycyclohexane (CHO)/EPO catalyzed by the cesium pivalate.

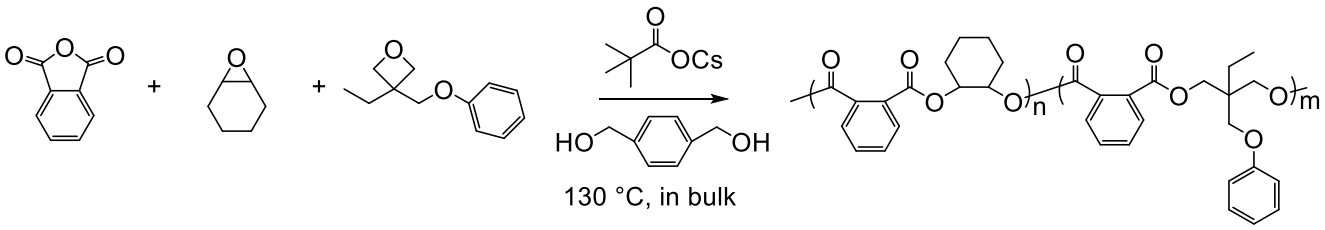

Scheme 3.5. Copolymerization of PA/CHO/EPO catalyzed by the cesium pivalate.

In an argon-filled glovebox, cesium pivalate (18.6 mg, 0.04 mmol), BDM (5.5 mg, 0.04 mmol), PA (88.8 mg, 0.6 mmol), CHO (58.8 mg, 0.6 mmol), and EPO (691.9 mg, 3.6 mmol) were placed in an oven-dried reaction vessel with a magnetic stir. The reaction mixture was stirred at 130 °C under an argon atmosphere in an oil bath. During polymerization, a crude aliquot was time-regularly obtained from the system by a syringe in an argon flow and monitored by ^{1}H NMR spectroscopy and SEC to determine monomer conversion and molar mass. After the defined time, the polymerization was terminated by diluting the reaction mixture with dichloromethane (CH_2Cl_2). The reaction mixture was purified by reprecipitation from a CH_2Cl_2 solution into cold methanol, and the obtained polymers were purified again by dialysis. The purified polymers were dried under vacuum at room temperature for the next analysis.

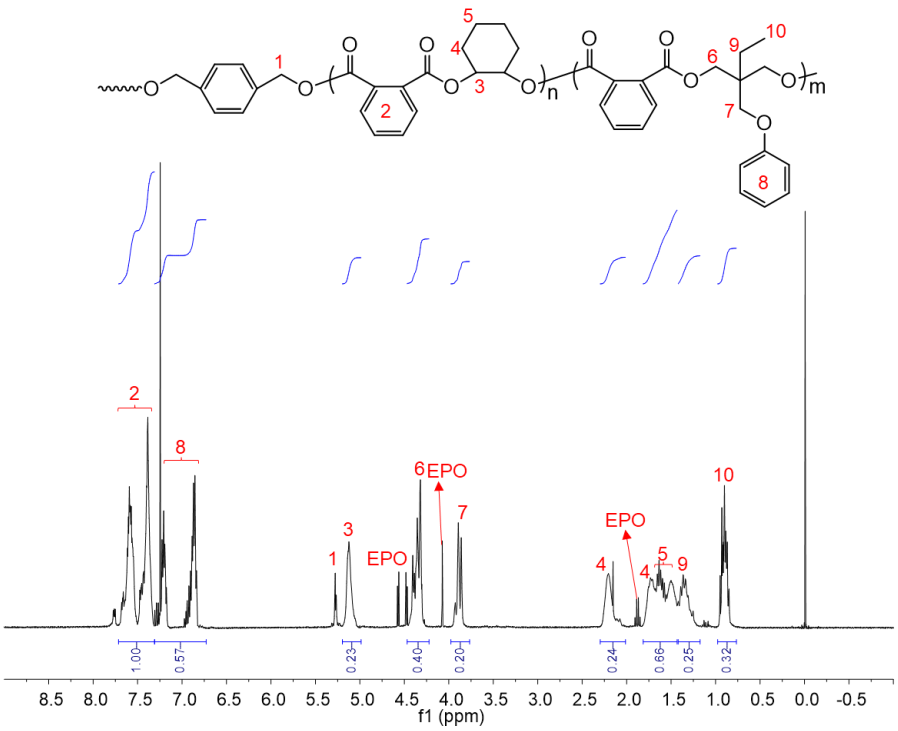

Figure 3.2. ^{1}H NMR ($CDCl_3$) spectrum of the resultant polymer synthesized from PA, CHO, and EPO. (entry 1 in Table 3.3).

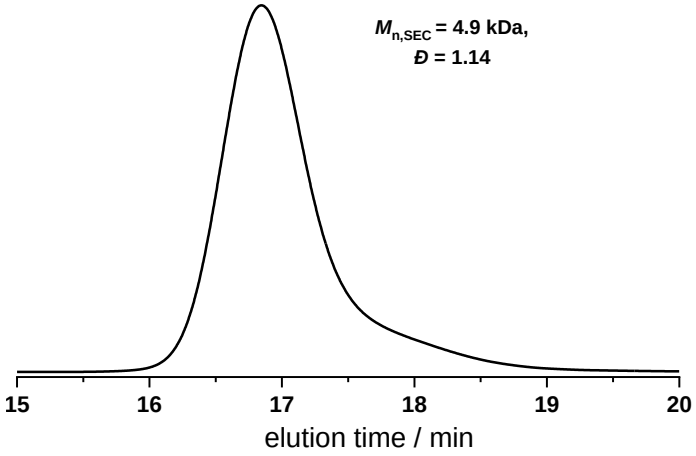

Figure 3.3. SEC (THF) trace of the resultant polymer synthesized from PA, CHO, and EPO. (entry 1 in Table 3.3).

Copolymerization of PA/allyl glycidyl ether (AGE)/EPO catalyzed by the cesium pivalate.

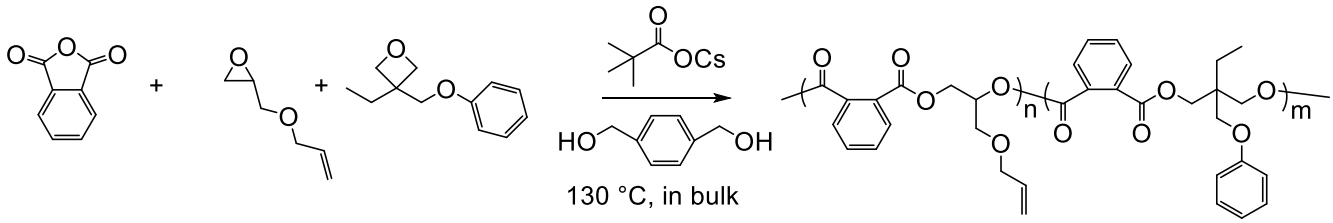

Scheme 3.6. Copolymerization of PA/AGE/EPO catalyzed by the cesium pivalate.

In an argon-filled glovebox, cesium pivalate (18.6 mg, 0.04 mmol), BDM (5.5 mg, 0.04 mmol), PA (88.8 mg, 0.6 mmol), AGE (68.5 mg, 0.6 mmol), and EPO (691.9 mg, 3.6 mmol) were placed in an oven-dried reaction vessel with a magnetic stir. The reaction mixture was stirred at 130 °C under an argon atmosphere in an oil bath. During polymerization, a crude aliquot was time-regularly obtained from the system by a syringe in an argon flow and monitored by ^{1}H NMR spectroscopy and SEC to determine monomer conversion and molar mass. After the defined time, the polymerization was terminated by diluting the reaction mixture with

dichloromethane (CH_2Cl_2). The reaction mixture was purified by reprecipitation from a CH_2Cl_2 solution into cold methanol, and the obtained polymers were purified again by dialysis. The purified polymers were dried under vacuum at room temperature for the next analysis.

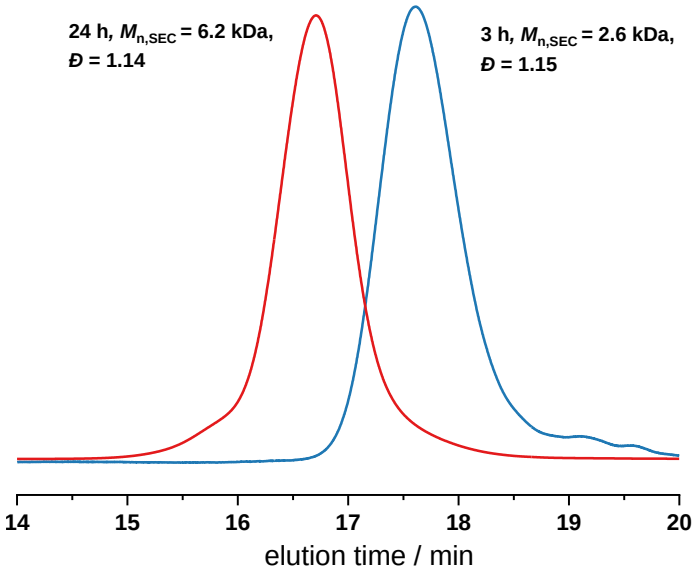

Figure 3.4. SEC (THF) trace of the resultant polymer synthesized from PA, AGE, and EPO (entry 3 in Table 3.3).

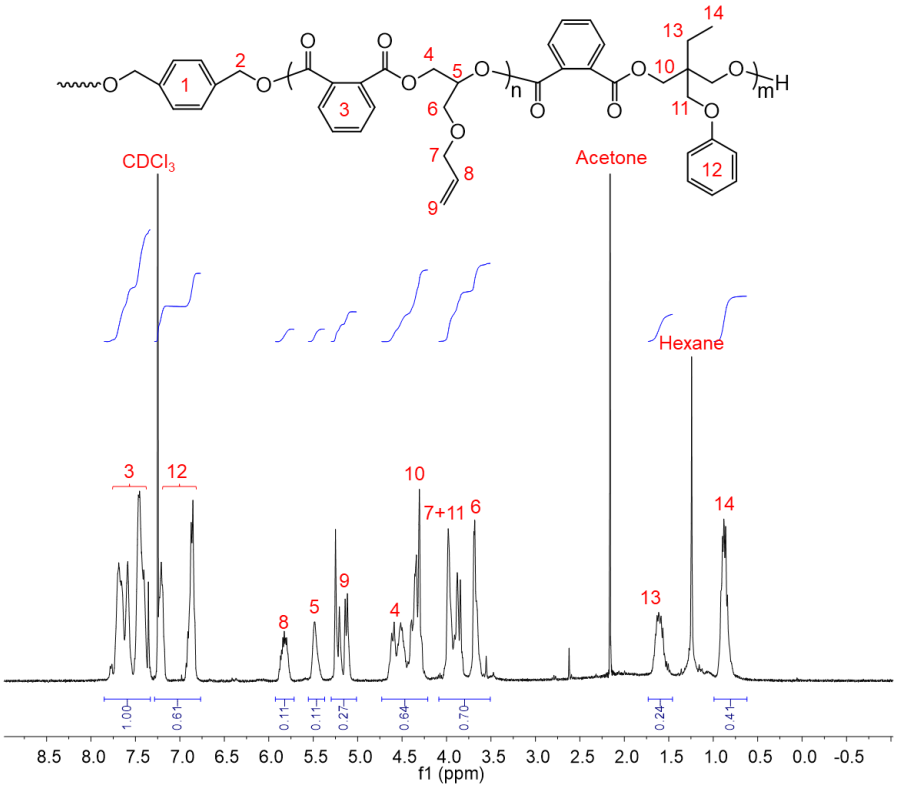

Figure 3.5 ^{1}H NMR ($CDCl_3$) spectrum of the resultant polymer synthesized from PA, AGE, and EPO (entry 3 in Table 3.3).

The polymerization from the mixture of DA, CHO, NA, and EPO catalyzed by cesium pivalate.

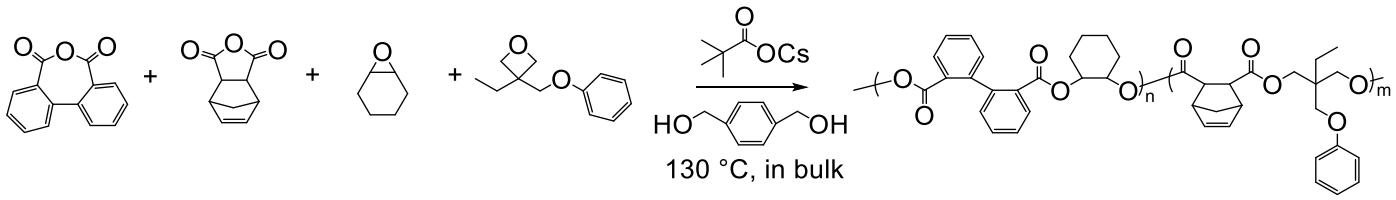

Scheme 3.7. Polymerization from the mixture of DA, CHO, NA, and EPO catalyzed by cesium pivalate.

In an argon-filled glovebox, cesium pivalate (18.6 mg, 0.04 mmol), BDM (5.5 mg, 0.04 mmol), DA (134.5 mg, 0.6 mmol), CHO (117.6 mg, 1.2 mmol), NA (197.0 mg, 1.2 mmol), and EPO (1230.1 mg, 6.4 mmol) were placed in an oven-dried reaction vessel with a magnetic stir. The reaction mixture was stirred at 130 °C under an argon atmosphere in an oil bath. During polymerization, a crude aliquot was time-regularly obtained from the system by a syringe in an argon flow and monitored by ^{1}H NMR spectroscopy and SEC to

determine monomer conversion and molar mass. After the defined time, the polymerization was terminated by diluting the reaction mixture with dichloromethane (CH_2Cl_2). The reaction mixture was purified by reprecipitation from a CH_2Cl_2 solution into cold methanol, and the obtained polymers were purified again by dialysis. The purified polymers were dried under vacuum at room temperature for the next analysis.

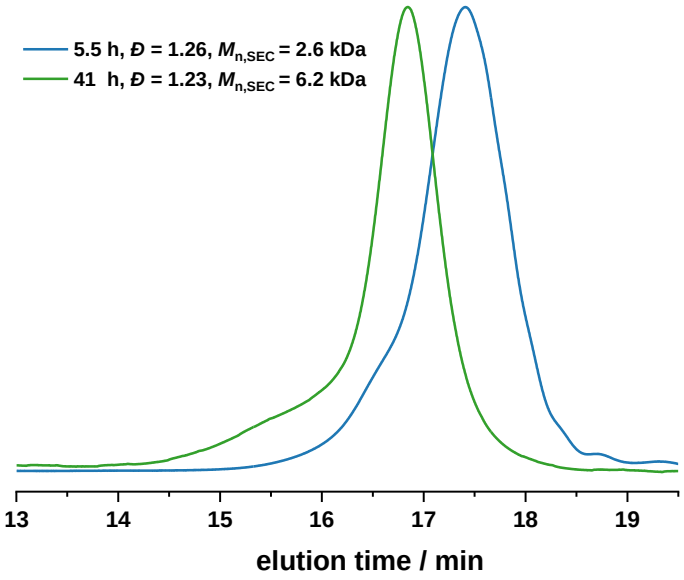

Figure 3.6. SEC (THF) trace of the resultant polymer synthesized from DA, CHO, NA, and EPO (entry 2 in Table 3.4).

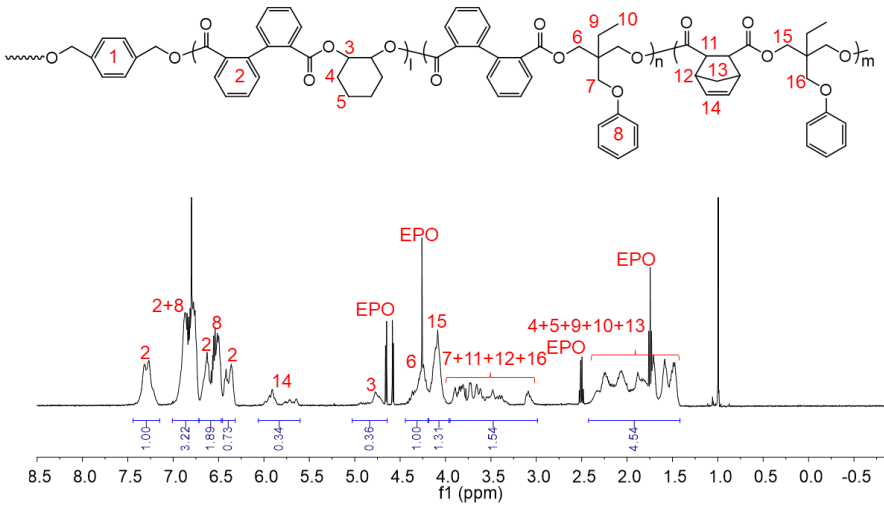

Figure 3.7. ^{1}H NMR ($CDCl_3$) spectrum of the resultant polymer synthesized from DA, CHO, NA, and EPO (entry 2 in Table 3.4).

The polymerization from the mixture of PA, Benzyl Glycidyl Ether (BGE), NA, and TO catalyzed by cesium pivalate.

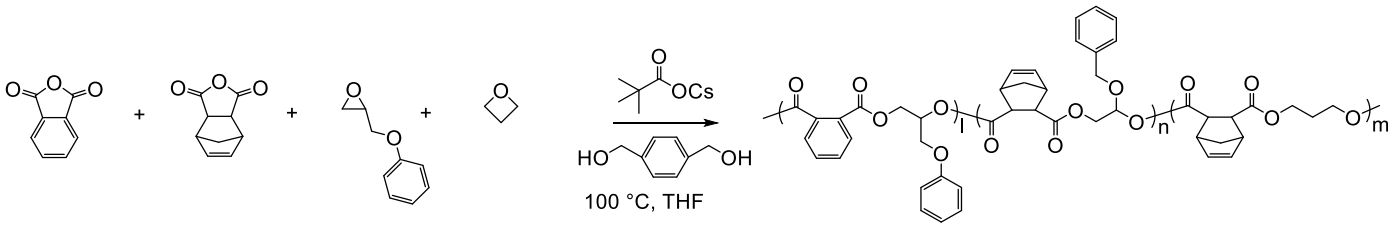

Scheme 3.8. Polymerization from the mixture of PA, Benzyl Glycidyl Ether (BGE), NA, and TO catalyzed by cesium pivalate.

In an argon-filled glovebox, cesium pivalate (18.6 mg, 0.04 mmol), BDM (5.5 mg, 0.04 mmol), PA (88.8 mg, 0.6 mmol), BGE (98.5 mg, 0.6 mmol), NA (98.5 mg, 0.6 mmol), TO (52.3 mg, 0.9 mmol), and THF (400 µl) were placed in an oven-dried reaction vessel with a magnetic stir. The reaction mixture was stirred at 110 °C under an argon atmosphere in an oil bath. During polymerization, a crude aliquot was time-regularly obtained from the system by a syringe in an argon flow and monitored by ^{1}H NMR spectroscopy and SEC to determine monomer conversion and molar mass. After the defined time, the polymerization was terminated

by diluting the reaction mixture with dichloromethane (CH_2Cl_2). The reaction mixture was purified by reprecipitation from a CH_2Cl_2 solution into cold methanol, and the obtained polymers were purified again by dialysis. The purified polymers were dried under vacuum at room temperature for the next analysis. Other polymerizations of two different anhydrides/epoxides/oxetanes were performed as same procedure.

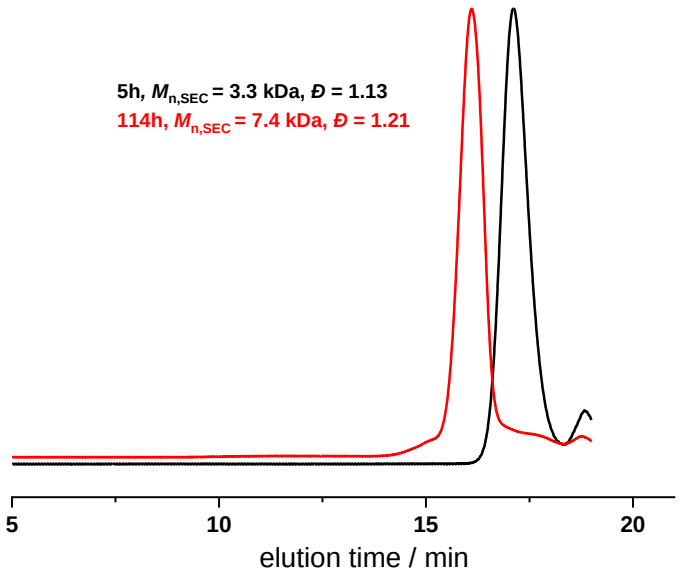

Figure 3.8. SEC (THF) trace of the resultant polymer synthesized from PA, BGE, NA, and TO (entry 4 in Table 3.4).

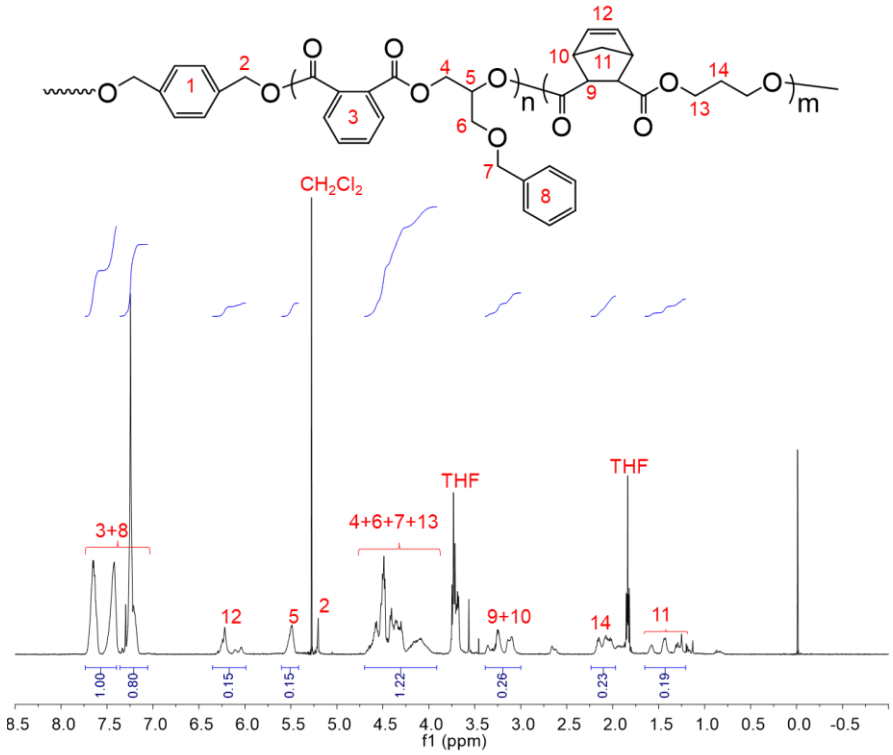

Figure 3.9 ^{1}H NMR ($CDCl_3$) spectrum of the resultant polymer synthesized from PA, BGE, NA, and TO (entry 4 in Table 3.4).

3.3 Results and Discussion

3.3.1 Terpolymerization of one epoxide and two cyclic anhydrides for one-step synthesis of block polyester

To investigate sequential incorporation based on the reactivity differences among the anhydrides (Scheme 3.2), the author attempted polymerization from a phthalic anhydride (PA), 5-norbornene-endo-2,3-dicarboxylic anhydride (NA), and ethyl glycidyl ether (EGE) mixture, which led to a block-like copolymer rather than a random copolymer. Using EGE as the model with *t*-$BuCO_2Cs$ and 1,4-benzenedimethanol (BDM) as the catalyst and initiator, respectively, ring-opening copolymerization (ROCOP) was performed at 100 °C with an $[PA]_0/[NA]_0/[EGE]_0/[BDM]_0/[t\text{-}BuCO_2Cs]$ ratio of 25/25/150/2/1 (entry 1, Table 3.1). Specifically, PA/EGE ROAC occurred first, as evidenced by the decreased ^{1}H NMR signals at 8.0 and 7.9 ppm (proton 3') corresponding to PA and the appearance of ^{1}H NMR signals associated with poly(PA-*alt*-

EGE) at 5.5–5.4 ppm (proton 5) and 7.4–7.8 ppm (proton 3) (Figures 3.10 and 3.11). During this period, no signals appeared at 5.1–4.9 ppm (proton 14) and the signal at 6.3 ppm (proton 12', NA) unchanged, indicating that NA remained intact without poly(NA-*alt*-EGE) formation. At 98.4% PA conversion, NA/EGE ROAC turned on and poly(NA-*alt*-EGE)-*b*-poly(PA-*alt*-EGE)-*b*-poly(NA-*alt*-EGE) triblock copolymers were formed. The polymerization showed a high degree of control, as demonstrated by a narrow and monomodal distribution ($Đ$ = 1.10; entry 1, Table 3.1, Figure 3.12), and high selectivity, with a tapered region fraction of 1.6% (entry 1, Table 3.1). ^{1}H NMR signals associated with both blocks were observed (Figure 3.13) and diffusion-ordered NMR spectroscopy (DOSY) showed only one diffusion coefficient (Figure 3.14), further confirming the formation of copolymers rather than poly(PA-*alt*-EGE) and poly(NA-*alt*-EGE) blends. The chemoselectivity of the polymerization system depends on the anhydride insertion order, which follows the reactivity ratio. Wurm and co-workers reported that block-like copolymer formation via one-step polymerization from a monomer mixture requires reactivity ratios of $r_1 > 20$ and $r_2 < 0.02$.[29] The largest difference in comonomer reactivity to date has been reported for the anionic polymerization of sulfonyl-activated aziridines and ethylene oxide (EO) to produce block copolymers ($r_1 = 265$, $r_2 = 0.004$).[29]

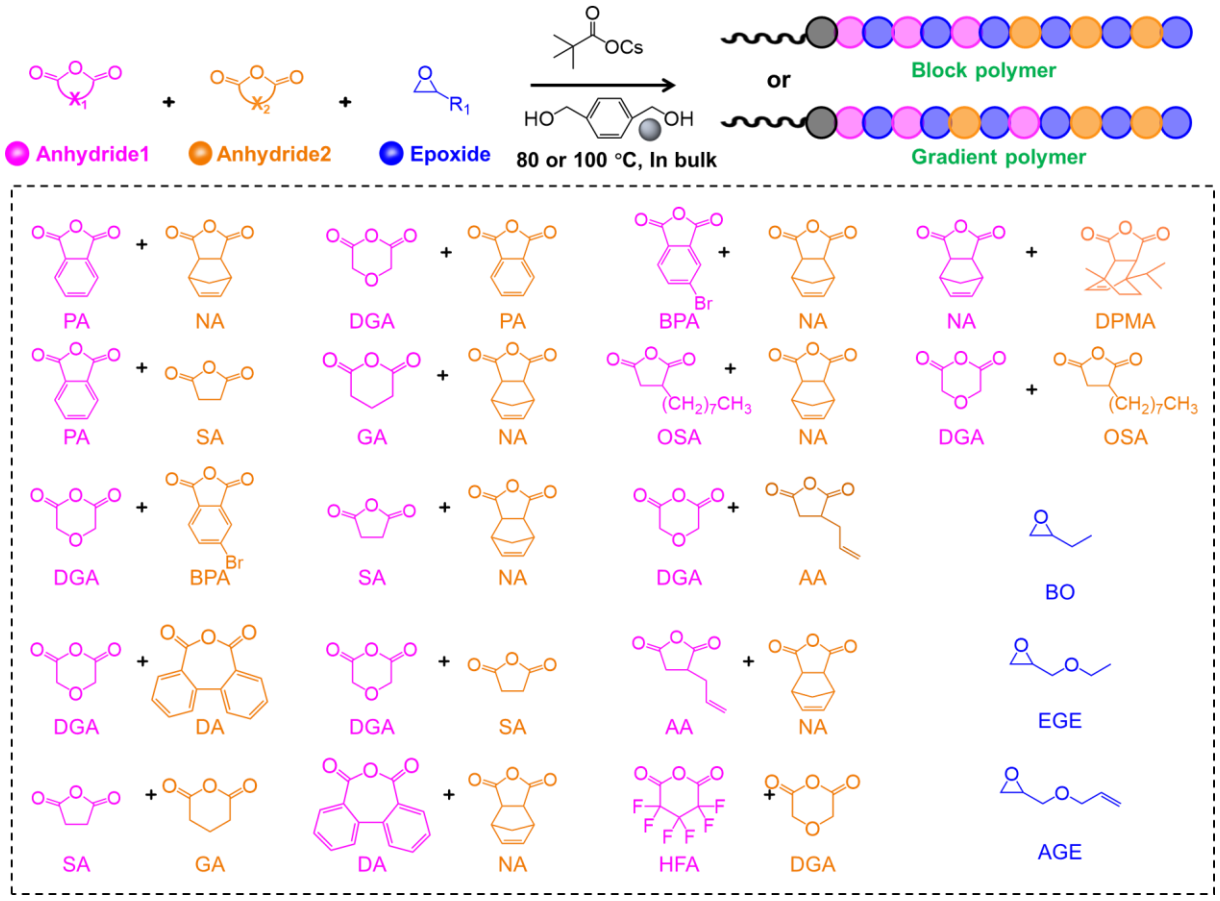

Scheme 3.9. Competitive copolymerization of two anhydrides/epoxide catalyzed by *t*-$BuCO_2Cs$.

Table 3.1. Competitive copolymerization of two anhydrides/EGE catalyzed by *t*-$BuCO_2Cs$ [a]

Entry	[anhydride1]/[anhydride2]	$[anhydride1]_0/[anhydride2]_0/[epoxide]_0/[I]_0/[cat.]_0$	Time (h)	Conv.[b][%] (anhydrides)	Copolymer type	$M_{n,th}$[c] (kDa)	$M_{n,SEC}$[d] (kDa)	$Đ$[d]
1	PA/NA	25/25/150/2/1	1.8	PA>99, NA=96.2	Block-like	6.5	4.8	1.10
2[e]	PA/NA	25/125/250/2/1	16	PA>99, NA=61.3	Block-like	13.5	10.7	1.15
3	PA/SA	25/25/150/2/1	2.5	PA>99, SA>99	Medium gradient	5.8	4.5	1.39
4[f]	DGA/BPA	25/25/150/2/1	3.7	DGA>99, BPA>99	Medium gradient	7.3	4.1	1.34
5	DGA/DA	25/25/150/2/1	2.0	DGA>99, DA>99	Medium gradient	6.9	4.8	1.37
6	SA/GA	25/25/150/2/1	5.0	SA>99, GA>99	Medium gradient	5.4	2.7	1.34
7	DGA/PA	25/25/150/2/1	3.3	DGA>99, PA=73	Hard gradient	6.0	4.5	1.35
8	GA/NA	25/25/150/2/1	6.5	GA>99, NA=76	Block-like	5.4	2.1	1.20
9	SA/NA	25/25/150/2/1	5.0	SA>99, NA=71	Block-like	5.0	4.0	1.12
10	DGA/SA	25/25/150/2/1	6.0	DGA>99, SA=78	Block-like	4.8	3.7	1.15
11	DA/NA	25/25/150/2/1	1.4	DA>99, NA=82	Block-like	6.9	3.5	1.36
12[f]	BPA/NA	25/25/150/2/1	2.0	BPA>99, NA=90	Block-like	7.5	4.8	1.22
13	OSA/NA	25/25/150/2/1	3.5	OSA>99, NA>99	Block-like	7.4	4.5	1.21
14	DGA/AA	25/25/150/2/1	7.5	DGA>99, AA>99	Block-like	5.8	3.7	1.25
15	AA/NA	25/25/150/2/1	3.5	AA>99, NA>99	Block-like	6.5	4.8	1.26
16	HFA/DGA	25/25/150/2/1	1.0	HFA>99, DGA=85	Real block	6.9	3.3	1.45
17	NA/DPMA	25/25/150/2/1	29.0	NA>99, DPMA=87	Real block	7.7	5.5	1.23
18[e,g]	NA/DPMA	25/125/250/2/1	163	NA>99, DPMA=30.1	Real block	9.7	9.0	1.15
19	DGA/OSA	25/25/150/2/1	7.5	DGA>99, OSA>99	Real block	6.7	3.6	1.30

[a]Polymerization conditions: in the bulk at 100 °C under an Ar atmosphere. [b]Determined by ^{1}H NMR analysis ($CDCl_3$). [c]Calculated using $[anhydride1]_0/[I]_0$ × conv. × (M.W. of anhydride1 + M.W. of epoxide) + $[anhydride2]_0/[I]_0$ × conv. × (M.W. of anhydride2 + M.W. of epoxide) + (M.W. of initiator). [d]Determined by SEC (THF) with a PSt standard. [e]Polymerization temperature: 80 °C. [f]Epoxide: AGE. [g]Epoxide: BO.

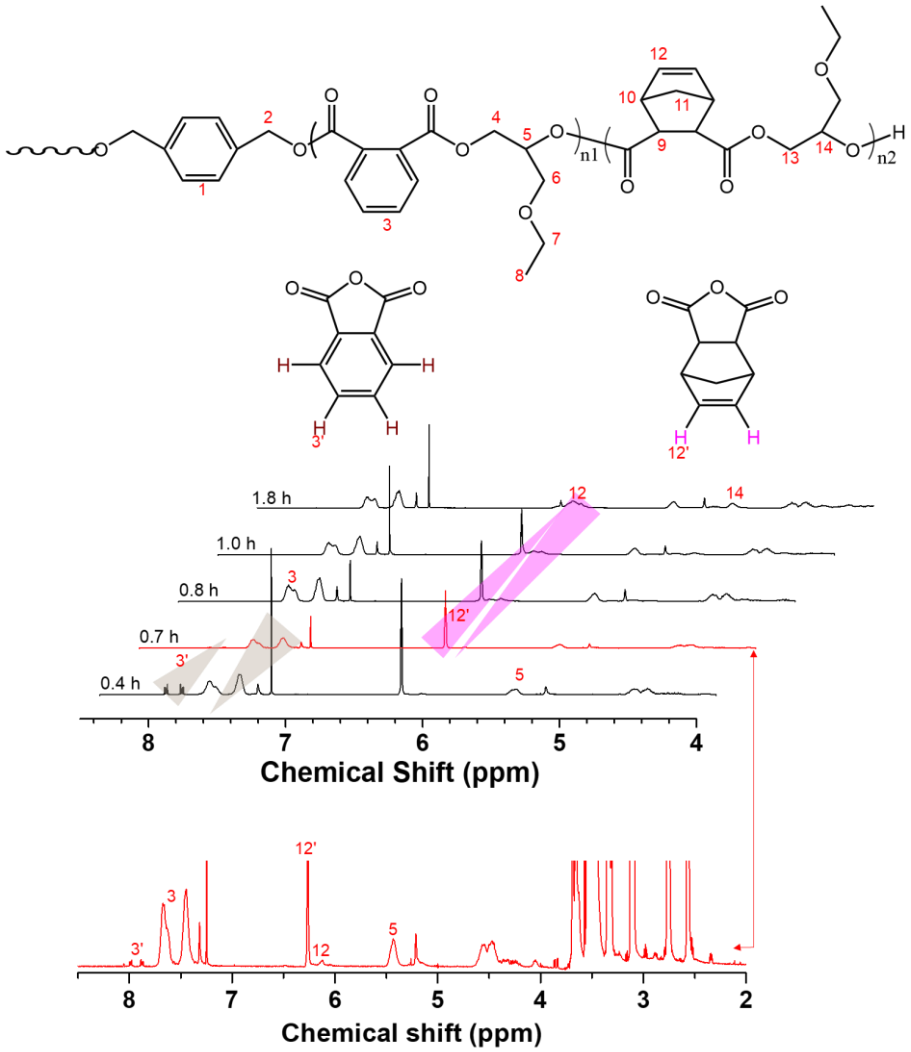

Figure 3.10. ^{1}H NMR ($CDCl_3$) spectra of crude aliquots withdrawn from the reaction system for monitoring the conversion of PA, NA and the formation of resultant copolymers (entry 1 in Table 3.1).

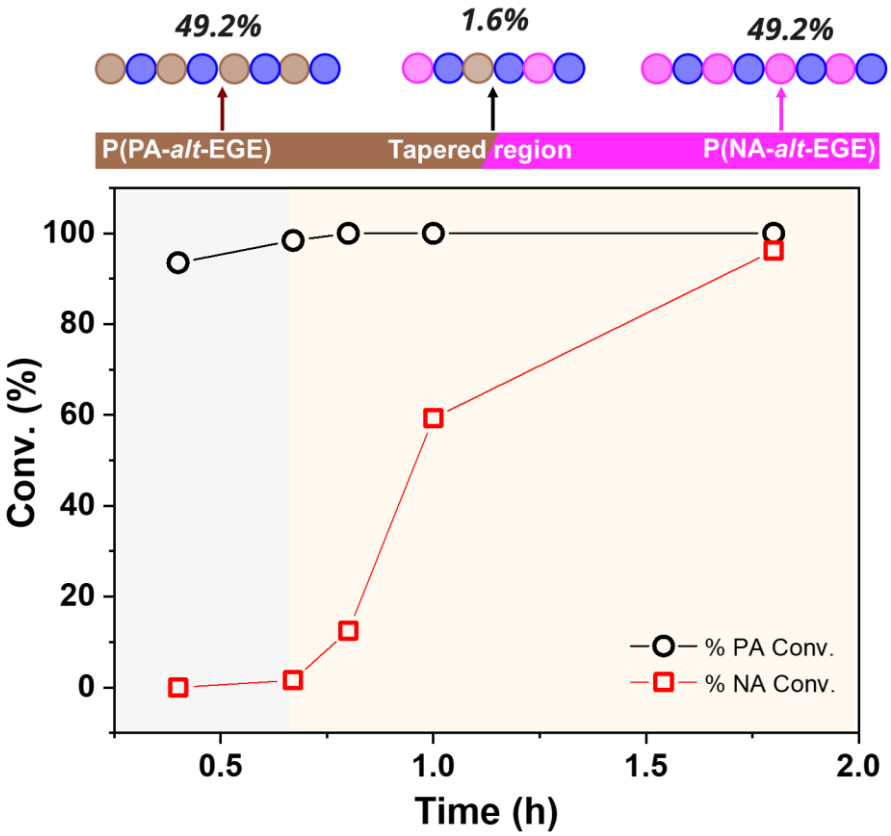

Figure 3.11. Plots of monomer conversion versus time. $[PA]_0/[NA]_0/[EGE]_0/[BDM]_0/[t\text{-}BuCO_2Cs]$ = 25/25/150/2/1 (entry 1 in Table 3.1). Conv. of PA and conv. of NA in the tapered region are 1.6% and 1.6%, respectively. The fraction of degree of polymerization (DP) of poly(PA-*b*-EGE) segment, tapered region, and poly(NA-*b*-EGE) segment are 49.2%, 1.6%, and 49.2%, respectively.

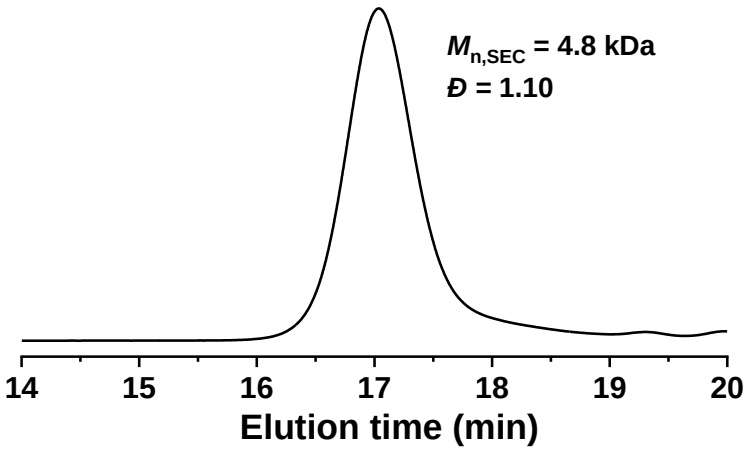

Figure 3.12. SEC (THF) trace of the resultant copolymer synthesized from PA, NA, and EGE (entry 1 in Table 3.1).

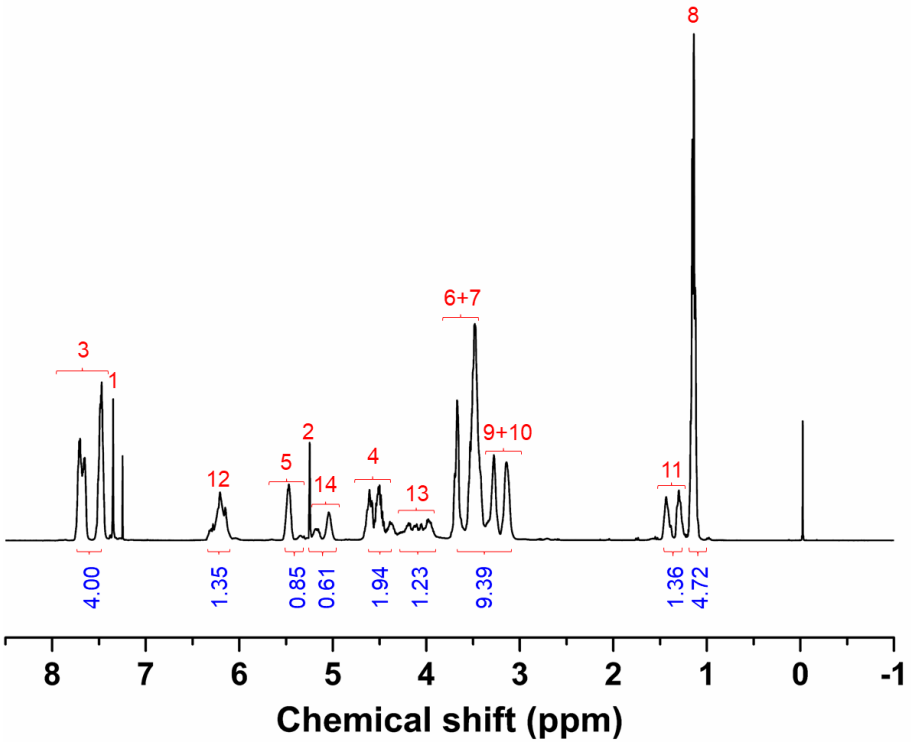

Figure 3.13. ^{1}H NMR ($CDCl_3$) spectrum of the resultant copolymer synthesized from PA, NA, and EGE (entry 1 in Table 3.1).

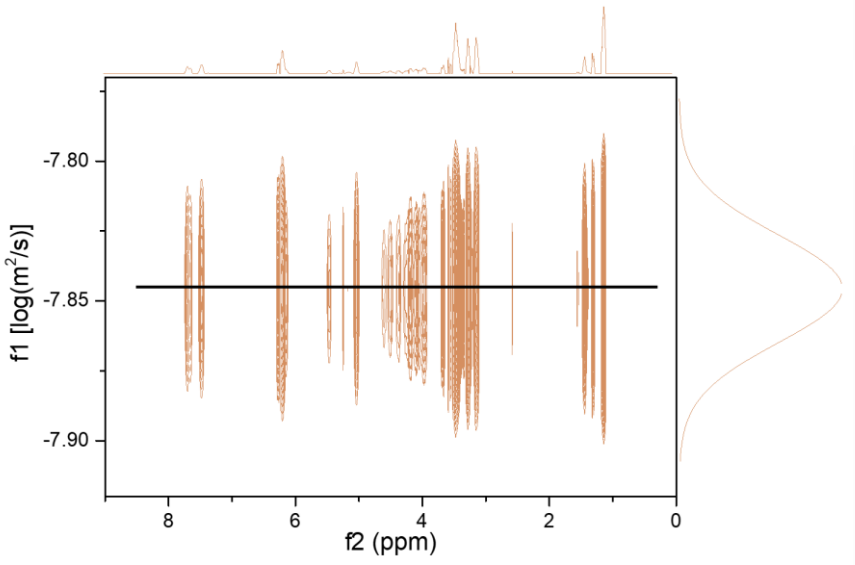

Figure 3.14. DOSY NMR ($CDCl_3$) spectrum of the resultant copolymer synthesized from PA, NA, and EGE (entry 1 in Table 3.1).

In the copolymerization system of PA/NA/EGE, anhydride/epoxide pair such as PA(A)/EGE(C) can be regarded as one monomer (AC), and the rate of monomer incorporation does not exhibit a strong dependence on the identity of terminal unit but instead is dictated solely by the nature of the anhydride (Figure 3.15). Therefore, a nonterminal copolymerization model (Beckingham–Sanoja–Lynd; BSL) was used to capture compositional drift data,[30] and the obtained reactivity ratios are shown in Table 3.2. Compared with previous systems, the reactivity difference between PA and NA was considerably larger (r_{PA} = 739.83, r_{NA} = 0.0055) (Figure 3.16), confirming that PA is more reactive than NA, which allowed the formation of a near perfect triblock polymer (entry 1, Table 3.2). When the PA/NA molar ratio was changed to 1/5 (r_{PA} = 704.83, r_{NA} = 0.0065), high chemoselectivity was maintained to produce a block-like copolymer with a tapered region of <5.6% (entry 2, Tables 3.1 and 3.2, Figures 3.17–3.19). Thus, the PA/NA ratio has little influence on the anhydride reactivity ratios or the chemoselectivity of the polymerization system.

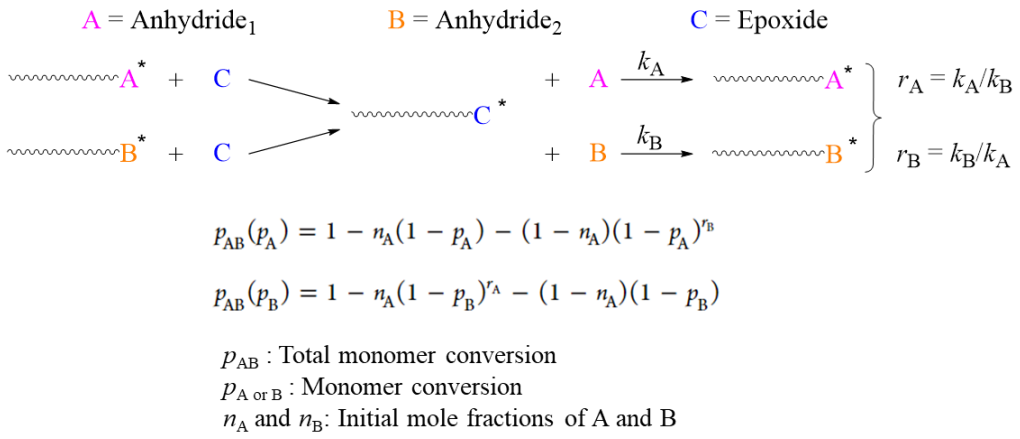

Figure 3.15. Reactivity ratios are defined by the ratios of the propagation rate constants for adding a monomer to a growing chain end of the same alcohol.

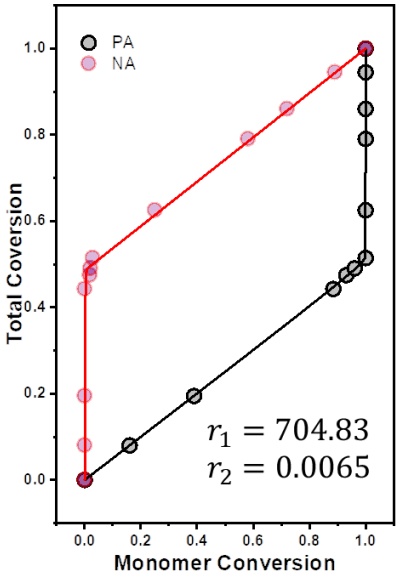

Figure 3.16. Total polymerization conversion plotted against monomer conversion and the data were obtained from time-resolved ^{1}H NMR spectra of a cesium pivalate-catalyzed copolymerization of PA/NA/EGE at 100 °C: a molar ratio of 25/125/250. Solid black and red lines represent fits to the experimental data using the nonterminal model.

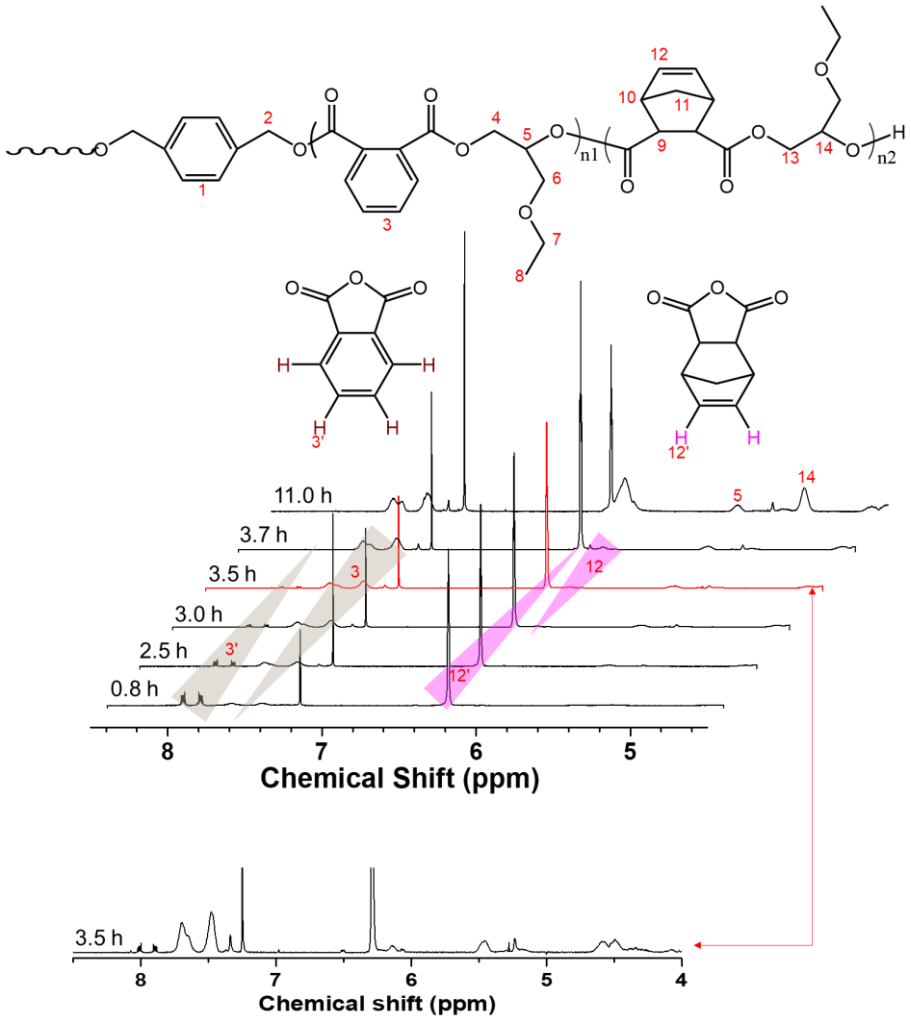

Figure 3.17. ^{1}H NMR ($CDCl_3$) spectra of crude aliquots withdrawn from the reaction system for monitoring the conversion of PA, NA and the formation of resultant copolymers (entry 2 in Table 3.1).

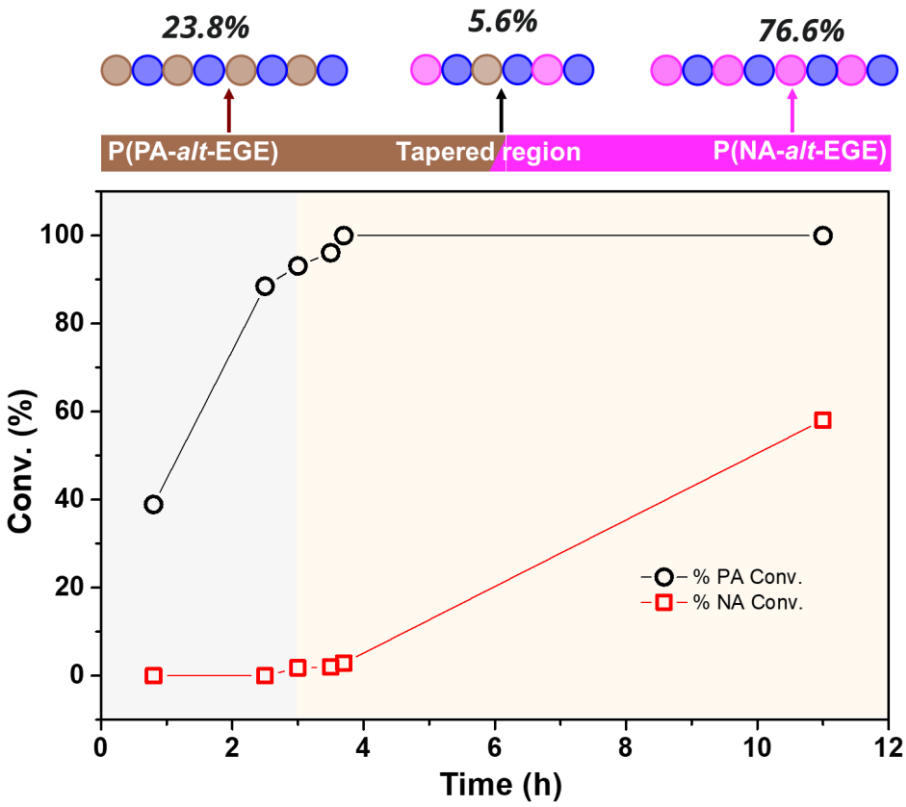

Figure 3.18. Plots of monomer conversion versus time. $[PA]_0/[NA]_0/[EGE]_0/[BDM]_0/[t\text{-}BuCO_2Cs]$ = 25/125/250/2/1 (entry 2 in Table 3.1). Conv. of PA and conv. of NA in the tapered region are 6.9% and 2.9%, respectively. The fraction of DP of poly(PA-*b*-EGE) segment, tapered region, and poly(NA-*b*-EGE) segment are 23.8%, 5.6%, and 76.6%, respectively.

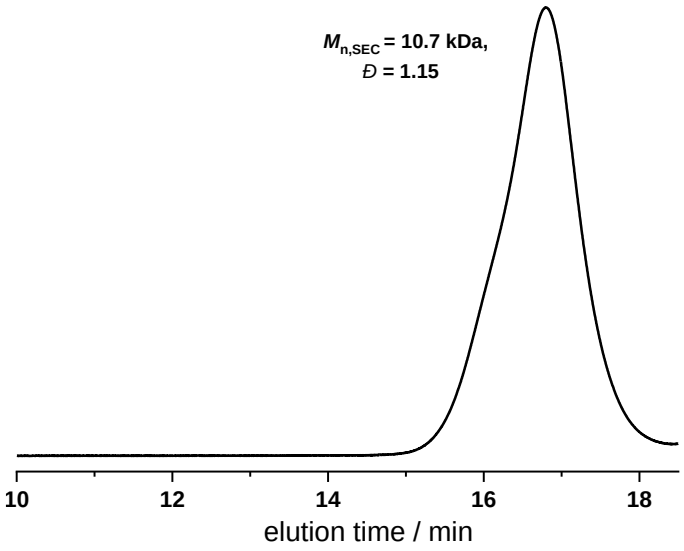

Figure 3.19. SEC (THF) trace of the resultant copolymer synthesized from PA, NA, and EGE (entry 2 in Table 3.1).

Table 3.2. Comonomer reactivity ratios and distributions for copolymerizations of two anhydrides/EGE.[a]

entry	Monomers (1/2)	Reactivity ratio r_1, r_2	Comonomer distribution	DP of tapered region and its fraction (%)
1	PA/NA	739.83, 0.0055	Block-like	0.4 (1.6)
[b]2	PA/NA	704.83, 0.0065	Block-like	2.7 (5.6)
[c]3	DGA/BPA	3.45, 0.33	Medium gradient	21.3 (85.2)
4	DGA/DA	4.51, 0.48	Medium gradient	20.8 (83.2)
5	PA/SA	4.59, 0.63	Medium gradient	20.1 (80.4)
6	SA/GA	4.78, 0.34	Medium gradient	19.6 (78.4)
7	DGA/PA	10.98, 0.034	Hard gradient	12.3 (49.2)
8	DGA/AA	448.02, 0.0263	Block-like	3.7 (14.9)
9	GA/NA	516.27, 0.0204	Block-like	2.9 (11.6)
10	DGA/SA	605.70, 0.0062	Block-like	2.4 (9.4)
11	SA/NA	634.02, 0.0057	Block-like	2.1 (8.3)
12	DA/NA	698.72, 0.0053	Block-like	1.4 (5.7)
13	OSA/NA	711.44, 0.0061	Block-like	1.4 (5.4)
14	AA/NA	730.55, 0.0058	Block-like	1.2 (4.7)
[c]15	BPA/NA	746.38, 0.0049	Block-like	0.4 (1.5)
16	HFA/DGA	816.39, 0.0036	Real block	0 (0)
17	NA/DPMA	814.83, 0.0047	Real block	0 (0)
[b,d]18	NA/DPMA	811.26, 0.0045	Real block	0 (0)
19	DGA/OSA	803.47, 0.0047	Real block	0 (0)

[a]Polymerization conditions: in the bulk at 100 °C under an Ar atmosphere. [b]Polymerization temperature: 80 °C and ratio of PA/NA is 1/5. [c]Epoxide: AGE. [d]Epoxide: BO. DP: degree of polymerization.

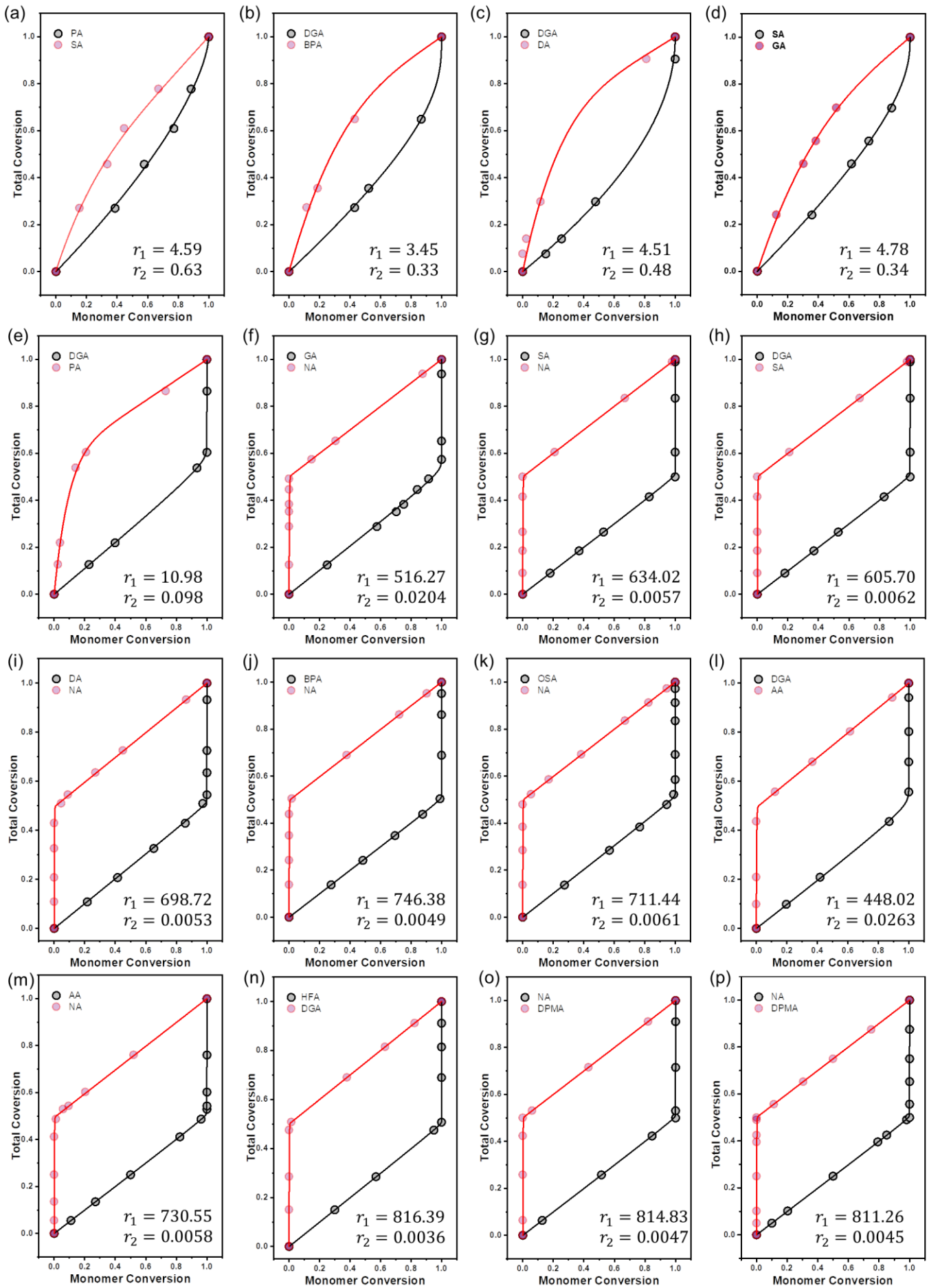
(a)
PA
SA
$r_1 = 4.59$
$r_2 = 0.63$
(b)
DGA
BPA
$r_1 = 3.45$
$r_2 = 0.33$
(c)
DGA
DA
$r_1 = 4.51$
$r_2 = 0.48$
(d)
SA
GA
$r_1 = 4.78$
$r_2 = 0.34$
(e)
DGA
PA
$r_1 = 10.98$
$r_2 = 0.098$
(f)
GA
NA
$r_1 = 516.27$
$r_2 = 0.0204$
(g)
SA
NA
$r_1 = 634.02$
$r_2 = 0.0057$
(h)
DGA
SA
$r_1 = 605.70$
$r_2 = 0.0062$
(i)
DA
NA
$r_1 = 698.72$
$r_2 = 0.0053$
(j)
BPA
NA
$r_1 = 746.38$
$r_2 = 0.0049$
(k)
OSA
NA
$r_1 = 711.44$
$r_2 = 0.0061$
(l)
DGA
AA
$r_1 = 448.02$
$r_2 = 0.0263$
(m)
AA
NA
$r_1 = 730.55$
$r_2 = 0.0058$
(n)
HFA
DGA
$r_1 = 816.39$
$r_2 = 0.0036$
(o)
NA
DPMA
$r_1 = 814.83$
$r_2 = 0.0047$
(p)
NA
DPMA
$r_1 = 811.26$
$r_2 = 0.0045$
Total Coversion
Monomer Conversion

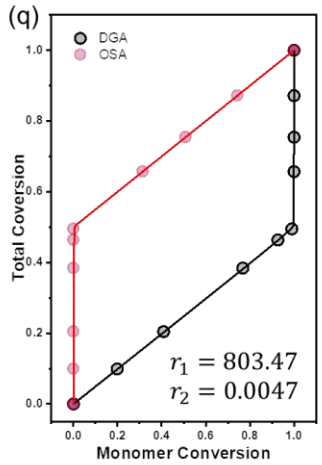

Figure 3.20. Total polymerization conversion plotted against monomer conversion in Table 3.2, and the data were obtained from time-resolved ^{1}H NMR spectra of a cesium pivalate-catalyzed copolymerization of EGE and two anhydrides at 100 °C: a molar ratio of 25/25/150. Solid black and red lines represent fits to the experimental data using the nonterminal model.

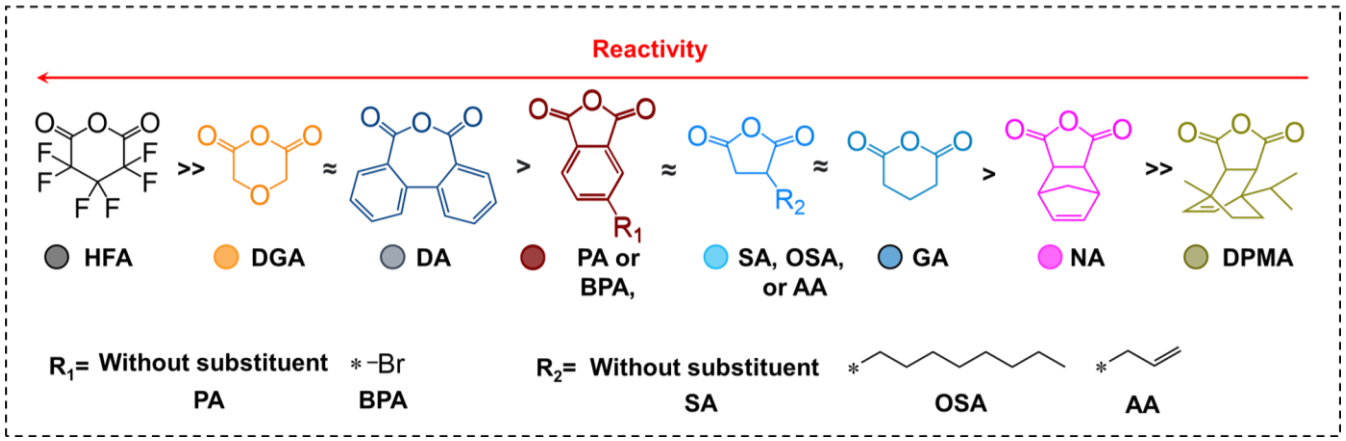

Figure 3.21. Established reactivity gradient among cyclic anhydrides.

With these results, the reactivity ratios between various anhydrides were systematically studied to build a reactivity gradient (Table 3.2, Figure 3.20, Figure 3.21). The copolymerization of EGE with a PA/ succinic anhydride (SA) mixture (r_{PA} = 4.59, r_{SA} = 0.63; Figure 3.20a, entry 5, Table 3.2) produced copolymers with medium gradient strengths (Figures 3.22–3.25). For the medium gradient, the separated blocks can be built, but its proportion is very small. In this study, the author suggest defining a soft gradient for reactivity ratios

of $r_1 \leq 5$ and $r_2 \geq 0.3$. The final products showed four ^{1}H NMR peaks corresponding to the main-chain methine protons of EGE at 5.6–5.0 ppm, in which the random insertion of PA and SA formed additional junction units (5.4–5.3 ppm for PA-EGE-SA (proton 10) and 5.3–5.2 ppm for SA-EGE-PA (proton 8); Figure 3.23). Monomer mixtures with smaller reactivity ratio differences ($2 < r_1 < 5$, $0.3 < r_2 < 0.7$; entries 3–6, Table 3.2), such as DGA/4-bromophthalic anhydride (BPA)/allyl glycidyl ether (AGE), diglycolic anhydride (DGA)/diphenic anhydride (DA)/EGE, and SA/glutaric anhydride (GA)/EGE, gave copolymers with medium gradient strengths (Figures 3.26–3.33). These copolymers showed monomodal distributions with relatively narrow dispersities ($Đ < 1.40$; entries 3–6, Table 3.1). However, the tapered region fraction (78.4–85.2%) varied depending on the anhydride reactivity ratios (entries 3–6, Table 3.2). Copolymers with medium-gradient microstructures, the properties of which differ considerably from those of random copolymers, have been applied as compatibilizers in polymer blends, which decreases domain size significantly when compared with block copolymers.[31, 32]

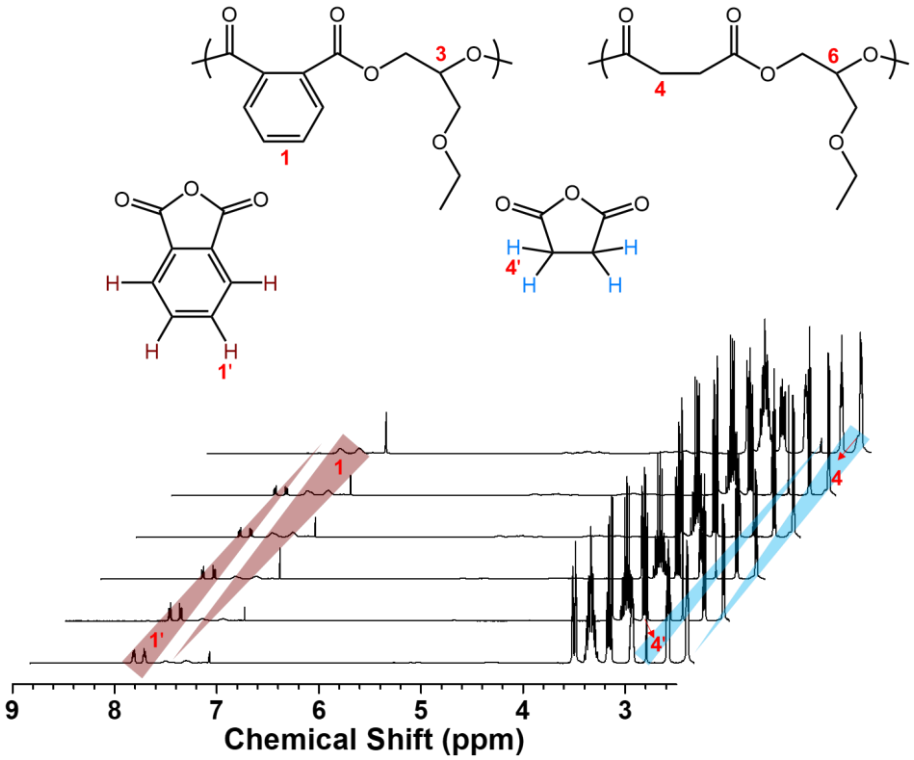

Figure 3.22. ^{1}H NMR ($CDCl_3$) spectra of crude aliquots withdrawn from the reaction system for monitoring the conversion of PA, SA, and the formation of resultant copolymers (entry 3 in Table 3.1).

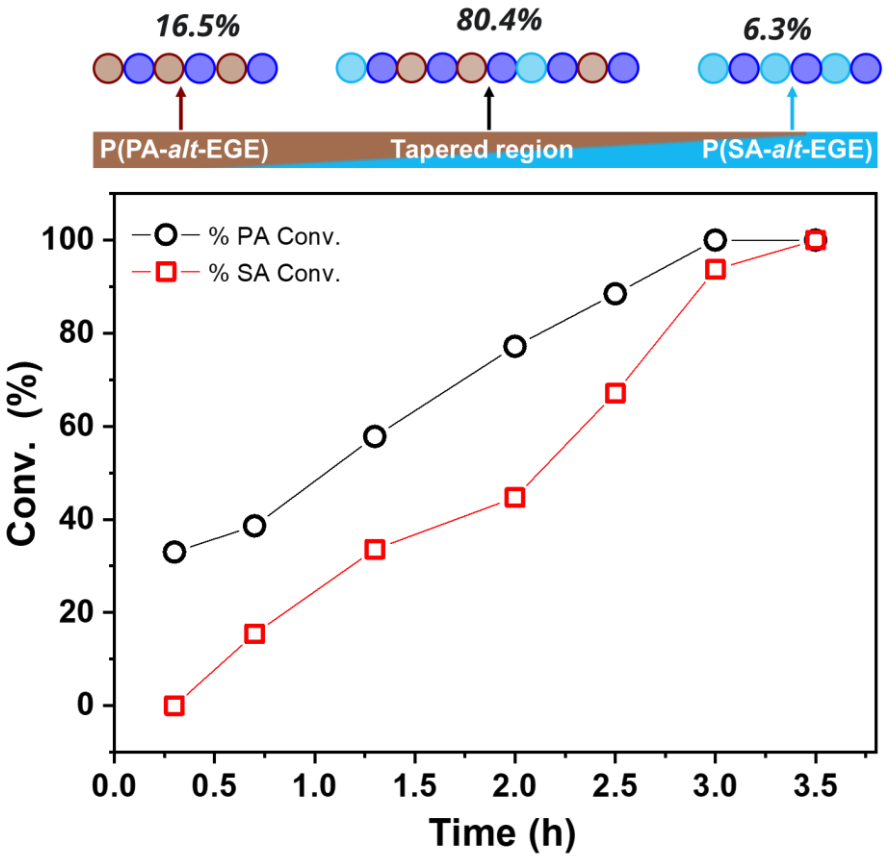

Figure 3.23. Plots of monomer conversion versus time. $[PA]_0/[SA]_0/[EGE]_0/[BDM]_0/[t\text{-}BuCO_2Cs]$ = 25/25/150/2/1 (entry 3 in Table 3.1). Conv. of PA and conv. of SA in the tapered region are 67.0% and 93.7%, respectively. The fraction of DP of poly(PA-*b*-EGE) segment, tapered region, and poly(SA-*b*-EGE) segment are 16.5%, 80.4%, and 6.3%, respectively.

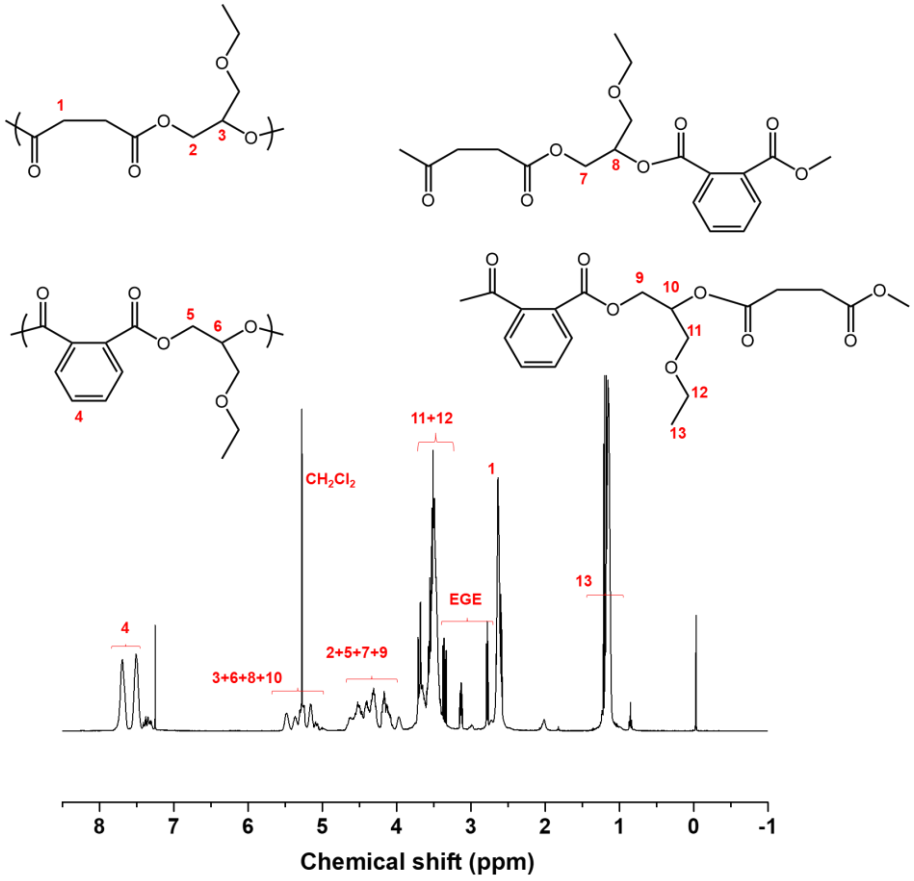

Figure 3.24. ^{1}H NMR ($CDCl_3$) spectrum of the resultant copolymer synthesized from PA, SA, and EGE (entry 3 in Table 3.1).

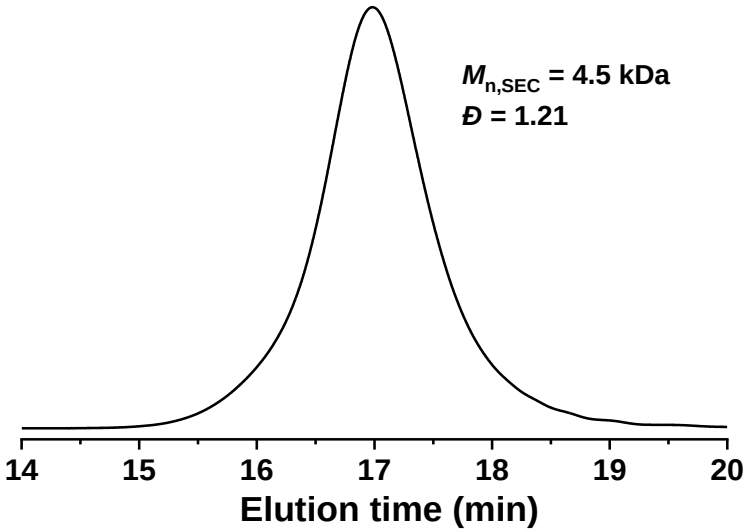

Figure 3.25. SEC (THF) trace of the resultant copolymer synthesized from PA, SA, and EGE (entry 3 in Table 3.1).

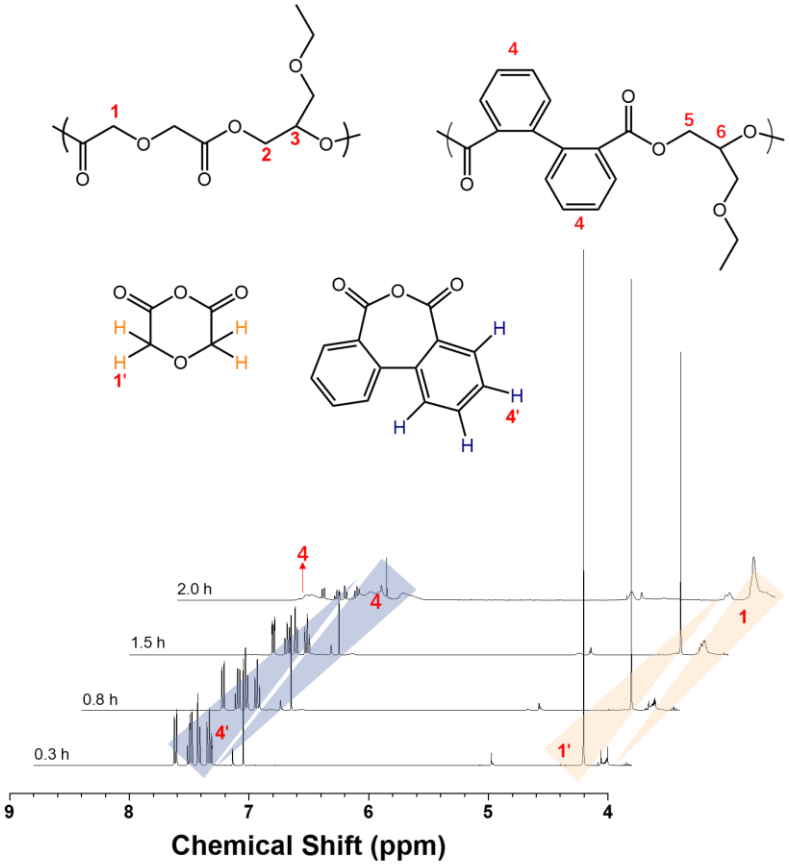

Figure 3.26. ^{1}H NMR ($CDCl_3$) spectra of crude aliquots withdrawn from the reaction system for monitoring the conversion of DGA, DA, and the formation of resultant copolymers (entry 5 in Table 3.1).

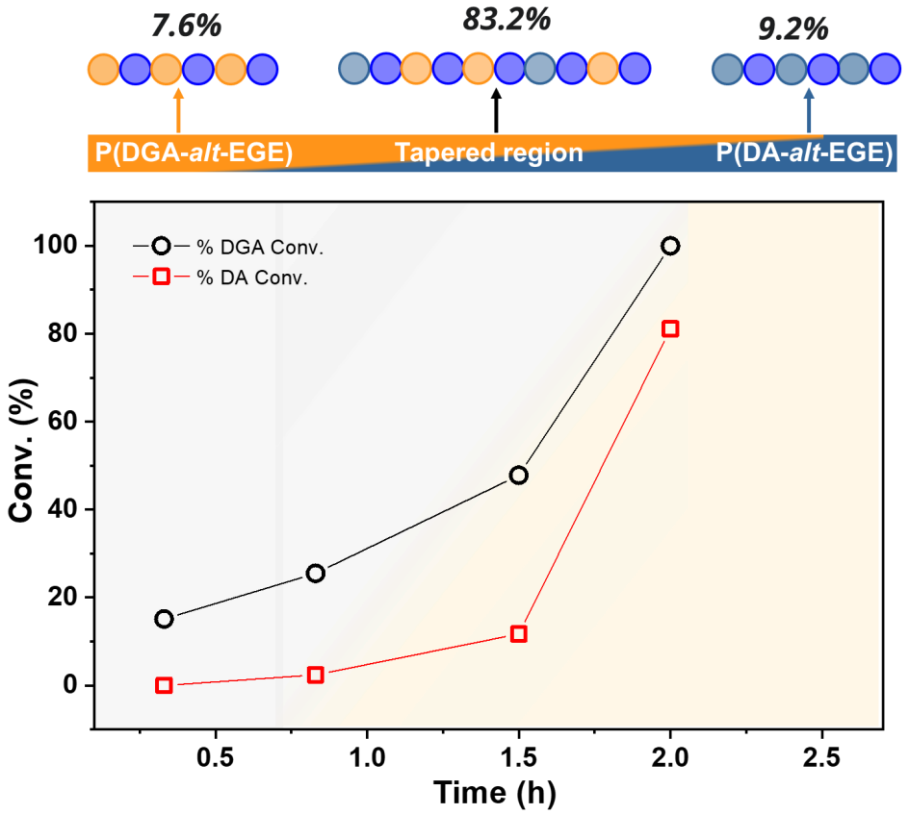

Figure 3.27. Plots of monomer conversion versus time. $[DGA]_0/[DA]_0/[AGE]_0/[BDM]_0/[t\text{-}BuCO_2Cs]$ = 25/25/150/2/1 (entry 5 in Table 1). Conv. of DGA and conv. of DA in the tapered region are 84.9% and 81.1%, respectively. The fraction of DP of poly(DGA-*b*-EGE) segment, tapered region, and poly(DA-*b*-EGE) segment are 7.6%, 83.2%, and 9.2%, respectively.

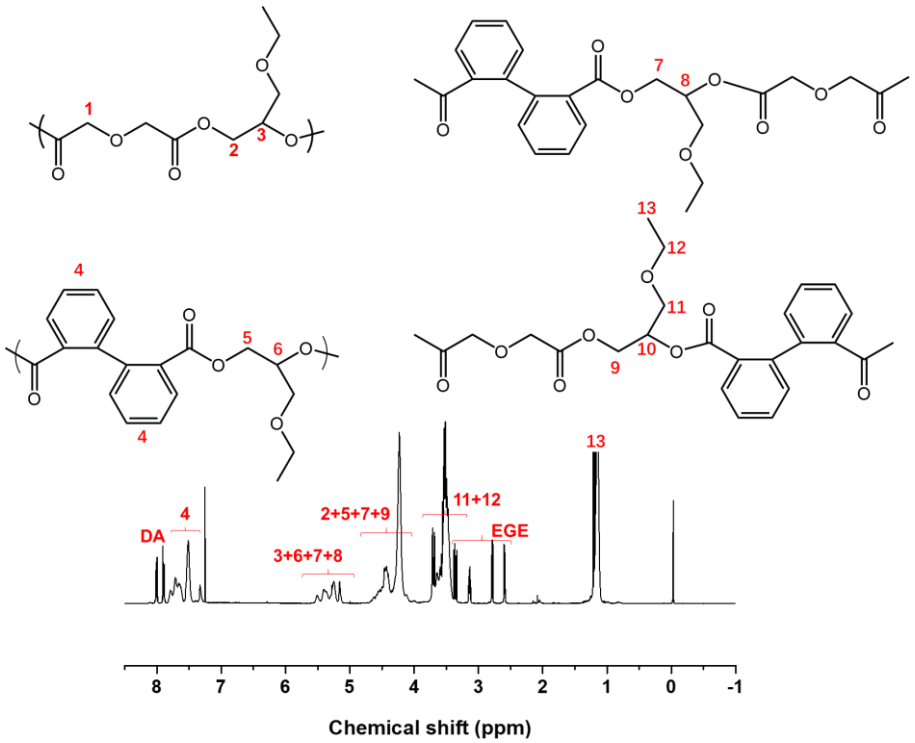

Figure 3.28. ^{1}H NMR ($CDCl_3$) spectrum of the resultant copolymer synthesized from DA, DGA, and EGE (entry 5 in Table 3.1).

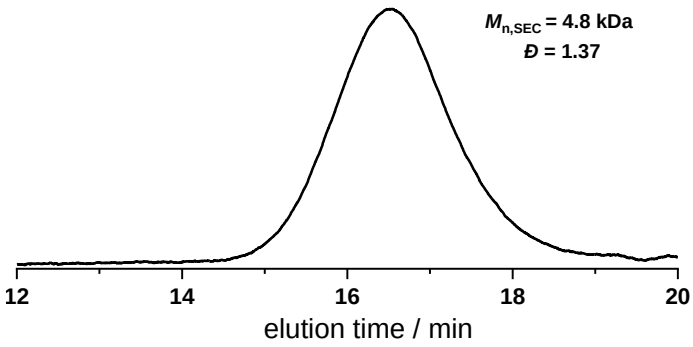

Figure 3.29. SEC (THF) trace of the resultant copolymer synthesized from DA, DGA, and EGE (entry 5 in Table 3.1).

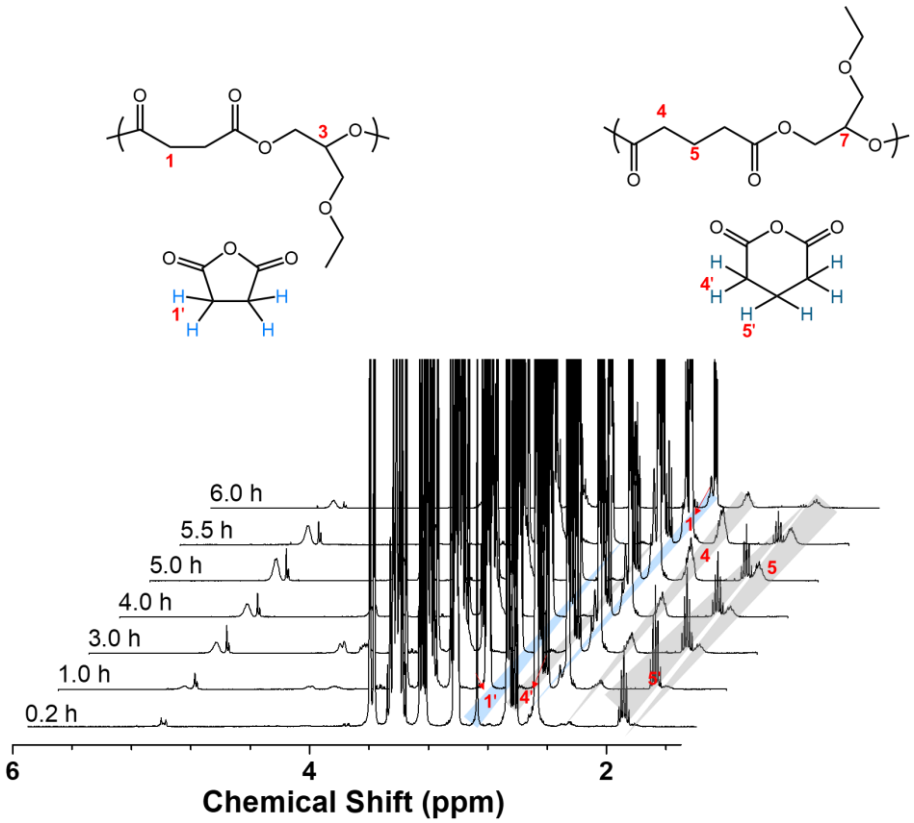

Figure 3.30. ^{1}H NMR ($CDCl_3$) spectra of crude aliquots withdrawn from the reaction system for monitoring the conversion of SA, GA, and the formation of resultant copolymers (entry 6 in Table 3.1).

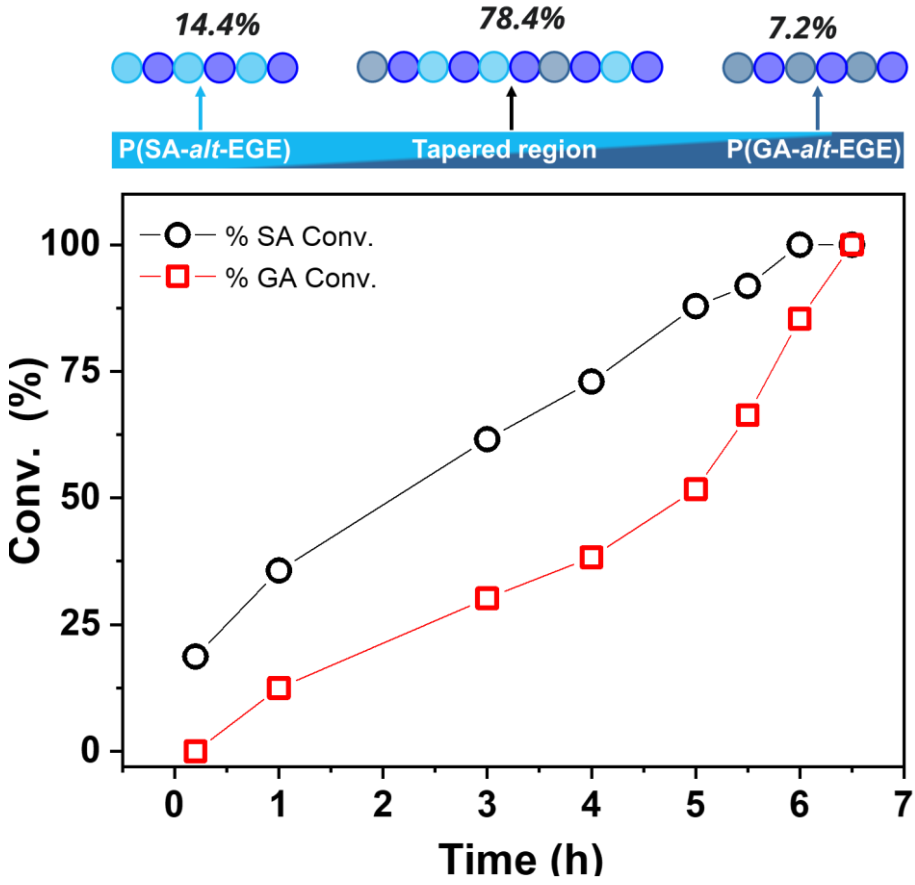

Figure 3.31. Plots of monomer conversion versus time. $[SA]_0/[GA]_0/[EGE]_0/[BDM]_0/[t\text{-}BuCO_2Cs]$ = 25/25/150/2/1 (entry 6 in Table 1). Conv. of SA and conv. of GA in the tapered region are 71.3% and 85.4%, respectively. The fraction of DP of poly(SA-*b*-EGE) segment, tapered region, and poly(GA-*b*-EGE) segment are 14.4%, 78.4%, and 7.2%, respectively.

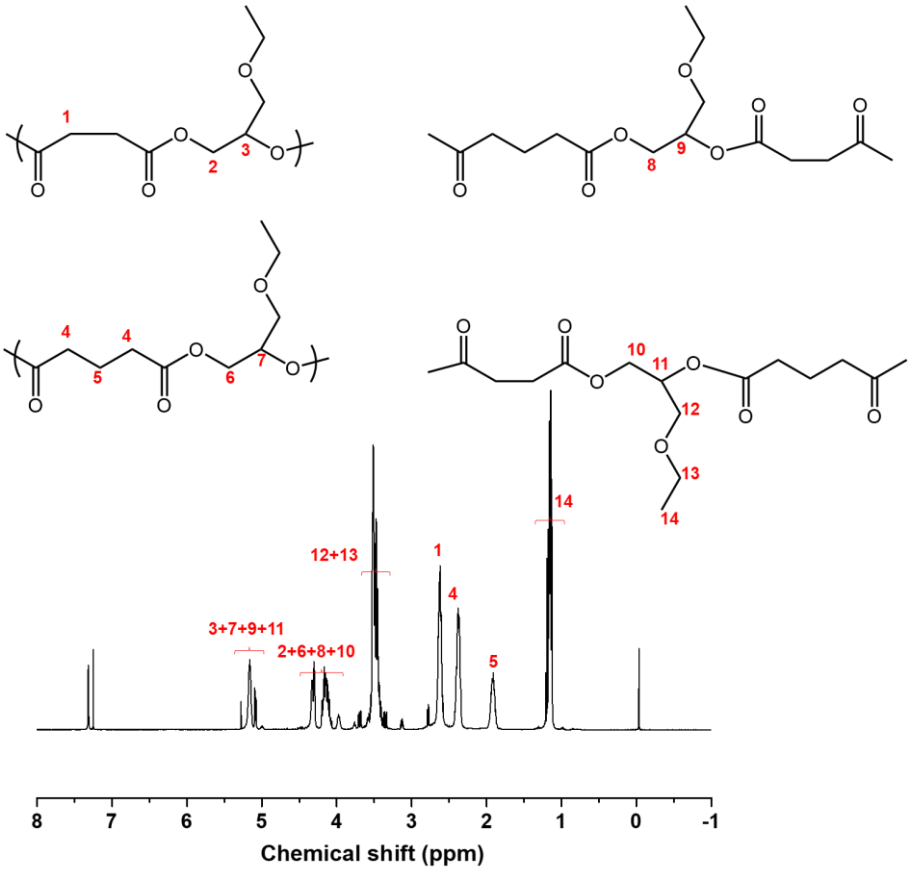

Figure 3.32. ^{1}H NMR ($CDCl_3$) spectrum of the resultant copolymer synthesized from SA, GA, and EGE (entry 6 in Table 3.1).

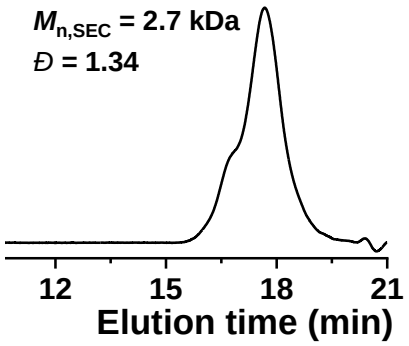

Figure 3.33. SEC (THF) trace of the resultant copolymer synthesized from SA, GA, and EGE (entry 6 in Table 3.1).

.

Further increasing the slope of the tapered microstructure can produce nominal "triblock" copolymers consisting of higher activity monomer A and lower activity monomer B blocks separated by a tapered middle block. Such copolymers are defined as hard-gradient copolymers.[29] A hard-gradient copolymer was synthesized from the DGA/PA/EGE mixture (r_{DGA} = 10.98, r_{PA} = 0.034; entry 7, Tables 3.1 and 3.2, Figure 3.20e), in which 39.4% of the terminal blocks consisted exclusively of poly(PA-*alt*-EGE) and the tapered middle segment contained 49.2% of the degree of polymerization (Figures 3.34–3.37). The ^{1}H NMR spectrum of the final products showed three peaks at 5.6–5.0 ppm, with an extra peak at 5.3–5.2 ppm (protons 8 and 10) resulting from the tapered segment (Figure 3.36).

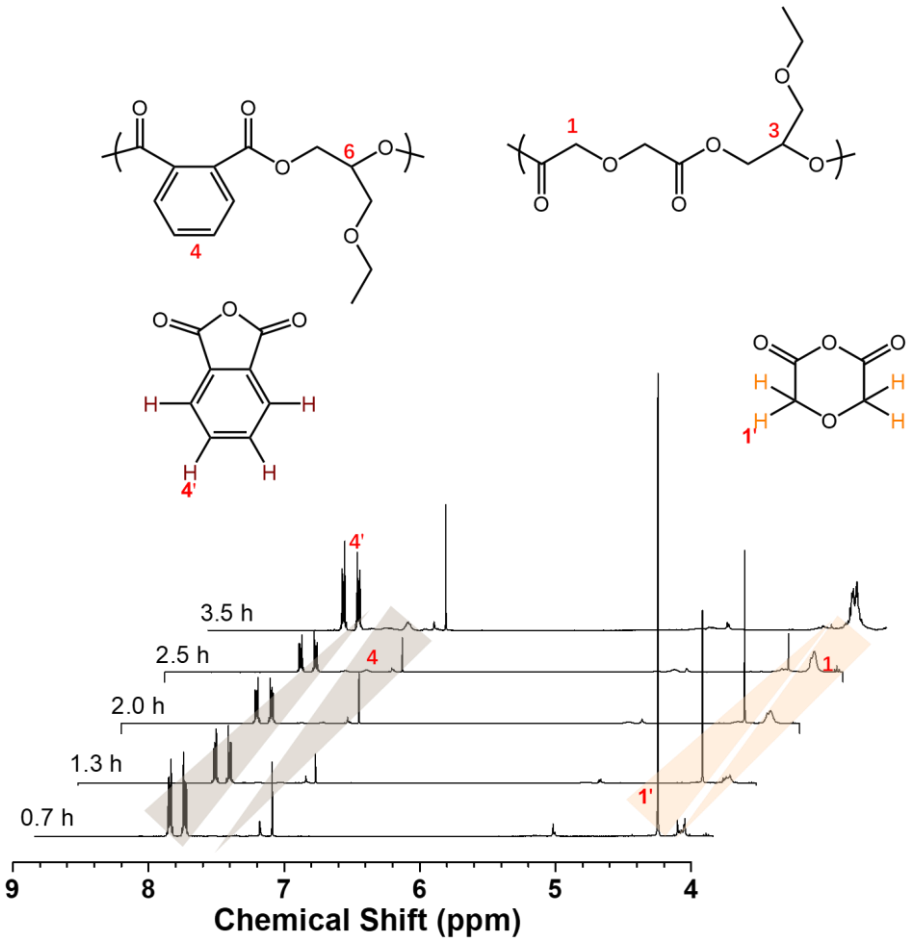

Figure 3.34. ^{1}H NMR ($CDCl_3$) spectra of crude aliquots withdrawn from the reaction system for monitoring the conversion of DGA, PA, and the formation of resultant copolymers (entry 7 in Table 3.1).

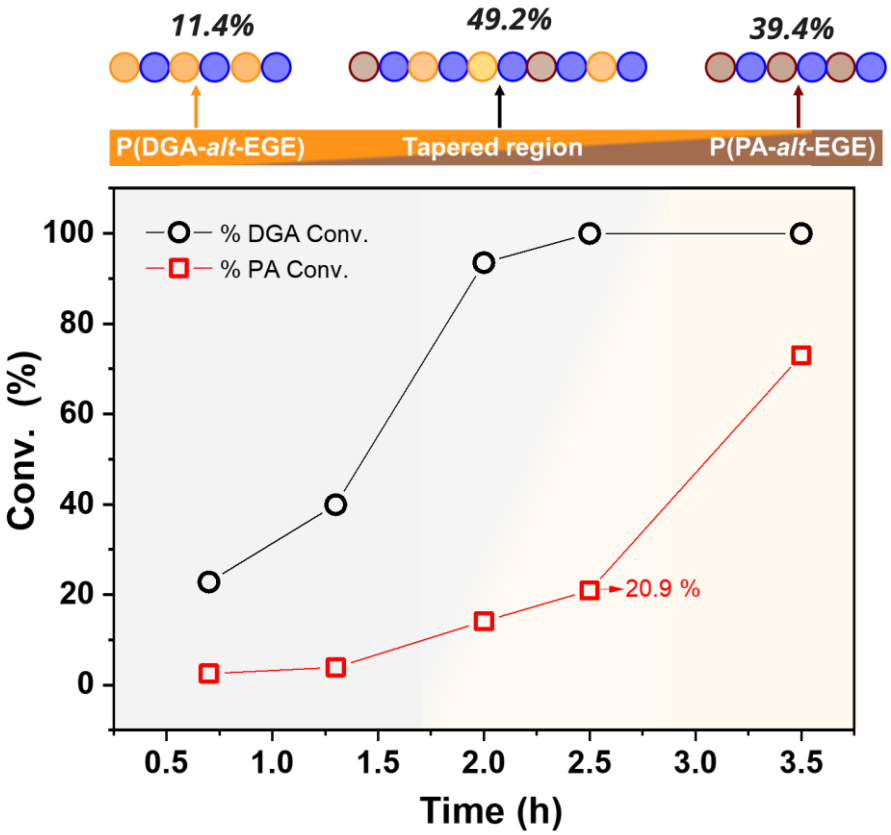

Figure 3.35. Plots of monomer conversion versus time. $[DGA]_0/[PA]_0/[EGE]_0/[BDM]_0/[t\text{-}BuCO_2Cs]$ = 25/25/150/2/1 (entry 7 in Table 3.1). Conv. of DGA and conv. of PA in the tapered region are 77.2% and 20.9%, respectively. The fraction of DP of poly(DGA-*b*-EGE) segment, tapered region, and poly(PA-*b*-EGE) segment are 11.4%, 49.2%, and 39.4%, respectively.

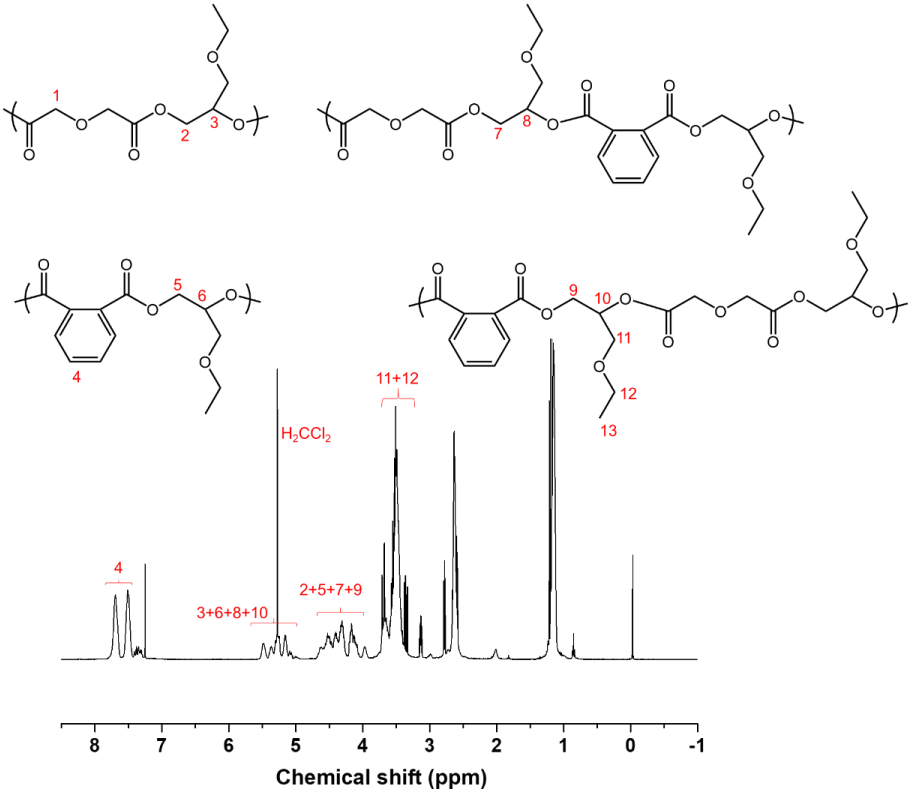

Figure 3.36. ^{1}H NMR ($CDCl_3$) spectrum of the resultant copolymer synthesized from PA, DGA, and EGE (entry 7 in Table 3.1).

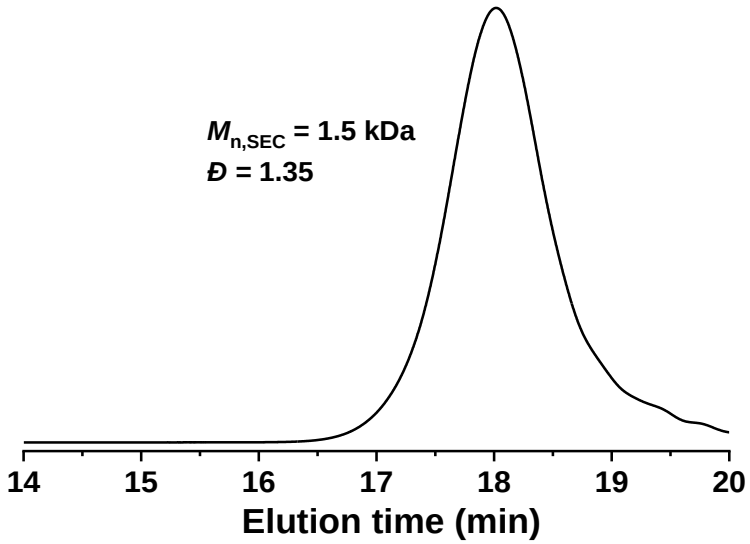

Figure 3.37. SEC (THF) trace of the resultant copolymer synthesized from PA, DGA, and EGE (entry 7 in Table 3.1).

Further increasing the reactivity ratio difference, such as for the GA/NA/EGE mixture (r_{GA} = 516.27, r_{NA} = 0.0204; entry 9, Table 3.2, Figure 3.20f), caused the gradient profile in the tapered block to become harder (11.6% tapered region) and a block-like copolymer was obtained. Reactivity ratios leading to block-like copolymers are typically in the order of around r_1 : 440–800 and r_2 : 0.0049–0.026. Because the tapered region was small, the additional ^{1}H NMR peak at 5.6–6.0 ppm was not observed (Figure 3.38). The copolymerization showed good control, as evidenced by the narrow dispersity ($Đ$ = 1.20; entry 8, Table 1, Figures 3.38–3.41). Replacing GA with SA further increased the reactivity ratio difference (r_{SA} = 634.02, r_{NA} = 0.0057; entry 11, Table 3.2) and gave a copolymer with a tapered region of only 8.4% with a narrow, monomodal distribution ($Đ$ = 1.12; entry 9, Table 3.1, Figures 3.42–3.45). In these block-like copolymers, the tapered microstructure fraction varied (1.5–14.9%) depending on the reactivity ratio (entries 8–15, Table 3.2). Moreover, competitive copolymerization provided a high degree of control with the obtained block-like copolymers having narrow, monomodal distributions ($Đ$ < 1.36; entries 7–15, Table 3.1, Figures 3.46–3.53).

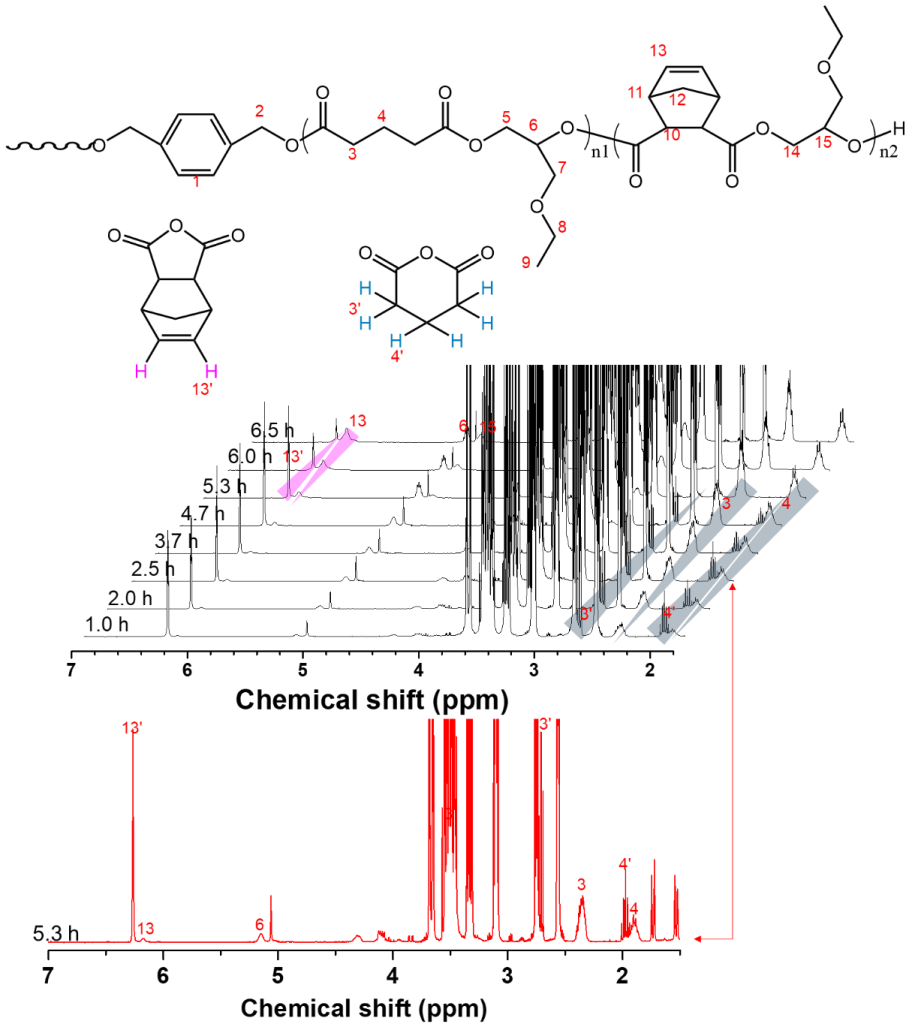

Figure 3.38. ^{1}H NMR ($CDCl_3$) spectra of crude aliquots withdrawn from the reaction system for monitoring the conversion of GA, NA, and the formation of resultant copolymers (entry 8 in Table 3.1).

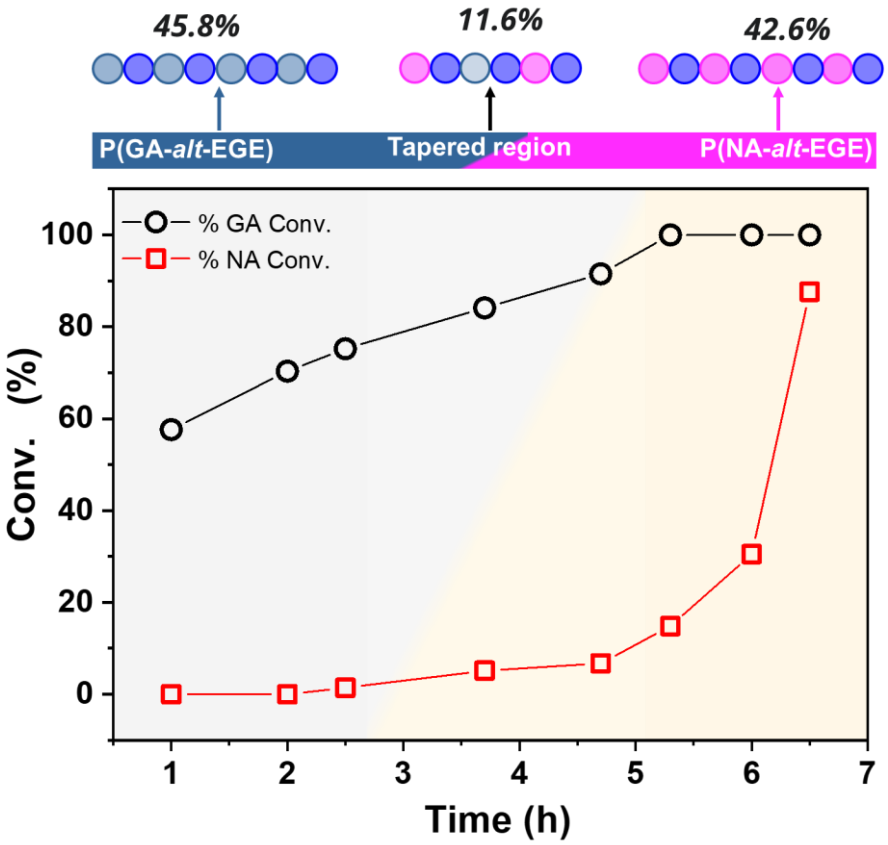

Figure 3.39. Plots of monomer conversion versus time. $[GA]_0/[NA]_0/[EGE]_0/[BDM]_0/[t\text{-}BuCO_2Cs]$ = 25/25/150/2/1 (entry 8 in Table 3.1). Conv. of DA and conv. of NA in the tapered region are 8.5% and 14.8%, respectively. The fraction of DP of poly(GA-*b*-EGE) segment, tapered region, and poly(NA-*b*-EGE) segment are 45.8%, 11.6%, and 42.6%, respectively.

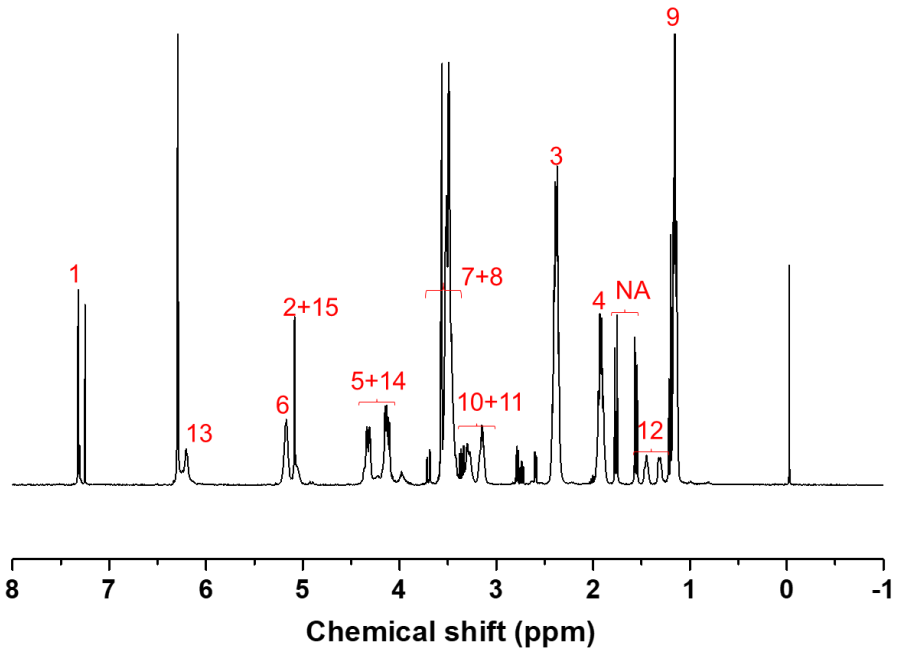

Figure 3.40. ^{1}H NMR ($CDCl_3$) spectrum of the resultant copolymer synthesized from NA, GA, and EGE (entry 8 in Table 3.1).

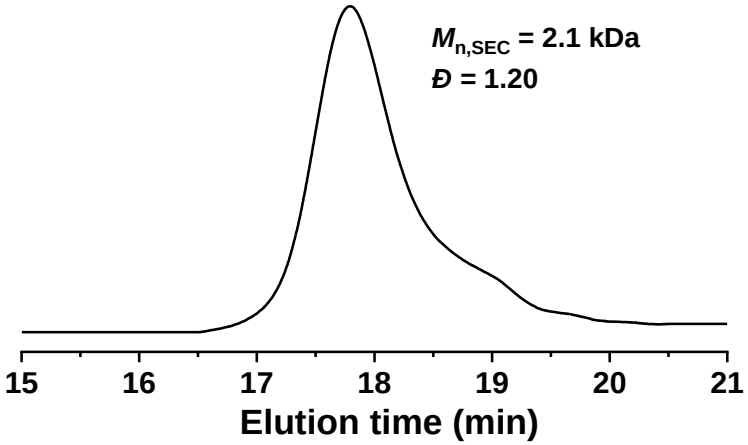

Figure 3.41. SEC (THF) trace of the resultant copolymer synthesized from NA, GA, and EGE (entry 8 in Table 3.1).

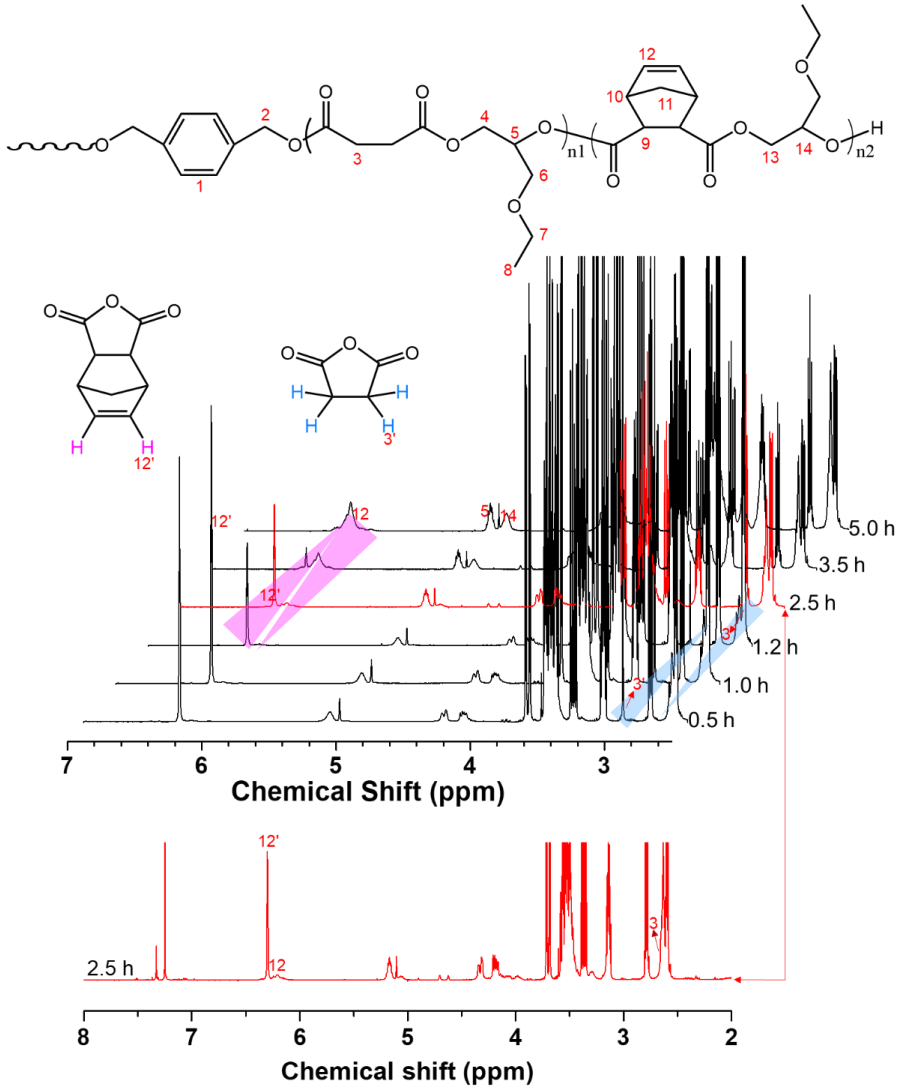

Figure 3.42. ^{1}H NMR ($CDCl_3$) spectra of crude aliquots withdrawn from the reaction system for monitoring the conversion of SA, NA and the formation of resultant copolymers (entry 9 in Table 3.1).

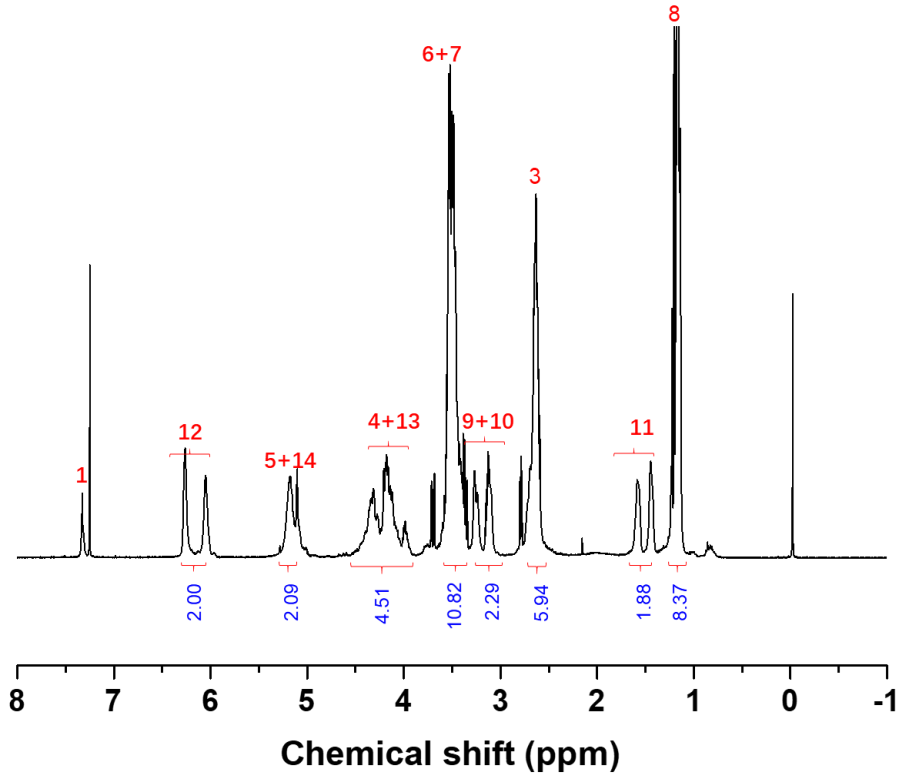

Figure 3.43. ^{1}H NMR ($CDCl_3$) spectrum of the resultant copolymer synthesized from NA, SA, and EGE (entry 9 in Table 3.1).

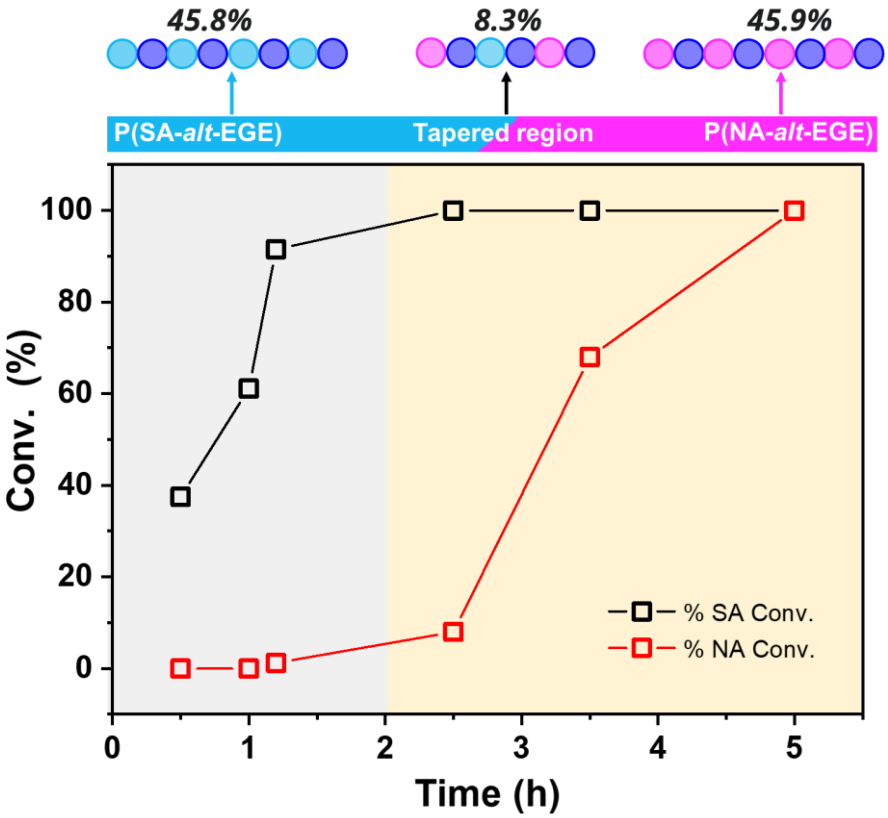

Figure 3.44. Plots of monomer conversion versus time. $[SA]_0/[NA]_0/[EGE]_0/[BDM]_0/[t\text{-}BuCO_2Cs]$ = 25/25/150/2/1 (entry 9 in Table 3.1). Conv. of SA and conv. of NA in the tapered region are 8.5% and 8.0%, respectively. The fraction of DP of poly(SA-*b*-EGE) segment, tapered region, and poly(NA-*b*-EGE) segment are 45.8%, 8.3%, and 45.9%, respectively.

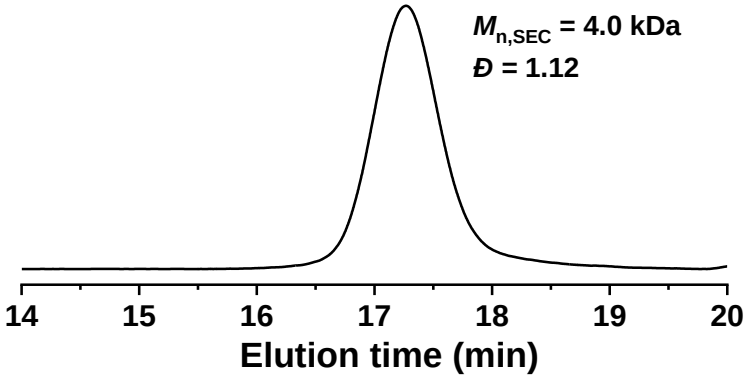

Figure 3.45. SEC (THF) trace of the resultant copolymer synthesized from NA, SA, and EGE (entry 9 in Table 3.1).

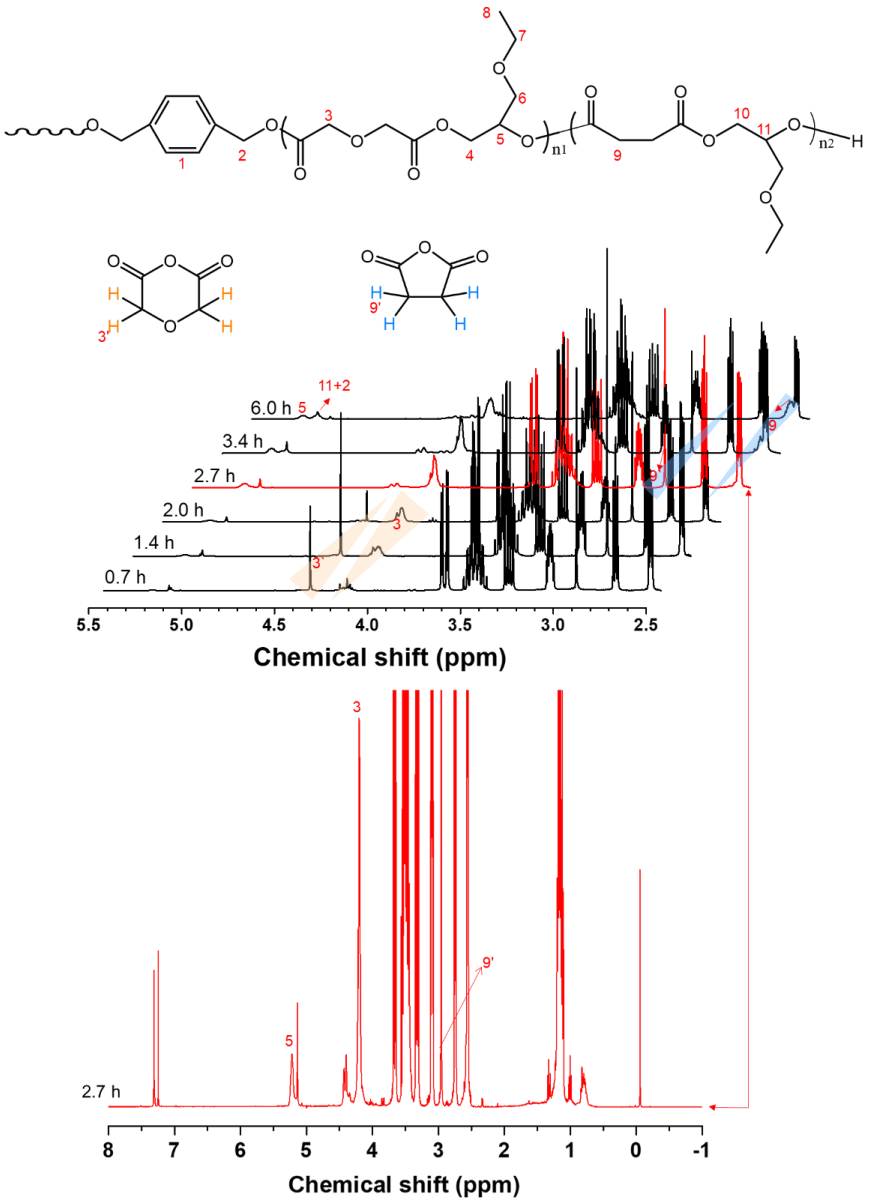

Figure 3.46. ^{1}H NMR ($CDCl_3$) spectra of crude aliquots withdrawn from the reaction system for monitoring the conversion of DGA, SA and the formation of resultant copolymers (entry 10 in Table 3.1).

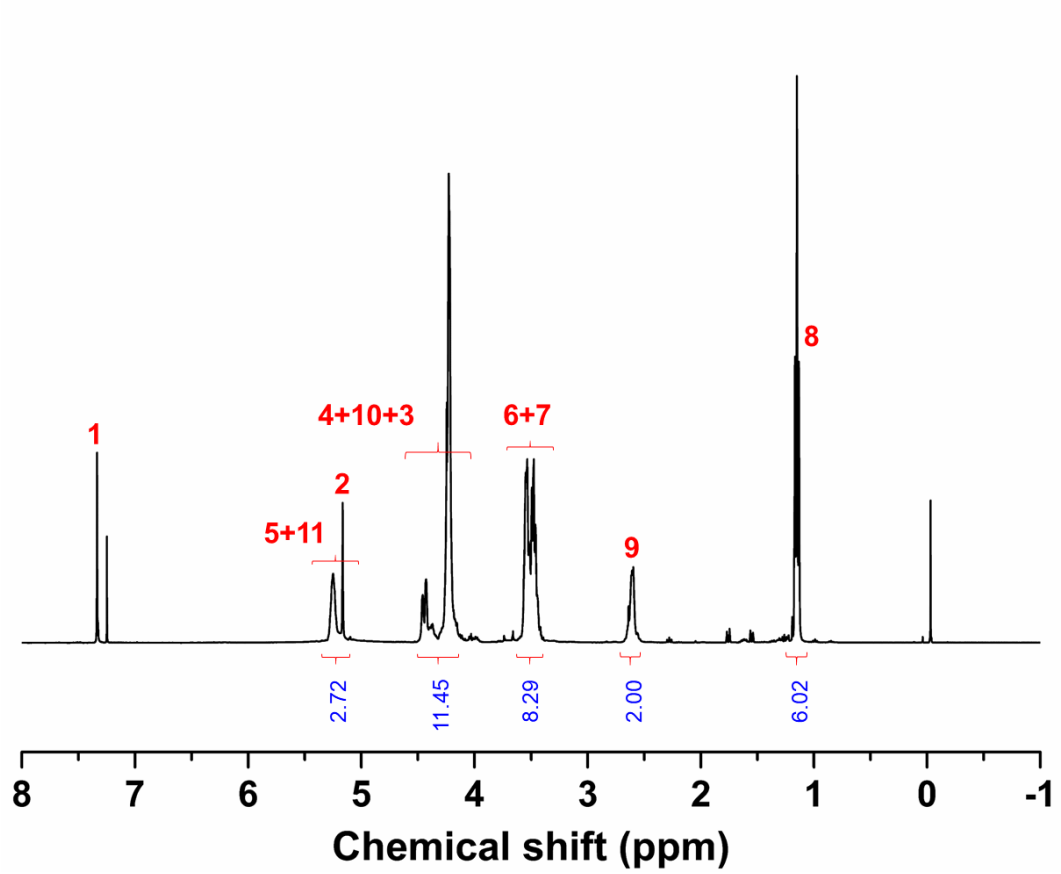

Figure 3.47. ^{1}H NMR ($CDCl_3$) spectrum of the resultant copolymer synthesized from DGA, SA, and EGE (entry 10 in Table 3.1).

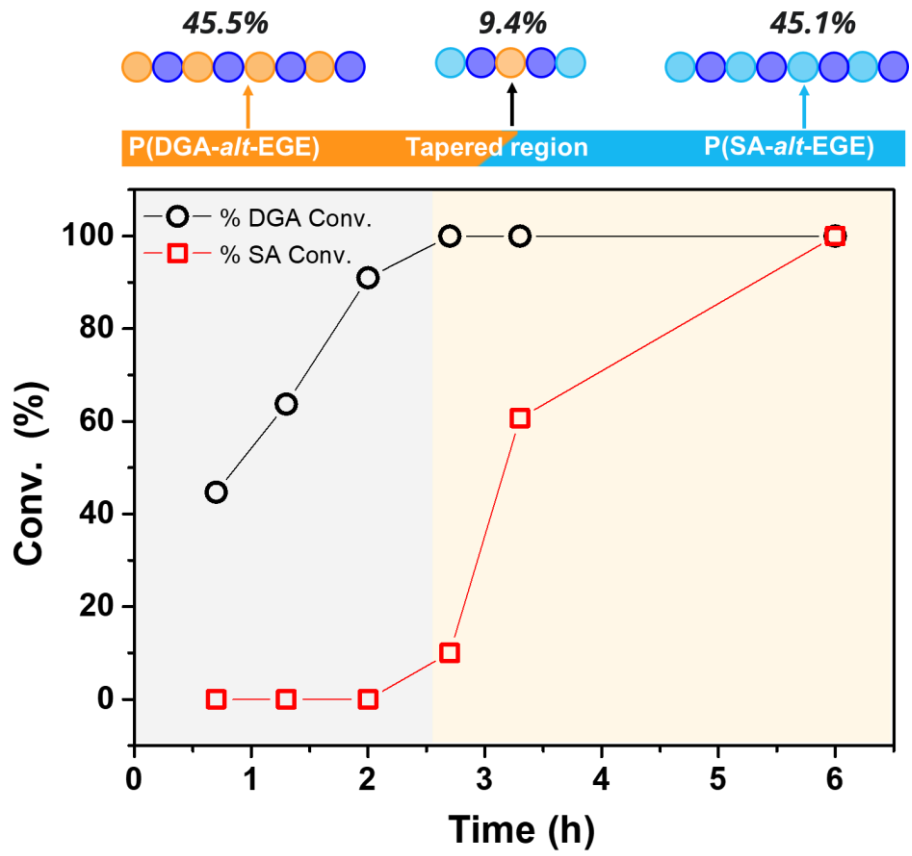

Figure 3.48. Plots of monomer conversion versus time. $[DGA]_0/[SA]_0/[EGE]_0/[BDM]_0/[t\text{-}BuCO_2Cs]$ = 25/25/150/2/1 (entry 10 in Table 3.1). Conv. of DGA and conv. of SA in the tapered region are 9% and 10%, respectively. The fraction of DP of poly(DGA-*b*-EGE) segment, tapered region, and poly(SA-*b*-EGE) segment are 45.5%, 9.4%, and 45.1%, respectively.

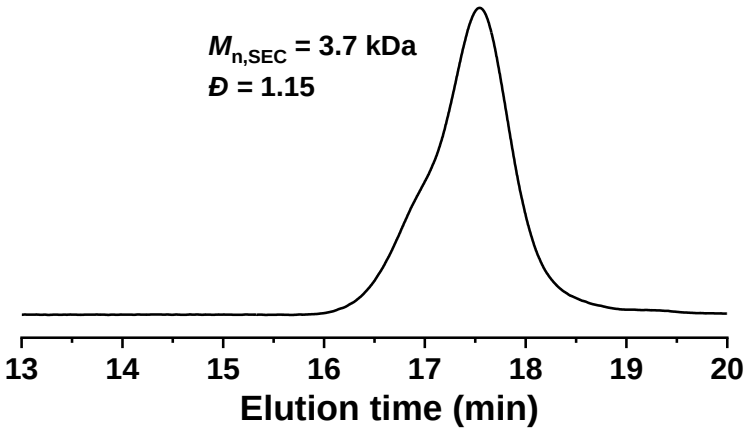

Figure 3.49. SEC (THF) trace of the resultant copolymer synthesized from DGA, SA, and EGE (entry 10 in Table 3.1).

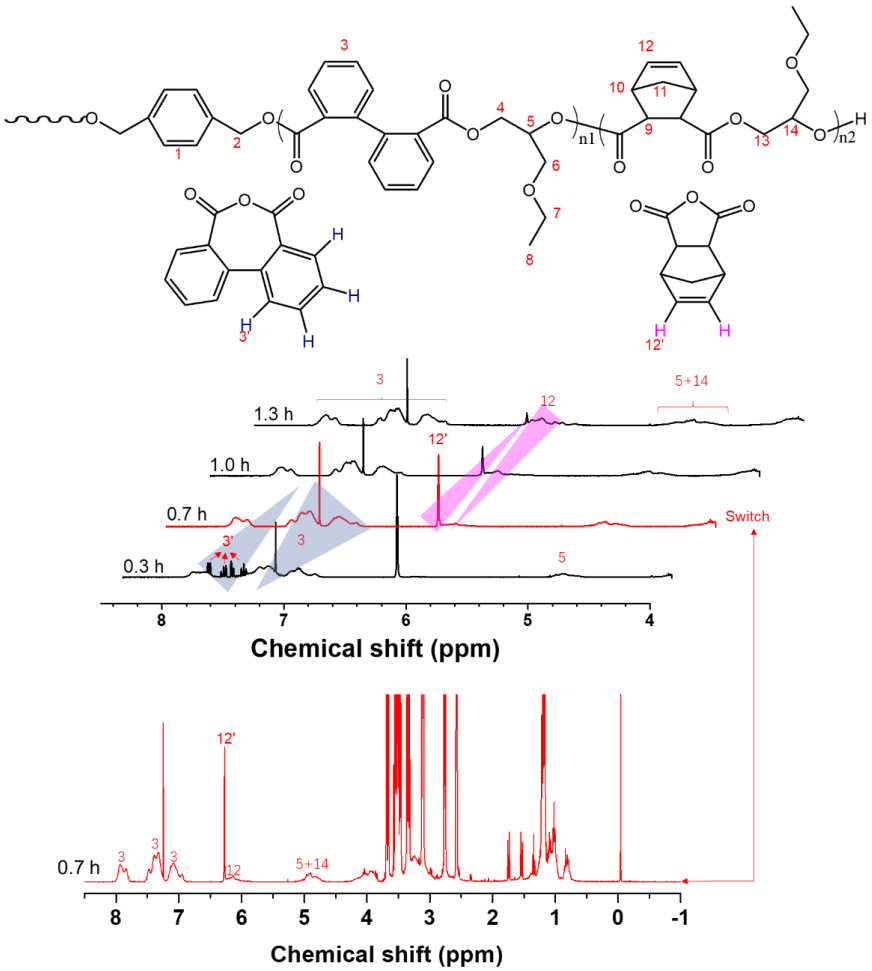

Figure 3.50. ^{1}H NMR ($CDCl_3$) spectra of crude aliquots withdrawn from the reaction system for monitoring the conversion of DA, NA and the formation of resultant copolymers (entry 11 in Table 3.1).

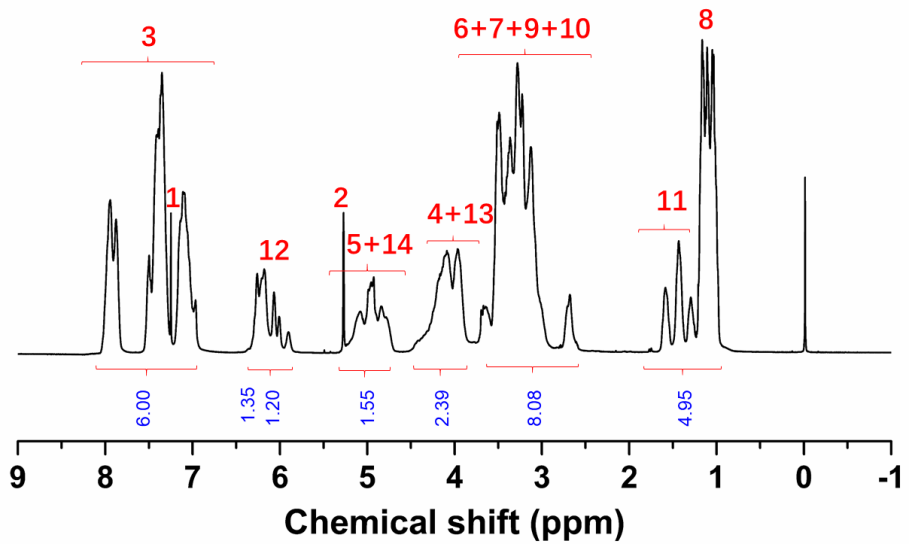

Figure 3.51. ^{1}H NMR ($CDCl_3$) spectrum of the resultant copolymer synthesized from DA, NA, and EGE (entry 11 in Table 3.1).

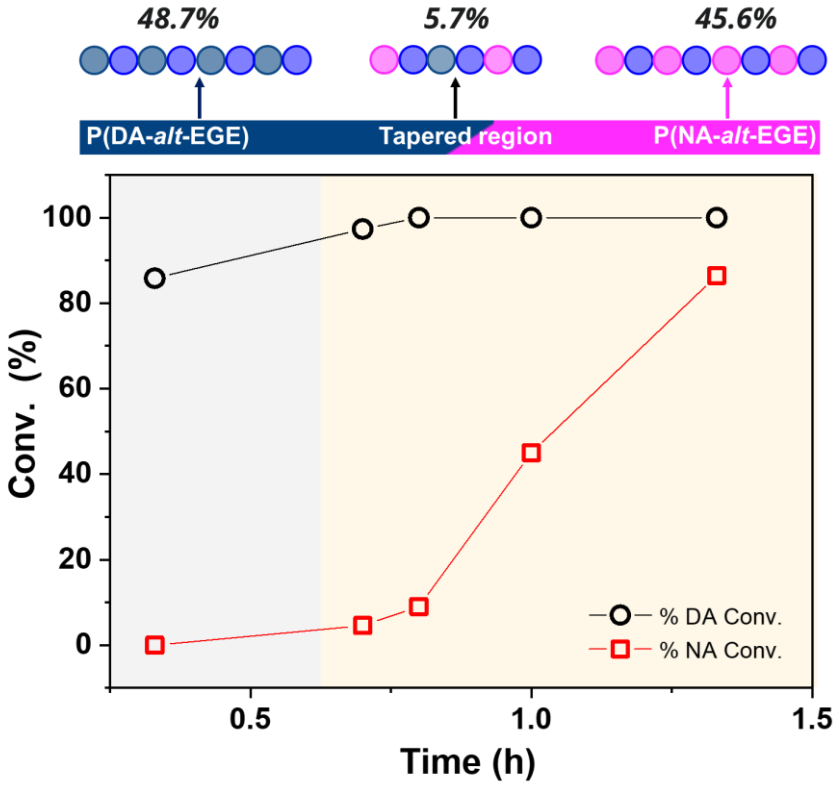

Figure 3.52. Plots of monomer conversion versus time. $[DA]_0/[NA]_0/[EGE]_0/[BDM]_0/[t\text{-}BuCO_2Cs]$ = 25/25/150/2/1 (entry 11 in Table 3.1). Conv. of DA and conv. of NA in the tapered region are 2.7% and 9%, respectively. The fraction of DP of poly(DA-*b*-EGE) segment, tapered region, and poly(NA-*b*-EGE) segment are 48.7%, 5.7%, and 45.6%, respectively.

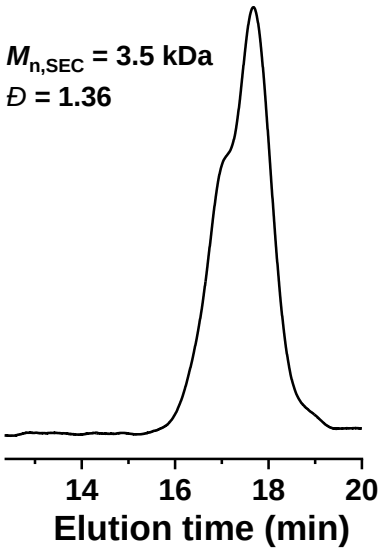

Figure 3.53. SEC (THF) trace of the resultant copolymer synthesized from DA, NA, and EGE (entry 11 in Table 3.1).

Using competitive anionic copolymerization, it is difficult to prepare "real" block copolymers similar to those obtained using sequential monomer addition. However, the extremely large reactivity ratio difference for 2,2,3,3,4,4-hexafluoropentanedioic anhydride (HFA)/DGA/EGE copolymerization (r_{HFA} = 816.39, r_{DGA} = 0.0036; entry 16, Table 3.2, Figure 3.20n) allowed the formation of a "real" triblock copolymer without a tapered region. ^{1}H NMR analysis showed that initial HFA/EGE copolymerization was followed by DGA/EGE ROAC. Owing to its extremely high reactivity, HFA was completely consumed in 1 min and then DGA began to react, leading to copolymers with relative broad dispersity ($Đ$ = 1.45; entry 16, Table 3.1, Figures 3.54–3.58). Similarly, the large reactivity ratio difference between NA and *rac*-*cis*-*endo*-1-isopropyl-4-methyl-bicyclo[2.2.2]oct-5-ene-2,3-dicarboxylic anhydride (DPMA) (r_{NA} = 814.83, r_{DPMA} = 0.0047; entry 17, Table 3.2, Figure 3.20o) resulted in the formation of perfect triblock copolymers (entry 17, Table 3.1, Figures 3.59–3.62). Even at an NA/DPMA molar ratio of 1/5, no DPMA-EGE or EGE-DPMA units were inserted in the P(NA-*alt*-EGE) block and a triblock copolymer without tapered regions was formed (entry 18, Tables 3.1 and 2, Figures 3.63–3.65). Typically, reactivity ratios of $r_1 > 800$ and $r_2 < 0.0049$ gave real block copolymers.

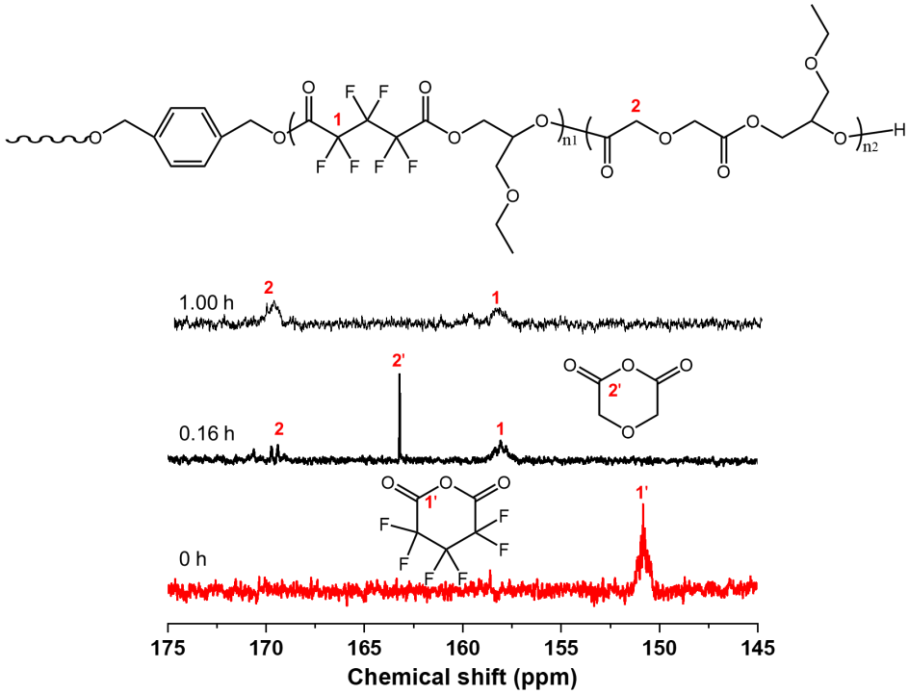

Figure 3.54. ^{13}C NMR ($CDCl_3$) spectra of crude aliquots withdrawn from the reaction system for monitoring the conversion of HFA, DGA and the formation of resultant copolymers (entry 16 in Table 3.1).

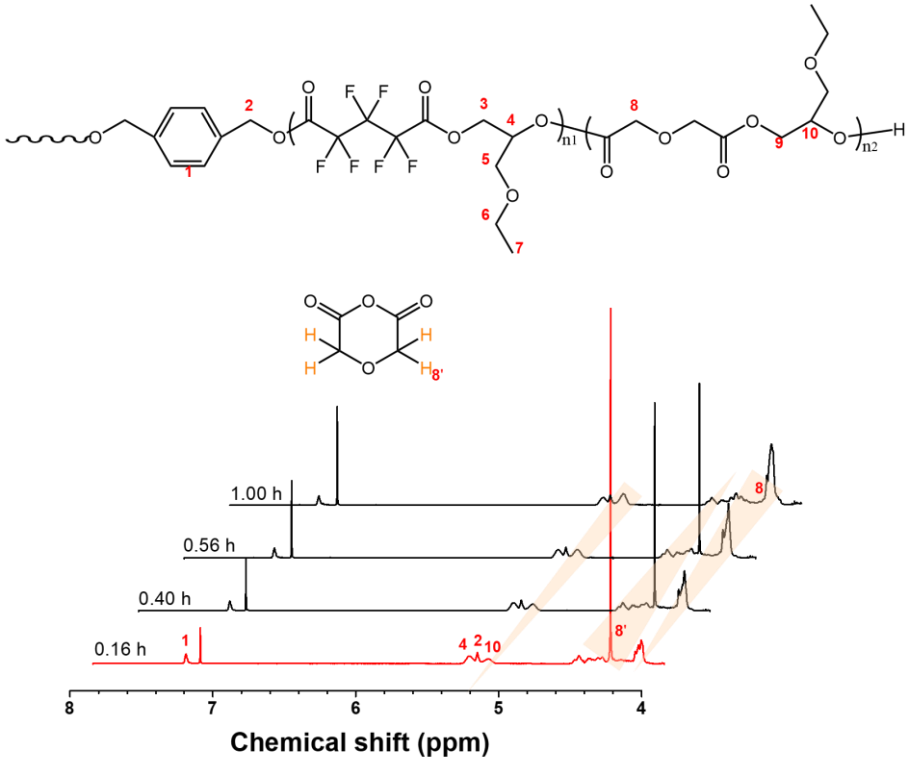

Figure 3.55. ^{1}H NMR ($CDCl_3$) spectra of crude aliquots withdrawn from the reaction system for monitoring the conversion of PA, NA and the formation of resultant copolymers (entry 16 in Table 3.1).

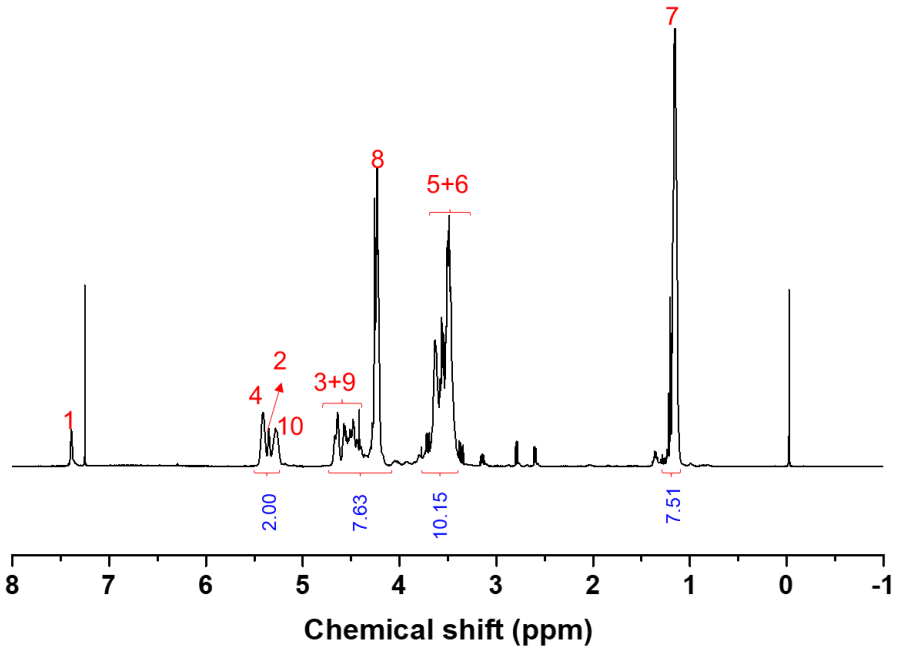

Figure 3.56. ^{1}H NMR ($CDCl_3$) spectrum of the resultant copolymer synthesized from DGA, HFA, and EGE (entry 16 in Table 3.1).

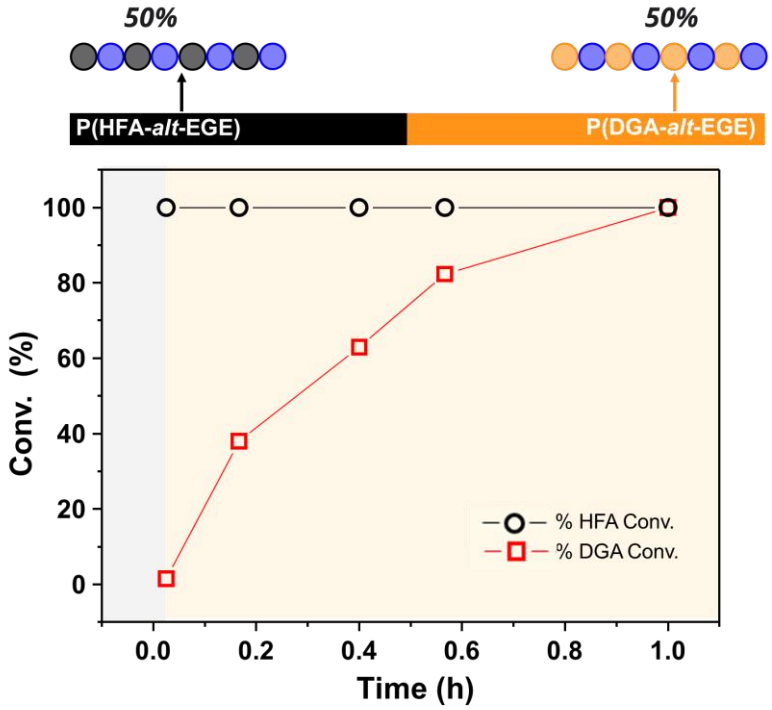

Figure 3.57. Plots of monomer conversion versus time. $[HFA]_0/[DGA]_0/[EGE]_0/[BDM]_0/[t\text{-}BuCO_2Cs]$ = 25/25/150/2/1 (entry 16 in Table 3.1). Conv. of HFA and conv. of DGA in the tapered region are 0% and 0%, respectively. The fraction of DP of poly(HFA-*b*-EGE) segment and poly(DGA-*b*-EGE) segment are 50% and 50%, respectively.

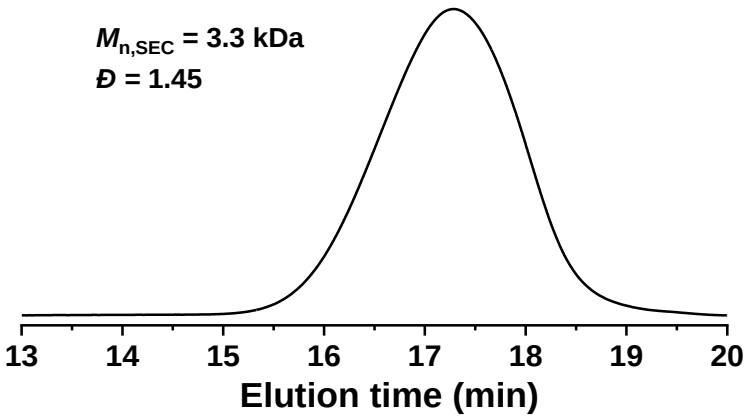

Figure 3.58. The SEC (THF) trace of the resultant copolymer synthesized from DGA, HFA, and EGE (entry 16 in Table 3.1).

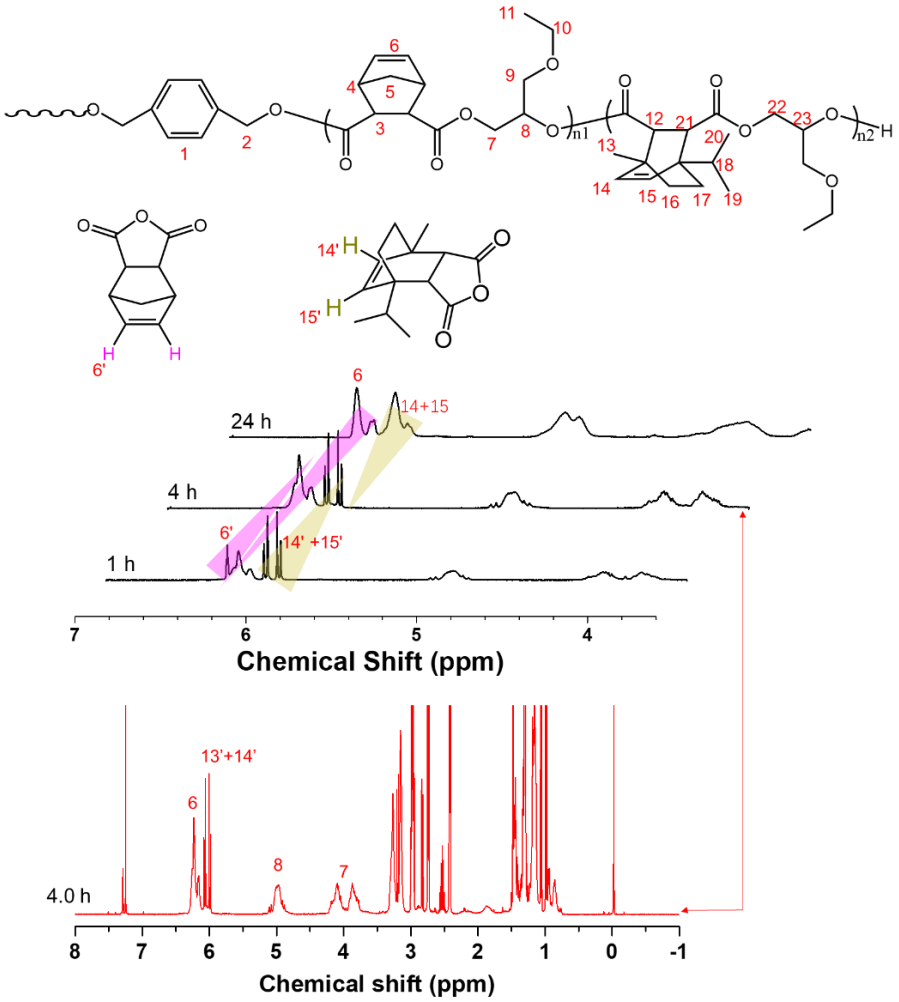

Figure 3.59. ^{1}H NMR ($CDCl_3$) spectra of crude aliquots withdrawn from the reaction system for monitoring the conversion of DPMA, NA and the formation of resultant copolymers (entry 17 in Table 3.1).

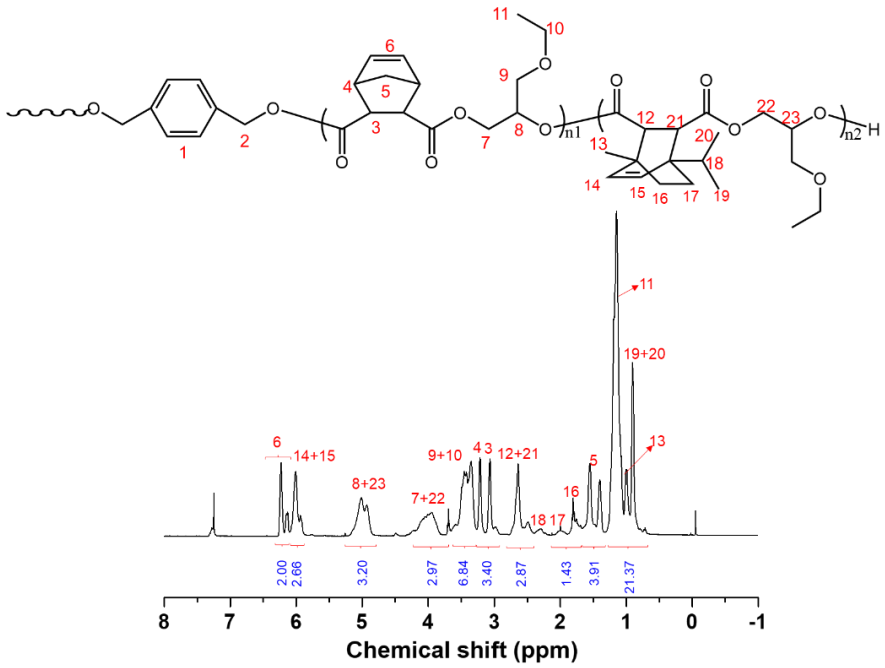

Figure 3.60. ^{1}H NMR ($CDCl_3$) spectrum of the resultant copolymer synthesized from NA, DPMA, and EGE (entry 17 in Table 3.1).

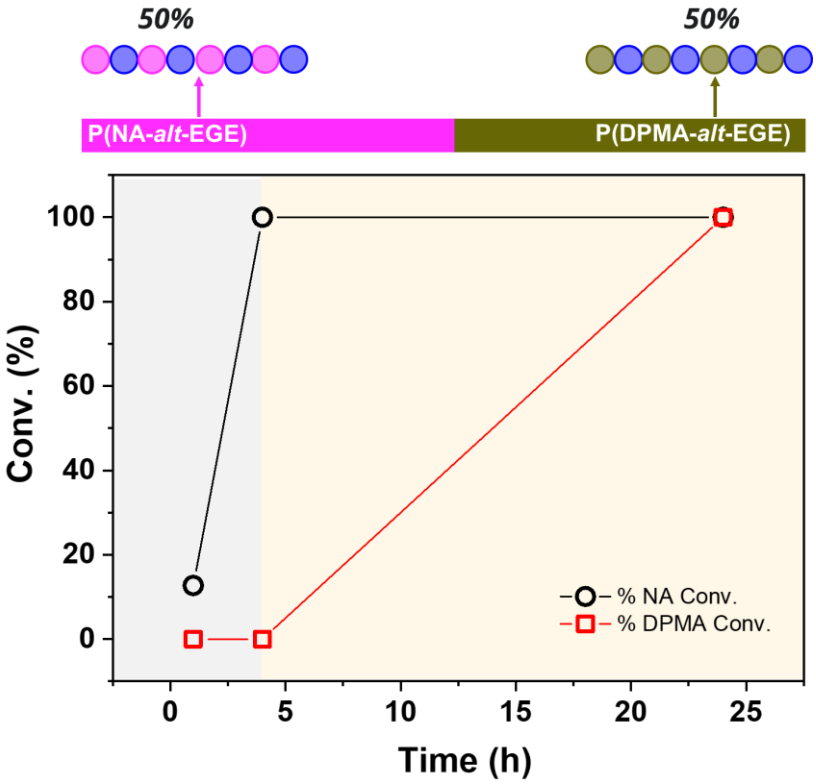

Figure 3.61. Plots of monomer conversion versus time. $[NA]_0/[DPMA]_0/[EGE]_0/[BDM]_0/[t\text{-}BuCO_2Cs]$ = 25/25/150/2/1 (entry 17 in Table 3.1). Conv. of NA and conv. of DPMA in the tapered region are 0% and 0%, respectively. The fraction of DP of poly(NA-*b*-EGE) segment and poly(DPMA-*b*-EGE) segment are 44.2% and 55.8%, respectively.

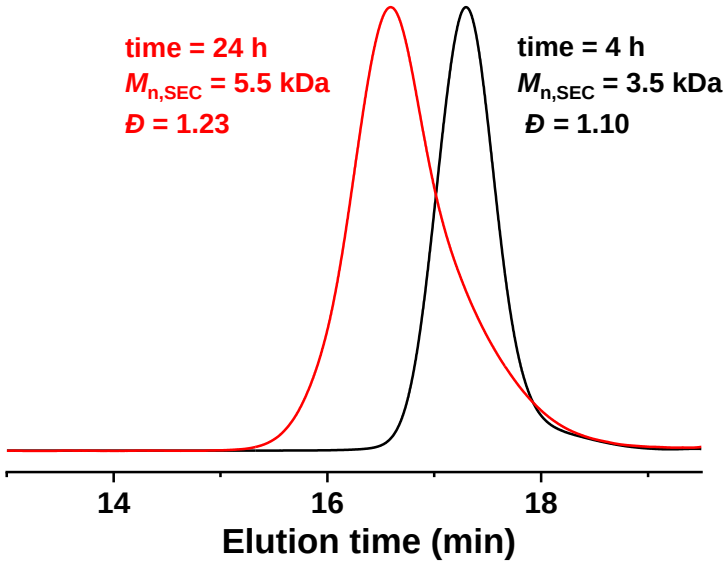

Figure 3.62. SEC (THF) trace of the resultant copolymer synthesized from NA, DPMA, and EGE (entry 17 in Table 3.1).

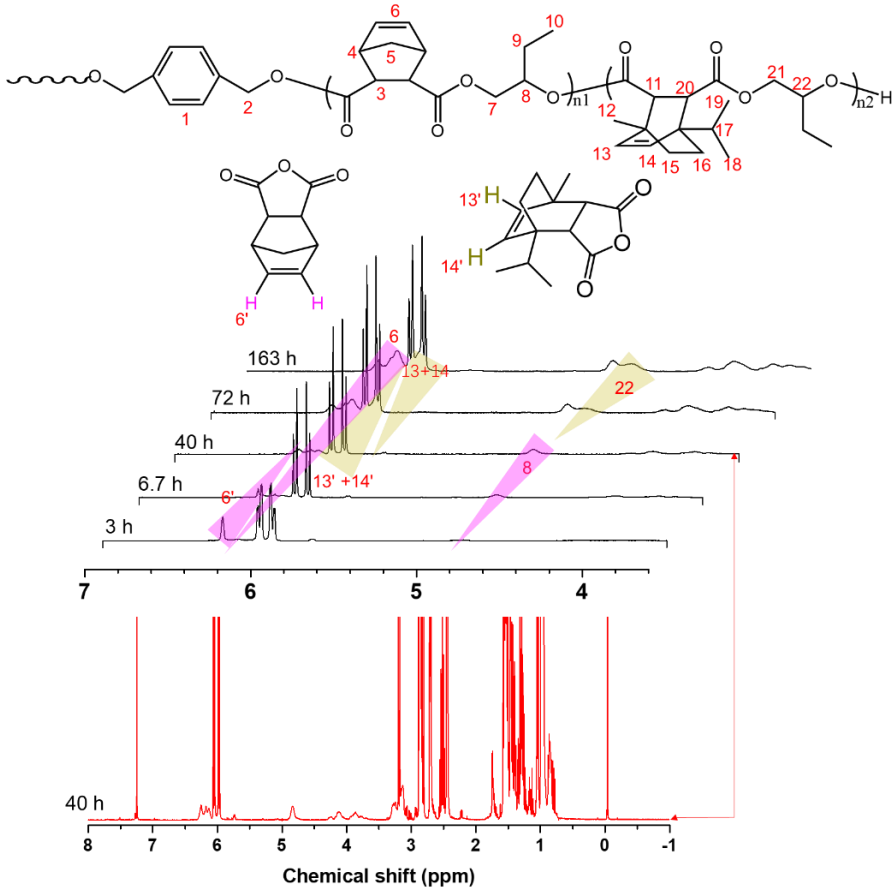

Figure 3.63. ^{1}H NMR ($CDCl_3$) spectra of crude aliquots withdrawn from the reaction system for monitoring the conversion of DPMA, NA and the formation of resultant copolymers (entry 18 in Table 3.1).

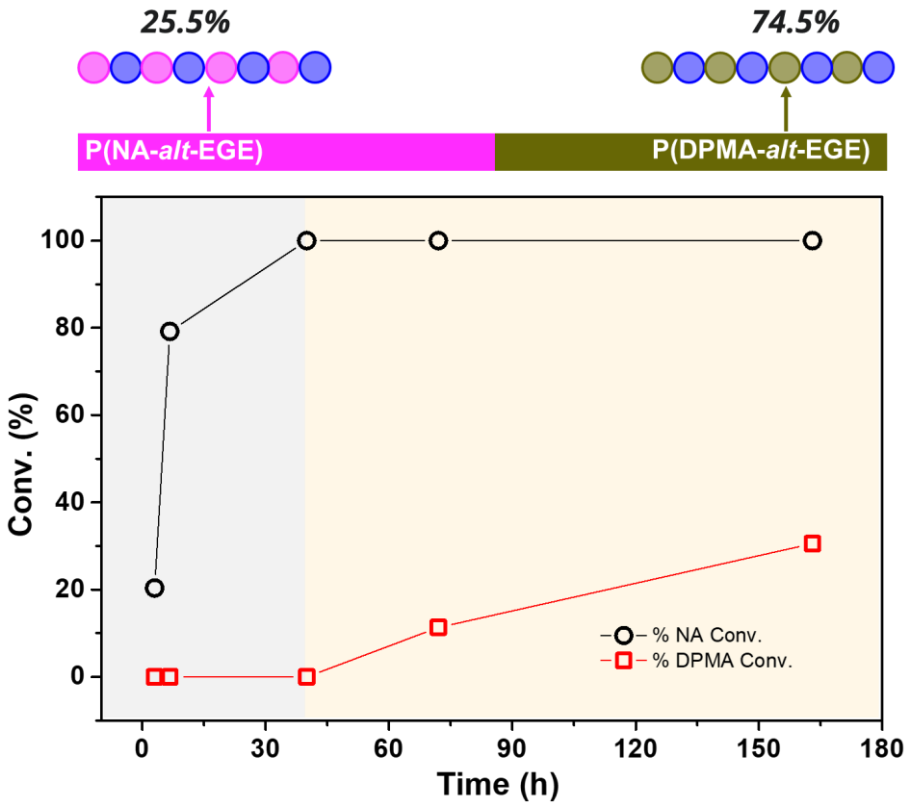

Figure 3.64. Plots of monomer conversion versus time. $[NA]_0/[DPMA]_0/[BO]_0/[BDM]_0/[t\text{-}BuCO_2Cs]$ = 25/125/250/2/1 (entry 18 in Table 3.1). Conv. of NA and conv. of DPMA in the tapered region are 0% and 0%, respectively. The fraction of DP of poly(NA-*b*-BO) segment and poly(DPMA-*b*-BO) segment are 25.5% and 74.5%, respectively.

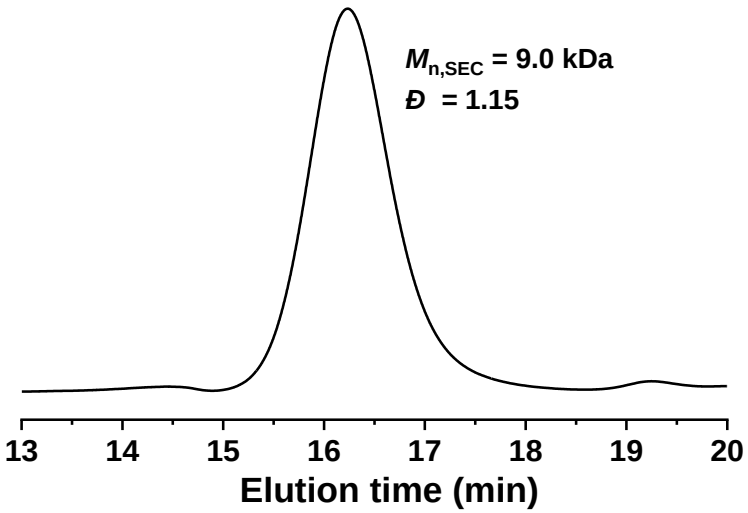

Figure 3.65. SEC (THF) trace of the resultant copolymer synthesized from NA, DPMA, and BO (entry 18 in Table 3.1).

3.3.2 Terpolymerization of oxetane and two cyclic anhydrides for one-step synthesis of block polyester

The author successfully established a reactivity gradient among different anhydrides as mentioned above. In light of this, with the switch of epoxide to oxetane, it is promising to maintain the sequential incorporation based on the difference in reactivity between these anhydrides. Thus, ring-opening copolymerization (ROCOP) of DA, NA, and EPO was conducted using *t*-$BuCO_2Cs$ and BDM as the catalyst and bidirectional initiator at 100 °C, with a $[DA]_0/[NA]_0/[EPO]_0/[BDM]_0/[t\text{-}BuCO_2Cs]$ ratio of 15/15/90/1/1. This experiment produced a triblock copolymer with a sharp junction between poly(DA-*alt*-EPO) and poly(NA-*alt*-EPO) rather than a random copolymer, as predicted. The ROAC of DA/EPO occurred first, as indicated by the decrease in ^1H NMR signals (proton 2', Figure 3.66a) due to DA and the appearance of ^1H NMR signals associated with poly(DA-*alt*-EGE) (proton 2, Figure 3.66a). Once the DA conversion reached 98.5% (Figure 3.66b), the ROAC of NA/EPO turned on and eventually formed triblock copolymers with a very small tapered section consisting of poly(NA-*alt*-EPO)-*b*-poly(DA-*alt*-EPO)-*b*-poly(NA-*alt*-EPO). The SEC analysis of the obtained

copolymers revealed a unimodal distribution ($Đ$ =1.26, Figure 3.66c), and the elution peak maximum shifted continuously toward shorter elution times (higher molecular weights) as copolymerization progressed (Figure 3.66c). The reactivity ratio between DA and NA indicates that DA is significantly more reactive than NA (here please mention the r values), forming a nearly perfect triblock polymer (Figures 3.1 and 3.67). Observing only one diffusion coefficient (Figure 3.68) in DOSY further demonstrated the formation of copolymers as opposed to blends of poly(DA-*alt*-EPO) and poly(NA-*alt*-EPO).

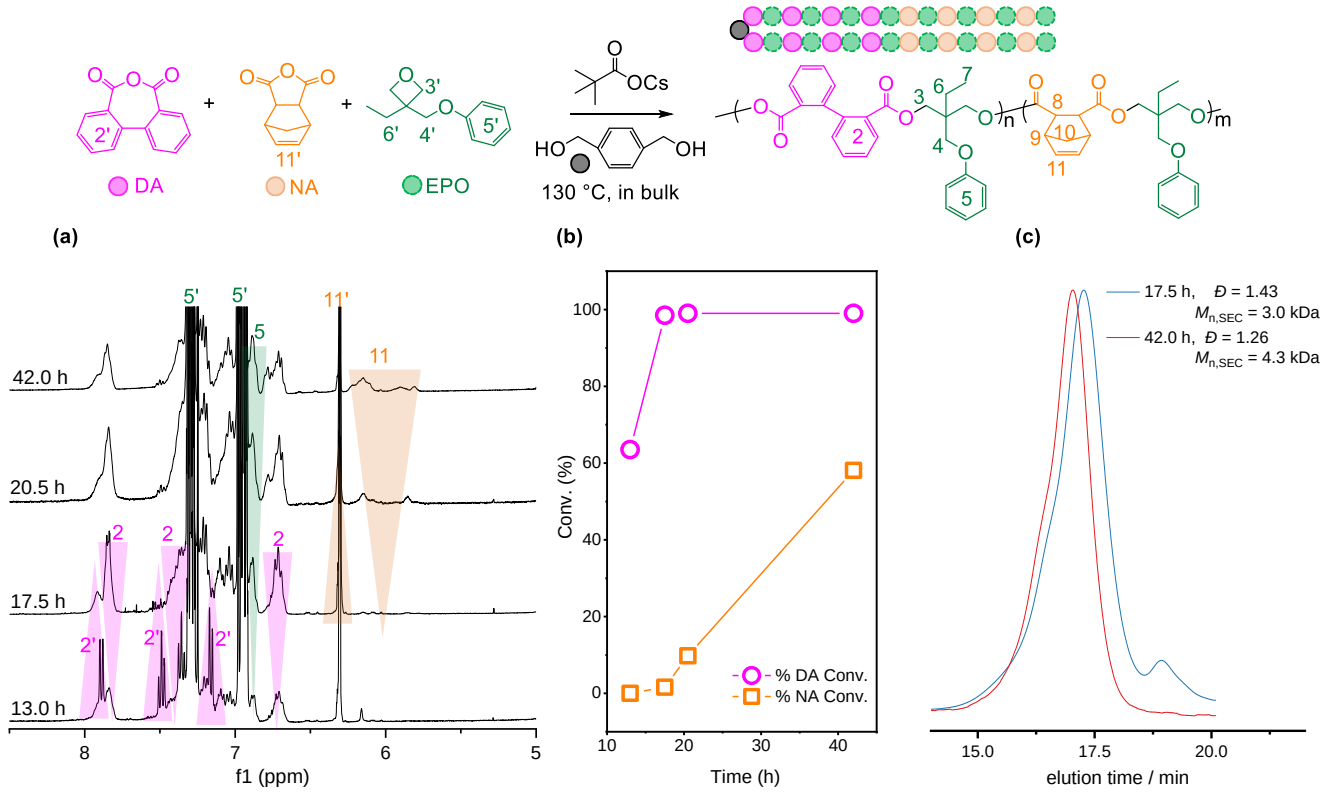

Figure 3.66. Polymerization from a mixture of DA/NA/EPO monitored by NMR spectrum and SEC: (a) The ^{1}H NMR ($CDCl_3$) spectrum of crude aliquots withdrawn from the reaction system for monitoring the conversion of DA, NA, EPO, and the formation of resultant polymers. (b) Plots of monomers conversion versus time. (c) Evolution of SEC traces (THF).

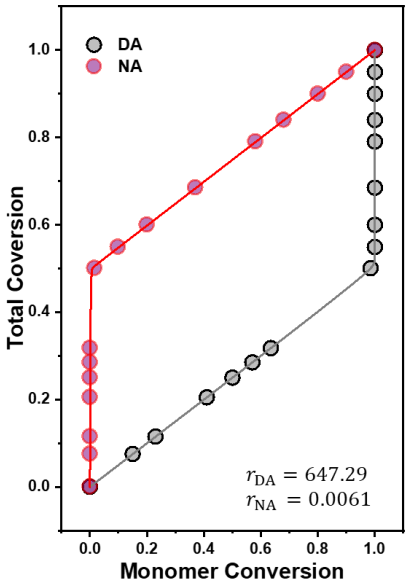

Figure 3.67. Total polymerization conversion plotted against monomer conversion and the data were obtained from time-resolved ^{1}H NMR spectra of a cesium pivalate-catalyzed copolymerization of DA/NA/EPO with a molar ratio of 15/15/90 at 130 °C. Solid black and red lines represent fits to the experimental data using the nonterminal model.

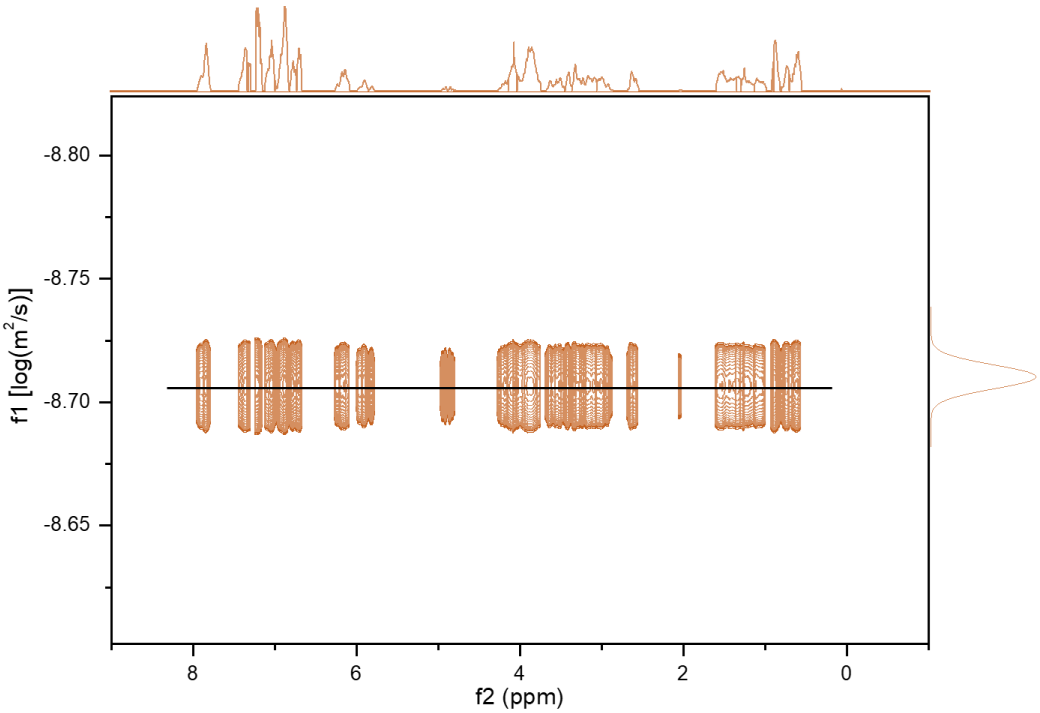

Figure 3.68. DOSY NMR ($CDCl_3$) spectrum of the resultant polymer synthesized from NA, DA, and EPO.

3.3.3 Terpolymerization of epoxide, oxetane, and cyclic anhydride for one-step synthesis of block polyester

As mentioned above, the cesium pivalate catalyst exhibited a high monomer selectivity and kinetic control for ROAC of anhydrides/epoxide as well as ROAC of anhydrides/oxetane. This motivates the author to create a new self-switchable polymerization system by using this catalyst to spontaneously connect ROAC of anhydrides/epoxide with ROAC of anhydrides/oxetane. The mixture of PA, EPO, and CHO was copolymerized using cesium pivalate and BDM as the catalyst and bidirectional initiator, respectively. The ^{1}H NMR analysis revealed that the initial PA/CHO copolymerization was followed by ROAC of PA/EPO to form perfect triblock copolymers devoid of a tapered region and with extremely narrow dispersity (entry 1 in Table 3.3 and Figures 3.2, 3.3, 3.69, and 3.70). The CHO and EPO reactivity ratio (Figure 3.71) revealed that the resultant polymers were almost consistent with a nearly perfect triblock copolymer. To further evaluate the catalytic pathway, copolymerization was conducted with the following ratios: $[PA]_0/[CHO]_0/[EPO]_0/[BDM]_0/[t\text{-}BuCO_2Cs]$: 45/15/90/1/1. After CHO was completely consumed and EPO conversion reached 7.2%, another 7.5 equiv of CHO was added to the reaction mixture, causing PA/EPO ROAC to temporarily cease and PA/CHO ROAC to commence. Perfect chemoselectivity was observed by ^{1}H NMR analysis of aliquots taken at regular intervals throughout the process (entry 2 in Table 3.3 and Figure 3.72). Extended reaction time initially caused the resonance signals of PA (proton 2' at 8.0 and 7.9 ppm) and CHO (proton 3' at 3.1 ppm) to decrease gradually. During this time period, there was no signal at 4.0−3.8 ppm (proton 6), indicating that poly(PA-*alt*-EPO) did not form. ROAC of PA/EPO begins only after CHO is completely consumed in 2 h (degree of polymerization (DP))of PA is 15.1, DP_{CHO} is 15.0, Figures 3.71a and c, as demonstrated by the decrease in signal at 4.1 ppm (proton 6') and the appearance of signal at 4.0−3.8 ppm (proton 6). 7.5 equiv of CHO was introduced to temporarily stop the ROAC of PA/EPO when conversion of EPO reached 7.2% in 19 h (DP_{PA} is 21.5, DP_{CHO} is 15, DP_{EPO} is 6.5, Figures 3.72a and c), and the ROAC

of PA/CHO restarted the propagation from the terminus of P(PA-*alt*-EPO)-*b*-P(PA-*alt*-CHO)-*b*-P(PA-*alt*-EPO). Only after CHO is completely consumed again in 21 h (DP_{PA} is 28.9, DP_{CHO} is 22.5, DP_{EPO} is 6.5, Figures 3.72a and c), does the ROAC of PA/EPO activate, resulting in the formation of a heptablock copolymer (Figures 3.72 and 3.73). SEC detects the narrow and unimodal *Đ*, and the molecular weight increases continuously with monomer consumption (Figures 3.72b), indicating that the propagation from the mixtures of PA, CHO, and EPO was well-controlled. The formation of triblock copolymers rather than blends was confirmed by DOSY NMR spectroscopy result displaying a single diffusion coefficient (Figures 3.72d).[49] To confirm that no EPO was incorporated into the poly(PA-*alt*-CHO) block during polymerization, a copolymerization was performed from a mixture of PA/CHO/EPO with a molar ratio of 15/15/90, and the process was terminated when PA was completely consumed. Utilizing MALDI-TOF MS, the chemical structure of the obtained polymer was analyzed. MALDI-TOF MS of poly(PA-*alt*-CHO) copolymers revealed six peaks, with the major series of peaks corresponding to poly(PA-*alt*-CHO) with BDM as initiator and CHO at two chain ends, and the minor series of peaks resulting from the sodium adduct of poly(PA-*alt*-CHO) with BDM or H_2O as initiator and two PAs or both PA and CHO at two chain ends, respectively (Figure 3.74). The alcohol end group continued to react with residual CHO instead of EPO, resulting in the formation of an ether link at the chain's terminus. This demonstrated that no EPO was inserted into the poly(PA-*alt*-CHO) and no transesterification side reaction occurred during terpolymerization.

Table 3.3. The self-switchable polymerizations from epoxide, oxetane, and cyclic anhydride catalyzed by *t*-$BuCO_2Cs$ [a]

entry	monomers	[anhydride1]$_0$/ [anhydride2]$_0$/ [epoxide]$_0$/[oxetane]$_0$/ [BDM]$_0$/[*t*-$BuCO_2Cs$]	Temp. (°C)	Time (h)	conv. [b] [%] (anhydride, epoxide, and oxetane)	$M_{n,\ th.}$ [c](kDa)	$M_{n,\ NMR.}$ [b](kDa)	$M_{n,\ SEC.}$ [d](kDa)	$Đ$ [d]
1	PA/CHO/EPO	30/15/90/1/1	130	19	PA = 89.5, CHO > 99, EPO = 13.2	7.9	7.1	4.9	1.14
2	PA/CHO/EPO	45/22.5/90/1/1	130	36	PA = 82.9, CHO > 99, EPO = 16.1	10.7	9.7	6.1	1.09
3	PA/AGE/EPO	30/15/90/1/1	130	24	PA = 96.3, AGE > 99, EPO = 15.6	8.8	7.6	6.2	1.14

[a]Polymerization conditions: Ar atmosphere. [b]Determined by ^{1}H NMR analysis of the obtained polymer in $CDCl_3$. [c]Calculated using [oxetane]$_0$/[I]$_0$ × conv. × (M.W. of anhydride + M.W. of oxetane) + [epoxide]$_0$/[I]$_0$ × conv. × (M.W. of anhydride + M.W. of epoxide) + (M.W. of initiator). [d]Determined by the SEC analysis of the obtained polymer in THF with a PSt standard.

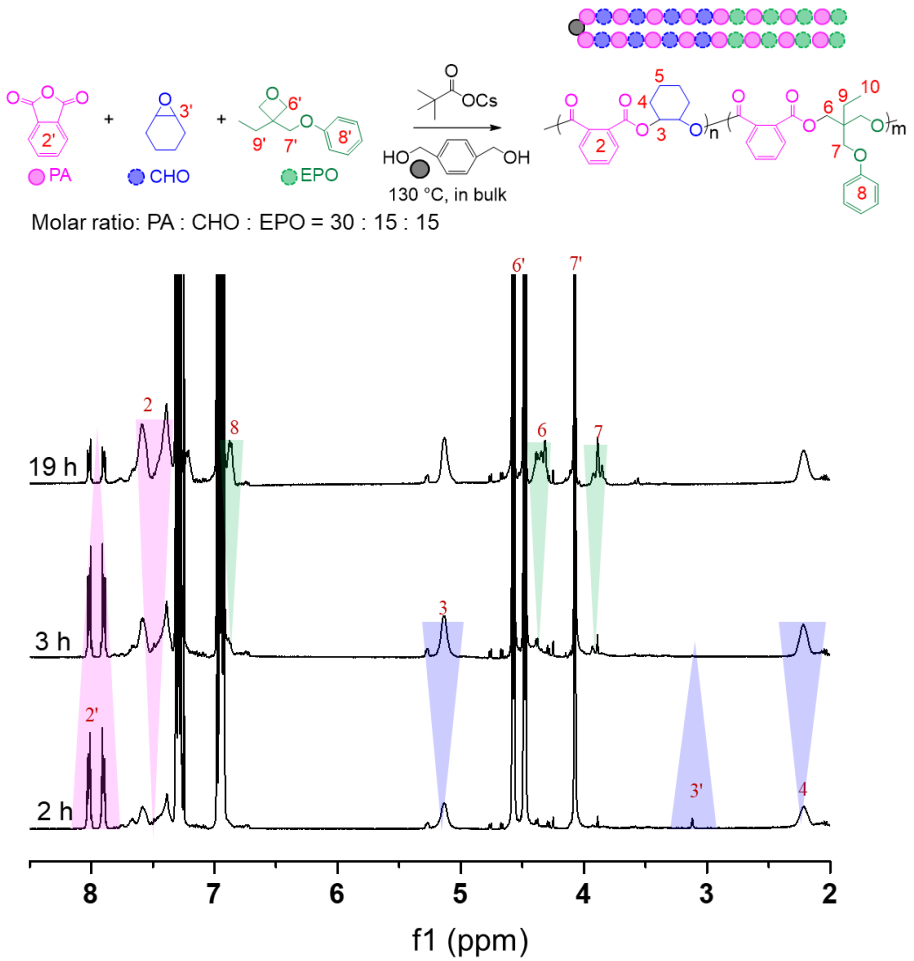

Figure 3.69. ^{1}H NMR ($CDCl_3$) spectra of crude aliquots withdrawn from the reaction system for monitoring the conversion of PA, CHO, EPO, and the formation of resultant polymers (entry 1 in Table 3.3).

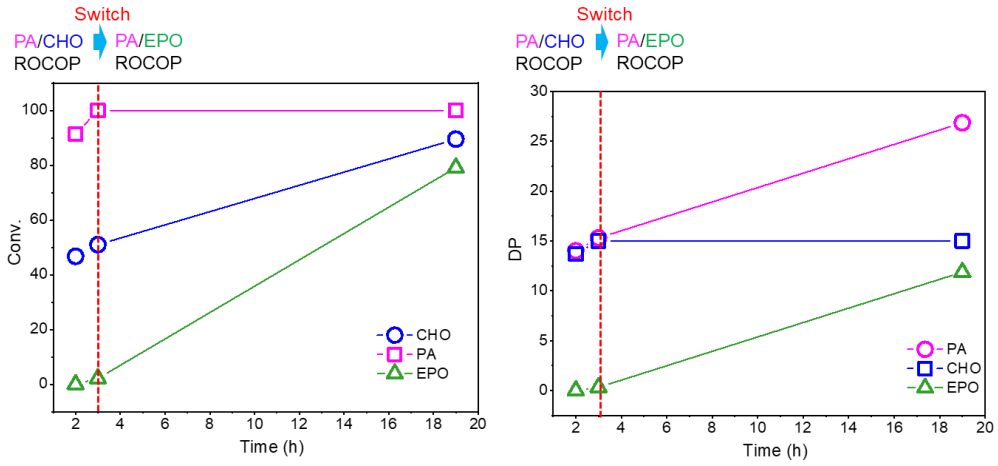

Figure 3.70. Plots of monomer conversion and degree of polymerization (DP) versus time. The polymerization of PA, CHO with EPO was performed at 130 °C (entry 1 in Table 3.3). The conv. of EPO is normalized.

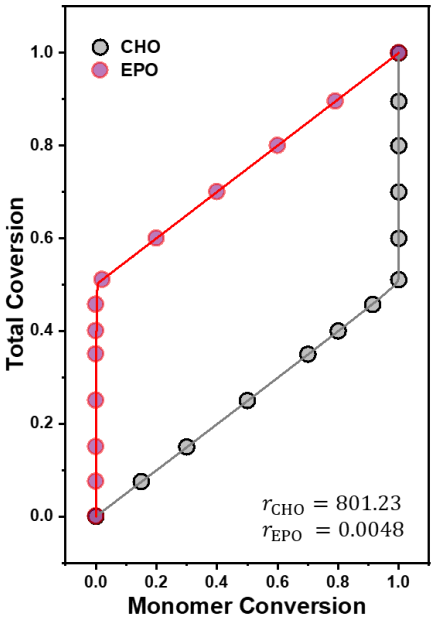

Figure 3.71. Total polymerization conversion plotted against monomer conversion and the data were obtained from time-resolved ^{1}H NMR spectra of a cesium pivalate-catalyzed copolymerization of PA/CHO/EPO with a molar ratio of 30/15/900 at 130 °C. Solid black and red lines represent fits to the experimental data using the nonterminal model.

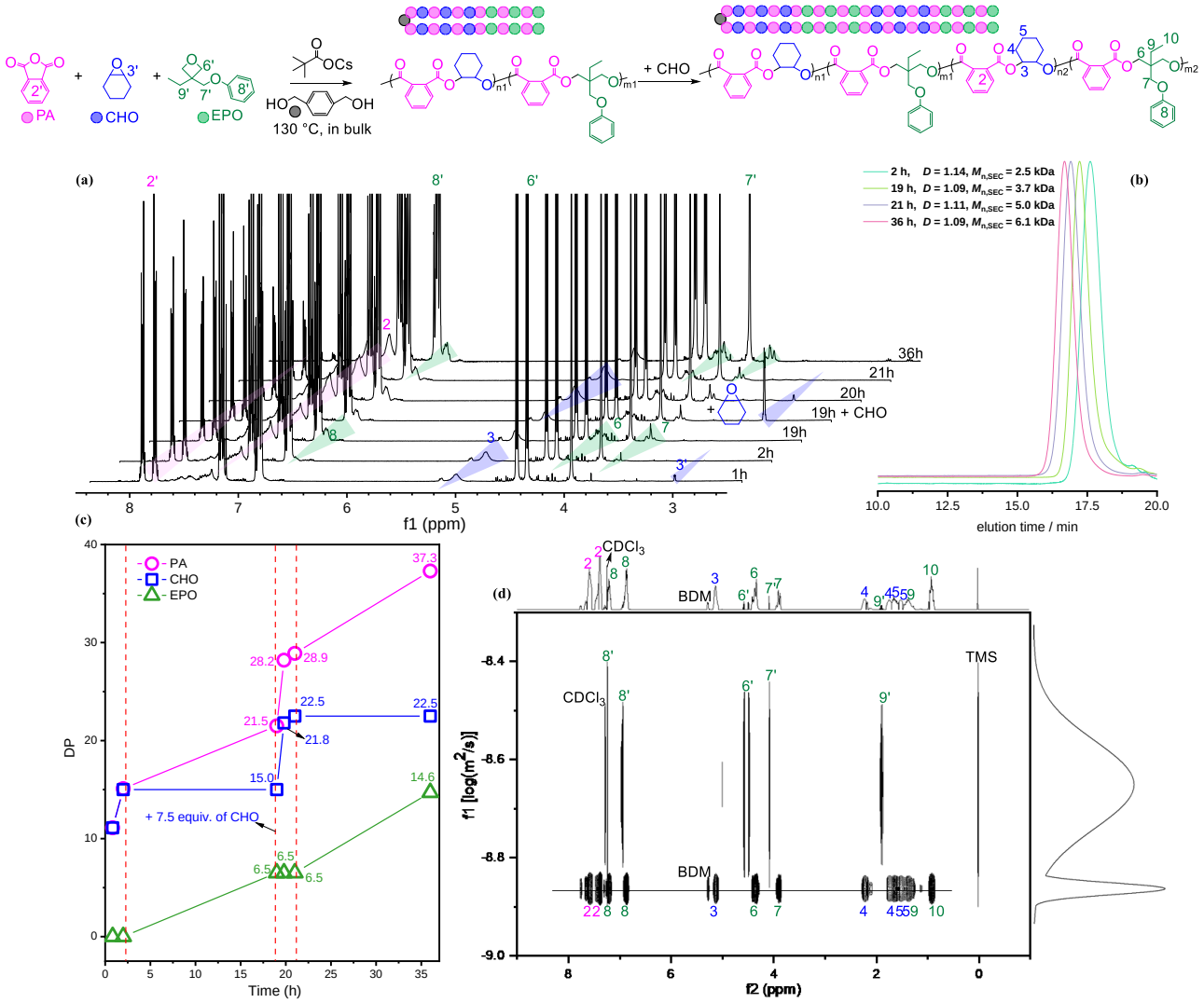

Figure 3.72. polymerization from a mixture of PA/CHO/EPO monitored by NMR spectrum and SEC (entry 2 in Table 3.3): (a) The ^{1}H NMR ($CDCl_3$) spectrum of crude aliquots withdrawn from the reaction system for monitoring the conversion of PA, CHO, EPO, and the formation of resultant polymers. (b) Evolution of SEC traces (THF). (c) Plots of the degree of polymerization (DP) versus time. (d) DOSY ($CDCl_3$) spectrum of resultant polymers.

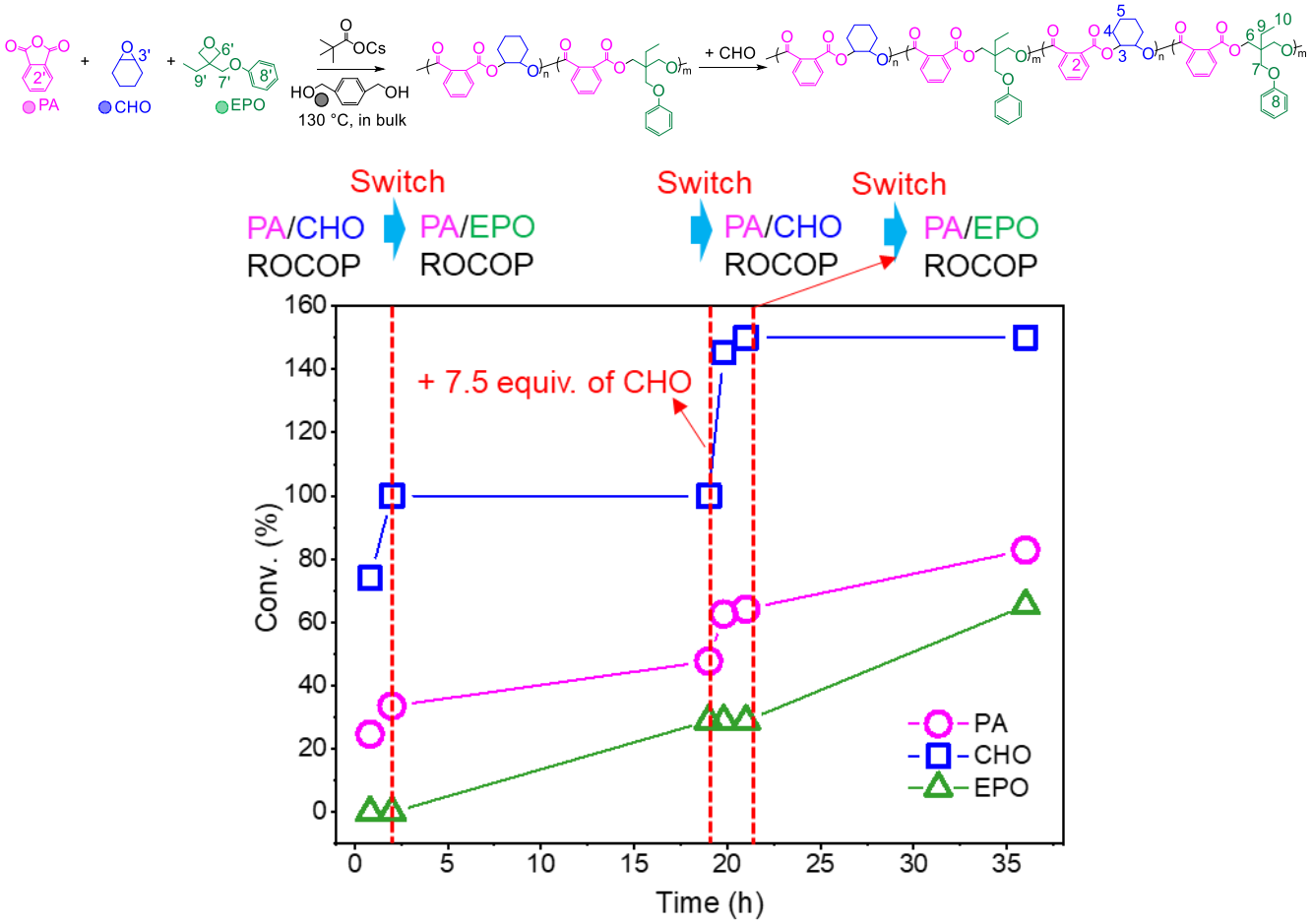

Figure 3.73. Plots of monomer conversion versus time. The polymerization of PA, CHO, and EPO was performed at 130 °C (entry 2 in Table 3.3). The conv. of EPO is normalized.

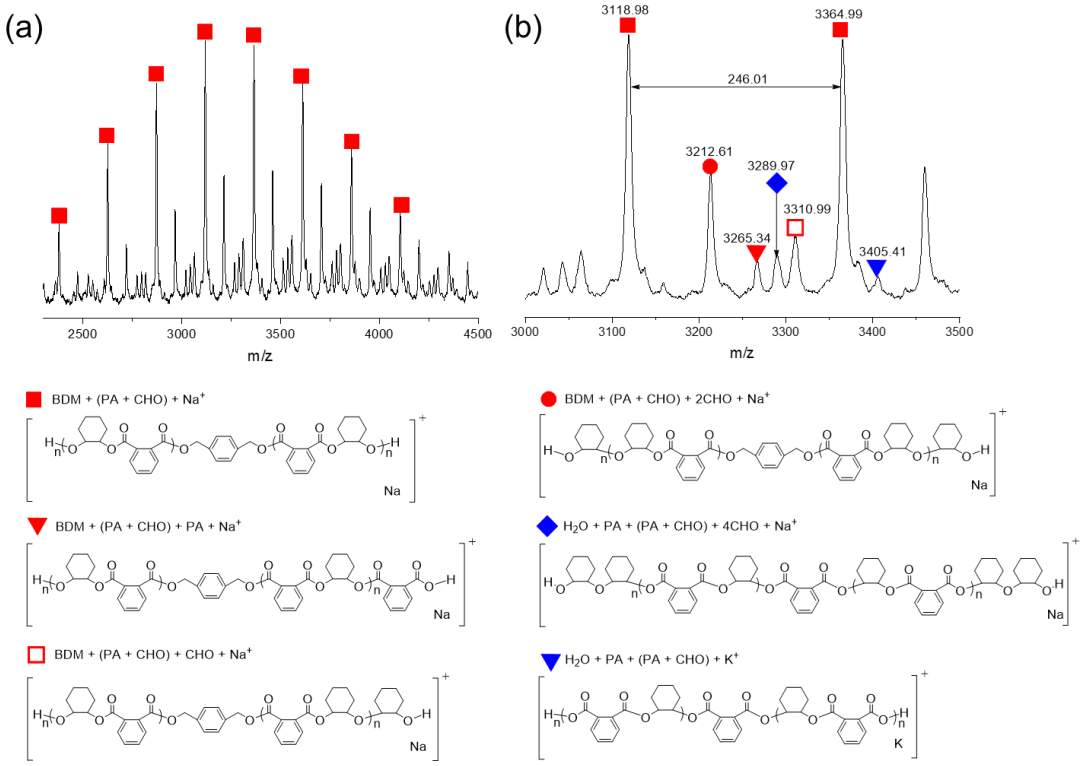

Figure 3.74. MALDI-TOF MS of the P(PA-*alt*-CHO) obtained by the polymerization of PA/CHO/EPO at 130 °C with a [*t*-BuCO$_2$Cs]/[BDM]$_0$/[PA]$_0$/[CHO]$_0$/[EPO]$_0$ ratio of 1/1/15/15/90. The conversion of PA is 100%.

The self-switchable polymerization was then applied to allyl glycidyl ether (AGE). The perfect BAB triblock copolymers, where the A and B blocks were prepared by ROAC of PA/AGE and ROAC of PA/EPO, respectively, were obtained by copolymerizing the mixture of PA/AGE/EPO, demonstrating a high degree of control (entry 3 in Table 3.3, Figures 3.4 and 3.5), as evidenced by a narrow dispersity and an increase in molecular weight with monomer consumption (Figure 3.75). The copolymerization of a PA/AGE/EPO mixture with a molar ratio of 15/15/90 was stopped when the reaction time reached 2 h. The MALDI-TOF MS result of the obtained polymer confirmed the absence of EPO incorporation and any transesterification side reaction during ROAC of PA/AGE. Because the major series of peaks corresponded to poly(PA-*alt*-AGE) containing BDM as an initiator and AGE and PA at two chain ends, and the minor series of peaks resulted from the sodium adduct of poly(PA-*alt*-AGE) containing BDM and two AGEs at two chain ends (Figure 3.76).

Following the reactivity order of anhydrides, the analysis of reactivity ratios revealed that these epoxides are significantly more active than EPO, following the current reactivity order: anhydrides >> epoxide >> oxetane.

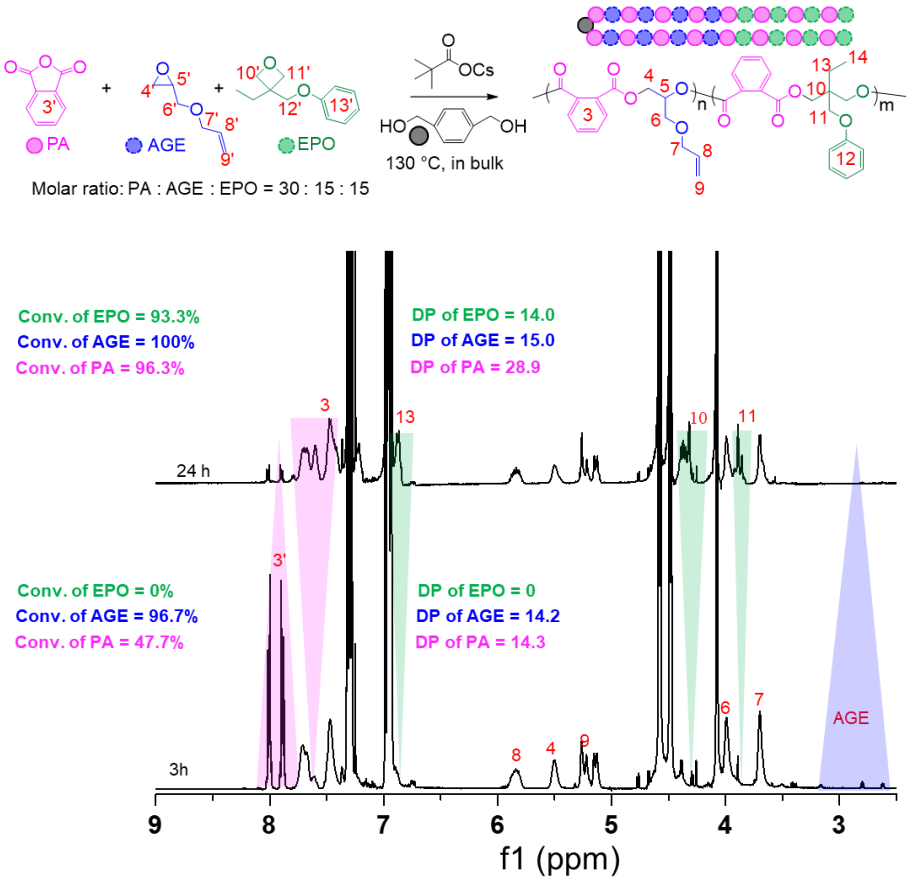

Figure 3.75. The ^{1}H NMR ($CDCl_3$) spectra of crude aliquots withdrawn from the reaction system for monitoring the conversion of PA, AGE, and EPO, and the formation of resultant polymers (entry 3 in Table 3.3). The conv. of EPO is normalized.

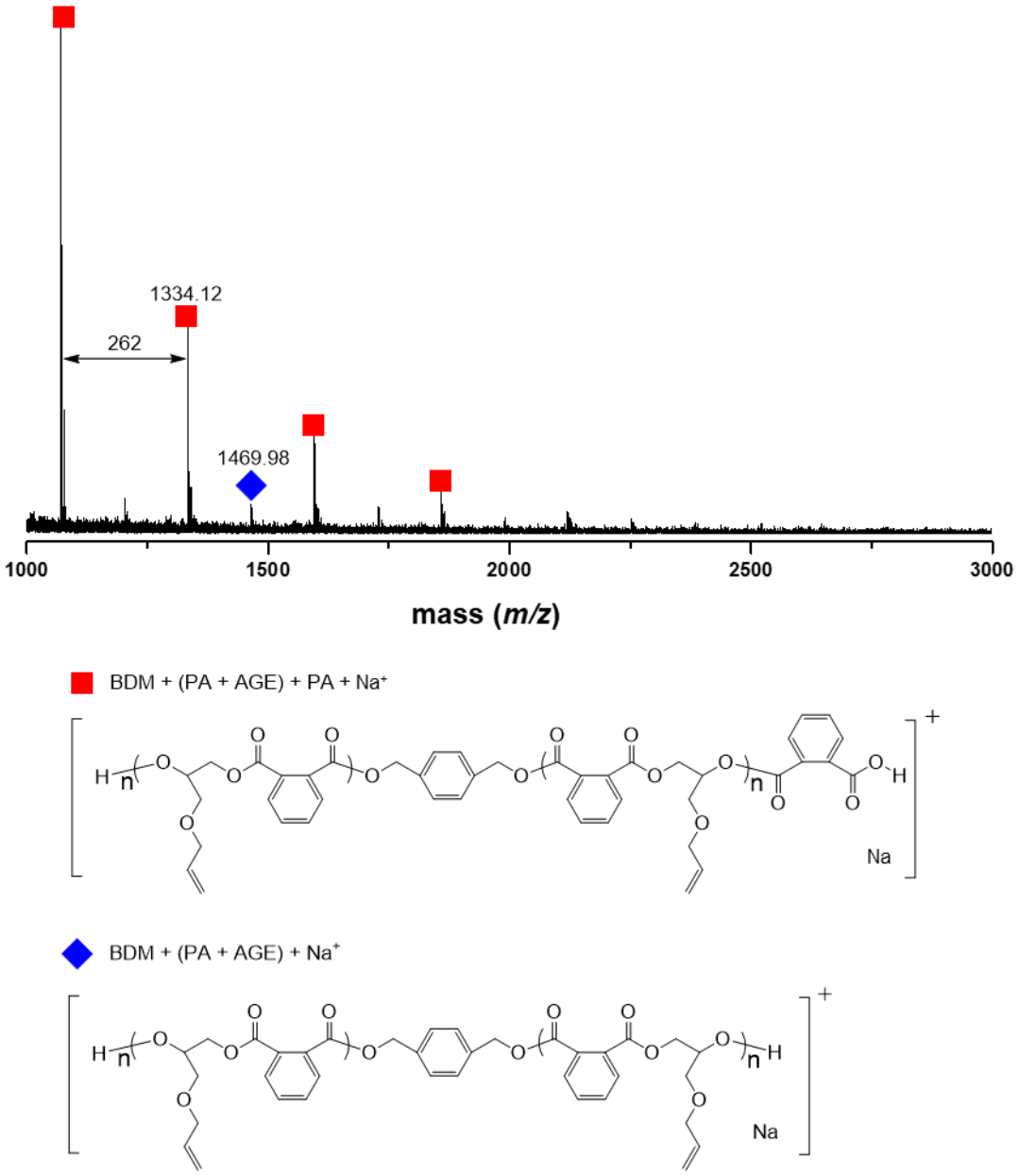

Figure 3.76. |MALDI-TOF MS of the poly(PA-*alt*-AGE) obtained by the polymerization of PA/AGE/EPO at 130 °C for 2h with a [*t*-$BuCO_2Cs$]/$[BDM]_0$/$[PA]_0$/$[AGE]_0$/$[EPO]_0$ ratio of 1/1/15/15/90. The conversion of PA is 79.3%.

3.3.4 Copolymerization of epoxide, oxetane, and two cyclic anhydrides for one-step synthesis of block polyester

Synchronous control of each unit structure in both blocks for self-switchable alternating copolymerization is a formidable obstacle; thus, no relevant reports have been published to date. Following

the above studies, using reactivity gradient among different anhydrides to combine with extremely large reactivity difference between epoxide and oxetane can provide an opportunity for multi-dimensional control of block copolymer. As a proof of concept, the cesium pivalate catalyst was used to attempt to link DA/CHO ROAC and NA/EPO ROAC, thereby establishing multidimensional controlled self-switchable alternating copolymerization. The mixture of DA, CHO, NA, and EPO was copolymerized using cesium pivalate and BDM as the catalyst and bidirectional initiator, respectively. The ^{1}H NMR spectra indicated that the ROAC of DA/CHO began immediately (Figure 3.77a), as evidenced by the simultaneous decrease of peaks due to DA (proton 2') and CHO (3') and the increase of poly(DA-*alt*-CHO) signals (proton 2). Within 2 h, the conversion of DA and CHO reached 99% (DP = 15) and 99% (DP = 15), respectively, and the conversion of NA and EPO reached 1.5 % (DP = 0.23) and 1.7 % (DP = 0.26) (Figures 3.77b and 3.77c), indicating that only a very small tapered section was formed. As the reaction progresses, the signal from the second-stage alternating units, i.e., poly(NA-*alt*-EPO), increases, resulting in the formation of the triblock tetrapolymer (entry 1 in Table 3.4). The SEC elution peak shifted to the higher molecular weight region while maintaining unimodal/narrow distributions ($Đ$ < 1.30, Figure 3.77d), indicating that ROCOP is well controlled without significant transesterification. By simply adjusting the molar ratio of DA/CHO/NA/EPO from 15:15:15:160 to 30:15:15:160, pentablock tetrapolymers were obtained from the polymerization of DA/CHO/NA/EPO with BDM as an initiator. In particular, due to reactivity order of DA >> NA for the alkoxide end group and reactivity order of CHO >> EPO for carboxylic end group, ROAC of DA/CHO occurred first. Upon complete consumption of CHO in 2 h, excess DA began to copolymerize with EPO, forming poly(DA-*alt*-EPO) block. Once the conversion of DA reached 100%, the ROAC of NA/EPO turned on and finally formed poly(NA-*alt*-EPO)-*b*-poly(DA-*alt*-EPO)-*b*-poly(DA-*alt*-CHO)-*b*-poly(DA-*alt*-EPO)-*b*-poly(NA-*alt*-EPO). As evidenced by SEC and ^{1}H NMR analyses, pentablock tetrapolymers with a tapered section of less than 3% was confirmed (entry 2 in Table 3.4, Figures 3.6, 3.7, 3.78, and 3.79). By changing the molar ratio of DA/CHO/NA/EPO from

30:15:15:160 to 15:30:30:160, DA/CHO ROAC first formed a poly(DA-*alt*-CHO) (Figure 3.80), followed by the serial incorporation of poly(NA-*alt*-CHO) and poly(NA-*alt*-EPO) blocks generated by NA/CHO ROAC and NA/EPO ROAC, respectively. Finally, poly(DA-*alt*-EPO)-*b*-poly(NA-*alt*-CHO)-*b*-poly(DA-*alt*-CHO)-*b*-poly(NA-*alt*-CHO)-*b*-poly(DA-*alt*-EPO) pentablock tetrapolymers were produced in an one-step procedure (entry 3 in Table 3.4, Figures 3.80–3.83) and showed different sequence structure from the above resulting copolymers, suggesting that various sequence-controlled block tetrapolymers can be synthesized by simply adjusting the molar ratio of the monomer mixture.

Table 3.4. The self-switchable polymerizations from epoxide, oxetane, and two cyclic anhydrides catalyzed by *t*-$BuCO_2Cs$ [a]

entry	monomers	$[anhydride1]_0/[anhydride2]_0/[epoxide]_0/[oxetane]_0/[BDM]_0/[t\text{-}BuCO_2Cs]$	Temp. (°C)	Time (h)	conv. [b] [%] (anhydride, epoxide, and oxetane)	$M_{n,th.}$ [c](kDa)	$M_{n,NMR}$ [b](kDa)	$M_{n,SEC}$ [d](kDa)	$Đ$[d]
1	DA/CHO/NA/EPO	15/15/15/160/1/1	130	30	DA > 99, CHO > 99, NA = 64.8, EPO = 6.0	8.5	11.7	4.9	1.28
2	DA/CHO/NA/EPO	30/15/15/160/1/1	130	56	DA > 99, CHO > 99, NA = 54, EPO = 14.4	14.1	40.0	6.2	1.23
3	DA/CHO/NA/EPO	15/30/30/160/1/1	130	41	DA > 99, CHO > 99, NA = 87.4, EPO = 6.7	13.5	27.8	6.0	1.23
4[e]	PA/BGE/NA/TO	15/15/15/22.5/1/1	110	114	PA > 99, BGE > 99, NA = 74.2, EPO = 49.3	7.3	7.0	7.4	1.21

[a] Polymerization conditions: Ar atmosphere. [b] Determined by ^{1}H NMR analysis of the obtained polymer in $CDCl_3$. [c] [c]Calculated using $[oxetane]_0/[I]_0$ × conv. × (M.W. of anhydride1 + M.W. of oxetane) + $[epoxide]_0/[I]_0$ × conv. × (M.W. of anhydride2 + M.W. of epoxide) + (M.W. of initiator). [d] Determined by the SEC analysis of the obtained polymer in THF with a PSt standard. [e] THF acted as solvent: $[PA]_0$ = 1.5.

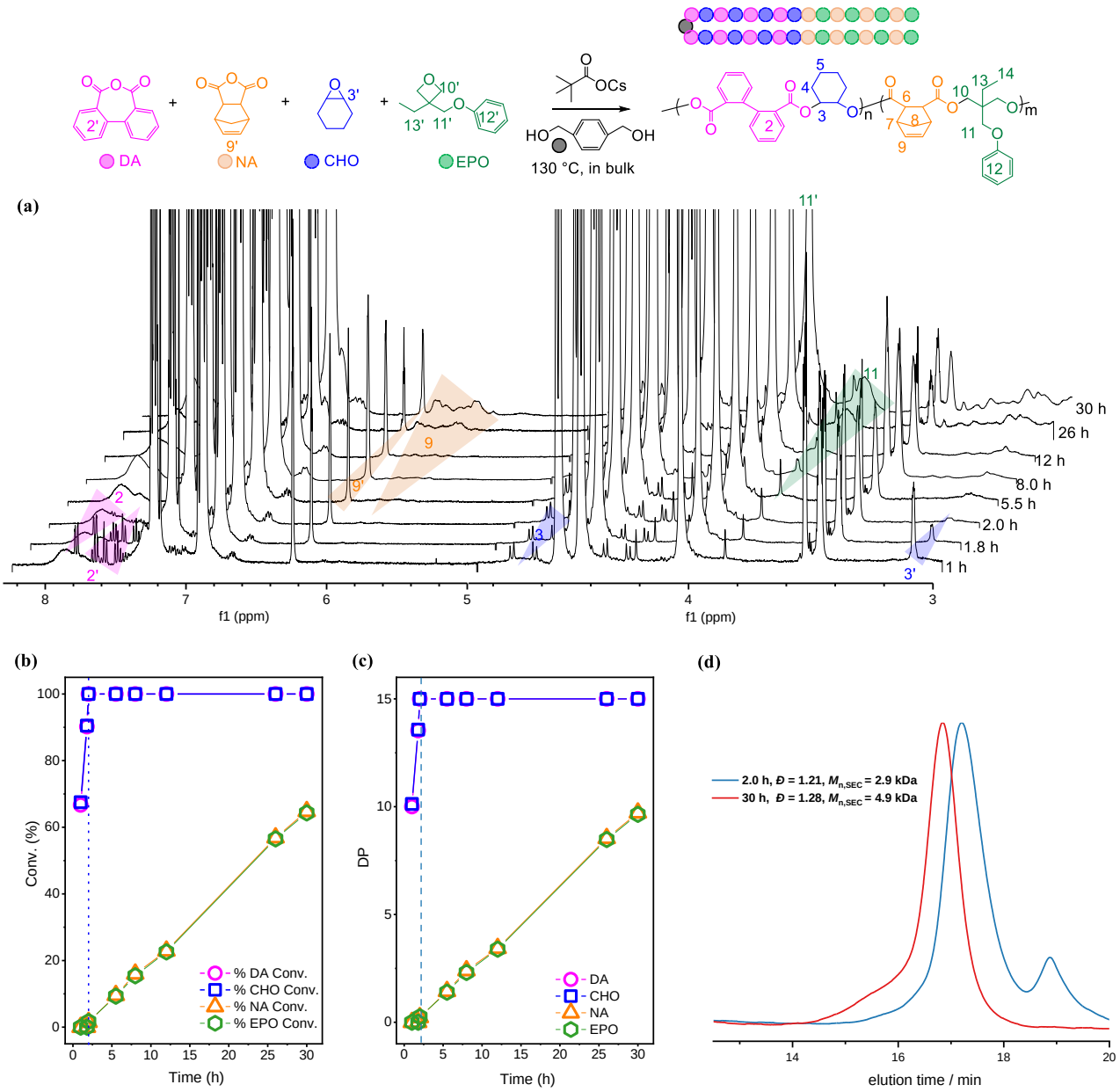

Figure 3.77. polymerization from a mixture of DA/CHO/NA/EPO monitored by NMR spectrum and SEC (entry 1 in Table 3.4): (a) The ^{1}H NMR ($CDCl_3$) spectrum of crude aliquots withdrawn from the reaction system for monitoring the conversion of DA, CHO, NA, EPO, and the formation of resultant polymers. (b) Plots of monomers conversion versus time and conversion of EPO are normalized. (c) Plots of the degree of polymerization versus time. (d) Evolution of SEC traces (THF).

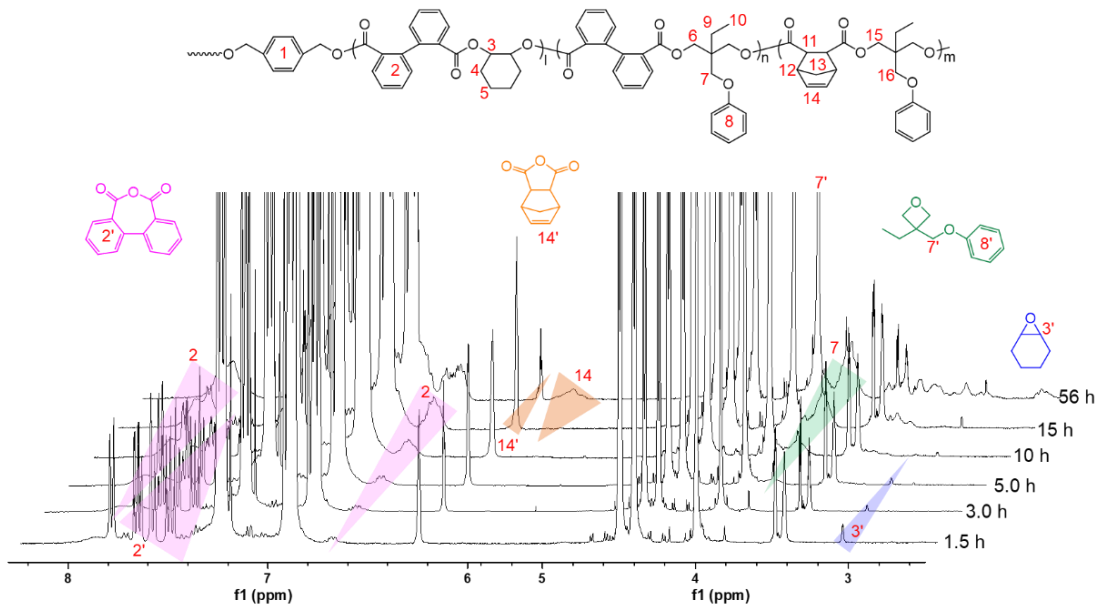

Figure 3.78. ^{1}H NMR ($CDCl_3$) spectra of crude aliquots withdrawn from the reaction system for monitoring the conversion of DA, CHO, NA, and EPO, and the formation of resultant polymers (entry 2 in Table 3.4).

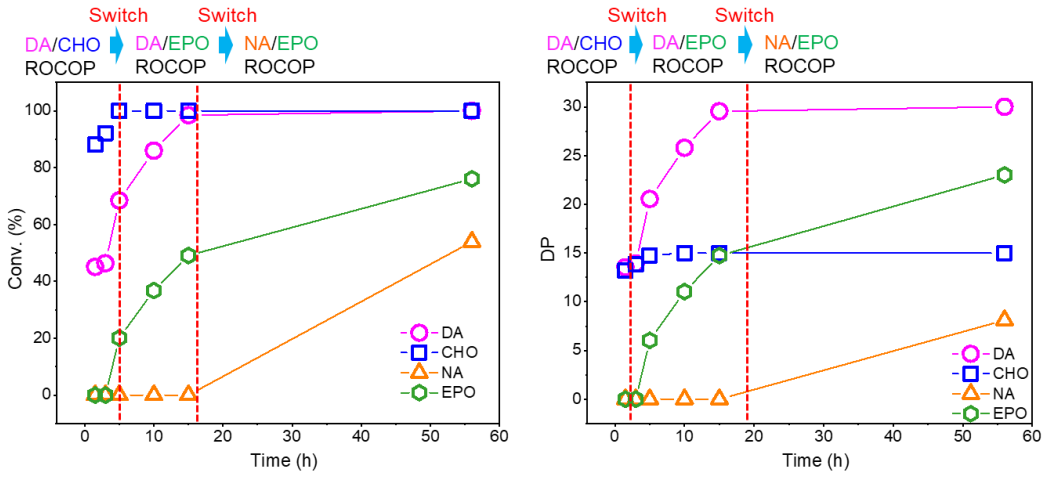

Figure 3.79. plots of monomer conversion DP versus time. The polymerization of DA, CHO, NA, and EPO was performed at 130 °C (entry 2 in Table 3.4). The conv. of EPO is normalized.

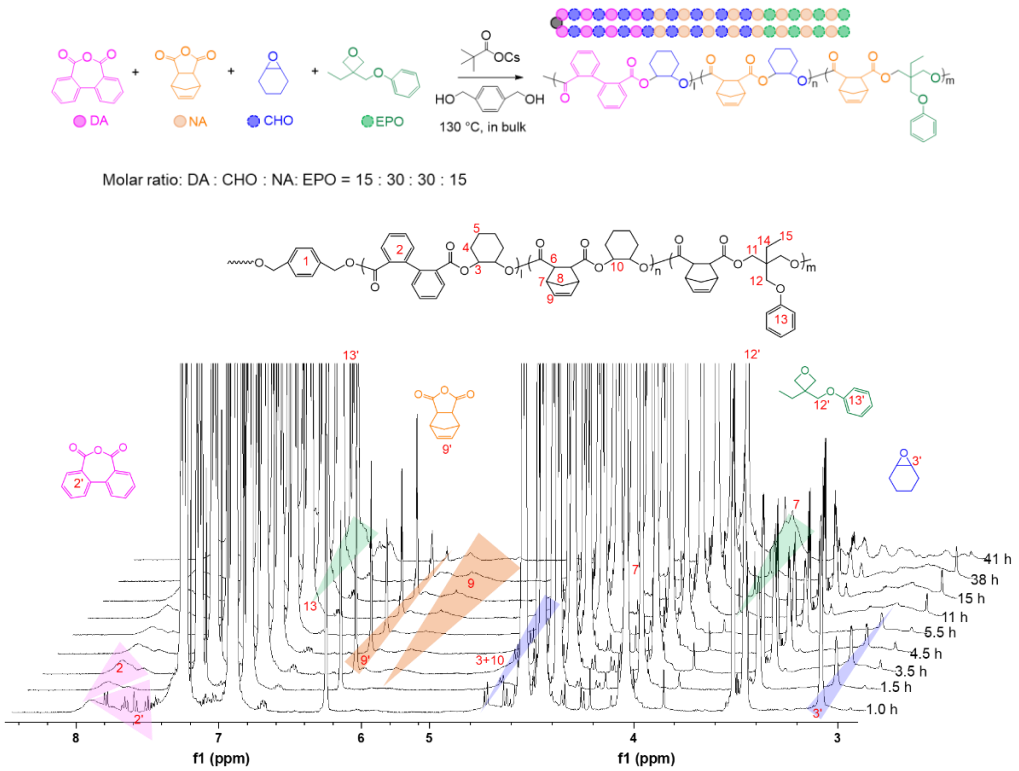

Figure 3.80. ^{1}H NMR ($CDCl_3$) spectra of crude aliquots withdrawn from the reaction system for monitoring the conversion of DA, CHO, NA, and EPO, and the formation of resultant polymers (entry 3 in Table 3.4).

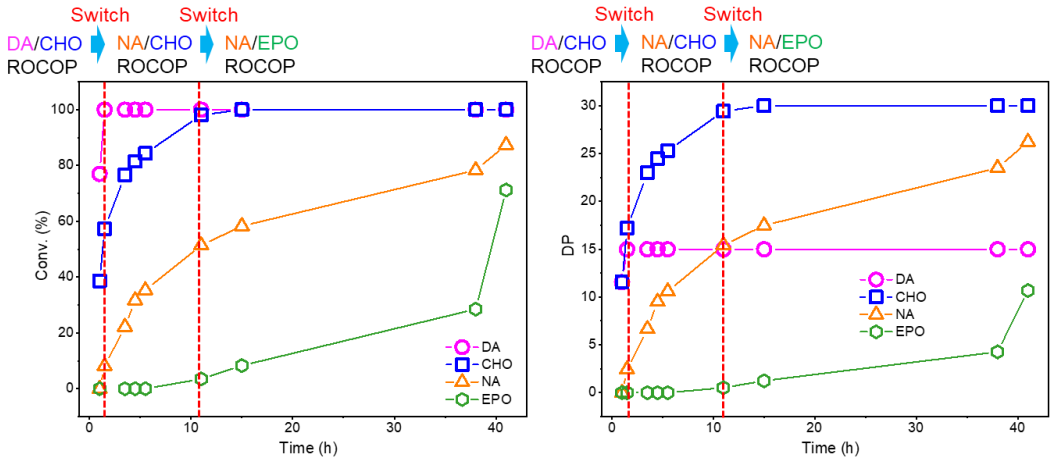

Figure 3.81. plots of monomer conversion and DP versus time. The polymerization of DA, CHO, NA, and EPO was performed at 130 °C (entry 3 in Table 3.4). The conv. of EPO is normalized.

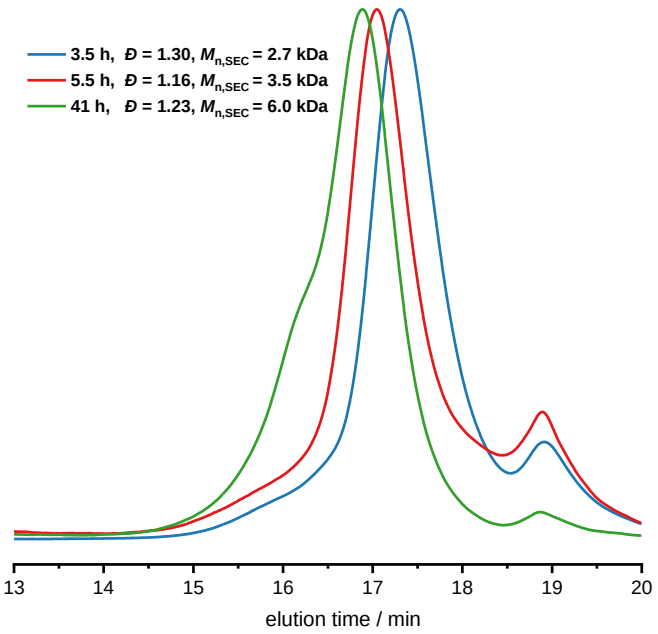

Figure 3.82. SEC (THF) trace of the resultant polymer synthesized from DA, CHO, NA, and EPO (entry 3 in Table 3.4).

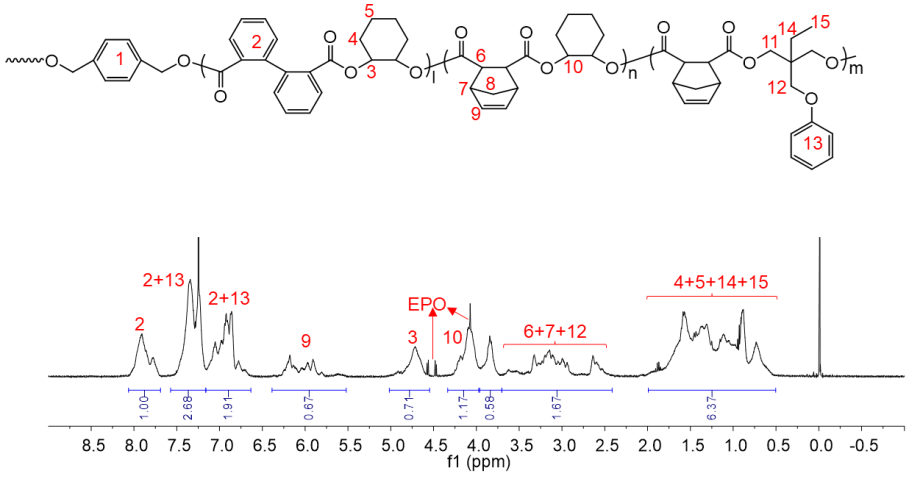

Figure 3.83. ^{1}H NMR ($CDCl_3$) spectrum of the resultant polymer synthesized from DA, CHO, NA, and EPO (entry 3 in Table 3.4).

The author also tried the other anhydrides, epoxides, and oxetanes combination to testify the versatility of the quarterpolymerization system. The quarterpolymerization from PA/benzyl glycidyl ether (BGE)/NA/TO

with the molar ratio of 15:15:15:22.5 was performed in 110 °C, leading to the triblock tetrapolymer with narrow dispersity (entry 4 in Table 3.4, Figures 3.8, 3.9, 3.84, and 3.85).

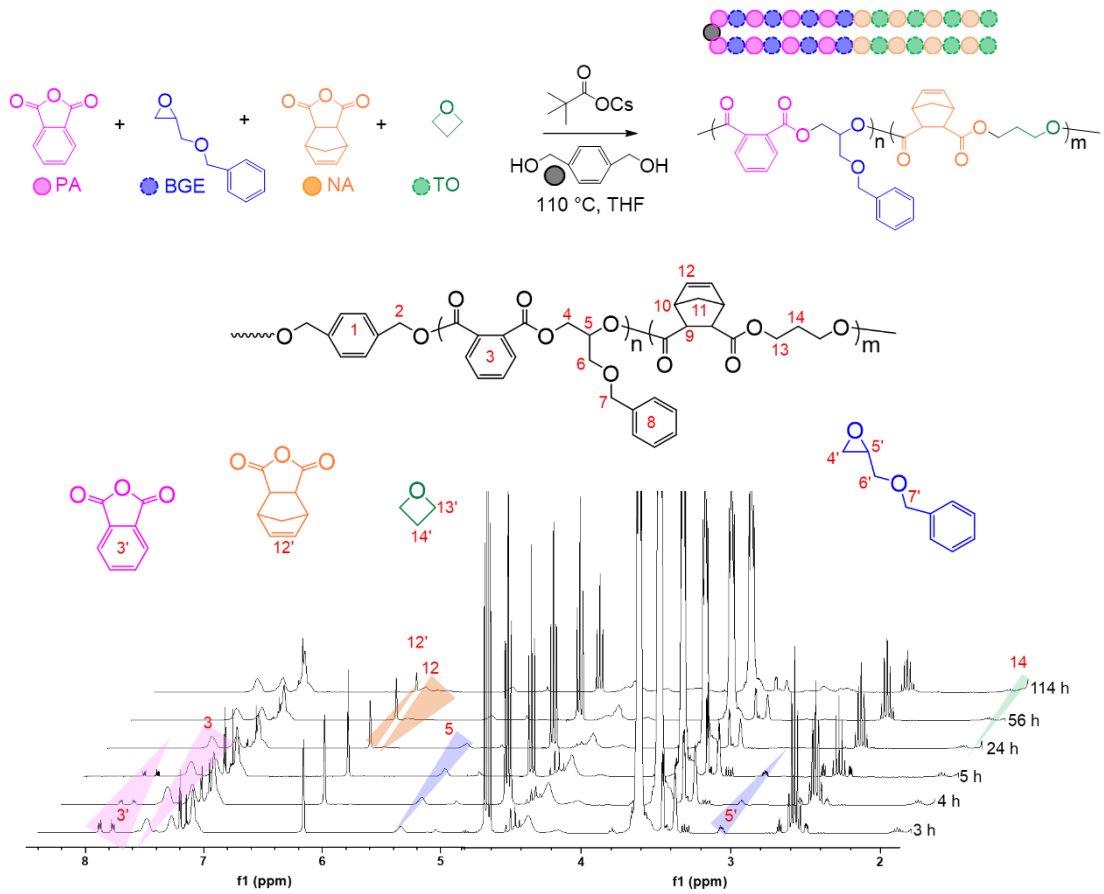

Figure 3.84. ^{1}H NMR ($CDCl_3$) spectra of crude aliquots withdrawn from the reaction system for monitoring the conversion of PA, BGE, NA, and TO, and the formation of resultant polymers (entry 4 in Table 3.4).

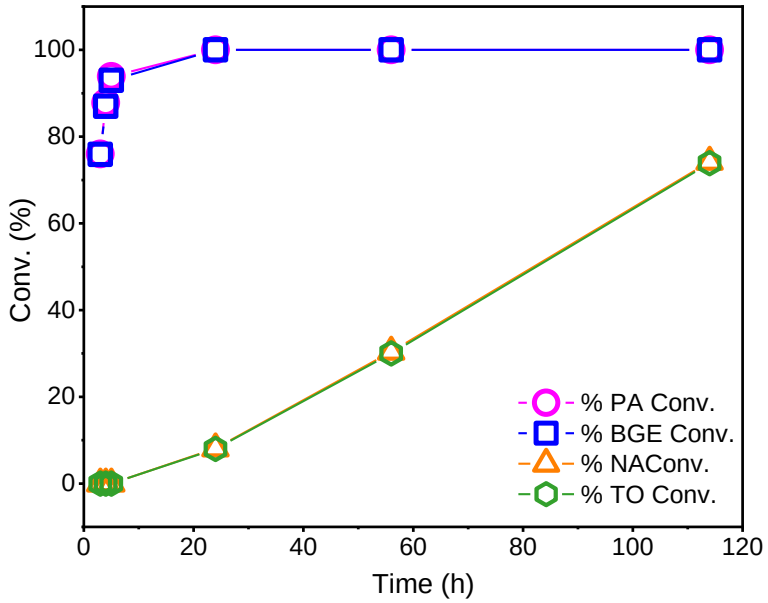

Figure 3.85. plots of monomer conversion versus time. The polymerization of PA, BGE, NA, and TO was performed at 100 °C (entry 4 in Table 3.4). The conv. of EPO is normalized.

3.4 Conclusion

In this chapter, the author applied cesium pivalate to connect two catalytic cycles among different epoxide/cyclic anhydrides ROAC, as well as oxetane/cyclic anhydrides ROAC, resulting in polyesters with various chain structures and monomer sequences. The polymerization behavior of ROAC with two epoxide/cyclic anhydrides ROAC catalytic cycles were deeply studied and summarized the reactivity trend of cyclic anhydrides.

Via incorporating oxetane monomer, the structures of synthesized polyester were further enriched. The reactivity trend of cyclic anhydrides on oxetane/cyclic anhydrides ROAC was confirmed as the same as that of epoxide/cyclic anhydrides ROAC. Based on the reactivity order of epoxides >> oxetane, ROCOP of epoxide, oxetane, and cyclic anhydride and ROCOP of epoxide, oxetane, and two cyclic anhydrides were implemented for one-step synthesis of block polyester with more flexible and adjustable mainchain structure and defined monomers sequence. This self-switchable copolymerization platform therefore promising and significant for both laboratory- and industrial-scale productions of block polymers with complex macromolecular architectures.

3.5 References

1. Bates, C. M.; Bates, F. S. 50th Anniversary Perspective: Block Polymers–Pure Potential. *Macromolecules*. **2017**, *50*, 3–22.
2. Eagan, J. M.; Xu, J.; Di Girolamo, R.; Thurber, C. M.; Macosko, C. W.; LaPointe, A. M.; Bates, F. S.; Coates, G. W. Combining Polyethylene and Polypropylene: Enhanced Performance with PE/IPP Multiblock Polymers. *Science*. **2017**, *355*, 814–816.
3. Cabral, H., Miyata, K., Osada, K., & Kataoka, K. Block copolymer micelles in nanomedicine applications. *Chemical reviews*. **2018**, *118*, 6844-6892.
4. Hsu, L. C.; Isono, T.; Lin, Y. C.; Kobayashi, S.; Chiang, Y. C.; Jiang, D. H.; Hung, C. C.; Ercan, E.; Yang, W. C.; Hsieh, H. C.; Tajima, K.; Satoh, T.; Chen, W. C. Stretchable OFET Memories: Tuning the Morphology and the Charge-Trapping Ability of Conjugated Block Copolymers Through Soft Segment Branching. *ACS Appl. Mater. Interfaces*. **2021**, *13*, 2932–2943.
5. Oh, J. Y.; Rondeau-Gagné, S.; Chiu, Y. C.; Chortos, A.; Lissel, F.; Wang, G. N.; Schroeder, B. C.; Kurosawa, T.; Lopez, J.; Katsumata, T.; Xu, J.; Zhu, C.; Gu, X.; Bae, W. G.; Kim, Y.; Jin, L.; Chung, J. W.; Tok, J. B. H.; Bao, Z. Intrinsically Stretchable and Healable Semiconducting Polymer for Organic Transistors. *Nature*. **2016**, *539*, 411–415.
6. Chiu, Y. C.; Otsuka, I.; Halila, S.; Borsali, R.; Chen, W. C. High-Performance Nonvolatile Transistor Memories of Pentacence Using the Green Electrets of Sugar-Based Block Copolymers and Their Supramolecules. *Adv. Funct. Mater.* **2014**, *24*, 4240–4249.
7. Hsueh, H. Y.; Yao, C.; Ho, R. M. Well-ordered nanohybrids and nanoporous materials from gyroid block copolymer templates. *Chem Soc Rev*, **2015**, *44*, 1974-2018.
8. Bates, C. M.; Maher, M. J.; Janes, D. W.; Ellison, C. J.; Willson, C. G. Block copolymer lithography. *Macromolecules*, **2014**, *47*, 2-12.

9. Moad, G. RAFT Polymerization to Form Stimuli-Responsive Polymers. *Polym. Chem.* **2017**, *8*, 177–219.

10. Hillmyer, M. A.; Tolman, W. B. Aliphatic Polyester Block Polymers: Renewable, Degradable, and Sustainable. *Acc. Chem. Res.* **2014**, *47*, 2390–2396.

11. Ouchi, M.; Terashima, T.; Sawamoto, M. Transition Metal-Catalyzed Living Radical Polymerization: Toward Perfection in Catalysis and Precision Polymer Synthesis. *Chem. Rev.* **2009**, *109*, 4963–5050.

12. Matyjaszewski, K. Architecturally Complex Polymers with Controlled Heterogeneity. *Science*. **2011**, *333*, 1104–1105.

13. Hu, C.; Pang, X.; Chen, X. Self-Switchable Polymerization: A Smart Approach to Sequence-Controlled Degradable Copolymers. *Macromolecules*. **2022**, *55*, 1879–1893.

14. Asano, S.; Aida, T.; Inoue, S. Polymerization of Epoxide and *β*-Lactone Catalyzed by Aluminum Porphyrin. Exchange of Alkoxide or Carboxylate Group as Growing Species on Aluminum Porphyrin. *Macromolecules*. **1985**, *18*, 2057–2061.

15. Jeske, R. C.; Rowley, J. M.; Coates, G. W. Pre-rate-Determining Selectivity in the Terpolymerization of Epoxides, Cyclic Anhydrides, and CO_2: A One-Step Route to Diblock Copolymers. *Angew. Chem. Int. Ed. Engl.* **2008**, *120*, 6130–6133.

16. Romain, D. C.; Williams, C. K. Chemoselective Polymerization Control: From Mixed-Monomer Feedstock to Copolymers. *Angew. Chem. Int. Ed. Engl.* **2014**, *53*, 1607–1610.

17. Stößer, T., Mulryan, D., & Williams, C. K. Switch Catalysis To Deliver Multi-Block Polyesters from Mixtures of Propene Oxide, Lactide, and Phthalic Anhydride. *Angew. Chem. Int. Ed. Engl.* **2018**, *57*, 16893-16897.

18. Chen, T. T. D.; Zhu, Y.; Williams, C. K. Pentablock Copolymer from Tetracomponent Monomer Mixture Using a Switchable Dizinc Catalyst. *Macromolecules.* **2018**, *51*, 5346–5351.

19. Plajer, A. J.; Williams, C. K. Heterotrimetallic Carbon Dioxide Copolymerization and Switchable Catalysts: Sodium Is the Key to High Activity and Unusual Selectivity. *Angew. Chem. Int. Ed. Engl.* **2021**, *60*, 13372–13379.

20. Kerr, R. W. F.; Williams, C. K. Zr(IV) Catalyst for the Ring-Opening Copolymerization of Anhydrides (A) with Epoxides (B), Oxetane (B), and Tetrahydrofurans (C) to Make ABB- and/or ABC-Poly(ester-*alt*-ethers). *J. Am. Chem. Soc.* **2022**, *144*, 6882–6893.

21. Kernbichl, S.; Reiter, M.; Adams, F.; Vagin, S.; Rieger, B. CO_2-Controlled One-Pot Synthesis of AB, ABA Block, and Statistical Terpolymers from *β*-Butyrolactone, Epoxides, and CO_2. *J. Am. Chem. Soc.* **2017**, *139*, 6787–6790.

22. Zhang, D.; Boopathi, S. K.; Hadjichristidis, N.; Gnanou, Y.; Feng, X. Metal-Free Alternating Copolymerization of CO_2 with Epoxides: Fulfilling "Green" Synthesis and Activity. *J. Am. Chem. Soc.* **2016**, *138*, 11117–11120.

23. Zhang, Y. Y.; Yang, G. W.; Xie, R.; Zhu, X. F.; Wu, G. P. Sequence-Reversible Construction of Oxygen-Rich Block Copolymers from Epoxide Mixtures by Organoboron Catalysts. *J. Am. Chem. Soc.* **2022**, *144*, 19896–19909.

24. Luo, H.; Zhou, Y.; Li, Q.; Zhang, B.; Cao, X.; Zhao, J.; Zhang, G. Oxygenated Boron Species Generated In Situ by Protonolysis Enables Precision Synthesis of Alternating Polyesters. *Macromolecules*. **2023**, *56*, 1907–1920.

25. Ji, H. Y., Wang, B., Pan, L., Li, Y. S. One-Step Access to Sequence-Controlled Block Copolymers by Self-

Switchable Organocatalytic Multicomponent Polymerization. *Angew. Chem. Int. Ed. Engl.* **2018**, 57, 16888-16892.

26. Yang, G. W., Zhang, Y. Y., Xie, R., & Wu, G. P. Scalable bifunctional organoboron catalysts for copolymerization of CO_2 and epoxides with unprecedented efficiency. *J. Am. Chem. Soc.* **2020**, *142*, 12245-12255.
27. Zhang, Y. Y., Yang, G. W., Xie, R., Zhu, X. F., Wu, G. P. Sequence-Reversible Construction of Oxygen-Rich Block Copolymers from Epoxide Mixtures by Organoboron Catalysts. *J. Am. Chem. Soc.* **2022**, *144*, 19896-19909.
28. Van Zee, N. J., Coates, G. W. Alternating copolymerization of propylene oxide with biorenewable terpene-based cyclic anhydrides: a sustainable route to aliphatic polyesters with high glass transition temperatures. *Angewandte Chemie* **2015**, *127*, 2703-2706.
29. Gleede, T., Markwart, J. C.; Huber, N.; Rieger, E. F.; Wurm, R.; Competitive copolymerization: access to aziridine copolymers with adjustable gradient strengths. *Macromolecules* **2019**, 52, 9703-9714.
30. Beckingham, B. S.; Sanoja, G. E.; Lynd, N. A.; Simple and accurate determination of reactivity ratios using a nonterminal model of chain copolymerization. *Macromolecules* **2015**, 48, 6922-6930.
31. Ganesan V, Kumar N A, Pryamitsyn V. Blockiness and sequence polydispersity effects on the phase behavior and interfacial properties of gradient copolymers. *Macromolecules* **2012**, *45*, 6281-6297.
32. Mok M M, Torkelson J M. Imaging of phase segregation in gradient copolymers: Island and hole surface topography. *J. Polym. Sci. B Polym. Phys.* **2012**, *50*, 189-197.

Chapter 4

Self-switchable Copolymerization: From Complex Monomer Mixtures to Poly(amide ester)-Based Block Copolymers

4.1 Introduction

Self-switchable polymerization systems, developed by researchers in recent years to achieve the efficient synthesis of block copolymers, possess improved efficiency, molecular weight, and sequence controllability, as well as a wider selection of monomers. However, achieving simultaneous and thorough adjustment of the chemical structures of the different blocks in the one-step-synthesized block copolymers remains a significant challenge, limiting the diversification of thermomechanical properties and microphase separation in the resulting block copolymers. To address this limitation, researchers have utilized novel monomers instead of conventional epoxide, anhydride, cyclic ester, carbonate, and CO_2 monomers in the synthesis of block copolymers with distinct block chemical structures. For instance, Hadjichristidis et al. reported poly(amide ester)-*b*-polyesters synthesized from an anhydride, *N*-tosylaziridine (TAz), and epoxide monomer mixture in a one-step procedure.[1] Similarly, Li et al. developed a metal complex catalyst to synthesize polyester-*b*-poly(ester-*alt*-thioester)s from an epoxide, anhydride, and thioanhydride monomer mixture in a single step.[2] Although these catalytic systems have significantly enhanced the inner chemical structural diversity of one-step-synthesized block copolymers, these copolymers still typically exhibit only a single glass transition temperature (T_g). This implies that the two blocks possess similar polarities, which prevent phase separation between them. For these terpolymerizations, two polymerization cycles involve the same monomer, thereby limiting the adjustment of the chemical nature (or polarity) difference between the two blocks.

The use of different monomers enables control of the chemical nature difference between the two blocks. In this chapter, the author discussed a self-switchable copolymerization system for the synthesis of quaterpolymer from two different anhydrides, TAz and an epoxide, as well as a terpolymer from a TAz, anhydride, and cyclic carbonate, using *t*-BuP_2 as a catalyst (Figure 4.1). The newly synthesized block copolymers exhibited two T_g values, and the microphase separation was confirmed via small-angle X-ray scattering (SAXS) measurements. This approach provides a platform for the synthesis of block copolymers

with adjustable block chemical structures, thus paving the way for fabricating block copolymers with the desired microphase-separated morphology.

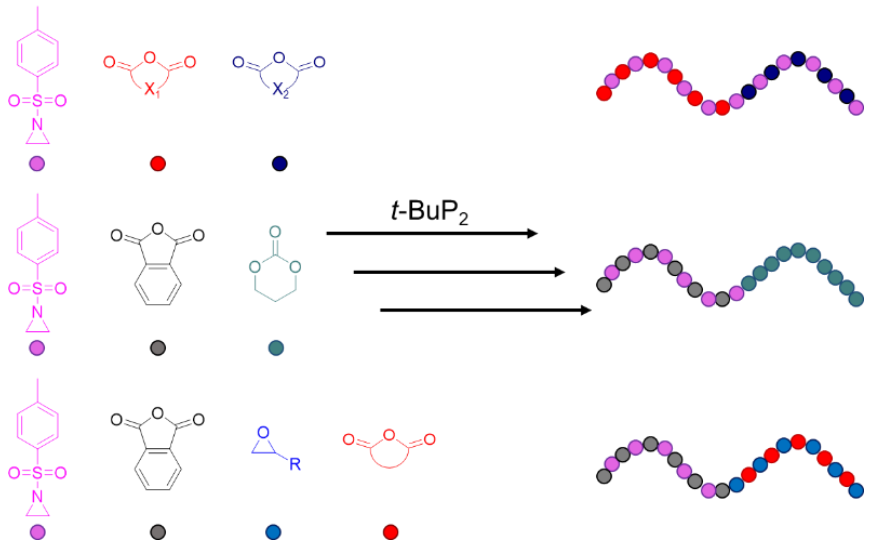

Figure 4.1. Illustration of block copolymer synthetic routes and the chemical structure difference between the two blocks.

4.2 Experimental Section

4.2.1 Materials:

Trimethylene carbonate (TMC; >98%, TCI) was recrystallized from dry tetrahydrofuran before use. 2-ethylhexyl glycidyl ether (EHGE; >98.0%, TCI) was distilled over CaH_2 under reduced pressure and stored under nitrogen atmosphere. 5-Norbornene-*endo*-2,3-dicarboxylic anhydride (NA; > 99%, Sigma−Aldrich), diglycolic anhydride (DGA; >98.0%, TCI), succinic anhydride (SA; >95.0%, TCI), diphenic anhydride (DA; >98.0%, TCI), phthalic anhydride (PA; >98.0%, TCI), 4-bromophthalic anhydride (BA; >97.0%, TCI), and glutaric anhydride (GA; >98.0%, TCI) were recrystallized in THF and then purified by sublimation before use. *N*-Tosylaziridine (TAz; 98%, Sigma−Aldrich) was dried over phosphorus pentoxide under a high vacuum for 72 h before use. 1,4-Benzenedimethanol (BDM; >99.0%, TCI) and 1-*tert*-butyl-2,2,4,4,4-pentakis(dimethylamino)-2λ^5,4λ^5-catenadi(phosphazene) (*t*-BuP_2, 2.0 M in THF, Sigma−Aldrich) were used as received.

4.2.2 Instrument:

The polymerization was carried out in a gas purification system (molecular sieves and copper catalyst) equipped MBRAUN stainless steel glovebox in a dry argon atmosphere (H_2O, O_2 <0.1 ppm). The moisture and oxygen contents in the glovebox were monitored with MB-MO-SE 1 and MB-OX-SE 1, respectively.

The size exclusion chromatography (SEC) was performed using a Shodex GPC-101 system equipped with a Shodex K-G guard column and a set of two Shodex K-805L columns (linear, 8 mm × 300 mm; bead size, 5 μm; exclusion limit, 4×10^6). The measurement was performed in THF (flow rate, 1.0 mL min^{-1}) at 40 °C. Polystyrene (PS) standard samples were used for calibration.

JEOL JNM-ECS400 instrument or a JEOL JNM-ECX400P instrument was used for ^1H NMR, and DOSY NMR spectral measurement was conducted at room temperature with the JEOL JNM-ECX400P instrument. DOSY NMR analyses were carried out at room temperature using the ledbpgp2s sequence with at least 15 gradient increments.

A Hitachi High-Technologies DSC7000X was used for differential scanning calorimetry (DSC), and the experiment was performed under an N_2 atmosphere. Polymer sample for DSC measurement was heated to 200 °C, cooled to −100 °C, and heated again to 200 °C at the heating and cooling rates of 10 °C min^{-1} and 20 °C min^{-1}, respectively.

Small-angle X-ray scattering (SAXS) experiments for the block copolymer samples were performed at the BL-6A beamline of the Photon Factory of High Energy Accelerator Research Organization (KEK, Tsukuba, Japan). The X-ray wavelength and exposure time were 1.50 Å (8.27 keV) and 60 s, respectively. A PILATUS3 1M 4 (Dectris Ltd., Switzerland) detector, with 981 × 1043 pixels at a pixel size of 172 × 172 μm and a counter depth of 20 bits (1,048,576 counts) was used for data acquisition. The sample-to-detector distance was calibrated using the scattering patterns of silver behenate (Nagara Science Co., Ltd., Japan). The SAXS data were acquired under ambient conditions, and 1D profiles were obtained as plots of scattering intensity as

functions of scattering vector (q), where $q = (4\pi/\lambda)\sin(\theta/2)$ (λ, wavelength; θ, scattering angle).

4.2.3 Synthetic detail

Synthesis of poly(TAz-*alt*-PA)-*b*-poly(TAz-*alt*-DGA)-*b*-poly(TAz-*alt*-PA)

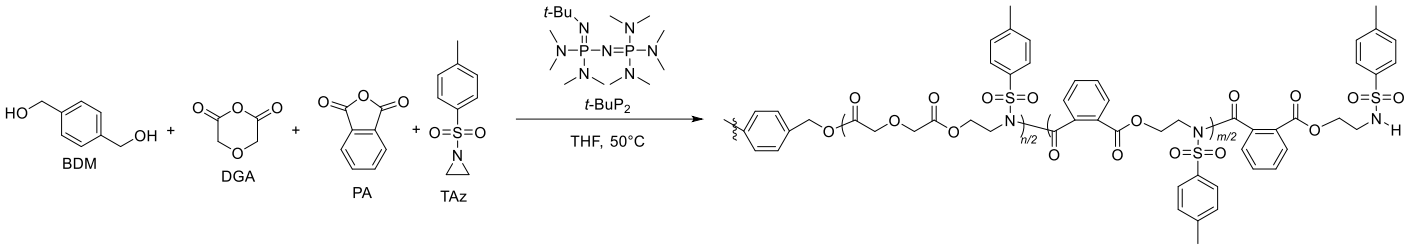

Scheme 4.1. Copolymerization from the mixture of DGA, PA, and TAz.

In the glovebox, diglycolic anhydride (DGA) (34.7 mg, 0.3 mmol), phthalic anhydride (PA) (44.2 mg, 0.3 mmol), *N*-tosylaziridine (TAz) (117.9 mg, 0.6 mmol), and BDM (5.5 mg, 39.9 μmol) were mixed in a Schleck flask. 0.6 mL THF was added to dissolve the mixture, and *t*-BuP_2 (11.9μL, 23.9 μmol) was introduced to start the polymerization. Then, the Schleck flask was taken out from the glovebox. The reaction was conducted with stirring at 50 °C. ^{1}H NMR measurement was used to monitor polymerization. After 7 h, benzoic acid was added to terminate the polymerization. The crude product was purified via reprecipitation with methanol.

Synthesis of poly(TAz-*alt*-GA)-*b*-poly(TAz-*alt*-DGA)-*b*-poly(TAz-*alt*-GA)

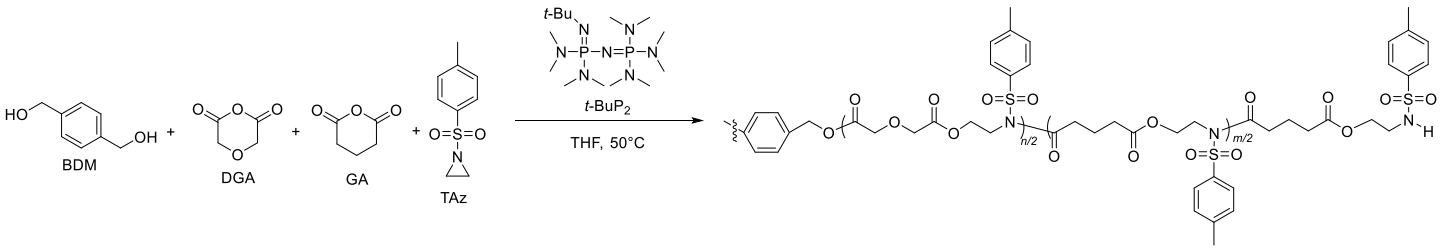

Scheme 4.2. Copolymerization from the mixture of DGA, GA, and TAz.

In the glovebox, DGA (69.4 mg, 0.60 mmol), glutaric anhydride (GA) (68.4 mg, 0.6 mmol), TAz (237.6 mg, 1.2 mmol), and BDM (5.5 mg, 39.9 μmol) were mixed in a Schleck flask. 0.6 mL THF was added to

dissolve the mixture, and *t*-BuP$_2$ (11.9μL, 23.9 μmol) was introduced to start the polymerization. Then, the Schleck flask was taken out from the glovebox. The reaction was conducted with stirring at 50 °C. ^{1}H NMR measurement was used to monitor polymerization. After 13 h, benzoic acid was added to terminate the polymerization. The crude product was purified via reprecipitation with methanol.

Synthesis of poly(TAz-*alt*-DA)-*b*-poly(TAz-*alt*-DGA)-*b*-poly(TAz-*alt*-DA)

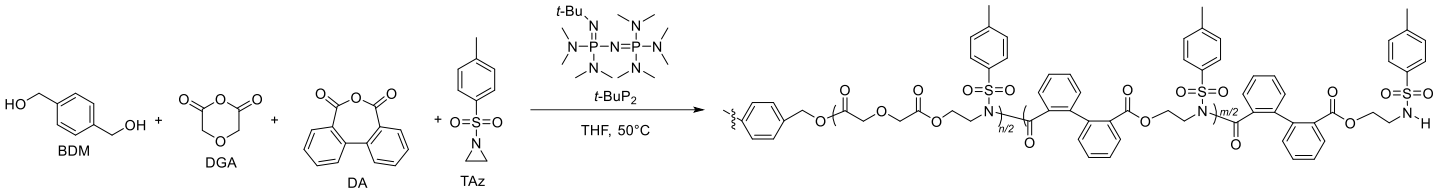

Scheme 4.3. Copolymerization from the mixture of DGA, DA, and TAz.

In the glovebox, DGA (34.7 mg, 0.3 mmol), diphenic anhydride (DA) (67.2 mg, 0.3 mmol), TAz (117.9 mg, 0.6 mmol), and BDM (5.5 mg, 39.9 μmol) were mixed in a Schleck flask. 0.6 mL THF was added to dissolve the mixture, and *t*-BuP$_2$ (11.9μL, 23.9 μmol) was introduced to start the polymerization. Then, the Schleck flask was taken out from the glovebox. The reaction was conducted with stirring at 50 °C. ^{1}H NMR measurement was used to monitor polymerization. After 7 h, benzoic acid was added to terminate the polymerization. The crude product was purified via reprecipitation with methanol.

Synthesis of poly(TMC)-*b*-poly(TAz-*alt*-PA)-*b*-poly(TMC)

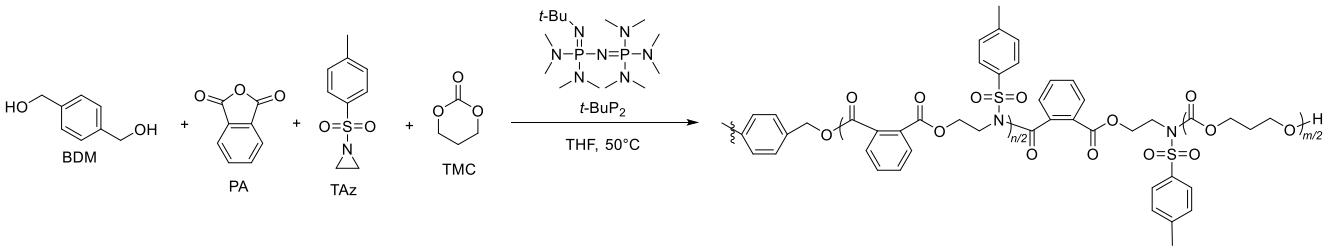

Scheme 4.4. Copolymerization from the mixture of TMC, PA, and TAz.

In the glovebox, PA (117.9 mg, 0.797 mmol), TAz (165.1 mg, 0.837 mmol), trimethylene carbonate (TMC) (284.6 mg, 2.79 mmol), and BDM (5.5 mg, 39.9 μmol) were mixed in a Schleck flask. 0.8 mL THF

was added to dissolve the mixture, and *t*-BuP_2 (11.9μL, 23.9 μmol) was introduced to start the polymerization. Then, the Schleck flask was taken out from the glovebox. The reaction was conducted with stirring at 50 °C. ^{1}H NMR measurement was used to monitor polymerization. After 26 h, benzoic acid was added to terminate the polymerization. The crude product was purified via reprecipitation with methanol.

Synthesis of poly(EHGE-*alt*-NA)-*b*-poly(TAz-*alt*-PA)-*b*-poly(EHGE-*alt*-NA)

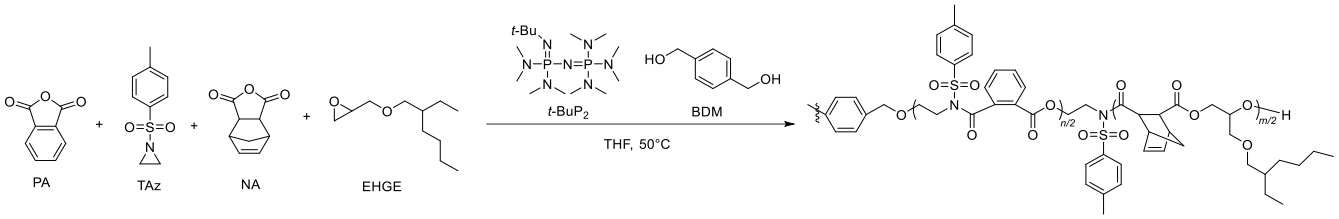

Scheme 4.5. Copolymerization from the mixture of PA, NA, EHGE and TAz.

In the glovebox, PA (88.5 mg, 0.598 mmol), TAz (117.9 mg, 0.598 mmol), 5-norbornene-*endo*-2,3-dicarboxylic anhydride (NA) (98.1 mg, 0.598 mmol), 2-ethylhexyl glycidyl ether (EHGE) (444.8 mg, 2.39 mmol), and BDM (5.5 mg, 39.9 μmol) were mixed in a Schleck flask. *t*-BuP_2 (11.9μL, 23.9 μmol) was introduced to start the polymerization. Then, the Schleck flask was taken out from the glovebox. The reaction was conducted with stirring at 50 °C. ^{1}H NMR measurement was used to monitor polymerization. After 45 h, benzoic acid was added to terminate the polymerization. The crude product was purified via reprecipitation with methanol.

4.3 Results and Discussion

4.3.1 Terpolymerization of one aziridine and two cyclic anhydrides for one-step synthesis of block poly(amide ester)-*b*-polyester

According to the previous report, the phosphazene base (*t*-BuP_2) exhibited excellent molecular weight controllability on the aziridine/cyclic anhydride ROAC, and the synthesized poly(amide ester) showed perfect alternating structure based on mass spectral analysis results.[3] To guarantee good molecular weight controllability on this terpolymerization, the *t*-BuP_2 was selected as the catalyst with a 1,4-benzenedimethanol (BDM) initiator to carry out the polymerization. DGA was selected for copolymerization with PA and TAz because of its superior reactivity according to last chapter. Polymerization of a mixture of monomers containing TAz, PA, and DGA was conducted at 50 °C. The molar ratio, $[TAz]_0/[PA]_0/[DGA]_0/[t\text{-}BuP_2]/[BDM]_0$, was 15/7.5/7.5/0.6/1.0 (entry 1 in Table 4.1, Figure 4.2). Monomer consumption during polymerization was monitored using ^{1}H NMR spectroscopy (Figure 4.2b). After 5 h, 92.5% of DGA had been consumed. No ^{1}H NMR signal was detected for poly(PA-*alt*-TAz), and the signal for PA remained unchanged. DGA was completely consumed within 6 h, whereas 17.1% of PA reacted within the same time. These results indicated the formation of "block-like" poly(TAz-*alt*-PA)-*b*-poly(TAz-alt-DGA)-*b*-poly(TAz-*alt*-PA) with a 12.3% tapered region on the polymer chain.[4]

Table 4.1. Poly(amide ester)-based block copolymers synthesis [a]

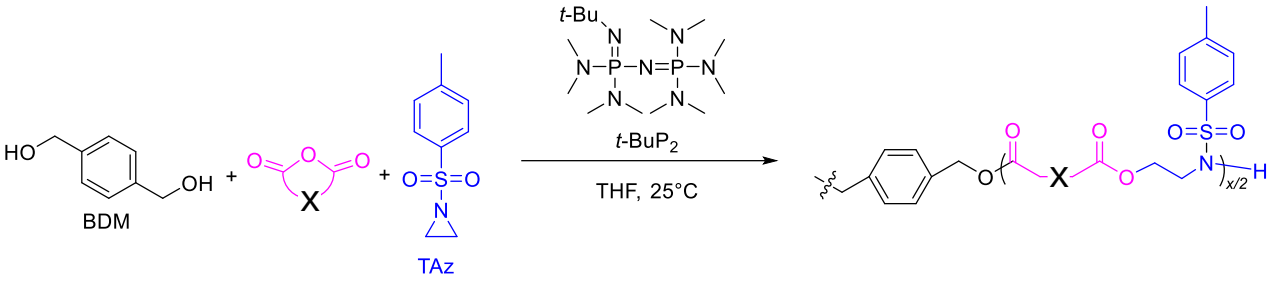

Entry	Monomers	$[TAz]_0/[anhydride_1]_0/[anhydride_2]_0/[Cat.]/[Ini.]_0$	Time (h)	Conv.[a] (%)	$M_{n,th}$ [b](Da)	$M_{n,NMR}$ [a](Da)	$M_{n,SEC}$ [c](Da)	$Đ$ [c]	Fraction of the tapered region (%)
1	TAz/PA/DGA	15/7.5/7.5/0.6/1.0	7	TAz = 95, PA = 68, DGA> 99	3,000	ND	2,500	1.26	12.3
2	TAz/DGA/GA	30/15/15/0.6/1.0	13	TAz = 85, DGA> 99, GA = 56	7,600	6,900	1,700	1.42	9.1
3	TAz/DA/DGA	15/7.5/7.5/0.6/1.0	7	TAz > 99, DA> 99, DGA> 99	5,500	5,500	2,700	1.69	18.4

[a]Polymerization was conducted in THF (solvent) at 50 °C; $[anhydride]_0$ = 1.0 mol/L. [a]Determined by ^{1}H NMR analysis ($CDCl_3$). [b]Calculated using $[anhydride1]_0/[Ini.]_0$ × conv. × (MW of anhydride1 + MW of TAz) + $[anhydride2]_0/[Ini.]_0$ × conv. × (MW of anhydride2 + MW of epoxide/TAz) + (MW of initiator) or $[anhydride1]_0/[I]_0$ × conv. × (MW of anhydride1 + MW of TAz) + (MW of initiator). [c]Determined by SEC (THF) with a PSt standard.

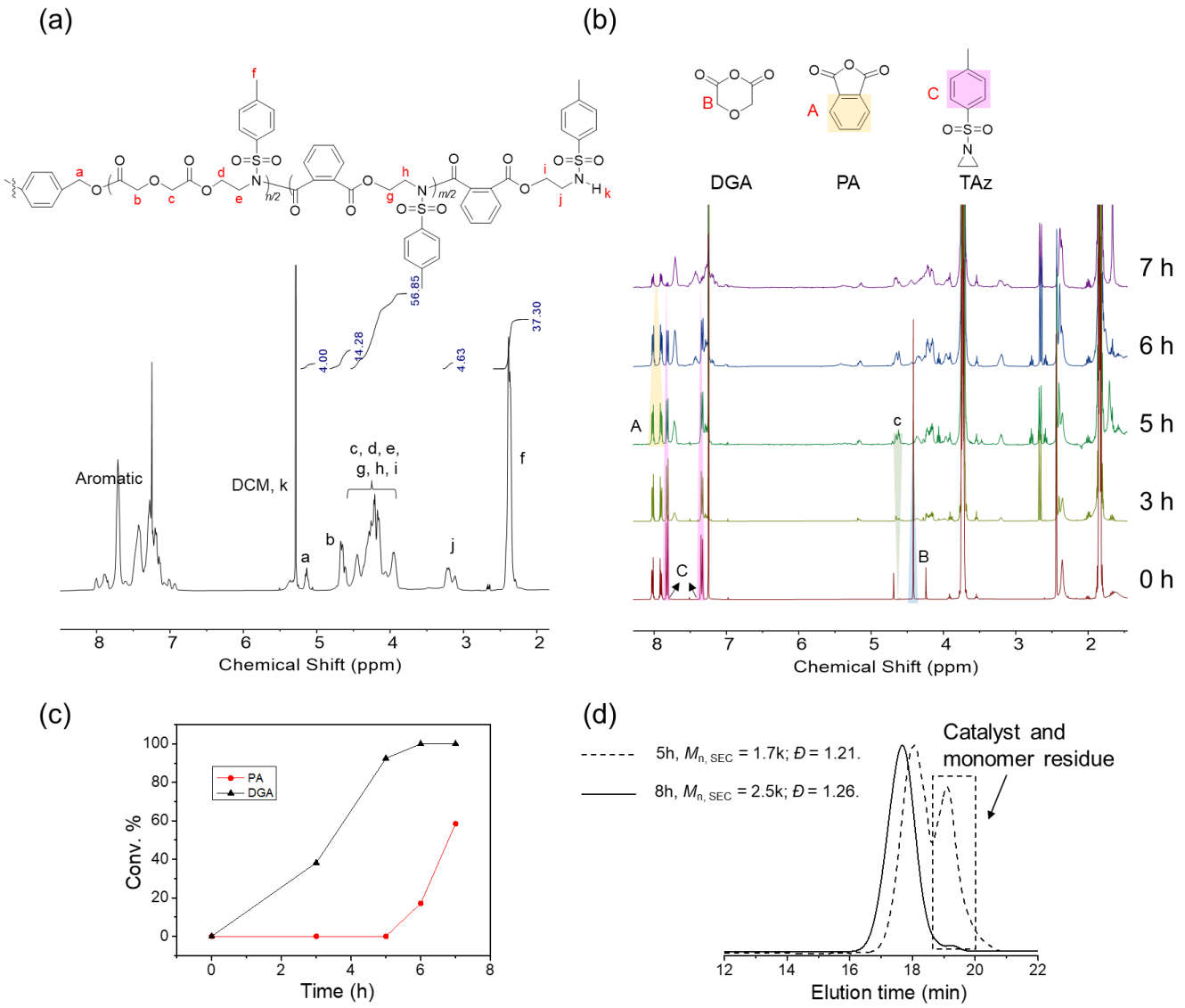

Figure 4.2. Copolymerization of TAz/DGA/PA catalyzed by *t*-BuP$_2$. (a) ^{1}H NMR spectrum of resulting poly(TAz-*alt*-PA)-*b*-poly(TAz-*alt*-DGA)-*b*-poly(TAz-*alt*-PA) ($CDCl_3$). (b) ^{1}H NMR spectra of crude aliquots withdrawn from the reaction system to monitor DGA and PA conversion ($CDCl_3$). (c) Monomer conversion over time (entry 1, Table 4.1). (d) Evolution of SEC traces (THF) (entry 1, Table 4.1).

The nonterminal Beckingham–Sanoja–Lynd (BSL) copolymerization model was employed to calculate the reactivity ratios (*r*) and determined that r_{DGA} and r_{PA} for the PA/DGA/TAz ROCOP system were 76.381 and 0.0103, respectively (Figure 4.3a). Notably, the reactivity difference between PA and DGA in the PA/DGA/TAz ROCOP system was much larger than that calculated for the previously reported

copolymerization system with epoxide; that is, PA/DGA/ethyl glycidyl ether (EGE) ROCOP (r_{DGA} = 10.98, r_{PA} = 0.034) produced a larger tapered region in the resulting poly(EGE-*alt*-PA)-*b*-poly(EGE-*alt*-DGA)-*b*-poly(EGE-*alt*-PA) (49.2%).[5] The increased anhydride reactivity difference of PA/DGA/TAz ROCOP compared to that of PA/DGA/EGE ROCOP is attributed to the weaker nucleophilicity of the secondary sulfonamide chain end relative to that of the alkoxide chain end, leading to a slower nucleophilic attack on the anhydride. Furthermore, GA, which has a lower copolymerization activity than does PA, was copolymerized with DGA in this system. Poly(DGA-*alt*-TAz) and poly(GA-*alt*-TAz) are difficult to reprecipitate in MeOH due to the low T_g nature of their main chains. Thus, the $[TAz]_0/[GA]_0/[DGA]_0/[t\text{-}BuP_2]$ /$[BDM]_0$ molar ratio was set as 30/15/15/0.6/1.0 to achieve a product with a higher molecular weight. The copolymerization resulted in a "block-like" poly(TAz-*alt*-GA)-*b*-poly(TAz-*alt*-DGA)-*b*-poly(TAz-*alt*-GA) with a less tapered region (9.1%) in the polymer chain (entry 2 in Table 4.1, Figure 4.4). A greater reactivity difference between GA and DGA was observed for the GA/DGA/TAz ROCOP system (r_{DGA} = 198.50, r_{GA} = 0.0023; Figure 4.3b). Based on the solubility difference of DA when compared with other anhydrides in THF, the copolymerization of TAz, DGA, and DA was implemented (entry 3 in Table 4.1, Figure 4.5). At the beginning of the polymerization, a white suspension of DA was observed at 50 °C. After 3 h, the DA solid started to diminish. The reaction was terminated after 7 h, yielding poly(TAz-*alt*-DA)-*b*-poly(TAz-*alt*-DGA)-*b*-poly(TAz-*alt*-DA) as a block-like copolymer with a tapered region of 18.4% in the polymer chain. The reactivity ratios r_{DA} and r_{DGA} were 50.821 and 0.0259, respectively (Figure 4.3c). Notably, the poly(EGE-*alt*-DA)-*b*-poly(EGE-*alt*-DGA)-*b*-poly(EGE-*alt*-DA) synthesized by the DA/DGA/EGE ROCOP system reported previously exhibited a medium gradient copolymer type with a tapered region of 83.2% and a smaller reactivity difference (r_{DGA} = 4.51, r_{DA} = 0.48).

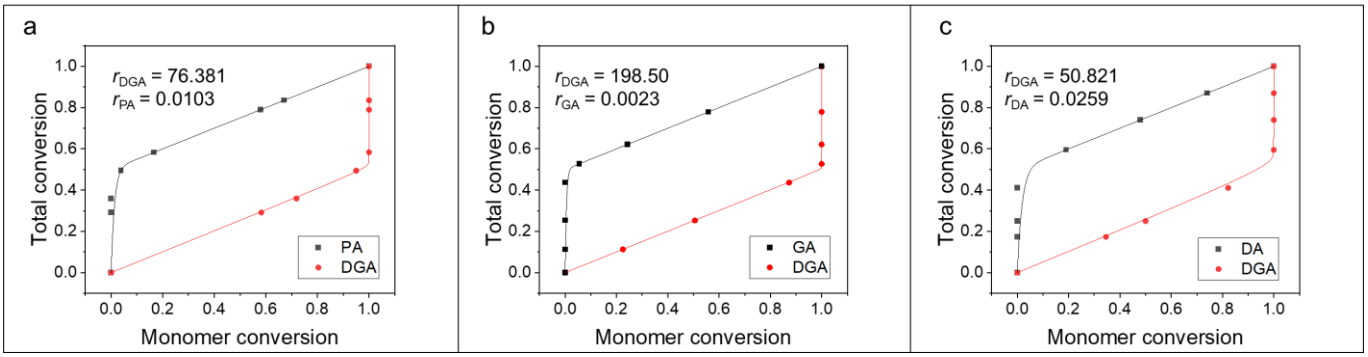

Figure 4.3. Total polymerization conversion plotted against monomer conversion and the data were obtained from time-resolved ^{1}H NMR spectra: (a) DGA/PA/TAz (entry 1 in Table 4.1); (b) DGA/GA/TAz (entry 2 in Table 4.1); (c) DGA/DA/TAz (entry 3 in Table 4.1).

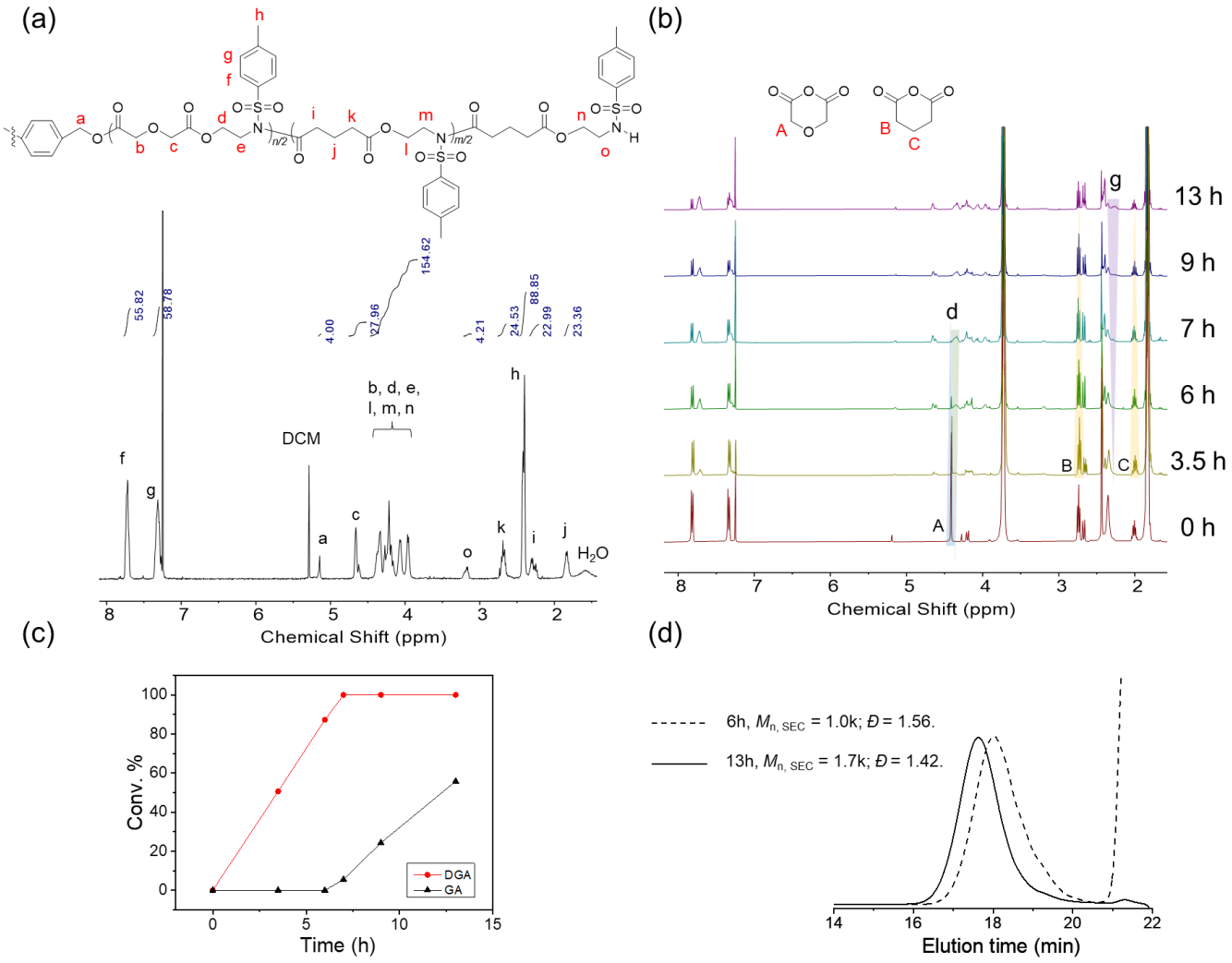

Figure 4.4. Copolymerization of TAz/DGA/GA catalyzed by *t*-BuP_2. (a) ^{1}H NMR spectrum of the resulted poly(TAz-*alt*-GA)-*b*-poly(TAz-*alt*-DGA)-*b*-poly(TAz-*alt*-GA) ($CDCl_3$). (b) ^{1}H NMR spectra of crude aliquots withdrawn from the reaction system to monitor DGA and GA conversion ($CDCl_3$). (c) Monomer conversion over time. (Entry 2 in Table 4.1) (d) Evolution of SEC traces (THF) (entry 2 in Table 4.1).

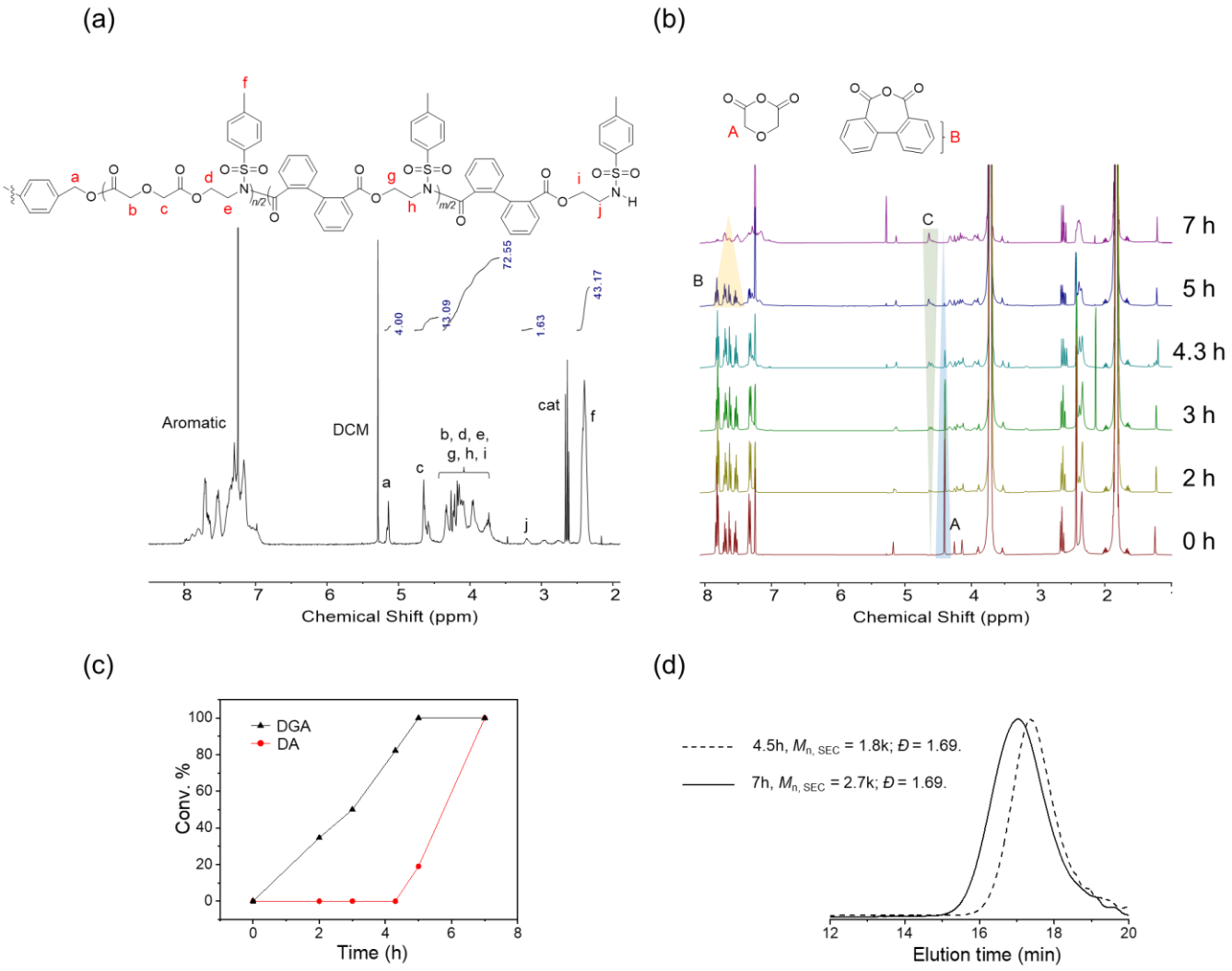

Figure 4.5. Copolymerization of TAz/DGA/DA catalyzed by *t*-BuP$_2$. (a) ^{1}H NMR spectrum of the resulted poly(TAz-*alt*-DA)-*b*-poly(TAz-*alt*-DGA)-*b*-poly(TAz-*alt*-DA) ($CDCl_3$). (b) ^{1}H NMR spectra of crude aliquots withdrawn from the reaction system to monitor DGA and DA conversion ($CDCl_3$). (c) Monomer conversion over time. (entry 3 in Table 4.1). (d) Evolution of SEC traces (THF) (entry 3 in Table 4.1).

4.3.2 Terpolymerization of cyclic carbonate, aziridine, and cyclic anhydride for one-step synthesis of block poly(amide ester)-*b*-polycarbonate

Based on the observations that the ROCOP of TAz with different anhydrides only delivers "block-like" poly(amide ester) with significantly tapered regions, a combination of a TAz/anhydride ROCOP catalytic cycle and cyclic carbonate ROP was devised for the one-step synthesis of a "real" block copolymer. The TMC

ROP catalytic cycle was selected to combine with a PA/TAz ROAC catalytic cycle for the one-step synthesis of a poly(amide ester)-*b*-polycarbonate (Figure 4.6).

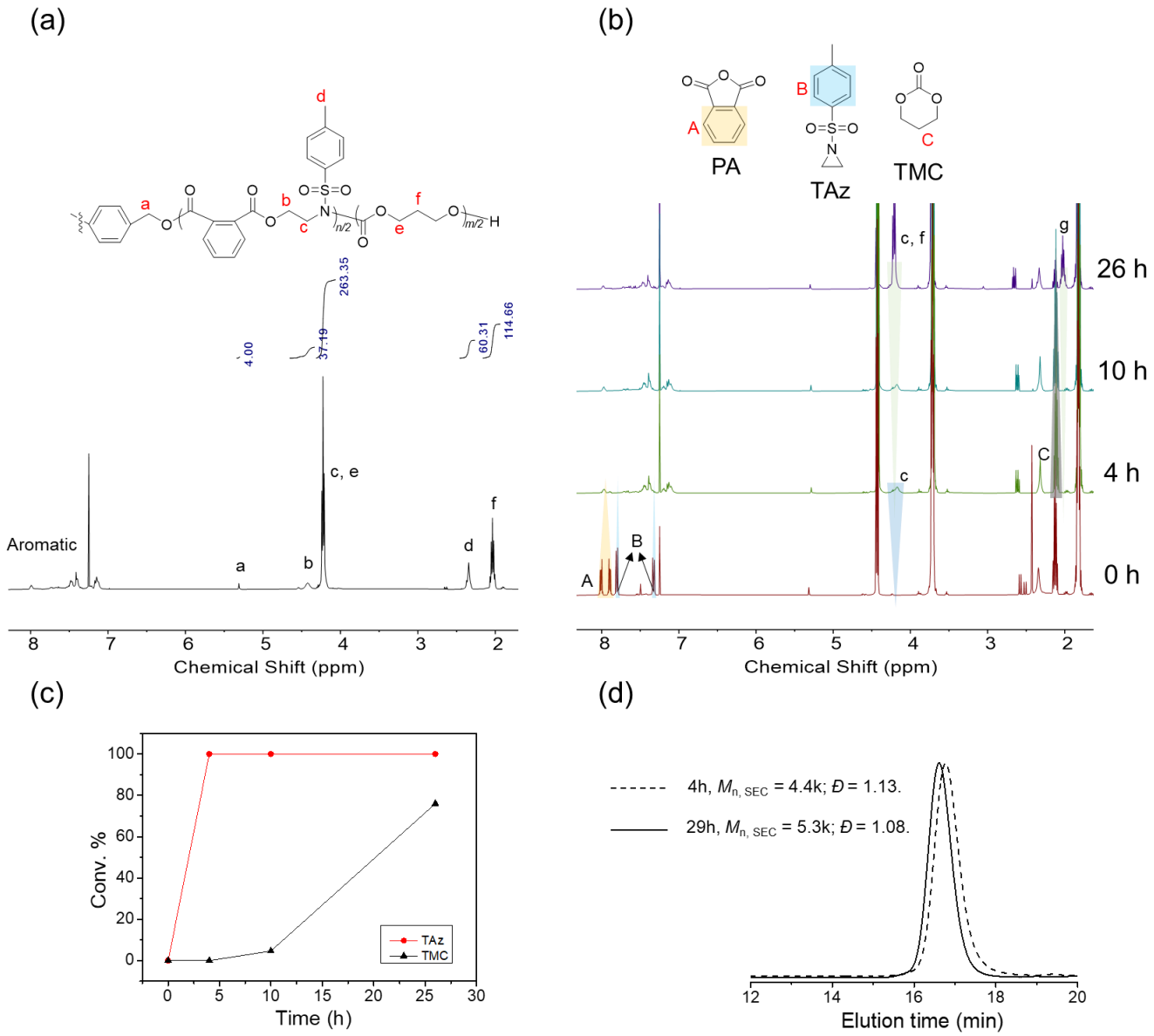

Figure 4.6. Copolymerization of TAz/PA/TMC catalyzed by *t*-BuP_2. (a) ^{1}H NMR spectrum of resulting poly(TMC)-*b*-poly(TAz-*alt*-PA)-*b*-poly(TMC) ($CDCl_3$). (b) ^{1}H NMR spectra of crude aliquots withdrawn from the reaction system to monitor TAz and TMC conversion ($CDCl_3$). (c) Monomer conversion over time. (d) Evolution of SEC traces (THF).

The polymerization was performed at 50 °C with a $[TAz]_0/[PA]_0/[TMC]_0/[t\text{-}BuP_2]/[BDM]_0$ molar ratio of 22/20/70/0.6/1.0. To enable a high initiation efficiency for TMC ROP when TAz and PA are fully consumed, a slightly higher amount of TAz relative to that of PA was added to ensure the presence of a secondary sulfonamide chain end on the first poly(TAz-*alt*-PA) block. The copolymerization behavior was monitored by ^{1}H NMR spectroscopy. After 4 h, the ^{1}H NMR signals assigned to PA (7.89–8.07 ppm, proton "A") and TAz (7.79–7.87 ppm; 7.32–7.39 ppm, proton "B") completely disappeared, and no signal was observed at this stage (1.98–2.10 ppm, proton "h") for poly(TMC) (Figure 4.6b). This indicated that the first block consisted entirely of poly(TAz-*alt*-PA) without TMC insertion. Owing to the low initiation efficiency of the secondary sulfonamide chain end, only 4.6% TMC reacted 6 h after TAz was fully consumed. After changing the chain end to alkoxide by insertion of a TMC unit, polymerization proceeded smoothly, with the reaction of 76% TMC after 26 h. The SEC trace showed a shift in molecular weight from a low-molecular-weight region (first poly(TAz-*alt*-PA) block, $M_{n,SEC}$ = 4,400) to a high-molecular-weight region (poly(TMC)-*b*-poly(TAz-*alt*-PA)-*b*-poly(TMC) $M_{n,SEC}$ = 5,300), whereas the molecular weight dispersity remained narrow ($Đ_{poly(TAz\text{-}alt\text{-}PA)\ block}$ = 1.13, $Đ_{poly(TMC)\text{-}b\text{-}poly(TAz\text{-}alt\text{-}PA)\text{-}b\text{-}poly(TMC)}$ = 1.08). The diffusion ordered NMR spectroscopy (DOSY) profile of the resulting poly(TMC)-*b*-poly(TAz-*alt*-PA)-*b*-poly(TMC) showed a single diffusion coefficient, indicating a covalent connection between the poly(TMC) and poly(TAz-*alt*-PA) blocks (Figure 4.7). This observation confirmed the successful synthesis of the "real" triblock poly(TMC)-*b*-poly(TAz-*alt*-PA)-*b*-poly(TMC).

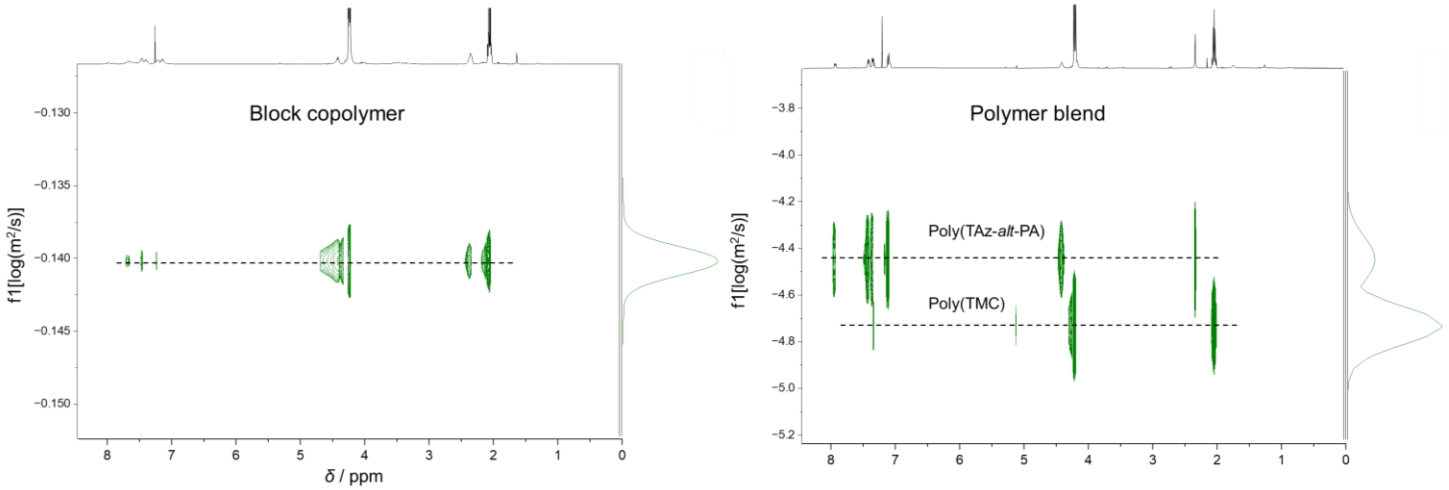

Figure 4.7. DOSY spectra of the poly(TMC)-*b*-poly(TAz-*alt*-PA)-*b*-poly(TMC) triblock copolymer and poly(TMC)/poly(TAz-*alt*-PA) polymer blend.

4.3.3 Copolymerization of epoxide, aziridine, and two cyclic anhydrides for one-step synthesis of poly(amide ester)-*b*-polyester

The combination of epoxide/anhydride ROCOP and TAz/anhydride ROCOP holds great promise for the preparation of poly(ester)-*b*-poly(amide ester)s. Hadjichristidis reported the one-step synthesis of diblock dialternating terpolymers from a monomer mixture of PA, TAz, and PO.[1] However, the synthesized block copolymers exhibited a single T_g value, indicating that no phase separation occurred between the two blocks. This is because, in these terpolymerizations, two polymerization cycles involve the same monomer (i.e., PA), thus limiting the ability to adjust the chemical nature difference between the two blocks. Based on these results, a quaterpolymer synthesized from PA, TAz, NA, and EHGE was devised. In accordance with the previous results, the reactivity gradient was expected to follow the order of PA >> TAz >> NA >> EHGE and thereby enable the one-step synthesis of poly(EHGE-*alt*-NA)-*b*-poly(TAz-*alt*-PA)-*b*-poly(EHGE-*alt*-NA) (Figure 4.8).

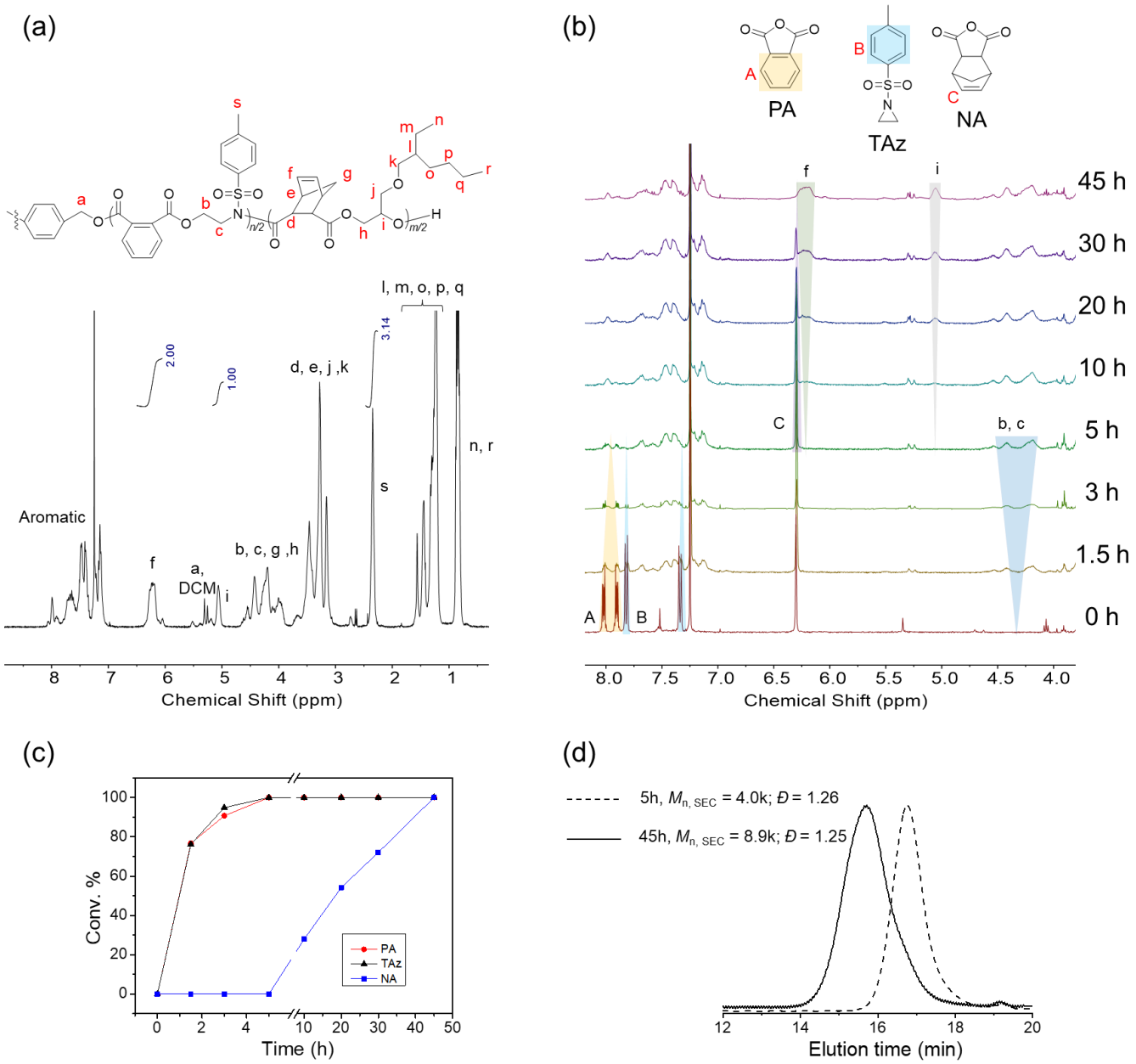

Figure 4.8. Copolymerization of TAz/PA/EHGE/NA catalyzed by *t*-BuP$_2$. (a) ^{1}H NMR spectrum of the resulting poly(EHGE-*alt*-NA)-*b*-poly(TAz-*alt*-PA)-*b*-poly(EHGE-*alt*-NA) ($CDCl_3$). (b) ^{1}H NMR spectra of crude aliquots withdrawn from the reaction system to monitor TAz, PA, and NA conversion ($CDCl_3$). (c) Monomer conversion during TAz, PA, NA, and EHGE ROCOP. (d) Evolution of SEC traces during TAz, PA, NA, and EHGE ROCOP (THF).

The reactivity differences between PA and NA and between TAz and EHGE were expected to allow for a high level of block sequence control, enabling flexible adjustment of the polymer chain from the four starting

monomers. TAz and PA were first copolymerized and then fully consumed within 5 h, resulting in poly(TAz-*alt*-PA), which exhibited a monomodal elution peak ($Đ$ = 1.26) in the SEC trace, with a molecular weight of 4,000 calculated via SEC analysis. No reaction between NA and EHGE was observed. Subsequently, the ROCOP of NA/EHGE turns on with a lower reaction rate. Polymerization was quenched after 45 h to yield the final copolymer with a higher molecular weight ($M_{n,\,SEC}$ = 8900, $Đ$ = 1.25). The covalent connection of the synthesized poly(EHGE-*alt*-NA)-*b*-poly(TAz-*alt*-PA)-*b*-poly(EHGE-*alt*-NA) was confirmed by DOSY NMR analysis (Figure 4.9), which indicated the successful synthesis of a "real" block poly(ester amide)-*b*-polyester.

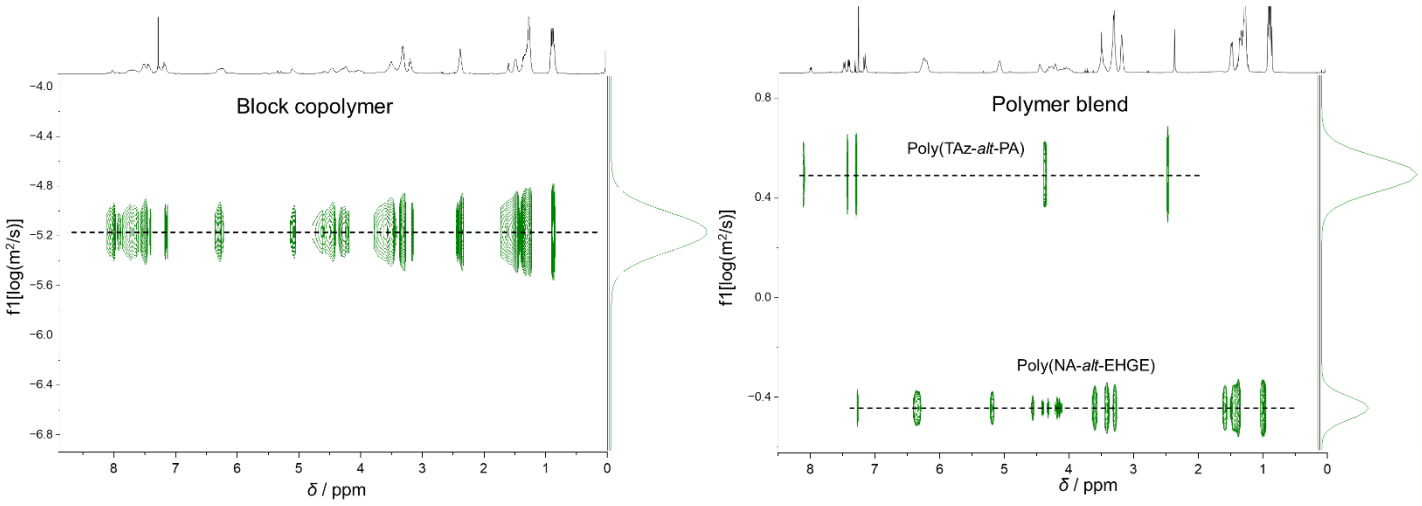

Figure 4.9. DOSY spectra of the poly(EHGE-*alt*-NA)-*b*-poly(TAz-*alt*-PA)-*b*-poly(EHGE-*alt*-NA) triblock copolymer and poly(EHGE-*alt*-NA)/poly(TAz-*alt*-PA) polymer blend.

4.3.4 Physical property investigation of synthesized block copolymers

The T_g is a crucial parameter for polymer materials, as it plays a significant role in determining the suitable application environments for the polymer. The synthesized "block-like" copolymer poly(TAz-*alt*-PA)-*b*-poly(TAz-*alt*-DGA)-*b*-poly(TAz-*alt*-PA) (entry 1 in Table 4.1) exhibited a single T_g of 59 °C (Figure 4.10), which lies between those of poly(TAz-*alt*-DGA) (45 °C) (figure 4.13) and poly(TAz-*alt*-PA) (114 °C).[3] The

same phenomenon was observed for the synthesized poly(TAz-*alt*-DA)-*b*-poly(TAz-*alt*-DGA)-*b*-poly(TAz-*alt*-DA) (entry 3 in Table 4.1) (Figure 4.11), with a T_g of 78 °C lying between the those of the two individual blocks. This finding indicates that the chemical nature (or polarity) difference between the two blocks is insufficient for microphase separation to take place. The insufficient difference in chemical nature (or polarity) of the blocks originates from their structural similarity, which is ascribed to the fact that they house a common TAz unit. On the other hand, the synthesized poly(TAz-*alt*-GA)-*b*-poly(TAz-*alt*-DGA)-*b*-poly(TAz-*alt*-GA) (entry 2 in Table 4.1) showed two distinct T_g values of 30 and 48 °C (Figure 4.12), which can be assigned to the individual blocks ($T_{g\ \text{poly(TAz-}alt\text{-GA)}}$ = 29 °C (figure 4.14), $T_{g\ \text{poly(TAz-}alt\text{-DGA)}}$ = 45 °C). The difference in the thermal property might be explained by the fraction of the tapered region. Poly(TAz-*alt*-GA)-*b*-poly(TAz-*alt*-DGA)-*b*-poly(TAz-*alt*-GA) shows the smallest tapered region (9.1%) among the three copolymers, which enables the phase separation between the poly(TAz-*alt*-DGA) and poly(TAz-*alt*-GA). However, SAXS measurements conducted on poly(TAz-*alt*-GA)-*b*-poly(TAz-*alt*-DGA)-*b*-poly(TAz-*alt*-GA) after annealing at 130 °C for 3.5 h did not reveal a distinct peak in the SAXS profile (Figure 4.15), indicating the absence of a nanoscale periodic structure. This could be due to the "block-like" nature of this copolymer and the weak segregation strength resulting from the insufficient molecular weight.

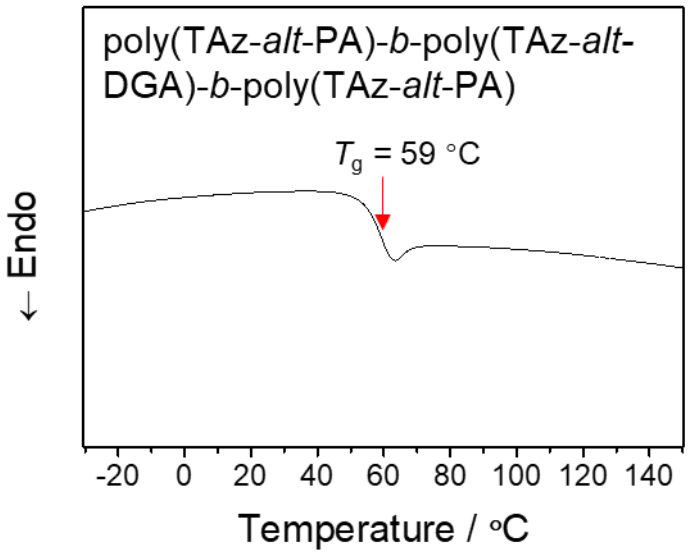

Figure 4.10. Second heating DSC curves of the synthesized poly(TAz-*alt*-PA)-*b*-poly(TAz-*alt*-DGA)-*b*-poly(TAz-*alt*-PA) (entry 1 in Table 4.1).

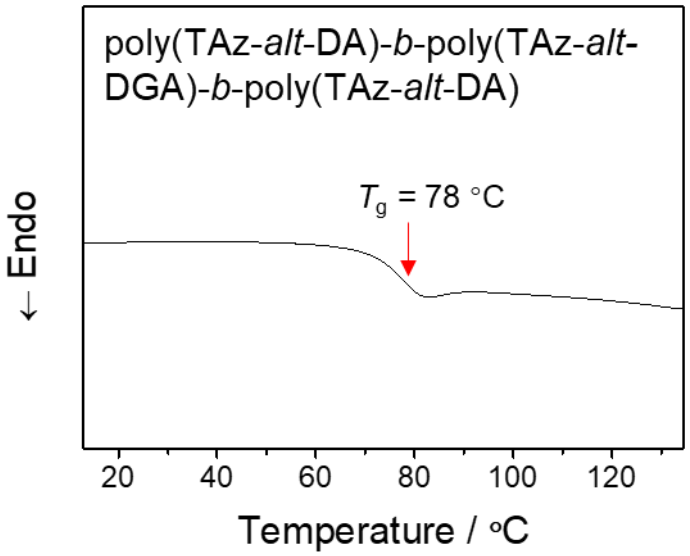

Figure 4.11. Second heating DSC curve of the synthesized poly(TAz-*alt*-DA)-*b*-poly(TAz-*alt*-DGA)-*b*-poly(TAz-*alt*-DA) (entry 3 in Table 4.1).

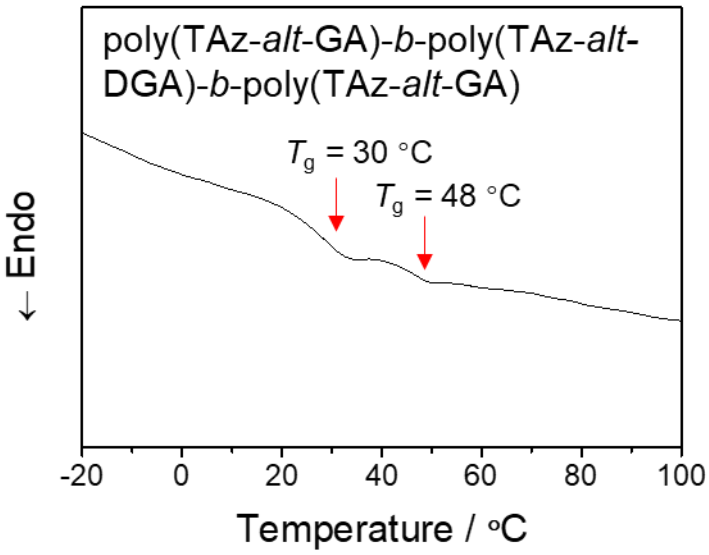

Figure 4.12. Second heating DSC curves of the synthesized poly(TAz-*alt*-GA)-*b*-poly(TAz-*alt*-DGA)-*b*-poly(TAz-*alt*-GA) (entry 2 in Table 4.1).

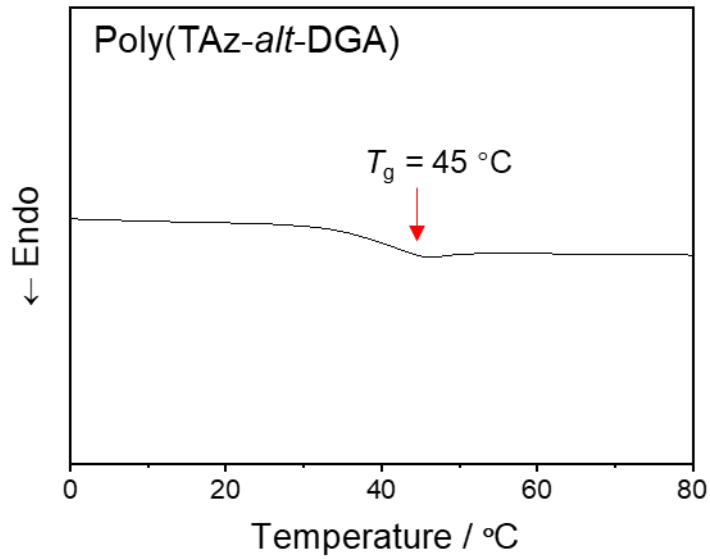

Figure 4.13. Second heating DSC curve of the synthesized poly(TAz-*alt*-DGA).

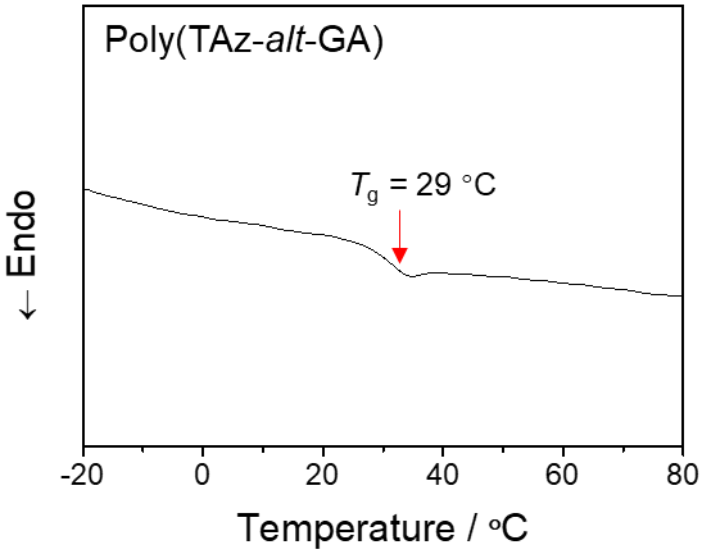

Figure 4.14. Second heating DSC curves of the synthesized poly(TAz-*alt*-GA).

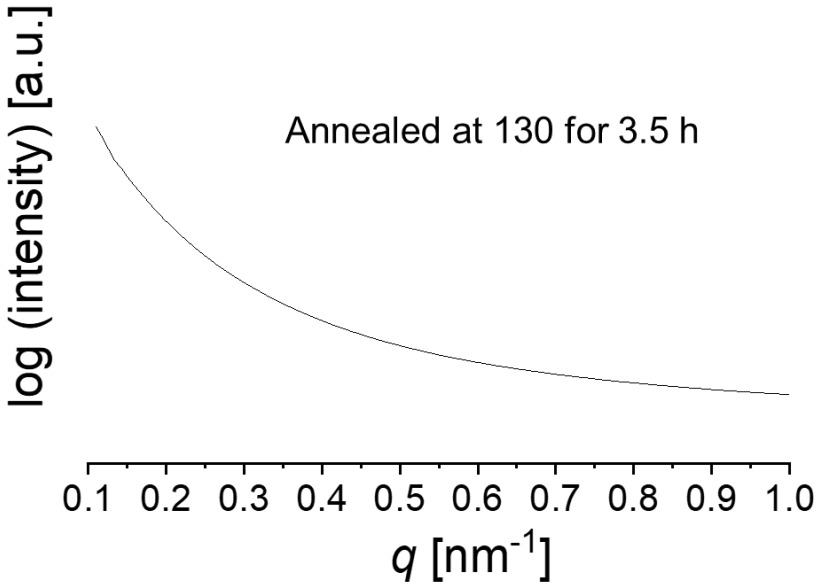

Figure 4.15. SAXS profile of poly(TAz-*alt*-GA)-*b*-poly(TAz-*alt*-DGA)-*b*-poly(TAz-*alt*-GA) (entry) after thermal annealing at 130 °C for 3.5 h (entry 2 in Table 4.1).

The synthesized "real" block copolymer poly(TMC)-*b*-poly(TAz-*alt*-PA)-*b*-poly(TMC) showed two distinct T_g values on the DSC curve (Figure 4.16a), corresponding to the poly(TAz-*alt*-PA) (T_g = 62 °C) and the poly(TMC) (T_g = –13 °C) blocks. Importantly, SAXS measurements confirmed distinct microphase separation in the copolymer. The SAXS profile of the thermally annealed sample (130 °C for 3.5 h) showed a

principal scattering peak (q^*) at 0.379 nm^{-1} (Figure 4.16b), from which a domain spacing (d) of 16.6 nm was calculated using the Bragg equation ($d = 2\pi/q^*$). However, the exact order of the periodic morphology could not be determined due to the absence of higher-order reflections. This is the first report of a block copolymer synthesized via self-switchable polymerization for which microphase separation was confirmed by SAXS measurements.

Similarly, the poly(EHGE-*alt*-NA)-*b*-poly(TAz-*alt*-PA)-*b*-poly(EHGE-*alt*-NA) quaterpolymer exhibited two distinct T_g values (T_g = –8 and 80 °C) on the DSC curve (Figure 4.16c). The microphase separation was also confirmed using SAXS analysis, which revealed a domain spacing of 28.3 nm in the copolymers (Figure 4.16d). These results indicate that the chemical nature (or polarity) difference between the two one-step-synthesized blocks was large enough to enable microphase separation. Thus, this four-component, self-switchable copolymerization provides a versatile block copolymer synthesis platform that allows for the flexible control of each block structure by a judicious selection of the four monomers. Moreover, it offers a wide range of possibilities for the precise modulation of block structure differences and holds great promise for the design of block copolymers with desired microphase separation behaviors.

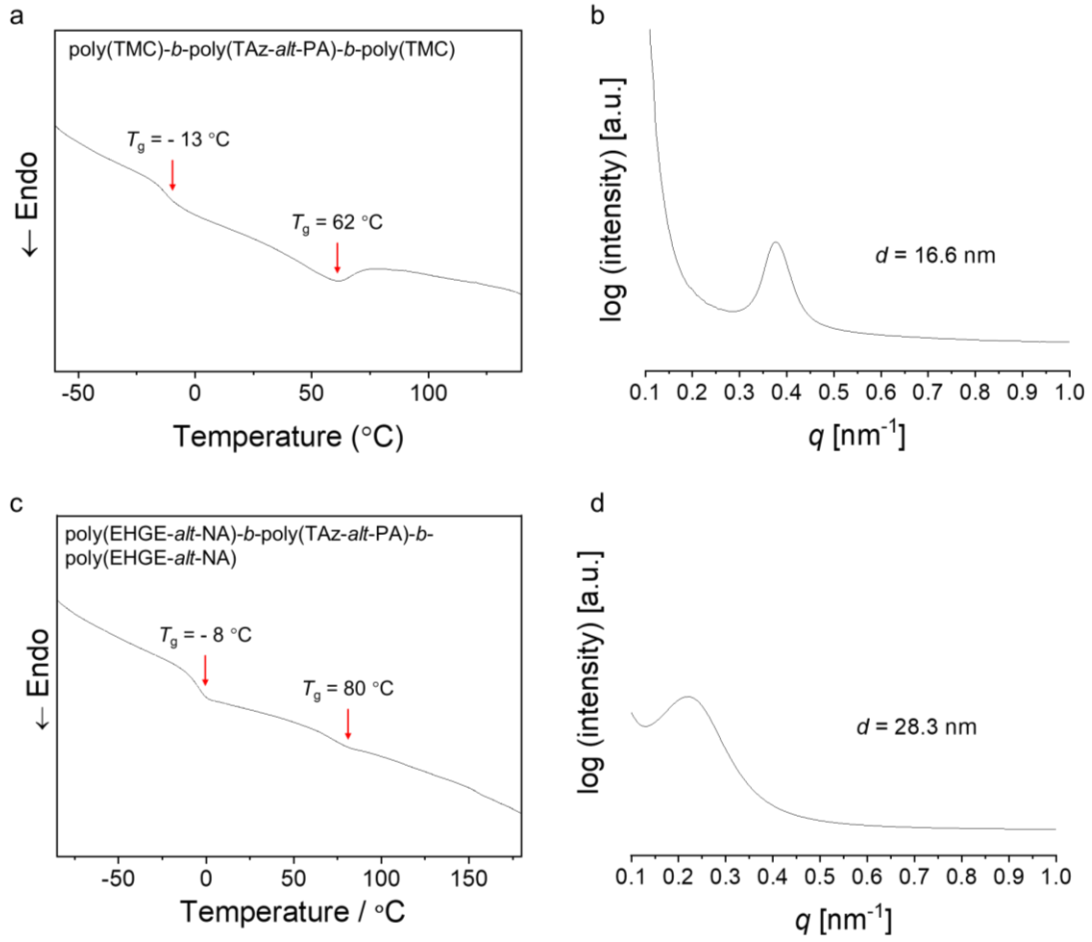

Figure 4.16. DSC thermograms of (a) poly(TMC)-*b*-poly(TAz-*alt*-PA)-*b*-poly(TMC) and (c) poly(EHGE-*alt*-NA)-*b*-poly(TAz-*alt*-PA)-*b*-poly(EHGE-*alt*-NA). SAXS profiles of (b) poly(TMC)-*b*-poly(TAz-*alt*-PA)-*b*-poly(TMC) and (d) poly(EHGE-*alt*-NA)-*b*-poly(TAz-*alt*-PA)-*b*-poly(EHGE-*alt*-NA). The samples were annealed at 130 °C for 3.5 h before measurement.

4.4 Conclusion

In this chapter, the author demonstrated that the copolymerization of TAz with two distinct anhydrides is an effective method for synthesizing poly(amide ester)-based block copolymers under mild conditions. By combining TAz/anhydride ROCOP and TMC ROP, the author successfully synthesized a “real” block poly(amide ester)-*b*-polycarbonate with a defined phase separation behavior that resulted in an improved block chemical structure relative to that achieved using the previously reported TAz ROCOP-based self-switchable system. Notably, the author demonstrated the one-step synthesis of “real” block copolymers composed of

poly(amide ester) and polyester that showed microphase separation by the four-component copolymerization of aziridine, epoxide, and two anhydrides. This approach enables the flexible adjustment of each block structure through the appropriate selection of the four starting monomers, providing a basis for the synthesis of block copolymers with the desired microphase-separated morphology.

4.5References

1. Xu J, Wang X, Hadjichristidis N. Diblock dialternating terpolymers by one-step/one-pot highly selective organocatalytic multimonomer polymerization. *Nat. Commun.* **2021**, *12*, 7124.
2. Chen, X. L., Wang, B., Song, D. P., Pan, L., Li, Y. S. One-step synthesis of sequence-controlled polyester-block-poly (ester-*alt*-thioester) by chemoselective multicomponent polymerization. *Macromolecules* **2022,** *55*, 1153-1164.
3. Xu, J.; Hadjichristidis, N. Well-Defined Poly(Ester Amide)-Based Homo- And Block Copolymers by One-Pot Organocatalytic Anionic Ring-Opening Copolymerization of *N*-Sulfonyl Aziridines and Cyclic Anhydrides. *Angew. Chem. Int. Ed. Engl.* **2021**, *60*, 6949–6954.
4. Gleede, T., Markwart, J. C., Huber, N., Rieger, E., & Wurm, F. R. Competitive copolymerization: access to aziridine copolymers with adjustable gradient strengths. *Macromolecules* **2019**, *52*, 9703-9714.
5. Xia, X., Gao, T., Li, F., Suzuki, R., Isono, T., Satoh, T. Sequential Polymerization from Complex Monomer Mixtures: Access to Multiblock Copolymers with Adjustable Sequence, Topology, and Gradient Strength. *Macromolecules* **2022**, *56*, 92-103.

Chapter 5

Binary Organocatalyzed Copolymerization: Toward Monomers Sequence Fully Controllable poly(ester-amide ester)

5.1 Introduction

In the previous chapters, the author demonstrated the self-switchable copolymerization for one-step synthesis of polyester-based block copolymers with various structures. Although block copolymers have received substantial attention, it is also essential to recognize the significance of random and gradient copolymers, which possess distinct physicochemical properties.[1–6] Consequently, tailoring the monomer sequence during copolymerization, particularly when derived from the same monomer mixture, could significantly improve the design of polymer materials, albeit posing a considerable challenge. In the case of copolymerization utilizing vinyl monomers, numerous reports exist on controlling the monomer sequence by adjusting the reaction conditions, including external stimulation,[7–10] catalyst,[11, 12] or solvent.[13] However, successful reports on controlling the monomer sequence in ring-opening polymerization (ROP) and ring-opening alternating copolymerization (ROAC) remain relatively scarce. For instance, Frey et al. demonstrated a shift in the copolymerization behavior in anionic ROP of two epoxides, changing it from random ($r_1 = r_2 = 1.00 \pm 0.02$) to gradient ($r_1 = 8.00 \pm 0.16$, $r_2 = 0.125 \pm 0.003$) by introducing a Lewis acid cocatalyst (Figure 5.1a).[14] Zhao and Ling et al. reported a copolymerization system involving epoxides and cyclic esters, using a binary catalyst pair comprising a phosphazene base and triethylborane (TEB) as a Brønsted base/Lewis acid combination. This system allowed for the tuning of copolymer monomer sequences by modifying the ratio of these two catalysts (Figure 5.1b).[15]

In the last chapters, the author has introduced multiple self-switchable copolymerization systems that encompass the ROAC of cyclic ethers and cyclic anhydrides, aziridines and cyclic anhydrides, ROP of cyclic esters, and cyclic carbonates. The remarkable versatility of these systems has facilitated the synthesis of various block copolymers with adjustable chemical structures through a combination of distinct catalytic cycles. The selectivity of copolymerization and control over monomer sequences predominantly relies on the inherent reactivity of different monomers under anionic polymerization conditions, where the primary

activation of the propagation chain ends occurs. Building upon the success of previous reports,[16–20] the author hypothesized that the introduction of a cocatalyst to selectively activate one of the monomers, thus permitting partial adoption of the "activated monomer mechanism," could effectively modify the monomer sequence in the resulting copolymers. With this hypothesis in mind, the author directed his focus toward the terpolymerization system involving epoxides, *N*-tosyl aziridine (TAz), and cyclic anhydrides, initially reported by Hadjichristidis et al.[21] In their study, a phosphazene base served as the catalyst, and the ROAC between TAz and cyclic anhydrides took place before the ROAC between epoxides and cyclic anhydrides. Owing to the structural differences between TAz and epoxides, epoxides would exhibit stronger interactions with a Lewis acid than TAz is anticipated. Consequently, the introduction of a Lewis acid cocatalyst has the potential to alter monomer selectivity.

During the investigation, Zhao and Carlotti et al. implemented a similar strategy in the copolymerization of aziridine and epoxides (as illustrated in Figure 5.1c).[22] They used a phosphazene base and TEB catalyst pair to synthesize polyether-*b*-polyamine block copolymers. Notably, the monomer sequence achieved in their work differed from that reported by Wurm et al.[23] Furthermore, Li et al. also utilized a phosphazene base and TEB catalyst pair in the terpolymerization of CO_2/epoxides/cyclic anhydrides, effectively enabling the tuning of the monomer sequence in the resulting poly(ester-carbonate) polymers (as shown in Figure 5.1d).[24] These studies collectively demonstrated the feasibility of controlling the monomer sequences by adjusting the catalyst pair ratio, thus providing supporting evidence for the author's hypothesis.

In this chapter, the author reports a *t*-BuP_1/TEB-catalyzed terpolymerization system involving epoxides/TAz/cyclic anhydrides. By changing the catalyst ratio, continuous monomer sequence regulation of the obtained poly(ester-amide ester) over the entire spectrum was achieved. The terpolymerization system allows unprecedented control over the monomer sequence spanning from ABA-type real block copolymers to gradient, random-like, reversed gradient, and reversed BAB-type block-like copolymers, from the same

combination of monomers (Figure 5.1e). To deepen the understanding of the reaction mechanism, the author also conducted density functional theory (DFT) calculations.

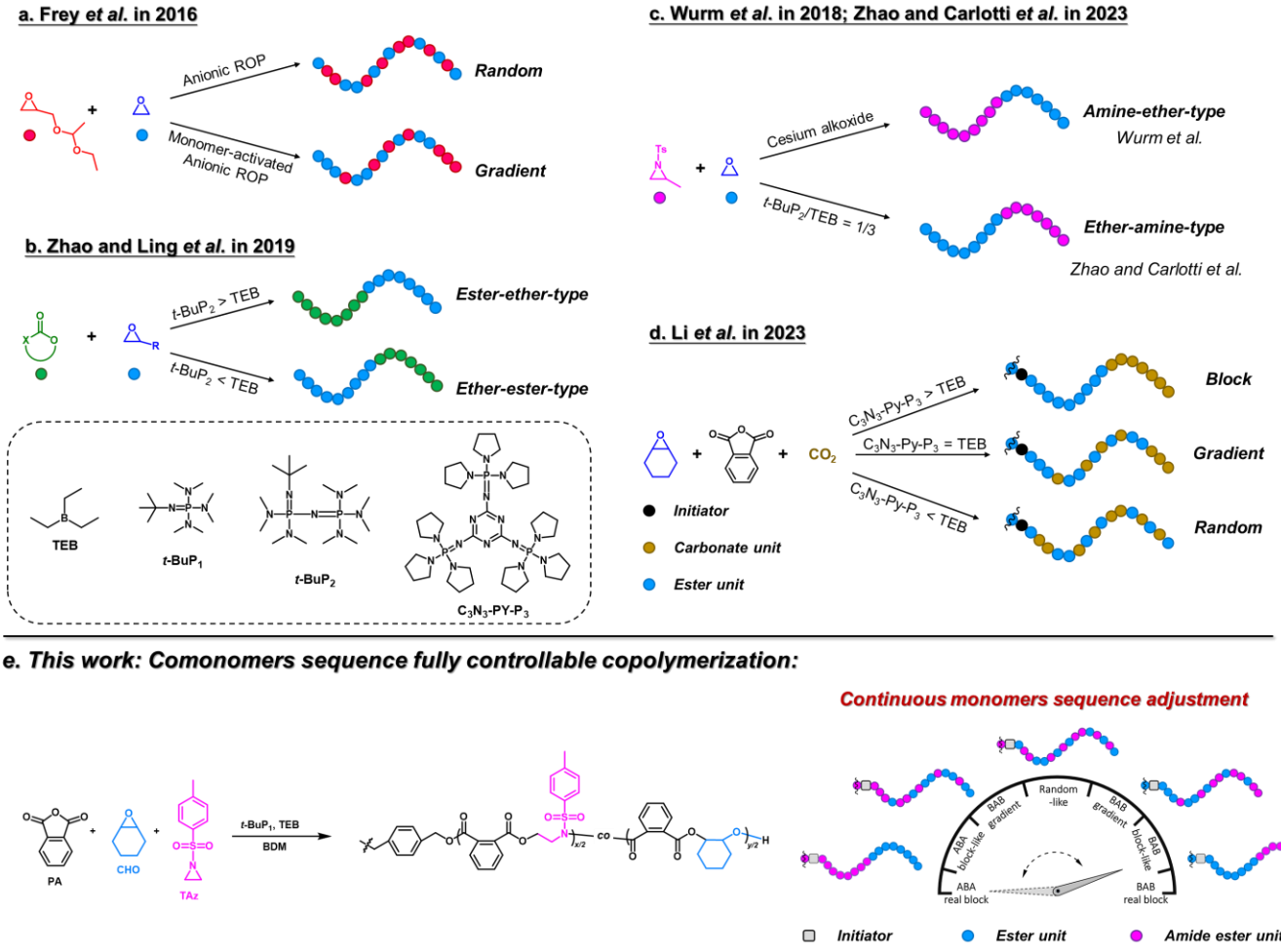

Figure 5.1. General scheme for monomer sequence controllable ring-opening copolymerization systems and the concept of this research.

5.2 Experimental Section

5.2.1 Materials:

Diglycolic anhydride (DGA; >98.0%, Tokyo Kasei Kogyo Co., Ltd. (TCI)), phthalic anhydride (PA; >98.0%, TCI), and glutaric anhydride (GA; >98.0%, TCI) were recrystallized in THF and then purified by sublimation before use. *N*-Tosylaziridine (TAz; 98%, Sigma−Aldrich) was dried over phosphorus pentoxide under a high vacuum for 72 h before use. 1,2-Epoxycyclohexane (CHO; >98.0%, TCI), 1,2-epoxyhexane (EH; >96.0%, TCI), (BO; >99.0%, TCI), and benzyl glycidyl ether (BGE; >97.0%, TCI) were

purified by distillation with CaH_2 under reduced pressure. Triethylborane solution (TEB; 1.0 M in THF, Sigma−Aldrich), 1,4-benzenedimethanol (BDM; >99.0%, TCI), trimethyl(phenyl)silane (TMPS; 99%, Sigma−Aldrich), and *N*′-*tert*-butyl-*N*,*N*,*N*′,*N*′,*N*″,*N*″-hexamethylphosphorimidic triamide (*t*-BuP_1, >98.0%, Sigma−Aldrich) were used as received.

5.2.2 Instrument:

The polymerization was carried out in a gas purification system (molecular sieves and copper catalyst) equipped MBRAUN stainless steel glovebox in a dry argon atmosphere (H_2O, O_2 <0.1 ppm). The moisture and oxygen contents in the glovebox were monitored with MB-MO-SE 1 and MB-OX-SE 1, respectively.

The size exclusion chromatography (SEC) is utilizing a Shodex GPC-101 system equipped with a Shodex K-G guard column and a set of two Shodex K-805L columns (linear, 8 mm × 300 mm; bead size, 5 μm; exclusion limit, 4×10^6). The measurement was performed in THF (flow rate, 1.0 mL min^{-1}) at 40 °C. Polystyrene (PS) standard samples were used for calibration.

JEOL JNM-ECS400 instrument or a JEOL JNM-ECX400P instrument was used for ^{1}H NMR, and DOSY NMR spectral measurement was conducted at room temperature with the JEOL JNM-ECX400P instrument. DOSY NMR analyses were carried out at room temperature using the ledbpgp2s sequence with at least 15 gradient increments.

DFT calculation was performed by Gaussian 16 C.01 package. All optimized structures and harmonic vibrational frequencies were obtained under B3LYP/6-31+g**.

5.2.3 Synthetic Details

t-BuP$_1$/TEB co-catalyzed ROAC from CHO and PA

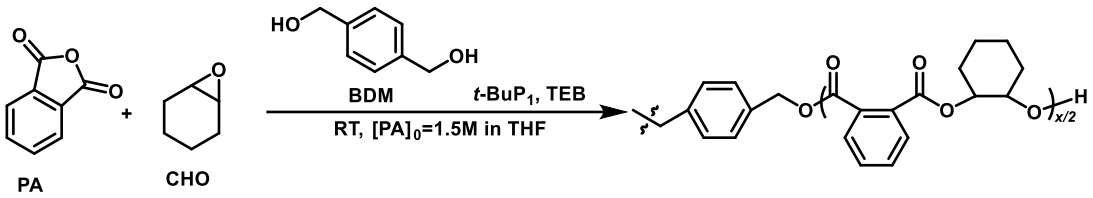

Scheme 5.2. *t*-BuP$_1$/TEB co-catalyzed ROAC from CHO and PA.

In the glovebox, a mixture was prepared by combining phthalic anhydride (PA) (128.5 mg, 0.868 mmol), cyclohexene oxide (CHO) (84.7 mg, 0.868 mmol), and BDM (6.0 mg, 43.4 μmol) in a Schlenk flask. To dissolve the mixture, 0.578 mL of tetrahydrofuran (THF) was added, and trimethylphenylsilane (TMPS) (35 mg, 0.232 mmol, as NMR inner standard) was included as an internal standard for calculating monomer conversion. The polymerization was initiated by introducing *t*-BuP$_1$ (10.2 mg, 43.4 μmol) and varying amounts of triethylborane (TEB). The reaction proceeded with stirring at room temperature inside the glovebox, and proton nuclear magnetic resonance (^{1}H NMR) spectroscopy was employed to monitor the progress of the polymerization. The crude product was purified via reprecipitation with methanol.

t-BuP$_1$/TEB co-catalyzed ROAC from TAz and PA

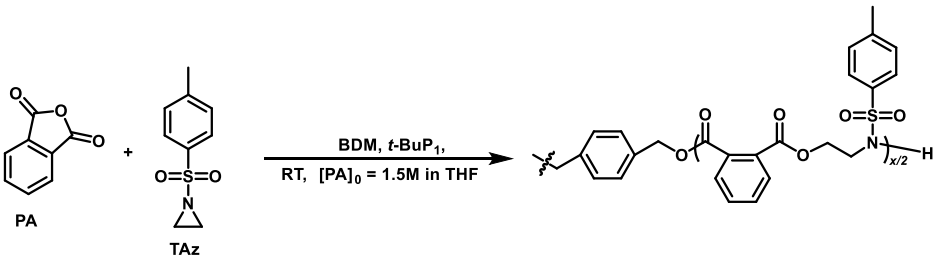

Scheme 5.3. *t*-BuP$_1$/TEB co-catalyzed ROAC from TAz and PA.

In the glovebox, a mixture was prepared by combining PA (128.5 mg, 0.868 mmol), TAz (171.1 mg,

0.868 mmol), and BDM (6.0 mg, 43.4 μmol) in a Schlenk flask. To dissolve the mixture, 0.578 mL of THF was added. TMPS (35 mg, 0.232 mmol) was included as an internal standard for calculating monomer conversion. The polymerization was initiated by introducing *t*-BuP$_1$ (10.2 mg, 43.4 μmol) and varying amounts of TEB. The reaction proceeded with stirring at room temperature inside the glovebox, and ^{1}H NMR spectroscopy was employed to monitor the progress of the polymerization. The crude product was purified via reprecipitation with methanol.

***t*-BuP$_1$/TEB co-catalyzed three components ROCOP in one-pot, two-step.**

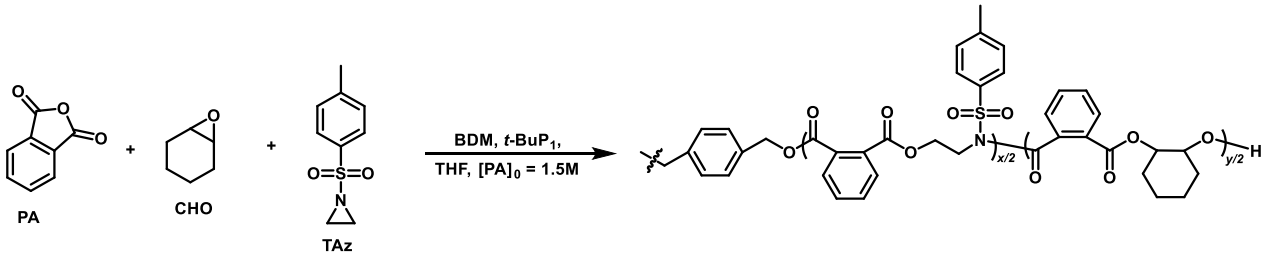

Scheme 5.4. *t*-BuP$_1$/TEB co-catalyzed three components ROCOP in one-pot, two-step.

In the glovebox, a mixture was prepared by combining PA (257.1 mg, 1.736 mmol), TAz (171.1 mg, 0.868 mmol), CHO (84.7 mg, 0.868 mmol), and BDM (6.0 mg, 43.9 μmol) in a Schlenk flask. To dissolve the mixture, 1.15 mL of THF was added. TMPS (35 mg, 0.232 mmol) was added as inner standard for monomer conversion calculation and *t*-BuP$_1$ (10.2 mg, 43.4 μmol) was introduced to start the polymerization at room temperature. ^{1}H NMR measurement was used to monitor polymerization. TEB (43.9μL, 43.9 μmol) was added into the Schlenk flask once TAz was all reacted. The crude product was later purified through reprecipitation with methanol.

***t*-BuP$_1$/TEB co-catalyzed three components ROCOP**

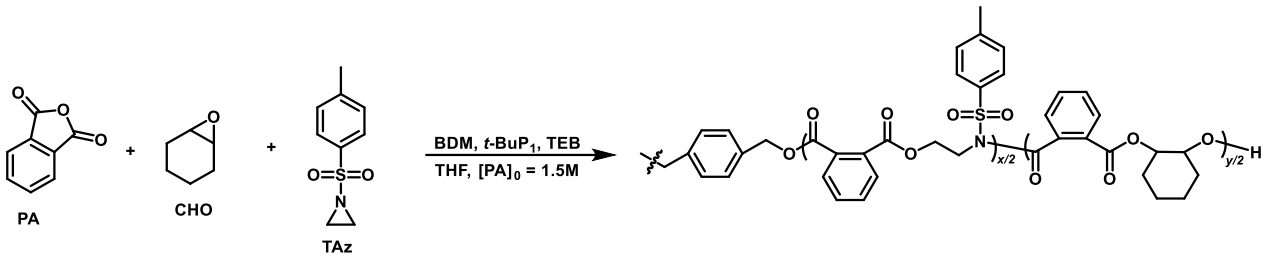

Scheme 5.5. *t*-BuP$_1$/TEB co-catalyzed three components ROCOP.

In the glovebox, a mixture was prepared by combining PA (257.1 mg, 1.736 mmol), TAz (171.1 mg, 0.868 mmol), CHO (84.7 mg, 0.868 mmol), and BDM (6.0 mg, 43.9 μmol) in a Schlenk flask. To dissolve the mixture, 1.15 mL of THF was added. TMPS (35 mg, 0.232 mmol) was added as internal standards for calculating monomer conversion. *t*-BuP$_1$ (10.2 mg, 43.4 μmol) and various amounts of TEB were introduced to initiate the polymerization. The reaction was carried out with stirring at room temperature inside the glovebox, and ^{1}H NMR spectroscopy was used to monitor the polymerization progress. The crude product was subsequently purified through reprecipitation with methanol.

5.3 Results and Discussion

5.3.1 *t*-BuP$_1$/TEB binary organocatalyzed CHO/PA and TAz/PA ROAC

The investigation was initiated with experimental studies to assess the impact of TEB on the ROAC of epoxides and cyclic anhydrides, and the ROAC of aziridine and cyclic anhydrides, using model monomers including TAz, CHO, and PA. The ROAC reactions were conducted at room temperature under an inert Ar atmosphere, with BDM as the initiator and THF as the solvent. The phosphazene base *t*-BuP$_1$ was employed as a catalyst to activate the initiator or the propagating chain ends. The initial PA concentration ([PA]$_0$) was set to 1.5 mol L^{-1}, and the initial ratio ([BDM]$_0$/[*t*-BuP1]/[PA]$_0$/[TAz or CHO]$_0$) was set as 1.0/1.0/20/20, with varying equivalents of TEB.

Table 5.1. CHO/PA ROAC and TAz/PA ROAC in different TEB loading [a]

Entry	Monomer	$[BDM]_0/[t\text{-}BuP_1]/[TEB]$	temp. (°C)	Time (%)	[b]Conv. (%)	TOF (h^{-1})
1	CHO/PA	1.0/1.0/0.0	RT	199	24.8	0.0249
2	CHO/PA	1.0/1.0/0.25	RT	28	73.8	0.528
3	CHO/PA	1.0/1.0/0.50	RT	12	64.5	1.075
4	CHO/PA	1.0/1.0/0.75	RT	12	65.9	1.098
5	CHO/PA	1.0/1.0/1.0	RT	12	67.3	1.121
6	TAz/PA	1.0/1.0/0.0	RT	23	80.5	0.700
7	TAz/PA	1.0/1.0/0.25	RT	51	85.7	0.336
8	TAz/PA	1.0/1.0/0.50	RT	145	88.9	0.123
9	TAz/PA	1.0/1.0/0.75	RT	477	0	0
10	TAz/PA	1.0/1.0/1.0	RT	477	0	0

[a]The copolymerization was performed under Ar with BDM as catalyst at a $[BDM]_0/[TAz]_0$ or $/[epoxide]_0/[anhydride]_0$ molar ratio of 1/20/20, $[anhydride]_0$ = 1.5M in THF. [b]Determined by ^1H NMR analysis ($CDCl_3$).

The use of *t*-BuP_1 as the sole catalyst in the ROAC of CHO and PA resulted in a slow polymerization rate, with only 24.7% CHO conversion observed after 199 h (Table 5.1, entry 1). The introduction of TEB significantly accelerated the polymerization rate, with 73.8% and 64.5% consumption of CHO achieved in 28 and 12 h with the addition of 0.25 and 0.5 eq. of TEB, respectively (Table 5.1, entries 2 and 3). Further increase in the TEB amount to 0.75 and 1 eq. did not significantly enhance the polymerization rate (Table 5.1, entry 4 and 5).

For the ROAC of TAz and PA, in the report by Hadjichristidis et al., a sole *t*-BuP_1 catalyst was used with a sulfonamide initiator at room temperature.[25] In this study, when the sulfonamide initiator was replaced with the alcohol initiator BDM, the TAz/PA ROAC maintained a high polymerization rate, with 80.5% of TAz consumed in 23 h at room temperature (Table 5.1, entry 6). The addition of 0.25 eq. of TEB, however, decreases the polymerization rate, resulting in the consumption of 85.7% of TAz in 51 h (Table 5.1, entry 7).

Further increase in the TEB loading decelerated the polymerization rate (0.50 eq. of TEB, Table 5.1, entry 8), and the polymerization was nearly halted with more than 0.75 eq. for the TEB (Table 5.1, entries 9 and 10).

These investigations revealed that TEB serves as an "activator" in the ROAC of CHO and PA, whereas acts as an "inhibitor" in the ROAC of TAz and PA. As shown in Figure 5.2, plotting the TOF value against the TEB loading shows that in the absence of a TEB, the TAz/PA ROAC exhibited substantially higher reactivity than the CHO/PA ROAC. However, as the amount of added TEB increases, the difference in their reactivity diminishes and eventually reverses. This observation suggests that by combining these two ROAC cycles and modulating the addition of TEB, it is feasible to establish a copolymerization system that offers full control over monomer sequences, including the generation of AB block, gradient, random, reversed gradient, and reversed BA block copolymers.

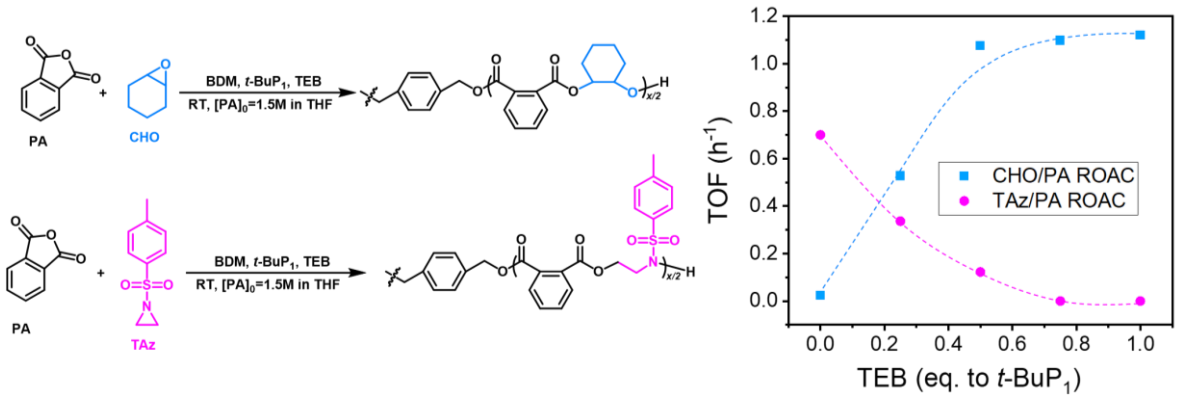

Figure 5.2. Plots of CHO/PA and TAz/PA ring-opening alternating copolymerization turnover frequency values (TOF) with different TEB addition amount.

5.3.2 Terpolymerization of CHO/TAz/PA with *t*-BuP$_1$/TEB binary catalyst system: establishment of monomer sequence-controlled copolymerization.

The terpolymerization of CHO/TAz/PA was initially conducted using only *t*-BuP$_1$, following the approach reported by Hadjichristidis and coworkers.[16] The terpolymerization was performed at 100 °C under

an Ar atmosphere at a $[BDM]_0/[t\text{-BuP1}]/[PA]_0/[CHO]_0/[TAz]_0$ molar ratio of 1.0/1.0/40/20/20 with an initial PA concentration of 1.5 mol L^{-1} in THF. Initially, TAz and PA reacted to form the poly(TAz-*alt*-PA) block.

Table 5.2. Synthesis of poly(CHO-*alt*-PA)-*co*-poly(TAz-*alt*-PA) with different monomer sequences [a]

entry	[TAz]/[anhydride]/[epoxide]	*t*-BuP1/TEB	temp. (°C)	conv. [b] (%)		time (h)	$M_{n,\,th}$ [c] (Da)	$M_{n,\,SEC}$ [d] (Da)	$Đ$ [d]
				TAz	CHO				
1	TAz/PA/CHO	1.0/0.0	100	100	65	34	10,100	4,800	1.13
2	TAz/PA/CHO	1.0/0.0→1.0/1.0	RT	100	89	210	11,300	8300	1.08
3	TAz/PA/CHO	1.0/0.10	RT	100	87	221.5	11,200	8,300	1.11
4	TAz/PA/CHO	1.0/0.25	RT	76	82	97	9,300	7,100	1.09
5	TAz/PA/CHO	1.0/0.5	RT	81	92	97	10,100	8,000	1.09
6	TAz/PA/CHO	1.0/0.75	RT	80	100	160	10,400	6,800	1.08
7	TAz/PA/CHO	1.0/1.0	RT	38	100	263	7,500	5,200	1.14
8	TAz/PA/CHO	1.0/1.0	RT→40	91	100	90 (RT); 70 (40 °C)	11,100	10,500	1.12

[a]The copolymerization was performed under Ar with BDM as catalyst at a $[BDM]_0/[TAz]_0/[anhydride]_0/[epoxide]_0$ molar ratio of 1/20/40/20, $[anhydride]_0$ = 1.5 mol L^{-1} in THF. [b]Determined by ^1H NMR analysis ($CDCl_3$). [c]Calculated using $[TAz]_0/[Ini]_0$ × conv. × (M.W. of anhydride + M.W. of TAz) + $[Epoxide]_0/[Ini]_0$ × conv. × (M.W. of anhydride + M.W. of Epoxide) + (M.W.of initiator). [d]Determined by SEC (THF) with a PSt standard

Following the complete consumption of TAz, the rate of copolymerization decelerated, and CHO conversion reached 65% after 33.5 h (Table 5.2, entry 1; Figures 5.3). However, no significant increase in molecular weight was discernible in the size exclusion chromatography (SEC) analysis (Figure 5.4). In a prior

report,[16] the copolymerization of cyclic anhydride with low-reactivity epoxide was hardly to initiate using the poly(TAz-*alt*-PA) segment under phosphazene base-catalyzed cyclic anhydride/epoxide/TAz self-switchable copolymerization. Only ethylene oxide (EO), propylene oxide (PO), and butylene oxide (BO) demonstrated the ability to copolymerize with cyclic PA and TAz, yielding diblock terpolymers with monomodal SEC elution peaks. To address this issue, a one-pot/two-step method was employed, wherein copolymerization was conducted at room temperature while maintaining other conditions constant (Figures 5.5 and 5.9a). TAz was fully consumed in 117 h to form the poly(TAz-*alt*-PA) block, and no further reaction of CHO was observed even after an additional 19 h. Subsequently, 1 equivalent of TEB was introduced into the reaction vessel, initiating the copolymerization of CHO and PA. 89% CHO had reacted after 74 h following the TEB addition. A distinct molecular weight shift from the poly(TAz-*alt*-PA) block to the poly(CHO-*alt*-PA)-*b*-poly(TAz-*alt*-PA)-*b*-poly(CHO-*alt*-PA) block copolymer was evident from SEC analysis, with the molecular weight distribution remaining narrow ($Đ$ = 1.09–1.08, Figure 5.6 and 5.7). The covalent linkage between each block of the resulting polymer was confirmed via diffusion-ordered NMR (DOSY) spectrum (Figure 5.8). Given the absence of a tapered region between each block, the resulting polymer is described as a "real-block" copolymer.

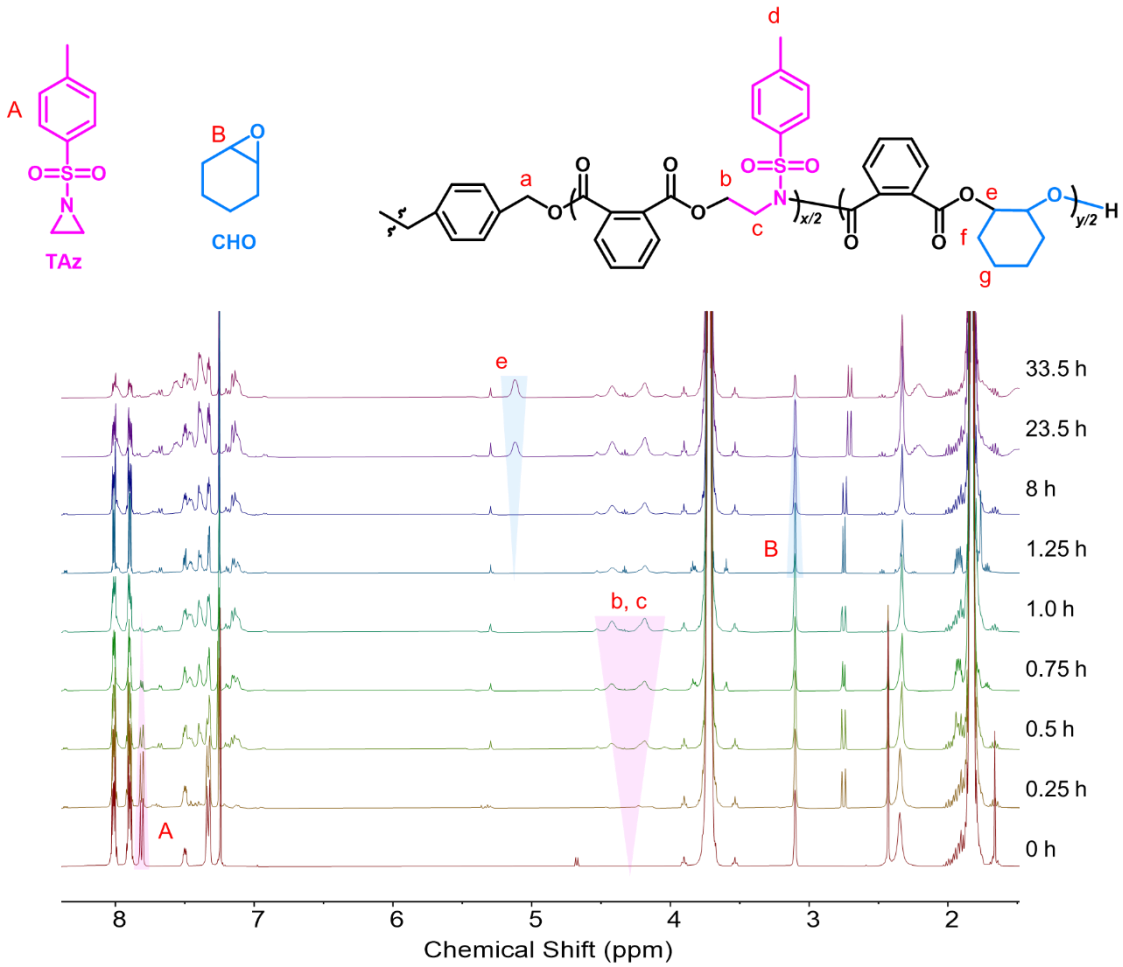

Figure 5.3. ^{1}H NMR spectra of crude aliquots withdrawn from the TAz/CHO/PA ROAC to monitor TAz and CHO conversion ($CDCl_3$) (polymerization was implemented under Ar atmosphere at 100 °C, *t*-BuP_1/TEB ratio was set as 1.0/0.0) (Table 5.2, entry 1).

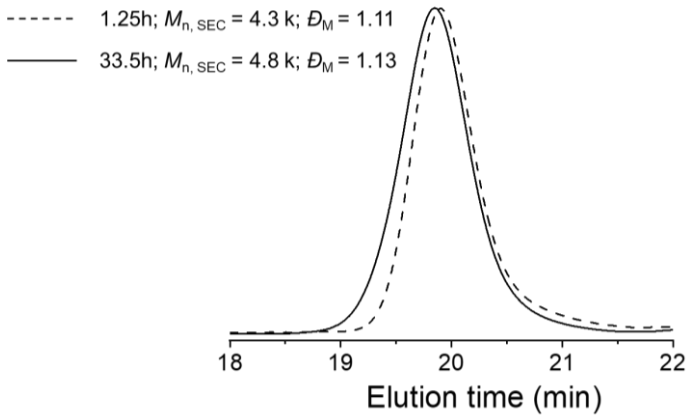

Figure 5.4. Evolution of SEC traces (THF) of synthesized poly(TAz-*alt*-PA)-*co*-poly(CHO-*alt*-PA) (polymerization was implemented under Ar atmosphere at 100 °C, *t*-BuP_1/TEB ratio was set as 1.0/0.0) (Table 1, entry 1).

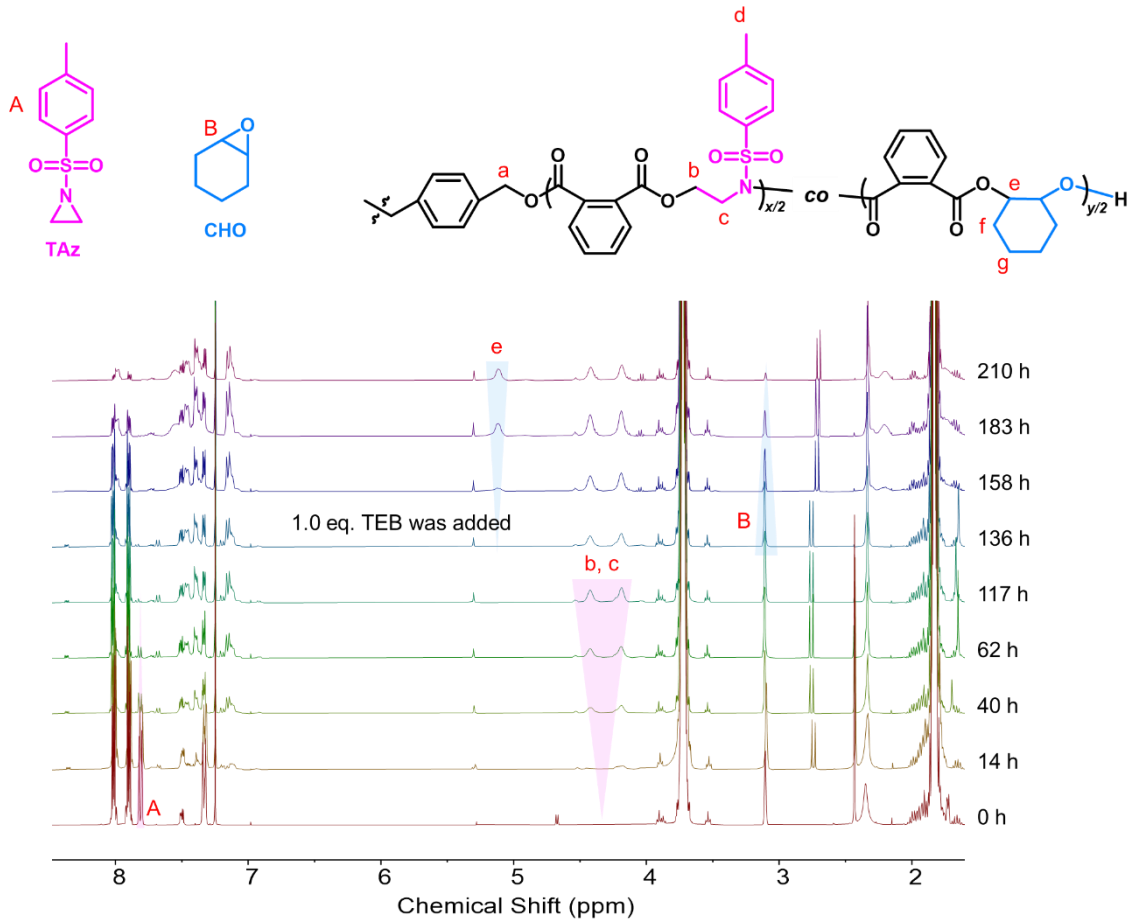

Figure 5.5. ^{1}H NMR spectra of crude aliquots withdrawn from the TAz/CHO/PA ROAC to monitor TAz and CHO conversion ($CDCl_3$) (polymerization was implemented under Ar atmosphere at room temperature, *t*-BuP_1/TEB ratio was set as 1.0/0.0 at the beginning, and 1.0 eq. TEB was added after136 hours) (Table 5.2, entry 2).

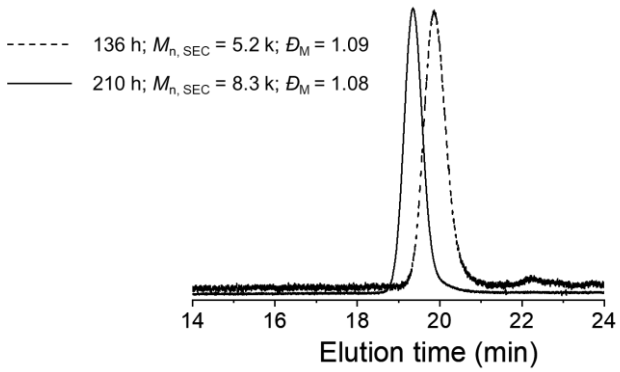

Figure 5.6. Evolution of SEC traces (THF) of synthesized poly(CHO-*alt*-PA)-*b*-poly(TAz-*alt*-PA)-*b*-poly(CHO-*alt*-PA) at136 hours and 210 hours (Table 5.2, entry 2).

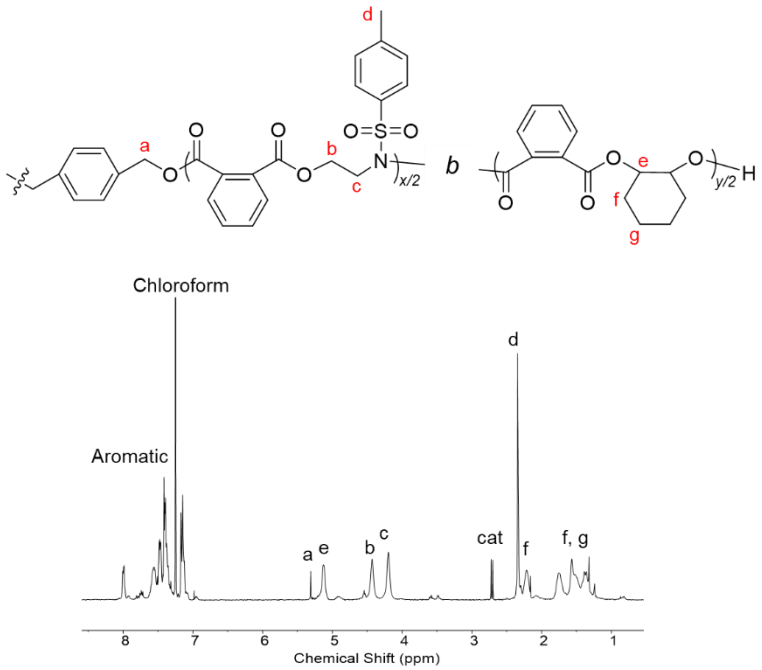

Figure 5.7. ^{1}H NMR spectrum of the synthesized poly(CHO-*alt*-PA)-*b*-poly(TAz-*alt*-PA)-*b*-poly(CHO-*alt*-PA) ($CDCl_3$) (Table 1, entry 2).

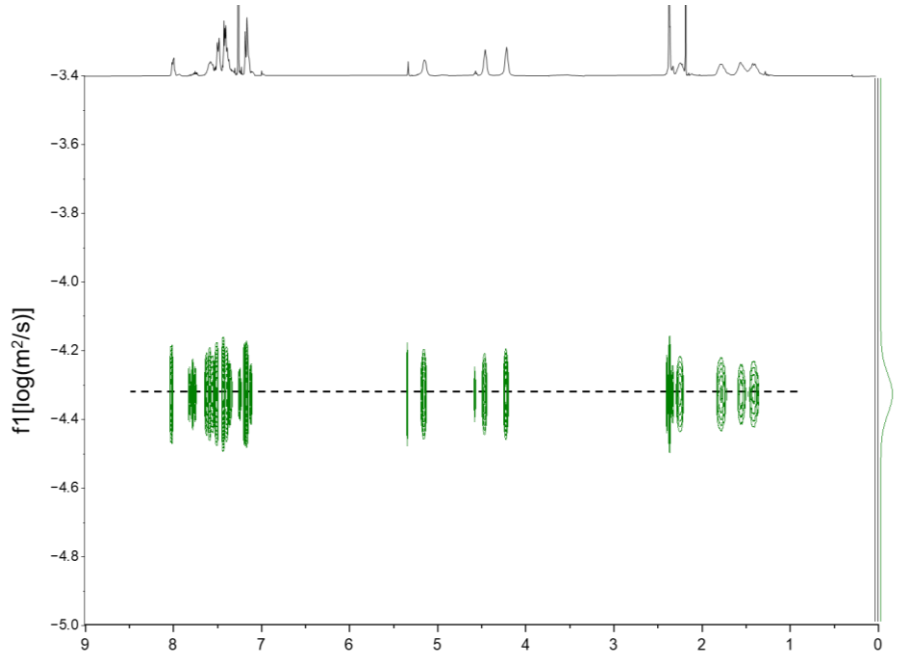

Figure 5.8. DOSY NMR spectrum of the synthesized poly(CHO-*alt*-PA)-*b*-poly(TAz-*alt*-PA)-*b*-poly(CHO-*alt*-PA) (Table 5.2 entry 2).

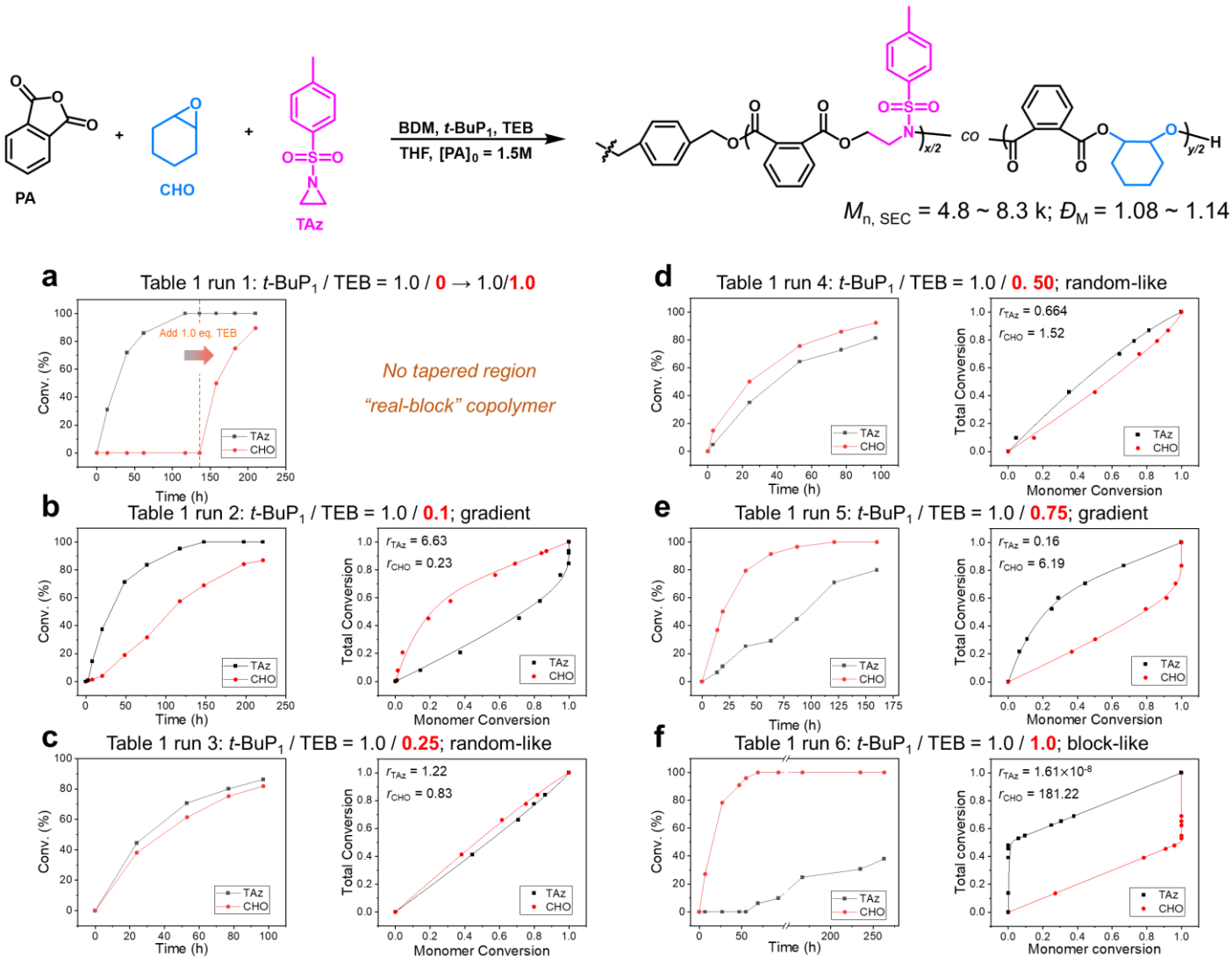

Figure 5.9. Copolymerization of *N*-tosyl aziridine, cyclohexane oxide, and phthalic anhydride with different *t*-BuP$_1$/TEB ratios. a) *t*-BuP$_1$/TEB = 1.0/0.0; b) *t*-BuP$_1$/TEB = 1.0/0.10; c) *t*-BuP$_1$/TEB = 1.0/0.25; d) *t*-BuP$_1$/TEB = 1.0/0.50; e) *t*-BuP$_1$/TEB = 1.0/ 0.75; f) *t*-BuP$_1$/TEB = 1.0/1.0.

Subsequently, CHO/TAz/PA terpolymerization was conducted by adding varying amounts of TEB while keeping the other reaction parameters constant at room temperature (Table 5.2, entries 2–6). Upon adding 0.1 eq. of TEB, although TAz still exhibited a higher reactivity, CHO began to react alongside TAz. For ease of discussion, the copolymer structures were classified into four categories based on the previous work by Wurm et al.: random-like ($r_1 \leq 2$ and $r_2 \geq 0.5$), gradient($2 \leq r_1 \leq 20$ and $0.05 \leq r_2 \leq 0.5$), block-like ($20 \leq r_1 \leq 800$ and $0.00125 \leq r_2 \leq 0.05$), and real block ($r_1 \geq 800$ and $r_2 \leq 0.00125$) (Figure 5.10).[26] Consequently, the

calculated reactivity ratios were r_{TAz} = 6.63 and r_{CHO} = 0.23. This finding indicates the formation of gradient terpolymers, with poly(TAz-*alt*-PA) being dominant in the center and poly(CHO-*alt*-PA) being dominant at the terminals (Figures 5.9b and 5.11–5.13).When 0.25 eq. of TEB was added, r_{TAz} and r_{CHO} were determined to be 1.22 and 0.83 (Figures 5.9c and 5.14–5.16), and the reactivity ratio became r_{TAz} = 0.66 and r_{CHO} = 1.52 when 0.5 eq. of TEB was added (Figures 5.9d and 5.17–5.19). As the reactivity ratios were close to 1.0, random-like sequences were formed under these two polymerization conditions. When the TEB amount increases to 0.75 eq., a reversed gradient terpolymer is created, where poly(CHO-*alt*-PA) units are concentrated at the center, whereas poly(TAz-*alt*-PA) is predominant at the terminals (Figures 5.9e and 5.20–5.22), with reactivity ratios of r_{TAz} = 0.16 and r_{CHO} = 6.19. Finally, the addition of 1.0 eq. of TEB (equal to *t*-BuP_1) resulted in CHO being consumed much more rapidly than TAz, yielding reactivity ratios of r_{TAz} = 0.0016 and r_{CHO} = 181.22. This result indicates the formation of a reversed BAB-type block-like poly(TAz-*alt*-PA)-*b*-poly(CHO-*alt*-PA)-*b*-poly(TAz-*alt*-PA) terpolymer (Table 5.2 run 7; Figures 5.9f and 5.23–5.25). Notably, as TAz consumption was sluggish under these conditions, the polymerization temperature increased from room temperature to 40 °C upon almost full conversion of CHO (Table 1, run 8; Figure 5.26). The resulting BAB block-like copolymer maintained a narrow molecular weight distribution ($Đ$ = 1.12; Figure 5.27), and covalent bonding between each block was confirmed via the DOSY NMR spectrum (Figure 5.28).

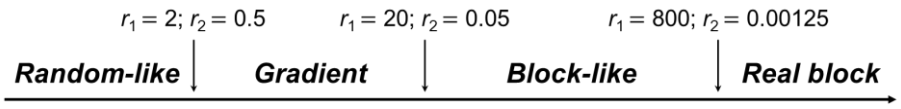

Figure 5.10. Monomer reactivity across diverse polymer sequence structures.

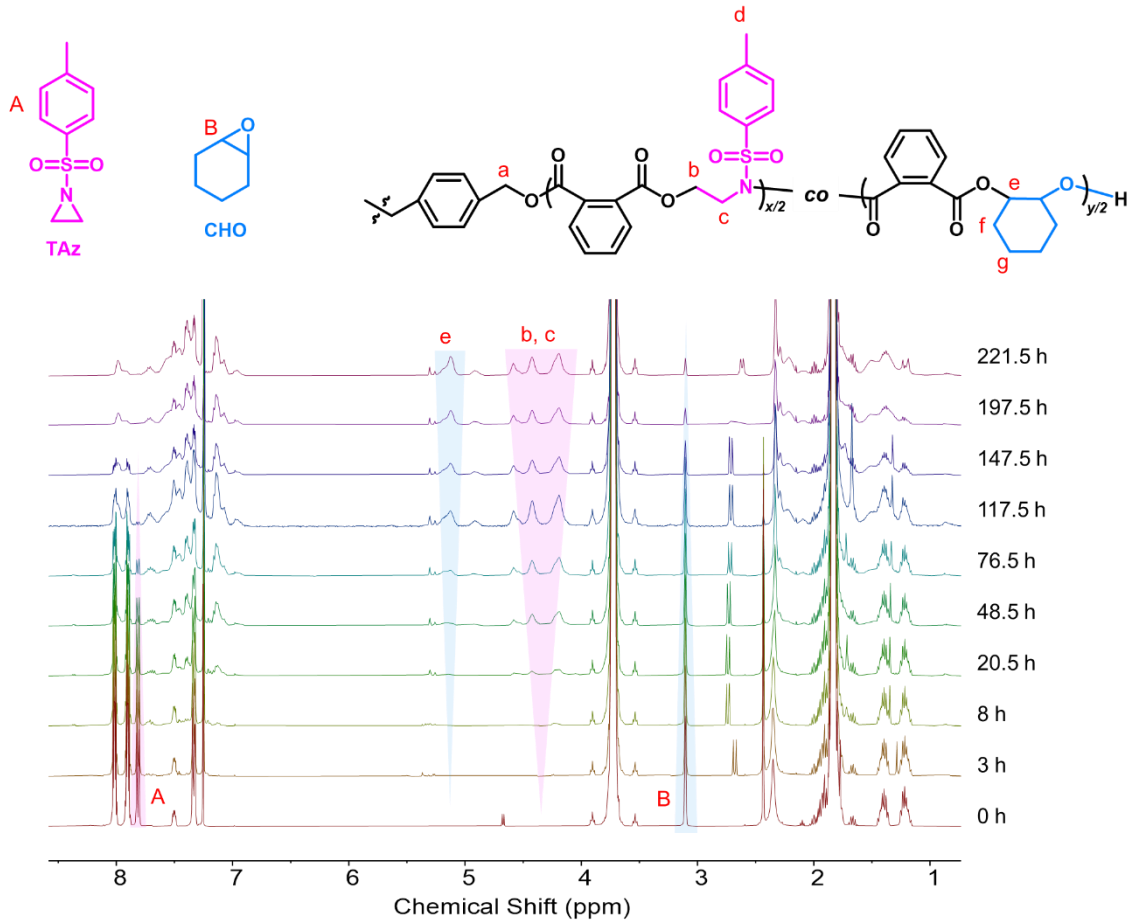

Figure 5.11. ^{1}H NMR spectra of crude aliquots withdrawn from the TAz/CHO/PA ROAC to monitor TAz and CHO conversion ($CDCl_3$) (polymerization was implemented under Ar atmosphere at room temperature, *t*-BuP_1/TEB ratio was set as 1.0/0.10) (Table 5.2, entry 3).

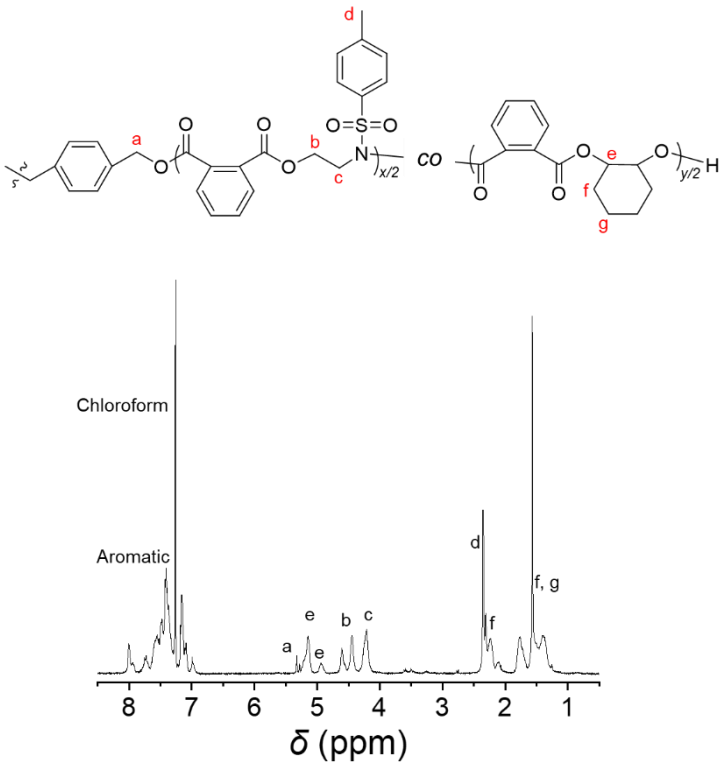

Figure 5.12. ^{1}H NMR spectrum of the synthesized poly(CHO-*alt*-PA)-*co*-poly(TAz-*alt*-PA) ($CDCl_3$) (polymerization was implemented under Ar atmosphere at room temperature, *t*-BuP_1/TEB ratio was set as 1.0/0.10) (Table 5.2, entry 3).

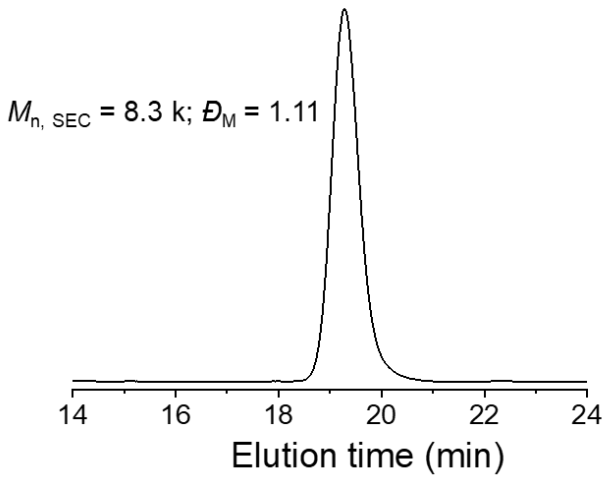

Figure 5.13. SEC trace (THF) of synthesized poly(CHO-*alt*-PA)-*co*-poly(TAz-*alt*-PA) (polymerization was implemented under Ar atmosphere at room temperature, *t*-BuP_1/TEB ratio was set as 1.0/0.1) (Table 5.2, entry 3).

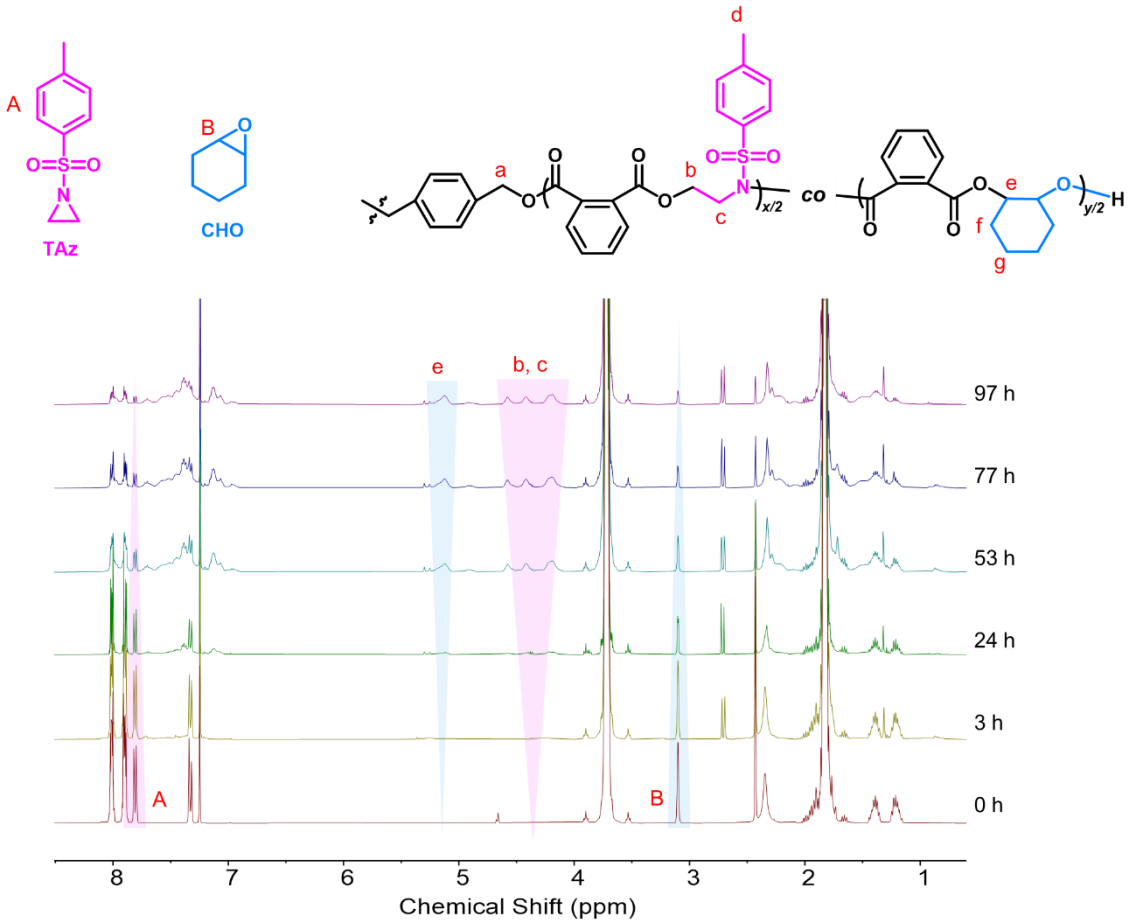

Figure 5.14. ^{1}H NMR spectra of crude aliquots withdrawn from the TAz/CHO/PA ROAC to monitor TAz and CHO conversion ($CDCl_3$) (polymerization was implemented under Ar atmosphere at room temperature, *t*-BuP_1/TEB ratio was set as 1.0/0.25) (Table 5.2, entry 4).

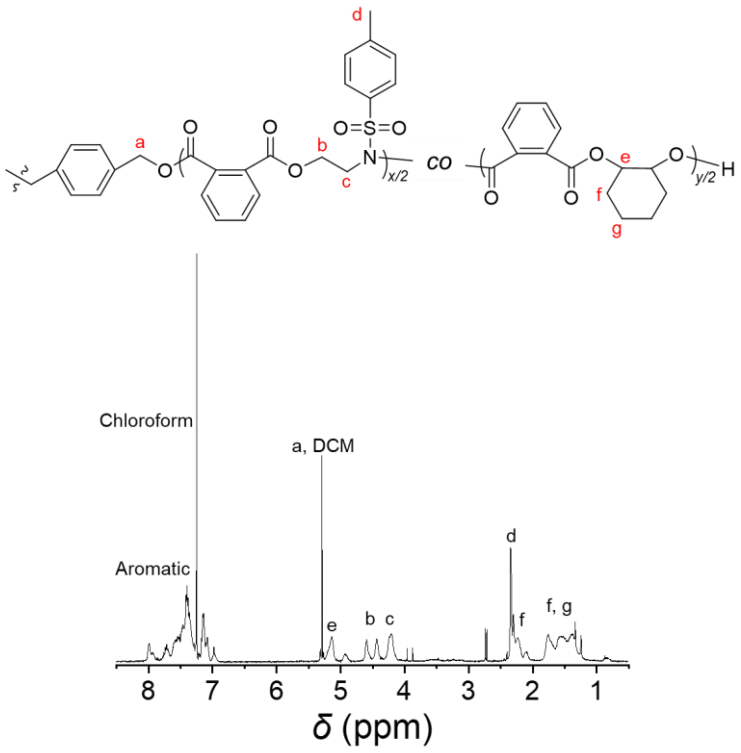

Figure 5.15. ^{1}H NMR spectrum of the synthesized poly(CHO-*alt*-PA)-*co*-poly(TAz-*alt*-PA) ($CDCl_3$) (polymerization was implemented under Ar atmosphere at room temperature, *t*-BuP_1/TEB ratio was set as 1.0/0.25) (Table 5.2, entry 4).

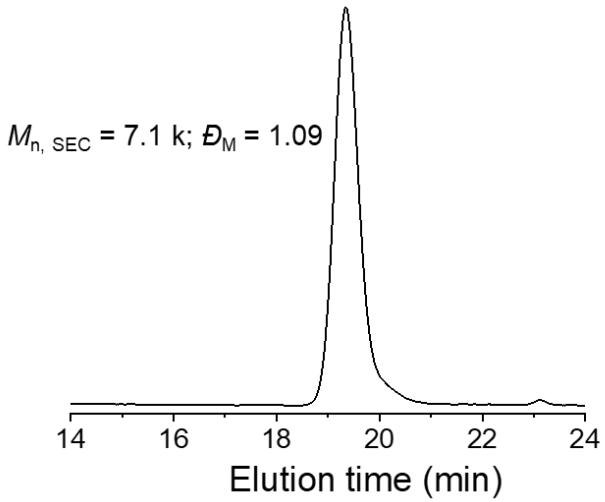

Figure 5.16. SEC trace (THF) of synthesized poly(CHO-*alt*-PA)-*co*-poly(TAz-*alt*-PA) (polymerization was implemented under Ar atmosphere at room temperature, *t*-BuP_1/TEB ratio was set as 1.0/0.25) (Table 5.2, entry 4).

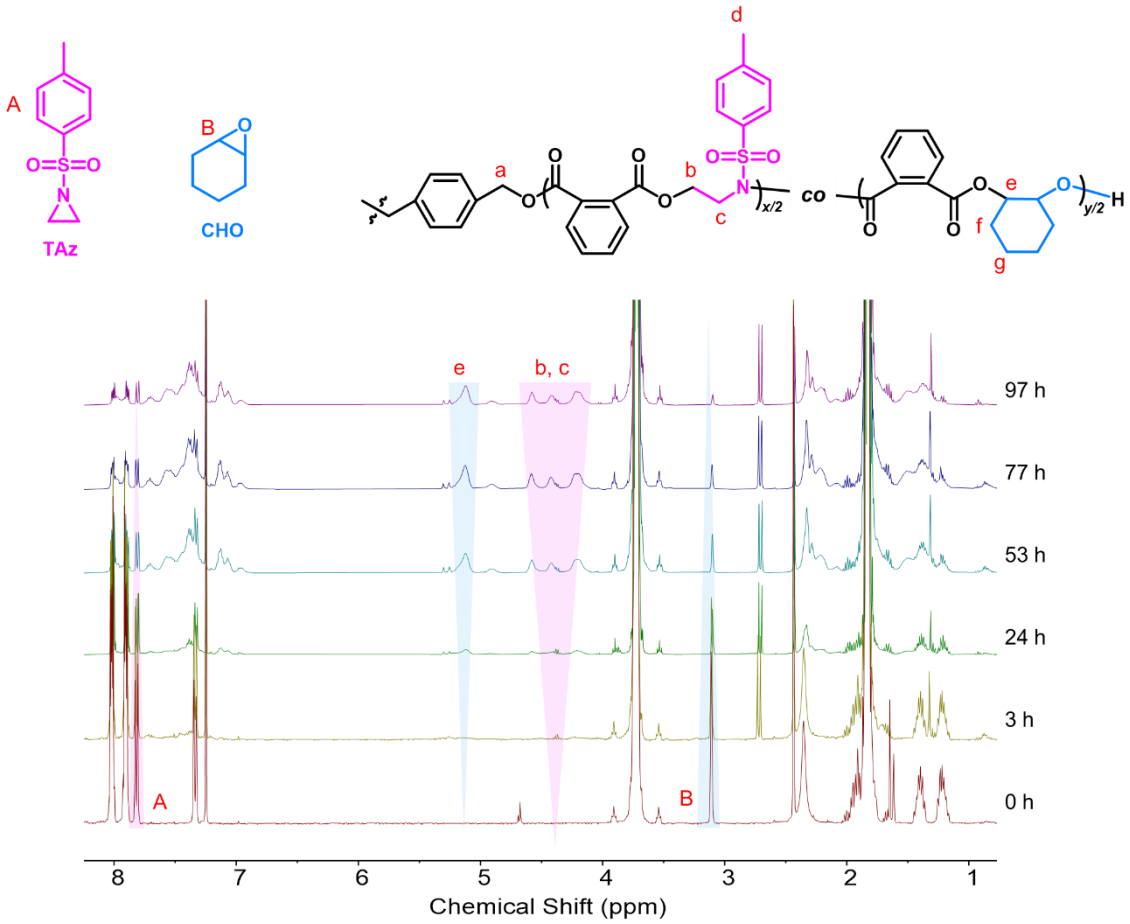

Figure 5.17. ^{1}H NMR spectra of crude aliquots withdrawn from the TAz/CHO/PA ROAC to monitor TAz and CHO conversion ($CDCl_3$) (polymerization was implemented under Ar atmosphere at room temperature, *t*-BuP_1/TEB ratio was set as 1.0/0. 50) (Table 5.2, entry 5).

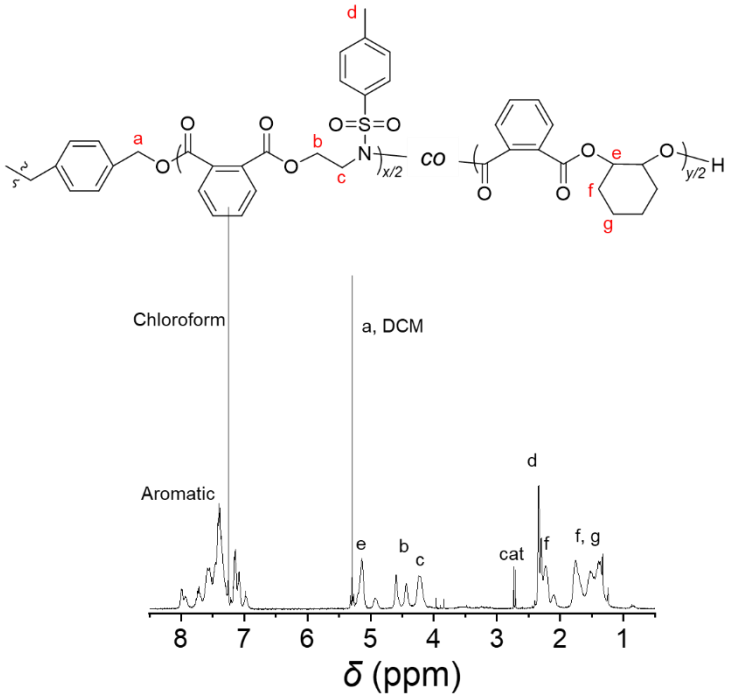

Figure 5.18. ^{1}H NMR spectrum of the synthesized poly(CHO-*alt*-PA)-*co*-poly(TAz-*alt*-PA) ($CDCl_3$) (polymerization was implemented under Ar atmosphere at room temperature, *t*-BuP_1/TEB ratio was set as 1.0/0.50) (Table 5.2, entry 5).

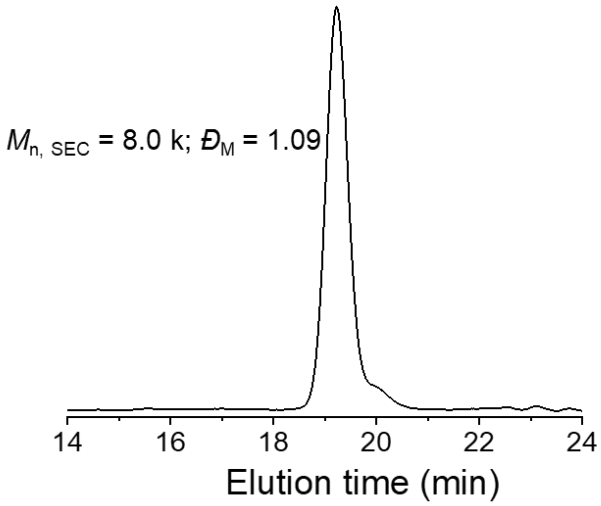

Figure 5.19. SEC trace (THF) of synthesized poly(CHO-*alt*-PA)-*co*-poly(TAz-*alt*-PA) (polymerization was implemented under Ar atmosphere at room temperature, *t*-BuP_1/TEB ratio was set as 1.0/0.5) (Table 5.2, entry 5).

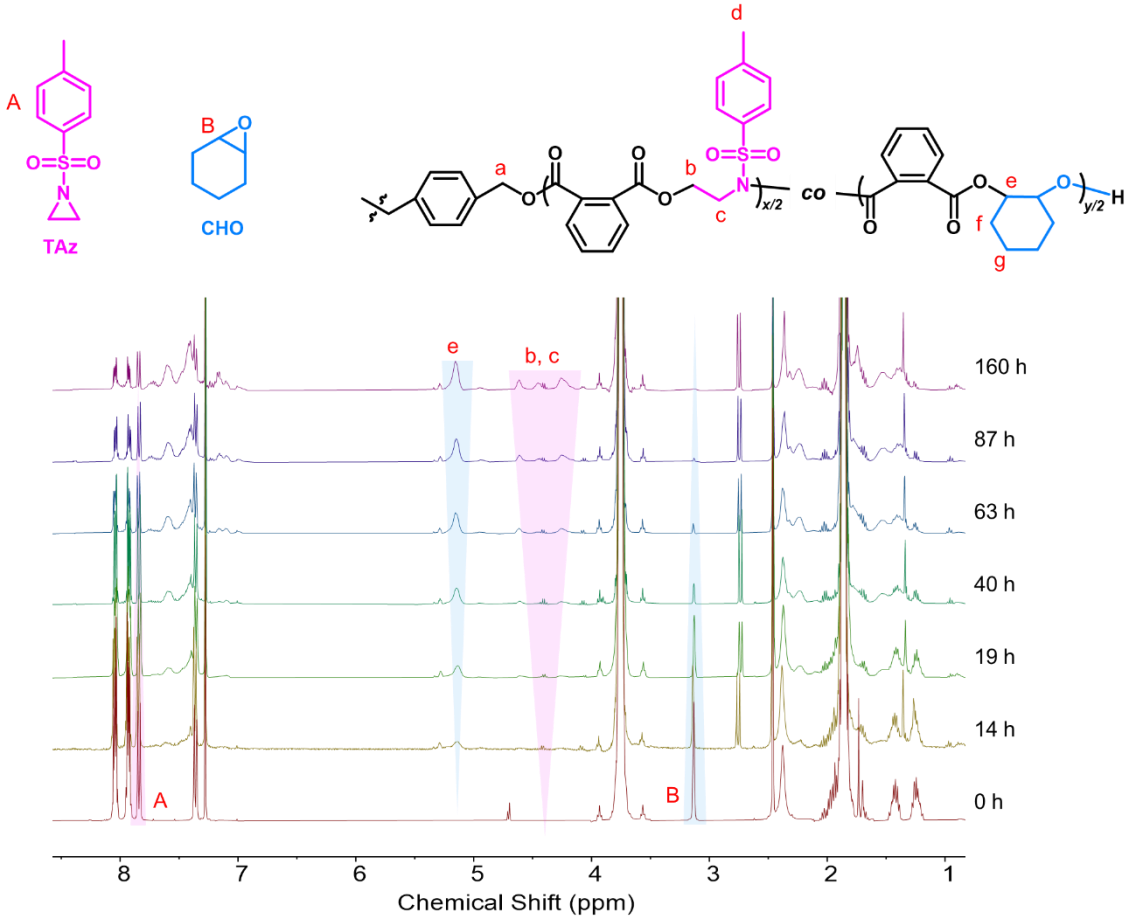

Figure 5.20. ^{1}H NMR spectra of crude aliquots withdrawn from the TAz/CHO/PA ROAC to monitor TAz and CHO conversion ($CDCl_3$) (polymerization was implemented under Ar atmosphere at room temperature, *t*-BuP_1/TEB ratio was set as 1.0/0.75) (Table 5.2, entry 6).

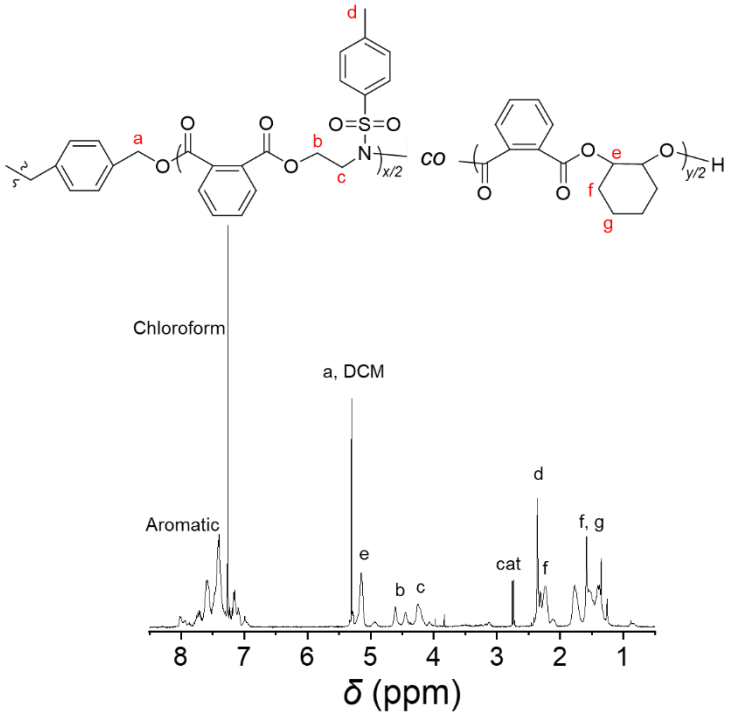

Figure 5.21. ^{1}H NMR spectrum of the synthesized poly(CHO-*alt*-PA)-*co*-poly(TAz-*alt*-PA) ($CDCl_3$) (polymerization was implemented under Ar atmosphere at room temperature, *t*-BuP_1/TEB ratio was set as 1.0/0.75) (Table 5.2, entry 6).

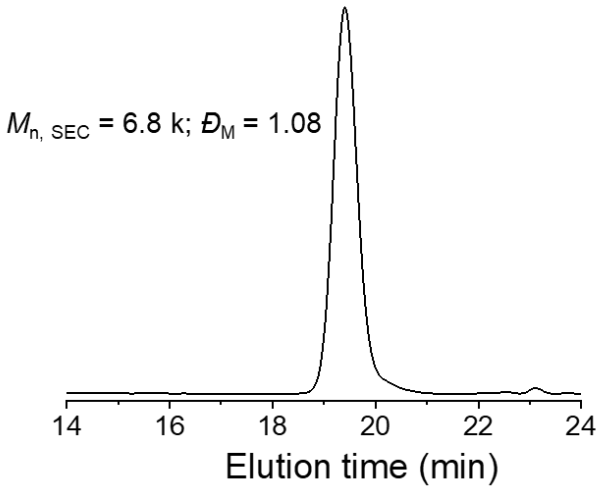

Figure 5.22. SEC trace (THF) of synthesized poly(CHO-*alt*-PA)-*co*-poly(TAz-*alt*-PA) (polymerization was implemented under Ar atmosphere at room temperature, *t*-BuP_1/TEB ratio was set as 1.0/0.75) (Table 5.2, entry 6).

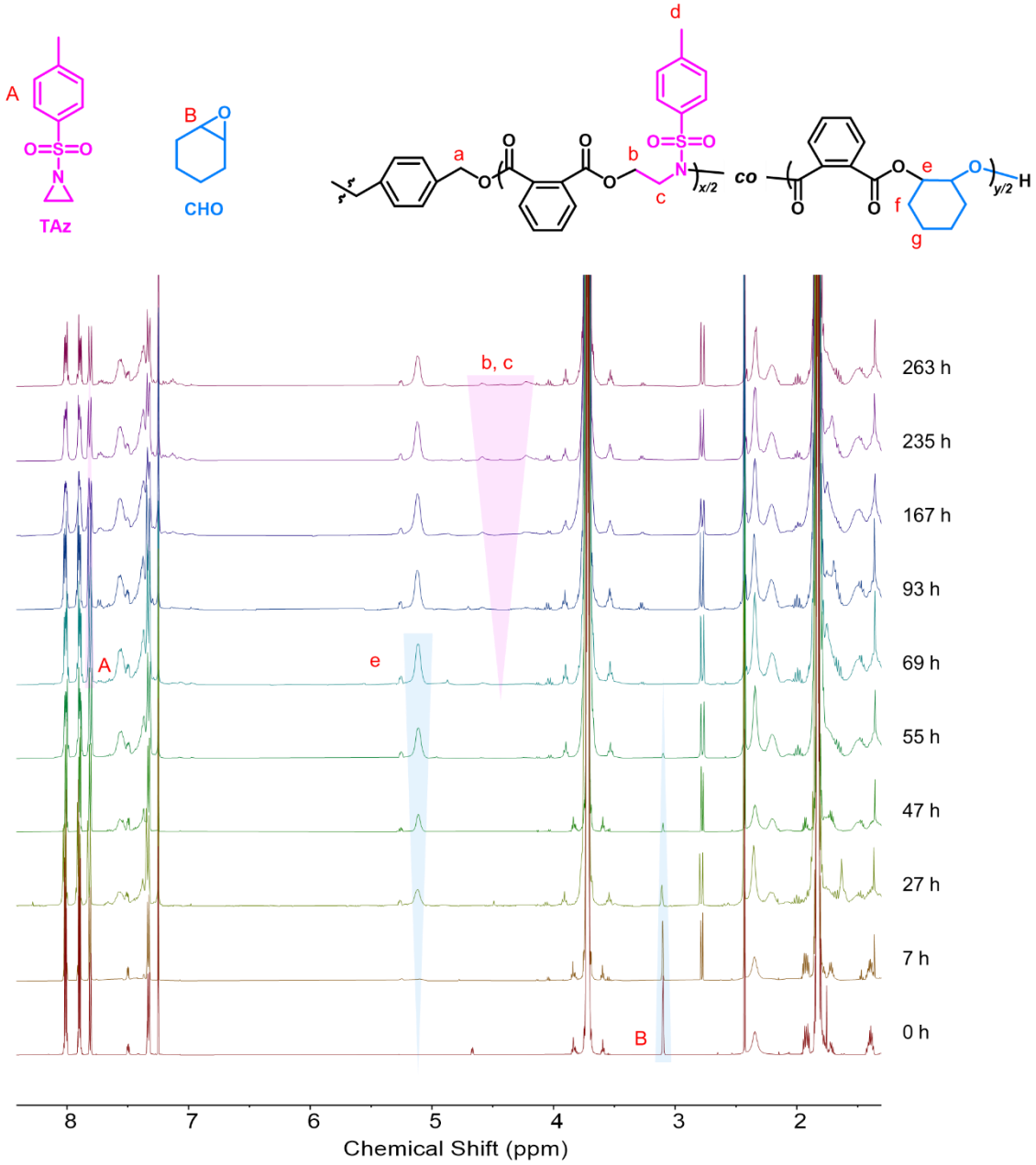

Figure 5.23. ^{1}H NMR spectra of crude aliquots withdrawn from the TAz/CHO/PA ROAC to monitor TAz and CHO conversion ($CDCl_3$) (polymerization was implemented under Ar atmosphere at room temperature, *t*-BuP_1/TEB ratio was set as 1.0/1.0) (Table 5.2, entry 7).

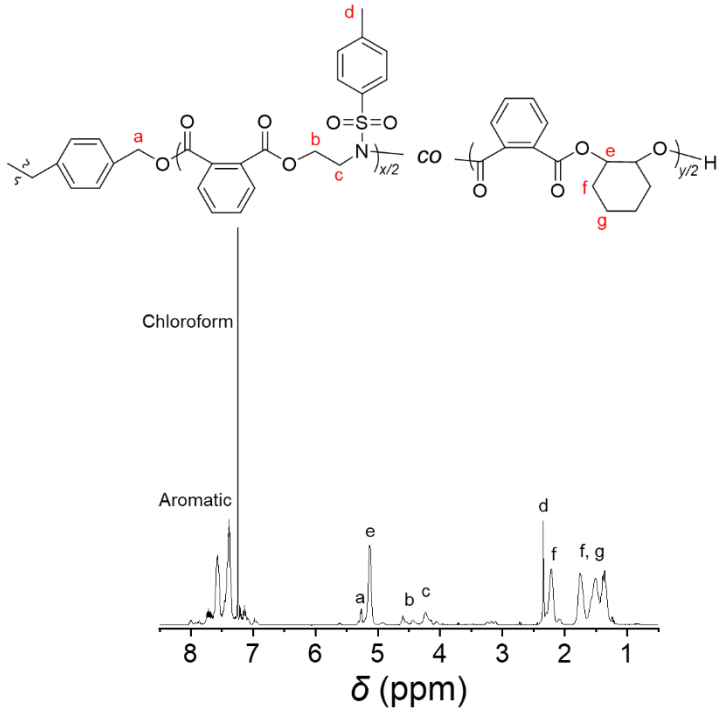

Figure 5.24. ^{1}H NMR spectrum of synthesized poly(TAz-*alt*-PA)-*b*-poly(CHO-*alt*-PA)-*b*-poly(TAz-*alt*-PA) ($CDCl_3$) (polymerization was implemented under Ar atmosphere at room temperature, *t*-BuP_1/TEB ratio was set as 1.0/1.0) (Table 5.2, entry 7).

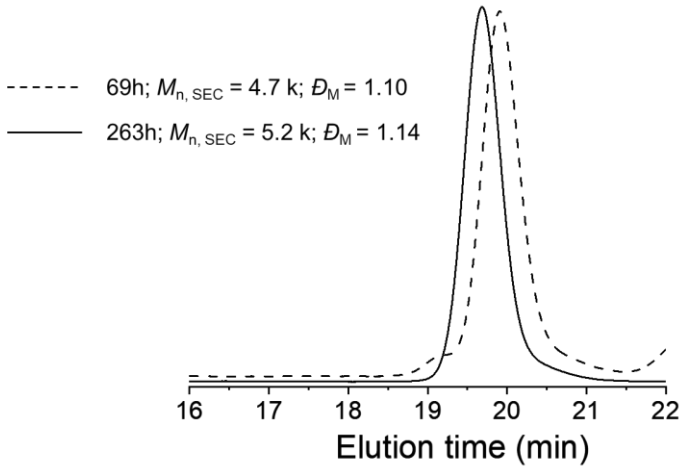

Figure 5.25. Evolution of SEC traces (THF) of synthesized poly(TAz-*alt*-PA)-*b*-poly(CHO-*alt*-PA)-*b*-poly(TAz-*alt*-PA) (polymerization was implemented under Ar atmosphere at room temperature, *t*-BuP_1/TEB ratio was set as 1.0/1.0) (Table 5.2, entry 7).

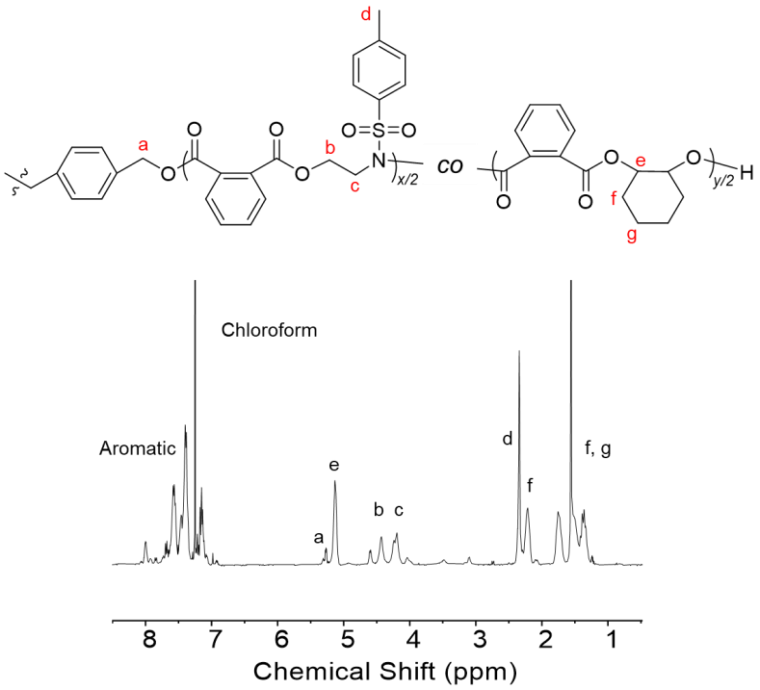

Figure 5.26. ^{1}H NMR spectrum of the synthesized poly(TAz-*alt*-PA)-*b*-poly(CHO-*alt*-PA)-*b*-poly(TAz-*alt*-PA) ($CDCl_3$) (polymerization was implemented under Ar atmosphere at room temperature for 90 hours and increased to 40 °C for 70 hours, *t*-BuP_1/TEB ratio was set as 1.0/1.0) (Table 5.2, entry 8).

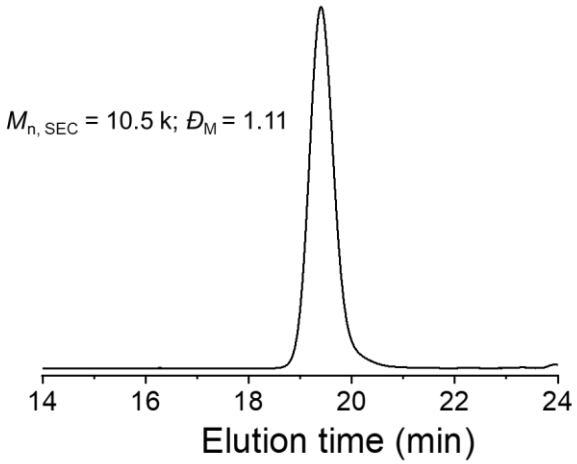

Figure 5.27. SEC traces of the synthesized poly(TAz-*alt*-PA)-*b*-poly(CHO-*alt*-PA)-*b*-poly(TAz-*alt*-PA) (THF) (Table 5.2, entry 8).

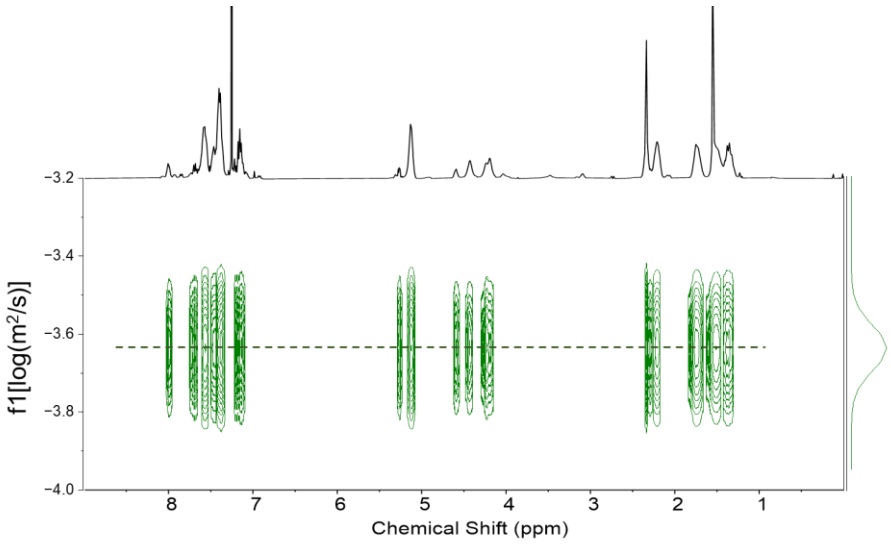

Figure 5.28. DOSY NMR spectrum of the synthesized poly(TAz-*alt*-PA)-*b*-poly(CHO-*alt*-PA)-*b*-poly(TAz-*alt*-PA) (Table 5.2 entry 8).

The ^{1}H NMR spectra of poly(TAz-*alt*-PA)-*co*-poly(CHO-*alt*-PA) with five different monomer sequences were compared to confirm the sequence structures of the synthesized polymers. As references, poly(TAz-*alt*-PA) and poly(CHO-*alt*-PA) alternating copolymers and a real-block poly(TAz-*alt*-PA)-*b*-poly(CHO-*alt*-PA)-*b*-poly(TAz-*alt*-PA) terpolymer synthesized via sequential monomer addition were used (Figure 5.29). The signals labeled "1" and "2" correspond to the protons from the BDM initiator connected with PA-CHO and PA-TAz units, respectively. By analyzing the relative peak intensities of "1" and "2" in the terpolymers, a clear shift in the initiation of the polymerization from PA-TAz to PA-CHO upon the addition of TEB is evident. Besides, the intensity of signals "3" and "4" corresponding to TAz unit in the chain-end gradually increased from run 3 to run 8 in table 1 confirmed a switch of PA/CHO ω chain-end to PA/TAz ω chain-end.[25] These findings underscore the consistency between the monomer sequence in the synthesized polymers and the reactivity ratio values established during polymerization, which can be continuously adjusted by modifying the ratio of binary catalysts.

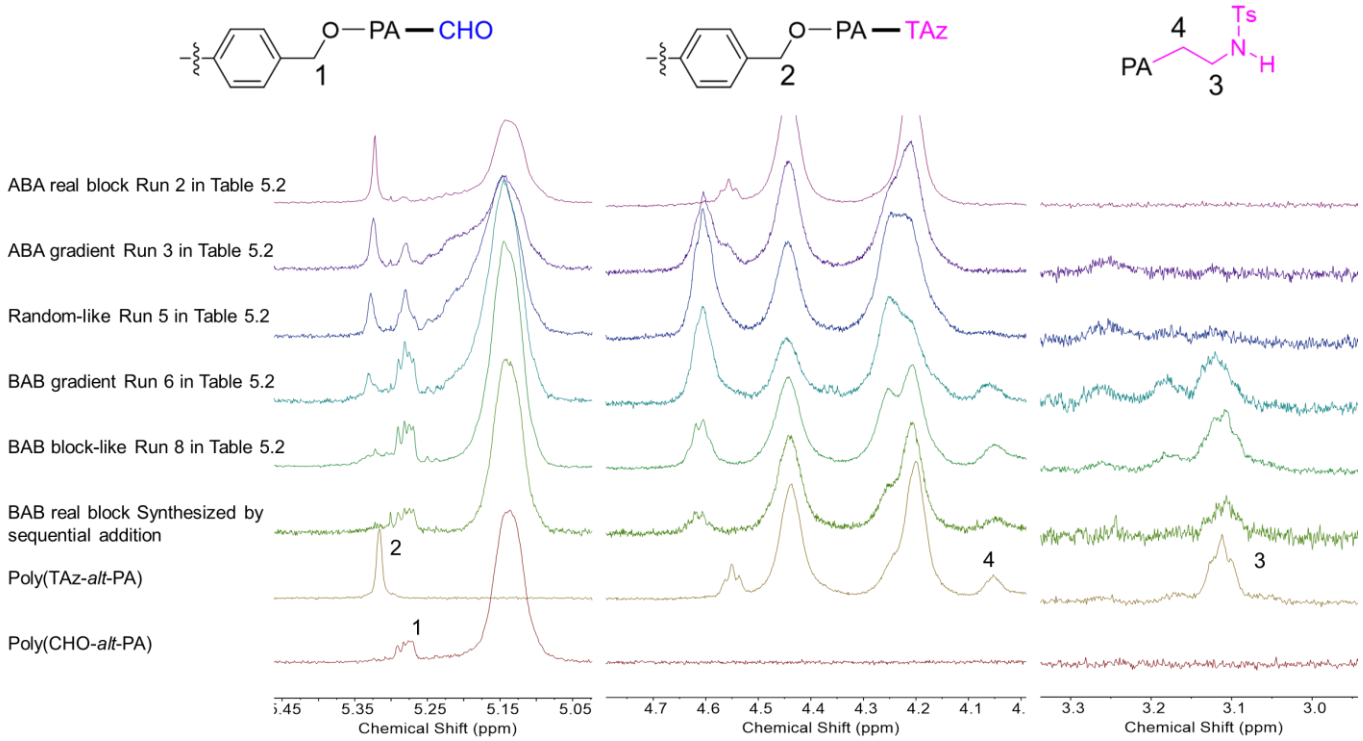

Figure 5.29. Assigning the α and ω chain-end signal of poly(CHO-*alt*-PA)-*co*-poly(TAz-*alt*-PA) with different monomer sequences on ^{1}H NMR.

5.3.3 DFT calculation of *t*-BuP_1/TEB-catalyzed CHO/TAz/PA ROAC

DFT calculations were conducted to assess the interactions between TEB and two different types of three-membered cyclic monomers, epoxides and aziridines, using CHO and TAz as the models for the preliminary study. Structure optimization was conducted, followed by calculation of the atomic charges (Figure 5.30). For TAz, the electron density of the two carbon atoms on the aziridine rings changed by less than 1% after interaction with TEB (Schemes 5.1a, C1, and C2). The distance between the oxygen atom on sulfonyl and the boron atom of TEB was calculated to be 3.23 Å in the TAz-TEB adduct, slightly shorter than the sum of the van der Waals radii of the oxygen and boron atoms (1.52 Å + 2.00 Å = 3.52 Å).

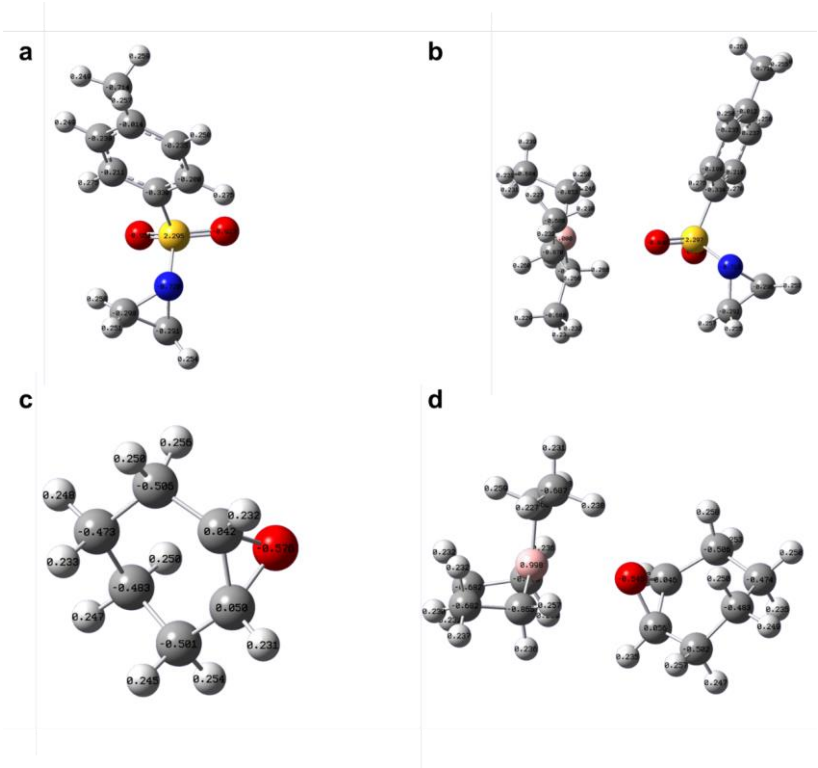

Figure 5.30. Optimized geometries and calculated charges on each atom. a). TAz; b). TAz-TEB adduct; c). CHO; d). CHO-TEB adduct.

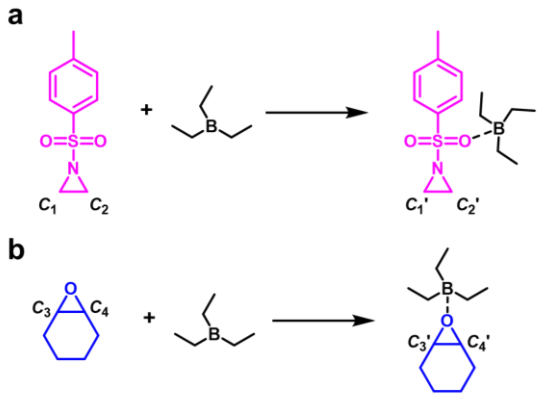

Electronic Charges Calculated on the α-carbon in the TAz and CHO

Carbon	Charge on TAz and CHO / e	Charge on TAz- and CHO- TEB adduct / e	Charge changes / %
C_1	-0.298	-0.296	0.7
C_2	-0.291	-0.291	0
C_3	0.042	0.046	9.5
C_4	0.050	0.056	12.0

Optimized geometry were performed using B3LYP/6–31+G**, atomic charges was computed by NBO theory.

Scheme 5.6. Charge changes after TEB is adducted to the substrate. a) TEB adducted with TAz; b) TEB adducted with CHO.

Consequently, the interaction between the TEB and TAz is expected to be weak. In contrast, after interacting with TEB, the electron density of the two carbon atoms on the epoxide ring of CHO changed significantly (Scheme 5.6b, C3, and C4), becoming 9.5% and 12.0% more positively charged, respectively, indicating greater susceptibility to nucleophilic attack. Moreover, the distance between the oxygen atom of CHO and the boron atom of TEB was calculated to be 2.55 Å, which was significantly shorter than that in the TEB-TAz adduct. These calculations suggest that TEB's monomer activation is much more significant for CHO than for TAz, which aligns with experimental observations.

The terpolymerization mechanism of epoxide/aziridine/cyclic anhydride ROCOP was further investigated using DFT calculations of the activation energy. The rate-determining step was simplified as the ring-opening of CHO and TAz by nucleophilic attack of a benzoate anion, both in the absence and presence of TEB. To reduce the computational load, the countercation [*t*-BuP$_1$-H]$^+$ was not included in the calculation. The calculated energy profiles for the ring opening of CHO and TAz without TEB are shown in Figure 5.33a.

Slightly difference in the activation Gibbs energies ($\Delta\Delta G^{\ddagger}$) between the ring opening of CHO and TAz (0.6 kcal/mol) was observed and ring-opening of TAz resulted more stable intermediate (initial reactants-E2: -3.1 kcal/mol; initial reactants-A2: -21.1 kcal/mol). This result is consistent with the experimental findings that the TAz/PA ROAC is more favored than the CHO/PA ROAC without a TEB.

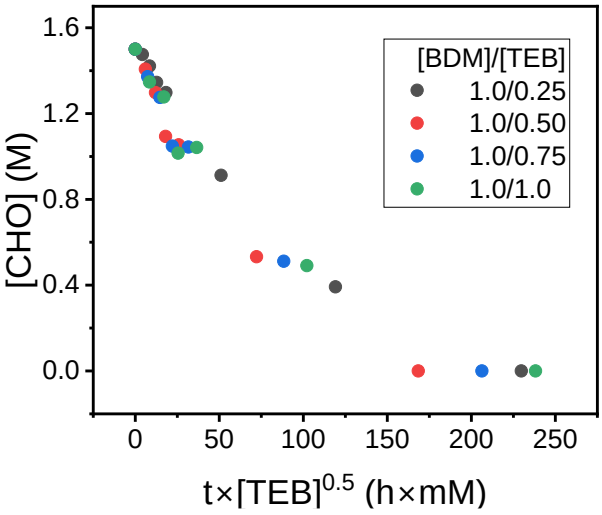

Figure 5.31. CHO decay versus normalized time scale showing 0.5th-order behavior in TEB at a variety of catalyst loadings.

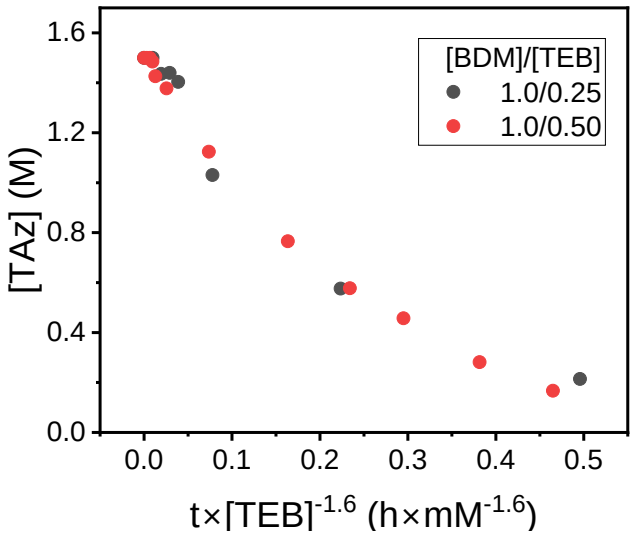

Figure 5.32. TAz decay versus normalized time scale showing 0.5th-order behavior in TEB at a variety of catalyst loadings.

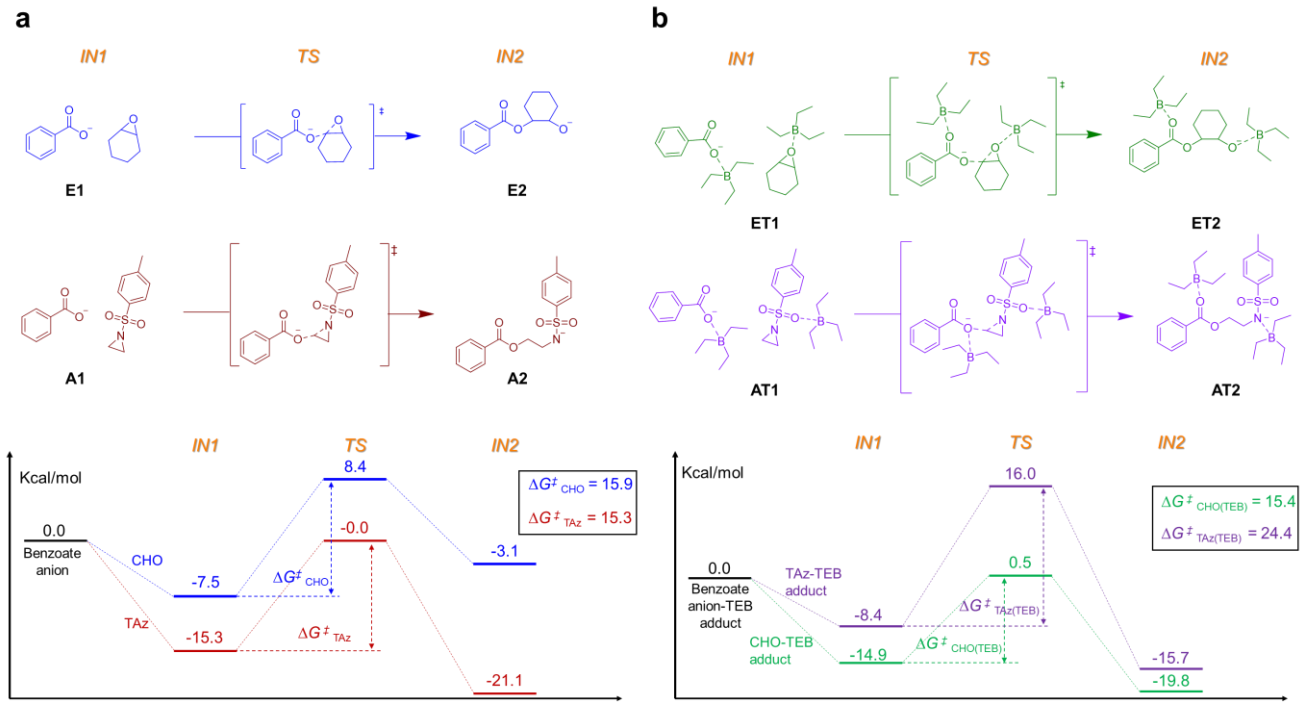

Figure 5.33. Density functional theory-calculated energy profile (ΔG, kcal mol^{-1}) for CHO and TAz ring opened by benzoate anion. a) without TEB involvement; b) with TEB involvement.

In the experimental study to assess the effect of TEB on both ROAC processes, the apparent reaction order of TEB on CHO/PA and TAz/PA ROAC was estimated as 0.5 and −1.6, respectively, using Burés's time-

normalized method (Figures 5.31 and 5.32).[27] The reaction order in TEB suggests the involvement of more than one molecule of TEB, interacting with the monomers and with the anionic chain end. With this consideration in mind, in the calculation of the ring-opening of CHO and TAz by the benzoate anion with TEB, two molecules of TEB were added: one interacting with the monomer and the other interacting with the benzoate anion (Figure 5.33b). The energy profiles show that the activation Gibbs energy ($\Delta G‡$) for the ring-opening of CHO was calculated to be 15.4 kcal/mol, which is 0.5 kcal/mol lower than without TEB. Moreover, $\Delta G‡$ for the ring-opening of TAz was calculated to be 24.4 kcal/mol, which is significantly higher than that for CHO, and 9.0 kcal/mol higher than TAz without TEB. These calculations align with the experimental results, indicating that TEB facilitates the ROAC of epoxide/cyclic anhydrides, but inhibits the ROAC of TAz/cyclic anhydrides.

5.4 Conclusion

In this chapter, the author introduced an innovative strategy for controlling the monomer sequence in the terpolymerization of epoxides, *N*-tosyl aziridine, and cyclic anhydrides using a binary catalyst system comprising a phosphazene base, *t*-BuP_1, and a Lewis acid, TEB. Varying the ratio of these two catalysts resulted in the fine-tuning of the poly(amide ester)-*co*-polyester terpolymers from real block structures to gradient, random-like, reversed gradient, and reversed block-like structures. This polymerization system demonstrated versatility across various epoxides and cyclic anhydride monomers, albeit with slight variations in polymerization behavior depending on the monomer combinations. Through a comprehensive mechanistic study that included experimental investigations to determine the apparent reaction order in TEB and density functional theory (DFT) calculations, the opposing effects of TEB on epoxides/cyclic anhydrides ROAC and TAz/cyclic anhydrides ROAC were elucidated. This strategy has the potential to be applied to diverse copolymerization systems, enabling the synthesis of polymers with precise and customizable monomer

sequences. Furthermore, this synthetic method offers a straightforward approach for producing copolymers with similar chemical compositions but varying monomer sequences, which can be valuable for exploring the relationship between the monomer sequences and polymer properties.

5.5References

1. Luo, W.; Xiao, M.; Wang, S.; Han, D.; Meng, Y. Gradient Terpolymers with Long ε-Caprolactone Rich Sequence Derived from Propylene Oxide, CO_2, and ε-Caprolactone Catalyzed by Zinc Glutarate. *Eur. Polym. J.* **2016**, 84, 245–255.

6. Zhou, Y.; Gao, Z.; Hu, C.; Meng, S.; Duan, R.; Sun, Z.; Pang, X. Facile Synthesis of Gradient Polycarbonate-Polyester Terpolymers from Monomer Mixtures Mediated by an Asymmetric Chromium Complex. *Macromolecules*. **2022**, 55, 9951–9959.

7. Nomura, N.; Akita, A.; Ishii, R.; Mizuno, M. Random Copolymerization of ε-Caprolactone with Lactide Using a Homosalen-Al Complex. *J. Am. Chem. Soc.* **2010**, 132, 1750–1751.

8. Jehanno, C.; Mezzasalma, L.; Sardon, H.; Ruipérez, F.; Coulembier, O.; Taton, D. Benzoic Acid as an Efficient Organocatalyst for the Statistical Ring-Opening Copolymerization of ε-Caprolactone and L-Lactide: A Computational Investigation. *Macromolecules*. **2019**, 52, 9238–9247.

9. Hua, X.; Liu, X.; Cui, D. Degradation Behavior of Poly(Lactide-*co*-Carbonate)s Controlled by Chain Sequences. *Macromolecules*. **2020**, 53, 5289–5296.

10. Judzewitsch, P. R.; Nguyen, T. K.; Shanmugam, S.; Wong, E. H. H.; Boyer, C. Towards Sequence-Controlled Antimicrobial Polymers: Effect of Polymer Block Order on Antimicrobial Activity. *Angew. Chem. Int. Ed. Engl.* **2018**, 57, 4559–4564.

11. Teator, A. J.; Lastovickova, D. N.; Bielawski, C. W. Switchable Polymerization Catalysts. *Chem. Rev.* **2016**, 116, 1969–1992.

12. Dadashi-Silab, S.; Doran, S.; Yagci, Y. Photoinduced Electron Transfer Reactions for Macromolecular Syntheses. *Chem. Rev.* **2016**, 116, 10212–10275.

13. Zhang, Z.; Zeng, T. Y.; Xia, L.; Hong, C. Y.; Wu, D. C.; You, Y. Z. Synthesis of Polymers with On-Demand Sequence Structures via Dually Switchable and Interconvertible Polymerizations. *Nat. Commun.* **2018**, 9, 2577.

14. Ida, S.; Ouchi, M.; Sawamoto, M. Template-Assisted Selective Radical Addition Toward Sequence-Regulated Polymerization: Lariat Capture of Target Monomer by Template Initiator. *J. Am. Chem. Soc.* **2010**, 132, 14748–14750.

15. Lin, F.; Wang, M.; Pan, Y.; Tang, T.; Cui, D.; Liu, B. Sequence and Regularity Controlled Coordination Copolymerization of Butadiene and Styrene: Strategy and Mechanism. *Macromolecules.* **2017**, 50, 849–856.

16. Liu, B.; Wang, X.; Pan, Y.; Lin, F.; Wu, C.; Qu, J.; Luo, Y.; Cui, D. Unprecedented 3,4-Isoprene and *cis*-1,4-Butadiene Copolymers with Controlled Sequence Distribution by Single Yttrium Cationic Species. *Macromolecules*. **2014**, 47, 8524–8530.

17. Fan, H.; Wang, J.; Tao, Z.; Huang, J.; Rao, P.; Kurokawa, T.; Gong, J. P. Adjacent Cationic–Aromatic Sequences Yield Strong Electrostatic Adhesion of Hydrogels in Seawater. *Nat. Commun.* **2019**, 10, 5127.

18. Herzberger, J.; Leibig, D.; Liermann, J. C.; Frey, H. Conventional Oxyanionic Versus Monomer-Activated Anionic Copolymerization of Ethylene Oxide with Glycidyl Ethers: Striking Differences in Reactivity Ratios. *ACS Macro Lett.* **2016**, 5, 1206–1211.

19. Liu, S.; Bai, T.; Ni, K.; Chen, Y.; Zhao, J.; Ling, J.; Ye, X.; Zhang, G. Biased Lewis Pairs: A General Catalytic Approach to Ether-Ester Block Copolymers with Unlimited Ordering of Sequences. *Angew. Chem. Int. Ed. Engl.* **2019**, 58, 15478–15487.
20. Xia, X.; Suzuki, R.; Gao, T.; Isono, T.; Satoh, T. One-Step Synthesis of Sequence-Controlled Multiblock Polymers with up to 11 Segments from Monomer Mixture. *Nat. Commun.* **2022**, 13, 163.
21. Xia, X.; Gao, T.; Li, F.; Suzuki, R.; Isono, T.; Satoh, T. Sequential Polymerization from Complex Monomer Mixtures: Access to Multiblock Copolymers with Adjustable Sequence, Topology, and Gradient Strength. *Macromolecules*. **2023**, 56, 92–103.
22. Xia, X.; Gao, T.; Li, F.; Suzuki, R.; Isono, T.; Satoh, T. Multidimensional Control of Repeating Unit/Sequence/Topology for One-Step Synthesis of Block Polymers from Monomer Mixtures. *J. Am. Chem. Soc.* **2022**, 144, 17905–17915.
23. Xia, X.; Suzuki, R.; Takojima, K.; Jiang, D. H.; Isono, T.; Satoh, T. Smart Access to Sequentially and Architecturally Controlled Block Polymers via a Simple Catalytic Polymerization System. *ACS Catal.* **2021**, 11, 5999–6009.
24. Gao, T.; Li, F.; Suzuki, R.; Li, H.; Yamamoto, T.; Xia, X.; Isono, T.; Satoh, T. One-Step Synthesis of Poly(Amide Ester)-Based Block Copolymers with Defined Phase Separation Behavior. *Macromolecules*. **2023**, 56, 8333–8343.
25. Xu, J.; Wang, X.; Hadjichristidis, N. Diblock Dialternating Terpolymers by One-Step/One-Pot Highly Selective Organocatalytic Multimonomer Polymerization. *Nat. Commun.* **2021**, 12, 7124.
26. Song, Q.; Qiu, H.; Liu, L.; Zhang, G.; Peruch, F.; Carlotti, S.; Zhao, J. Janus Effect of Lewis Acid Enables One-Step Block Copolymerization of Ethylene Oxide and *N*-Sulfonyl Aziridine. *Angew. Chem. Int. Ed. Engl.* **2023**, 62, e202300187.

27. Gleede, T.; Rieger, E.; Blankenburg, J.; Klein, K.; Wurm, F. R. Fast Access to Amphiphilic Multiblock Architectures by the Anionic Copolymerization of Aziridines and Ethylene Oxide. *J. Am. Chem. Soc.* **2018**, 140, 13407–13412.

28. Ma, Y.; You, X.; Zhang, J.; Wang, X.; Kou, X.; Liu, S.; Zhong, R.; Li, Z. Synthesis of Sequence-Specific Poly(Ester-Carbonate) Copolymers via Chemoselective Terpolymerization Controlled by the Stoichiometric Ratio of Phosphazene/Triethylborane. *Angew. Chem. Int. Ed. Engl.* **2023**, 62, e202303315.

29. Xu, J.; Hadjichristidis, N. Well-Defined Poly(Ester Amide)-Based Homo- and Block Copolymers by One-Pot Organocatalytic Anionic Ring-Opening Copolymerization of N-Sulfonyl Aziridines and Cyclic Anhydrides. *Angew. Chem. Int. Ed. Engl.* **2021**, 133, 7025–7030.

30. Xia, X.; Gao, T.; Li, F.; Suzuki, R.; Isono, T.; Satoh, T. Sequential Polymerization from Complex Monomer Mixtures: Access to Multiblock Copolymers with Adjustable Sequence, Topology, and Gradient Strength. *Macromolecules*. **2023**, 56, 92–103.

31. Burés, J. A Simple Graphical Method to Determine the Order in Catalyst. *Angew. Chem. Int. Ed. Engl.* **2016**, 55, 2028–2031.

Chapter 6

Conclusions

In this thesis, the author has developed a versatile platform for synthesizing polyesters with precisely controllable structures. In response to the current challenges associated with the unsustainable generation and disposal of polymer materials, polyester emerges as a viable option due to its recyclability facilitated by hydrolysable ester bonds, enabling chemical recycling into small molecules. Moreover, the use of renewable monomer resources for polyester synthesis further enhances its sustainability profile. To transition from petroleum-based polymers to polyesters and their derivatives, it is imperative to enhance the performance of polyester-based materials. This necessitates diverse polyester mainchains to cater to various needs in polymer-related fields, as well as precisely controlled structures to ensure optimal performance. Addressing these requirements, the author has established a platform comprising several polymerization systems for the production of polyester homopolymers, polyester block copolymers, and monomer sequence-controlled polyesters with well-defined structures. This platform offers a solution for large-scale polyester production while addressing concerns related to material performance and sustainability. A summary of this thesis is as follows:

In Chapter 2, the author has expounded upon the notable catalytic efficiency of cesium pivalate in epoxide/cyclic anhydride ring-opening alternating copolymerization (ROAC), oxetane/cyclic anhydride ROAC, and epoxide ring-opening polymerization (ROP) processes. Employing various combinations of epoxides and cyclic anhydrides has yielded a diverse array of polyester structures, all characterized by narrow molecular weight distributions. The advantageous properties of the cesium pivalate catalyst, such as its cost-effectiveness, ease of handling, and low toxicity, suggest promising applications in both laboratory and industrial-scale polyester production. Additionally, the successful execution of a one-pot/two-step synthesis for polyether-polyester block copolymers highlights the versatility of alkali metal carboxylate as a versatile catalyst capable of bridging different catalytic cycles.

In Chapter 3, cesium pivalate was employed to integrate two catalytic cycles involving various epoxide/cyclic anhydrides ROAC reactions, as well as oxetane/cyclic anhydrides ROAC reactions, resulting in the production of polyesters exhibiting diverse chain structures. The polymerization behavior of ROAC involving two epoxide/cyclic anhydrides ROAC catalytic cycles was extensively investigated, and the reactivity trends of cyclic anhydrides were summarized. Incorporating the oxetane monomer further enriched the structures of the synthesized polyesters. Utilizing the reactivity order of epoxides >> oxetane, ROCOP (Ring-Opening Copolymerization) of epoxide, oxetane, and cyclic anhydride, as well as ROCOP of epoxide, oxetane, and two cyclic anhydrides, were employed for the one-step synthesis of block polyester. This approach resulted in polymers with more flexible and adjustable mainchain structures and defined monomer sequences. Consequently, this self-switchable copolymerization platform holds promise and significance for both laboratory and industrial-scale production of block polymers with complex macromolecular architectures.

In Chapter 4, the author has showcased the efficacy of copolymerizing aziridine with two cyclic anhydrides to synthesize poly(amide ester)-based block copolymers under mild reaction conditions. Through the combination of aziridine/cyclic anhydride ROCOP and trimethylene carbonate ROP, the author successfully produced a "real" block poly(amide ester)-*b*-polycarbonate with well-defined phase separation behavior, which implied an enhanced block chemical structure compared to block copolymers synthesized via other self-switchable copolymerization systems. Importantly, by employing a four-component copolymerization of aziridine, epoxide, and two cyclic anhydrides, the author demonstrated the one-step synthesis of "real" block copolymers comprising poly(amide ester) and polyester, exhibiting microphase separation. This strategy allows for the flexible adjustment of each block's structure by selecting the appropriate combination of the four starting monomers, thereby laying the groundwork for synthesizing block

copolymers with desired microphase-separated morphologies.

In Chapter 5, the author has introduced an innovative approach to control monomer sequence in the terpolymerization of epoxides, aziridine, and cyclic anhydrides. This method utilizes a binary catalyst system consisting of phosphazene base (*t*-BuP_1) and Lewis acid (triethylborane). By adjusting the ratio of these two catalysts, precise monomer sequence control over the structure of the resulting poly(amide ester)-*co*-polyester terpolymers was achieved, ranging from real block structures to gradient, random-like, reversed gradient, and reversed block-like structures. A comprehensive mechanistic study, which included experimental investigations to determine the apparent reaction order in TEB and density functional theory calculations, elucidated the opposing effects of TEB on epoxides/cyclic anhydrides ROAC and TAz/cyclic anhydrides ROAC. This strategy holds promise for application in diverse copolymerization systems, enabling the synthesis of polymers with precise and customizable monomer sequences. Moreover, this synthetic approach offers a straightforward method for producing copolymers with similar chemical compositions but varying monomer sequences, which can be valuable for exploring the relationship between monomer sequences and polymer properties.

In conclusion, this research has established a versatile platform for high-value added polyester production. The alkali metal carboxylate-catalyzed ROAC systems outlined in Chapters 2 enable the efficient large-scale production of polyester homopolymers with diverse structures. Additionally, the self-switchable systems introduced in Chapters 3 and 4 offer a flexible approach for the one-step synthesis of polyester block copolymers. Furthermore, Chapter 5 presents a monomer sequence-controlled copolymerization system where the sequence of monomers in the synthesized polyester copolymers can be precisely manipulated by adjusting the cocatalyst ratio. These polymerization systems have significantly enhanced the synthesis of polyesters

with tailored structures, laying the groundwork for future investigations into the correlation between comonomer sequences and polyester properties. This advancement contributes to the development of sustainable polymer material systems.